8-8-2023

Script-based design toolkit for digitally fabricated concrete applied to terrain-responsive retaining wall design

Nada Abdel-Aziz
Mississippi State University, na627@msstate.edu

Script-based design toolkit for digitally fabricated concrete applied to terrain-responsive retaining wall design

By

Nada Abdel-Aziz

Approved by:

Abbey Franovich (Major Professor)
Warren C. Gallo
Duane McLemore
Peter R. Summerlin (Graduate Coordinator)
Scott T. Willard (Dean, College of Agriculture and Life Sciences)

A Thesis
Submitted to the Faculty of
Mississippi State University
in Partial Fulfillment of the Requirements
for the Degree of Master of Landscape Architecture
in Landscape Architecture
in the Department of Landscape Architecture

Mississippi State, Mississippi

August 2023

Name: Nada Abdel-Aziz

Date of Degree: August 8, 2023

Institution: Mississippi State University

Major Field: Landscape Architecture

Major Professor: Abbey Franovich

Title of Study: Script-based design toolkit for digitally fabricated concrete applied to terrain-responsive retaining wall design

Pages in Study: 185

Candidate for Degree of Master of Landscape Architecture

The potential of digitally fabricated concrete (DFC) to produce terrain responsive designs has not been thoroughly investigated. Existing research indicates diverse benefits of DFC, such as the rapid fabrication of customized geometries. This research clarifies the advantages and design processes involved in creating site-specific DFC structures. Existing literature is analyzed to provide an overview of fabrication methods and their impacts and constraints on design. Parametric scripting is used to develop an interactive toolkit that integrates aesthetic, structural, and fabrication considerations into the design process. This toolkit specifically focuses on unreinforced retaining walls with interchangeable modules for terrain analysis, wall form generation, structural analysis, and fabrication analysis. The toolkit provides valuable feedback, such as identifying optimum wall proportions, and enables rapid design explorations. The findings affirm the value of exploratory design tools in managing fabrication complexities. Additionally, by recreating an existing amphitheater, the research indicates that DFC can create site-specific geometries that draw from the surrounding terrain.

DEDICATION

To Nicole Columbus and Carly Shows, for our years of friendship, mirth, and solidarity.

ACKNOWLEDGEMENTS

I am deeply indebted to my advisor, Abbey Franovich, for her tireless and endless commitment, enthusiasm, and support. I admire how you give everything you have to what you do. I'm excited to see the impact you'll have on the profession. I am grateful to Cory Gallo, whose guidance and patience have been invaluable to me for the last six years. I would also like to thank Duane McLemore, for his boundless energy and enthusiasm in sharing his expertise. Special thanks to Peter Summerlin for creating the high-quality LIDAR drone capture 3D model used as the basis of the experimental demonstration. I would be remiss in not also mentioning his respectful, patient, and diligent efforts as graduate coordinator.

So long, and thanks for all the fish!

TABLE OF CONTENTS

DEDICATION ii

ACKNOWLEDGEMENTS iii

LIST OF TABLES vii

LIST OF FIGURES viii

CHAPTER

I. INTRODUCTION 1

1.1 Project Overview 1
1.2 Research Context 1
1.3 Research Objectives 4
1.4 Study organization 5

II. LITERATURE REVIEW 6

2.1 Overview of digital fabrication systems for concrete 6
2.1.1 Deposition-based systems 10
2.1.2 Particle bed-based systems 14
2.1.3 Formwork-based systems 16
2.2 Process Factors for DFC 22
2.2.1 Mechanical factors for DFC 22
2.2.1.1 Large-scale mobility factors 23
2.2.1.2 Small-scale mobility factors 27
2.2.1.3 Effects of mechanical factors on printable design resolution 34
2.2.2 Material factors for DFC 38
2.2.2.1 Material factors for deposition-based systems 38
2.2.2.2 Material factors for particle bed-based systems 40
2.2.2.3 Processes for “setting on demand” activation of concrete 45
2.3 Robotic construction processes in relation to site and terrain conditions 46

III. PROBLEM STATEMENT: RECIPROCAL PROCESSES BETWEEN DESIGN INTENT AND MACHINE SELECTION 51

3.1 Introduction 51
3.2 Research context and designer challenges identified for DFC 52

3.2.1 Understanding of design space for DFC 52
3.2.2 Complexity of design process for DFC 53
3.2.3 Print method suitability evaluation and comparisons 56
3.2.4 Application to landscape architecture and terrain responsive design 57
3.3 Defining terrain responsive design 60
3.4 Print method comparisons and selection process 68
3.4.1 Production environment 81
3.4.2 Print volume 83
3.4.3 Minimum feature size 84
3.4.4 Surface Slope 85
3.4.5 Perimeter lengths 86
3.4.6 Surface Continuity and self-intersection 88
3.5 Retaining wall considerations and variables 90

IV. METHODOLOGY: PARAMETRIC SCRIPTING APPLIED TO AN INTERACTIVE DESIGN TOOLKIT FOR AESTHETICS, STRUCTURE, AND FABRICATION 94

4.1 Introduction 94
4.2 Preparation of inputs 96
4.3 Toolkit phases and modules 96
4.4 Initial conditions processes 101
4.4.1 Terrain preparations and inputs 101
4.4.2 Path inputs 104
4.5 Terrain analysis processes 106
4.5.1 Brief process summary 106
4.5.2 Sectional versus volumetric approaches 107
4.5.3 Process considerations for terrain analysis 109
4.6 Form generation processes 112
4.6.1 Cross section distribution 112
4.6.2 Cross-section design 117
4.6.3 Random manipulation process 122
4.6.4 Resulting forms 124
4.7 Structural evaluation 126
4.7.1 Formulas and processes 126
4.7.2 Data preparations 129
4.7.3 Lateral pressure and weight 130
4.7.4 Resultant force and eccentricity 132
4.7.5 Sliding, crushing, and overturning risks 136
4.8 Printability evaluation processes 137
4.8.1 Layer contour analysis 138
4.8.2 Surface slopes 139
4.8.3 Print volume 141
4.9 Remote control panel and export options 143

V. RESULTS AND DISCUSSIONS: DEMONSTRATION OF DFC PROCESSES AND POTENTIALS WITH AN AMPHITHEATER APPLICATION 145

5.1 Experimental applications and purpose 145
5.2 Existing conditions of test case - MSU Amphitheater 146
5.3 Fabrication parameters 150
5.4 Series I: inventory stage 151
5.4.1 Series objectives and definitions 151
5.4.2 First series data 154
5.4.3 Observations 160
5.5 Series II: exploratory stage of design process 162
5.5.1 Series objectives and definitions 162
5.5.2 Iteration stages and actions 162
5.5.3 Observations 171

VI. CONCLUSIONS 174

6.1 Role of designer in emergent technology 174
6.2 Realized potentials of toolkit applications 175
6.3 Future potentials for toolkit applications 175
6.4 Research limitations 176
6.5 Potentials for future research 176
6.6 Conclusions 177

REFERENCES 179

LIST OF TABLES

Table 3.1 Commercial and academic case studies referenced for systematic discussion of digital fabrication of concrete (DFC) 70

Table 3.2 Parameter comparison for 3DCP, S3DCP and SPI 89

Table 4.1 All toolkit modules with identifier and short functional descriptions 97

Table 4.2 List of user inputs and their definitions for the Initial Conditions modules variable 106

Table 4.3 Cross-section organization 114

Table 4.4 User inputs for wall proportions 120

Table 4.5 User inputs for randomizing wall proportions 124

Table 4.6 Structural variables 132

Table 5.1 Soil volume, length, and height for each sub-piece within each wall 150

Table 5.2 Inputs for the formal variables for each iteration of the first series 152

Table 5.3 Definitions of dependent variables for structural analysis (output data) 153

Table 5.4 Definitions of dependent variables for printability analysis (output data) 153

Table 5.5 Definitions of dependent variables for material usage analysis (output data) 154

Table 5.6 Input and output data for iteration series with wall elevation multiplier as unfixed variable 154

Table 5.7 Input and output data for iteration series with wall width multiplier as unfixed variable 154

Table 5.8 Input and output data for iteration series with wall toe batter multiplier as unfixed variable. 155

Table 5.9 Input and output data for iteration series with wall front batter multiplier as unfixed variable. 155

LIST OF FIGURES

Figure 1.1 Example of digital fabrication in landscape architecture: Alexander Plaza, Mikyoung Kim Design 3

Figure 1.2 Precedent of 3D concrete printing applications in landscape architecture: 3D printed concrete in learning garden by Mississippi State University with Pikus3D, and 3D printed concrete park by Tsinghua University and AICT 3

Figure 1.3 Distinct agendas in digitally fabricated concrete, individualized designs that gain strength from their geometry and projects that focus on rapid production 4

Figure 2.1 Deposition-based manufacturing versus particle-based manufacturing 8

Figure 2.2 Diagram of different digital fabrication methods for concrete 9

Figure 2.3 3D Concrete Printing through extrusion of concrete (left), Spray-based "Shotcrete" 3D Concrete Printing through spraying of concrete (right) 11

Figure 2.4 Post-print processing of Spray-based "Shotcrete" 3D Concrete Printing 12

Figure 2.5 Injection 3D Concrete Printing in a limestone sand suspension: setup (left) and result (right) 12

Figure 2.6 Visualization of artificial reef module and printing setup: Module is printed in carrier bed and banded together into a slab. 13

Figure 2.7 Formwork fabricated by binder jetting sand for a material efficient slab 14

Figure 2.8 Selective cement activation where desired geometries are activated by precise application of cement to water, depowdering of final product 15

Figure 2.9 Selective paste intrusion where an aggregate layer has cement paste applied in areas to be hardened 16

Figure 2.10 KnitCandela, Mexico City, 2018, Product of KnitCrete flexible knitted textile formwork 17

Figure 2.11 Diagram of a foil-based robotic concrete casting setup and lab demonstration of roof section with a changing cross-section 18

Figure 2.12 Diagram of Smart Casting System by UTH Zurich Block group 20

Figure 2.13 Different geometry typologies demonstrated to date by UTH Zurich Block group.....21

Figure 2.14 Photograph of Cybe RC, diagram of the printing volume inside which the Cybe robot crawler can reach while printing concrete.....24

Figure 2.15 Single gantry frame printing setup (left) versus collaboration between multiple robots printing simultaneously (right).....26

Figure 2.16 Fabrication with partnering robots: a robot that builds the foundation, a robot that increases the wall height and a robot that refinishes the surface.....26

Figure 2.17 Various material supply strategies for in-situ mobile robotic concrete printing.....27

Figure 2.18 Tight bends and curvatures produced by a robotic arm 29

Figure 2.19 Tearing and texture issues with tight curvatures in 3DCP 29

Figure 2.20 Effects of machine turning radius on printable geometries, not to scale.....30

Figure 2.21 3D printed benches with gradual, loose curvatures with diagram of sectional design to meet turning radius requirement. 30

Figure 2.22 Printing bench on sloped base with a fixed nozzle orientation 32

Figure 2.23 Diagram of printing planes for a bridge module utilizing successive variable inclined printing planes 32

Figure 2.24 A typical robotic arm set up with incremental3D, printing modules for the Striatus bridge.....33

Figure 2.25 A robotic arm mounted within a gantry frame system 33

Figure 2.26 Overhang produced by a uniform layer angle versus a variable layer angle.....34

Figure 2.27 Nozzle movement and their effects on layer dimensions for S3DCP 35

Figure 2.28 Effects of layer height on fidelity of printed object to desired geometry.....36

Figure 2.29 Effects of minimum turning radius on fidelity of printed object to desired geometry 37

Figure 2.30 Effect of time delay after concrete mixing 39

Figure 2.31 Defects between printed layers built after initial setting time of concrete 40

Figure 2.32 Effects of water penetration on geometric fidelity 41
Figure 2.33 Effects of water penetration and particle size on geometric fidelity 41
Figure 2.34 Effects of water penetration and particle size on compressive strength 42
Figure 2.35 Levels of penetration of cement paste into aggregate bed 43
Figure 2.36 SPI with small scale particles 43
Figure 2.37 SPI with large scale particles 44
Figure 2.38 An example of mixing chambers for setting on demand 45
Figure 2.39 Examples of collaborative printing between two robots 47
Figure 2.40 In-Situ Fabricator using 3D laser scan to guide task 47
Figure 2.41 Real time height adjustment to accommodate ground plane deviations 48
Figure 2.42 Processes for robotic embankment undertaken by "HEAP", the robotic excavator 49
Figure 2.43 Trench detail from Tsinghua University's farmhouse prototype 50
Figure 3.1 Cross-sections of a wall design are evaluated for printability 55
Figure 3.2 Complex geometries require evaluation of serial sections throughout the wall. 56
Figure 3.3 Bibliographic statistics concerning extrusion-based 3D concrete printing with the disciplines of published articles and the project type 59
Figure 3.4 Diagram of research gaps that drive the study agenda 59
Figure 3.5 *Pulitzer Piece*, a sculpture inserted into the landscape to draw attention to the gentle terrain slope 61
Figure 3.6 Retaining wall variables identified for material reduction 63
Figure 3.7 Baseline scenario where wall dimensions are consistent irrespective of location within terrain 64
Figure 3.8 First scenario where wall width changes relative to location within terrain 65
Figure 3.9 Second scenario where wall batter changes relative to location within terrain 66
Figure 3.10 Third scenario where wall radii become more concave relative to location within terrain 67

Figure 3.11 Variations within one fabrication method 73

Figure 3.12 Various scales of products made by DFC 74

Figure 3.13 Levels of technology implementation 75

Figure 3.14 Production environments from factory conditions to in-situ printing 76

Figure 3.15 Diagram of DFC methods considered (listed from top to bottom): 3D Concrete Printing (3DCP), Spray-based 3D Concrete Printing (S3DCP), Injection-based 3D Concrete Printing (I3DCP), Selective Cement Activation (SCA) and Selective Paste Intrusion (SPI) 78

Figure 3.16 Range of geometric precision 79

Figure 3.17 Relative advantages of each digital concrete fabrication method considered 80

Figure 3.18 Examples of sloped surfaces in military experiments (precedent studies #8 and #9) with commercial example by CyBe Construction 82

Figure 3.19 Varying print volume forms 83

Figure 3.20 Examples of layer sizes and layer curvatures 85

Figure 3.21 High versus low curvature as an approximation for minimum feature size 85

Figure 3.22 Inclined plane printing strategies 86

Figure 3.23 Effect of time delays between layers 88

Figure 3.24 Initial considerations for a digitally fabricated concrete retaining wall 92

Figure 4.1 Zoomed out perspective of Grasshopper script 100

Figure 4.2 Drone point cloud model of existing conditions at MSU amphitheater 101

Figure 4.3 Preparations for input into the Grasshopper script; removal of existing retaining walls, a point grid projected onto the mesh, a reduced detail single surface approximating the existing terrain 102

Figure 4.4 Initial condition variables in the case of an unaltered terrain pre-construction 103

Figure 4.5 Initial condition variables determining attributes related to the base of the retaining wall and the splitting of the retaining wall into multiple segments 105

Figure 4.6 Major variables for terrain analysis modules 107

Figure 4.7 Conceptual considerations for sectional and volumetric approaches to terrain analysis and wall design 108

Figure 4.8 Creation of a terraced toe line and vertical wall seams in terrain analysis phase 110

Figure 4.9 Vertical and angled extrusions used to find the soil volume actively retained 111

Figure 4.10 Determination of soil volume actively retained 112

Figure 4.11 Subdivision of wall and soil 113

Figure 4.12 Generation of cross-section points for the wall segments 114

Figure 4.13 Matching process between soil sub-pieces and cross-sections 116

Figure 4.14 Diagram of variables determining wall proportions 118

Figure 4.15 Process for setting top of wall elevation 119

Figure 4.16 Generation of wall proportions by perpendicular vectors 121

Figure 4.17 Translation of randomly chosen cross-section points 123

Figure 4.18 Creation of sloped lines that describe the final wall form and adjustment process to match geometries between wall segments 125

Figure 4.19 Closed cross-section polylines that create the solid geometries 126

Figure 4.20 Lateral pressure and wall weight definition 127

Figure 4.21 Resultant force definition 128

Figure 4.22 Definition of overturning, crushing, and sliding risk. 129

Figure 4.23 Variables describing the wall base for structural evaluation 130

Figure 4.24 Volume variables for structural calculations 131

Figure 4.25 Diagram of process for finding weighted center of gravity 134

Figure 4.26 Preparations for resultant force calculations 134

Figure 4.27 Resultant force variables 136

Figure 4.28 Relationship of surface normal vectors, angle from vertical and angle from XY plane 141

Figure 4.29 Live feedback on printability issues during design process 142

Figure 4.30 Iterative design of station points for printer 143

Figure 4.31 Remote Control Panel interface.....144

Figure 5.1 Front view of Mississippi State Univ. amphitheater with long linear wall framing stage 147

Figure 5.2 Side walls and path of Mississippi State Univ. amphitheater 148

Figure 5.3 Footprint of existing walls (yellow) versus altered wall corners 149

Figure 5.4 Wall forms with wall elevation multiplier as unfixed variable (Sub-pieces with structural risks are depicted in red.) 156

Figure 5.5 Wall width multiplier as unfixed variable (Sub-pieces with structural risks are depicted in red.) 157

Figure 5.6 Wall toe batter multiplier as unfixed variable (Sub-pieces with structural risks are depicted in red.).....158

Figure 5.7 Wall front batter multiplier as unfixed variable (Sub-pieces with structural risks are depicted in red.).....159

Figure 5.8 Design stages for iteration 1, which begins with no pre-determined agenda.....164

Figure 5.9 Design for iteration 1, which begins with no pre-determined agenda.....165

Figure 5.10 Design stages for iteration 2, which begins with successful wall proportions found in the first series 166

Figure 5.11 Design for iteration 2, which begins with successful wall proportions found in the first series.....167

Figure 5.12 Initial design stages for iteration 3, which is based on manipulations of the front batter 168

Figure 5.13 Design for iteration 3, which is based on manipulations of the front batter 169

Figure 5.14 Design stages for iteration 4, which alters the level of detail of iteration 3 170

Figure 5.15 Design for iteration 4, which alters the level of detail of iteration 3.....171

Figure 5.16 Challenging geometries across the second series of wall iterations.....172

CHAPTER I

INTRODUCTION

1.1 Project Overview

This study consists of two parts. The first part involves assessing and identifying the most suitable digitally fabricated concrete (DFC) machine for constructing retaining walls on-site. The second part focuses on developing an interactive design environment that utilizes DFC to create retaining wall designs that respond to the terrain. The toolkit developed in the second study is specifically designed for the construction of unreinforced retaining walls using extrusion-based 3D concrete printing. The studies aim to address implementation challenges faced by designers working with DFC and demonstrate the potential benefits of DFC in the field of landscape architecture. The outcome of the second study is a prototype that helps overcome challenges in implementing DFC and provides a demonstration of the potential value of DFC in landscape architecture.

1.2 Research Context

Digital fabrication is often referred to as the fourth industrial revolution, which emphasizes the production of individualized products with rapid efficiency. While digital fabrication has found its place in the landscape architecture profession, particularly in the works of Mikyoung Kim (Figure 1.1), the application of DFC in the field has not been thoroughly explored. Figure 1.1 depicts a stone bench created by CNC milling of stone, a subtractive process. There is potential for the profession to adapt additive manufacturing processes.

Currently, landscape architecture primarily utilizes DFC for site furniture, such as benches and planters However, one notable exception is the Tsinghua University's 3D printed park in Shenzhen, China (Figure 1.2). 3D concrete printing is used to create paving, walls and sculptures for the park. Despite a limited number of existing precedents in landscape architecture, there are clear advantages of using DFC that could significantly impact the profession.

Architecture, engineering, and construction have made more significant advancement in DFC. These applications have focused on two major objectives. The first is facilitating individualized and highly complex geometries. Aside from aesthetic considerations, this has been widely applied in structural applications to reduce material consumption through efficient and complex geometries. The second motivator behind DFC applications have prioritized reducing labor, waste, and decreasing construction timelines, while also increasing automation in the construction industry (Figure 1.3).

One main goal of this study is to evaluate the existing applications and agendas of DFC for its applicability to landscape architecture. This includes evaluating its suitability for in-situ robotic construction, providing individualized design freedoms, and enabling structurally expressive design. Similarly, while there is a gap in landscape applications for DFC, there is also a gap in research. Most of the existing DFC research focuses on the material science and engineering aspects of the technology, with limited studies addressing design and construction challenges specific to landscape architecture. This study seeks to explore the role of designers in relationship to the development of emerging technologies, with a focus on developing design-oriented tools that manage the complexities of fabrication. Additionally, it explores how material properties and structural agendas contribute to the creation of a cohesive design language.

Figure 1.1 Example of digital fabrication in landscape architecture: Alexander Plaza, Mikyoung Kim Design

(*The Alexander Plaza | Mikyoung Kim Design*, n.d.)

Figure 1.2 Precedent of 3D concrete printing applications in landscape architecture: 3D printed concrete in learning garden by Mississippi State University with Pikus3D, and 3D printed concrete park by Tsinghua University and AICT

Left photo by Cory Gallo, (The First Park to Be Built Using 3D Printing Is in China - 3Dnatives, n.d.)

Figure 1.3 Distinct agendas in digitally fabricated concrete, individualized designs that gain strength from their geometry and projects that focus on rapid production

(Bhooshan et al. 2022, Xu et, al 2022)

This study builds upon the research completed in 2021 by Setareh Baniasadi titled, “The potential of 3D Concrete Printing technology in Landscape Architecture”. It also draws insights from a design-build project that utilized DFC for the Galloway Elementary learning garden and was completed by Mississippi State University in 2020 (Figure 1.2).

The precedent study and the previous experiences with DFC helped identify major implementation challenges faced by designers These challenges were further confirmed in the literature review. As a result, these identified challenges formed the basis for the research objectives.

1.3 Research Objectives

To aid designers in adopting DFC, this study explores the use of parametric scripting to create design tools for terrain responsive retaining walls. This entails the following objectives:

1. Translate the findings from the literature review on engineering and material science research into a framework that outlines the key considerations for designers when working with DFC

2. Conduct a comprehensive review of literature and precedent case studies to develop a systematic approach for selecting the fabrication system most suitable for a terrain responsive retaining wall

3. Create an interactive design environment using parametric scripting to assist non-expert designers in understanding and working with the fabrication limitations associated with deposition-based DFC. This interactive environment should integrate structural and material considerations to guide the design process effectively

4. Provide demonstrations of possible DFC applications to speculate on its value of the technology and potential contributions to the field of landscape architecture

1.4 Study organization

This thesis is organized by a literature review, problem statement, methodology, results and discussions, and conclusions. In Chapter II, the literature review utilizes existing literature to translate material and physical properties into design parameters relevant to the processes for DFC construction. Fabrication parameters, processes, and designer challenges are translated into a problem statement in Chapter III. The problem statement justifies three major objectives: the rationale for an 3D printed gravity wall, the focus on structurally expressive design, and the motivations for a fluid exploratory design process. In Chapter IV, the toolkit modules and calculations are described, including terrain analysis, form generation, structural analysis, and fabrication analysis. The Mississippi State University amphitheater is used as a test case application in Chapter V. This chapter documents material usages, structural evaluations, printability issues, and designer experiences that emerged during the use of the toolkit. In Chapter VI, the developed toolkit is used to discuss the values of exploratory design environments for digital fabrication as well as describe the potential values of DFC for terrain responsive design.

CHAPTER II

LITERATURE REVIEW

Digitally fabricated concrete (DFC) spans numerous fabrication methods, each with its own specific advantages and limitations. One particular method, 3D concrete printing has demonstrated successful implementation in real-world scenarios, such as single-family houses (Xu et al., 2022) and pedestrian bridges (Bhooshan et al., 2022). Existing research has also been conducted to measure the readiness of 3D concrete printing for real world applications (Ma et al., 2022).

To provide a comprehensive understanding of DFC, the following sections explore different DFC processes along with their mechanical and material limitations. This overview is supplemented with a discussion of factors and processes for in-situ concrete printing and robotic construction of terrain. By examining mechanics, material properties, and on-site fabrication, the study establishes a basis for a comparative selection process in Chapter III. This process aids in determining the most suitable fabrication method for terrain structures.

2.1 Overview of digital fabrication systems for concrete

DFC has been demonstrated by numerous research groups worldwide. However, with the diversity of fabrication methods being pursued, there is a strong need for a shared vocabulary to describe processes. A classification system is a necessary precursor for understanding the mechanics of the various fabrication systems and for judging the merits and limitations of each

system. Since 2012, there has been progress in proposing DFC process classification frameworks (Buswell et al., 2020).

More recent frameworks provide a two-prong process classification system for digital fabrication with concrete. DFC systems can be classified into two broad categories: deposition-based systems, such as 3D concrete printing (3DCP), and particle-based systems, such as selective cement activation. This distinction is based on whether the fabrication system utilizes layers of extruded wet cement or layers of dry particles selectively bound together, compared in Figure 2.1. However, these classification systems neglect to include digital fabrication methods that utilize digitally controlled or fabricated formwork.

In addition to deposition-based and particle-based systems, there is a third typology that involves formwork-based concrete fabrication. These three typologies-formwork-based, deposition-based, and particle bed-based- share similar advantages that are worth considering within the context of site-specific landscape structures. Figure 2.2 provides examples of each typology. All three typologies create a physical clone of a digital 3D computer model through robotic and mechanic systems, while minimizing physical human labor and material waste.

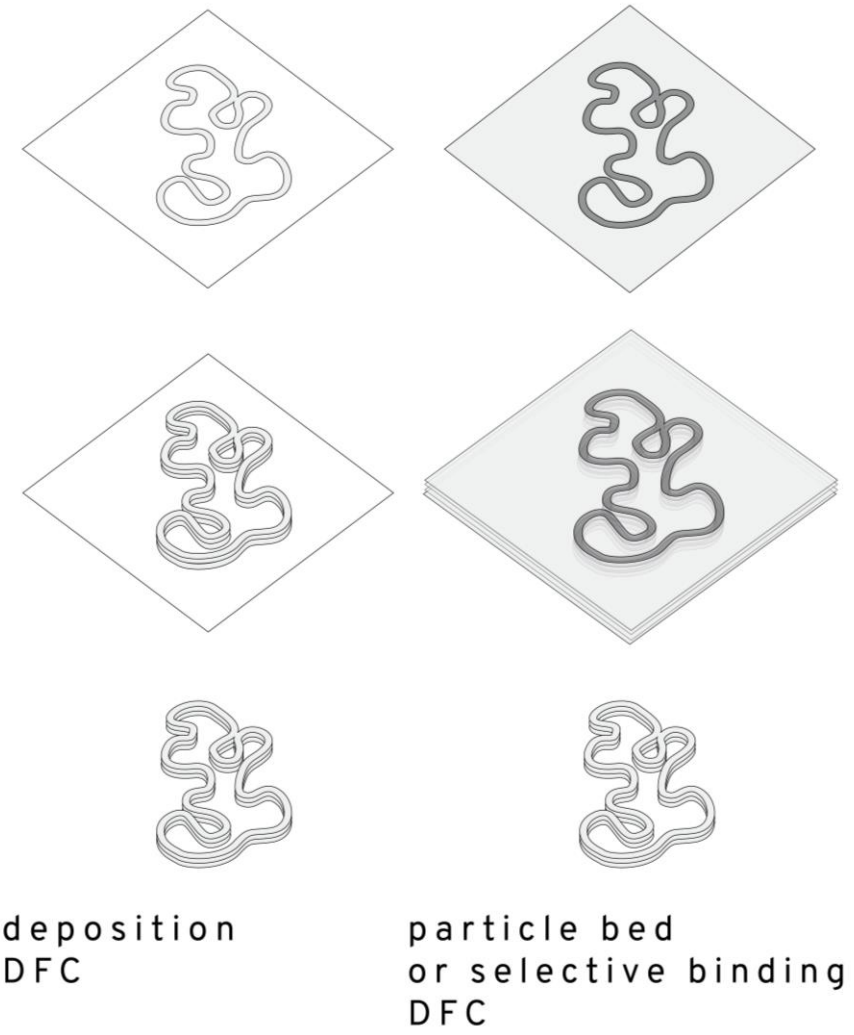

Figure 2.1 Deposition-based manufacturing versus particle-based manufacturing

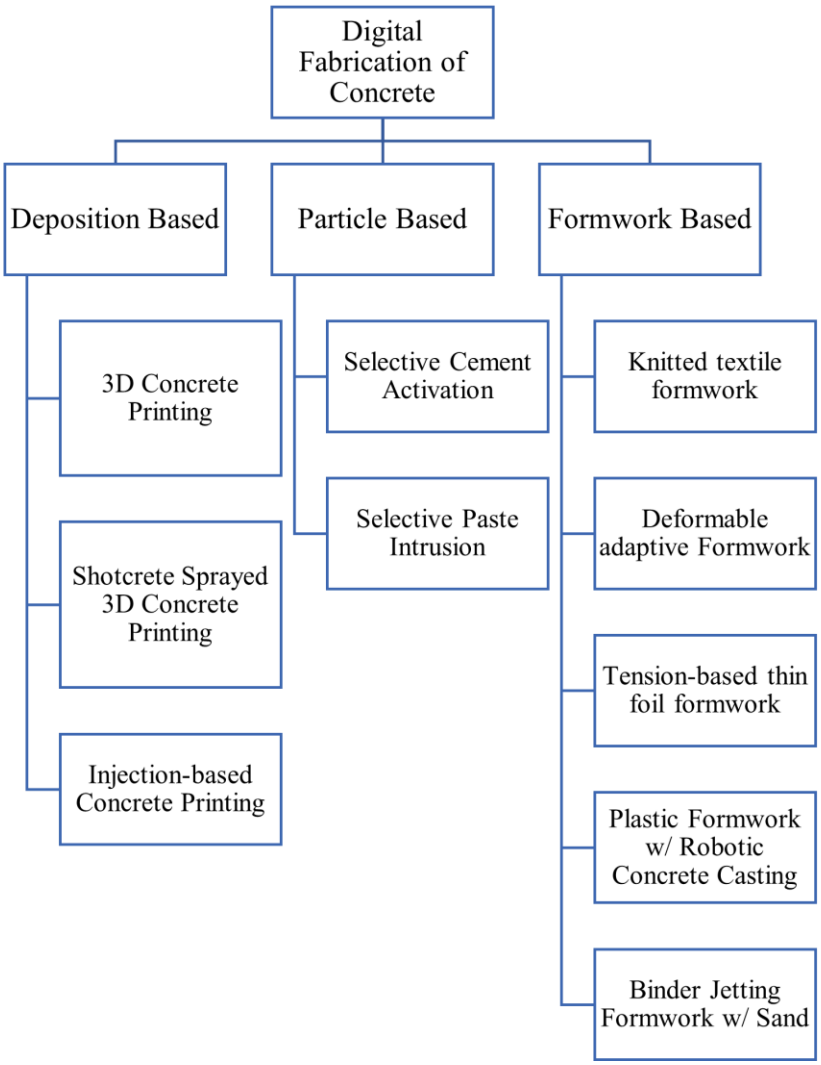

Figure 2.2 Diagram of different digital fabrication methods for concrete

DFC without formwork is heavily researched with prevalent case studies and demonstrative real-world applications, particularly in the context of 3DCP. This process depends on the successive layering of material to construct a three-dimensional object. Deposition-based systems are one example of DFC without formwork. These systems involve the layering of pre-mixed wet concrete through extrusion, pressurized spraying, or injection into a media bed. Particle bed systems are another example of DFC without formwork. These systems involve the

layering of dry materials and selectively wet, activate, or cement certain areas to build up a 3D shape through successive layers. These two classifications are generally referred to as additive manufacturing of concrete due to the substitution of form filling with additive layering of material (Kloft et al., 2021a).

2.1.1 Deposition-based systems

Extrusion-based 3DCP uses the pumping to extrude concrete through a nozzle to form consecutive layers, as shown in Figure 2.3. The hydration of concrete is controlled to ensure rapid curing, allowing the printer layers to quickly develop self-supporting strength and provide a stable base for subsequent wet layers. This rapid curing affects the range of geometries that can be printed. Extrusion-based 3DCP generally describes a continuous spiral of extruded concrete, where each layer is supported by the previous layer, causing openings or cantilevers to be challenging to produce. The rapid hardening of the concrete in 3DCP causes challenges with cold joint formation, reinforcement integration, and surface post-processing. Unlike other DFC methods that allow for reinforcement placement before printing or during, extrusion-based 3DCP typically uses the printed concrete as a permanent formwork into which more concrete with reinforcement is cast. However, there have been demonstrations of reinforcement integration during printing using fiber reinforcement and interlayer steel reinforcement (Asprone et al., 2018; Kloft, Empelmann, et al., 2020; Mechtcherine et al., 2021).

Spray-based “Shotcrete” 3D Concrete Printing (S3DCP) utilizes robotic systems to apply pressurized sprayed concrete in controlled layers, as shown in Figure 2.3. Shotcrete systems can accommodate a prepared base onto which material is sprayed, such as metal reinforcement or another building part. In some cases, shotcrete systems have been used in conjunction with

robotically placed reinforcement (Freund & Lowke, 2022). S3DCP also allows for a longer curing time for further processing of the finished surface (Hack & Kloft, 2020).

The extrusion and sprayed methods of 3DCP and S3DCP produce continuous surfaces without openings, limiting their suitability for creating structures with voids. In contrast, injection-based 3D Concrete Printing (I3DCP) involves the use of a carrier medium into which concrete can be injected in freeform, open geometries. The carrier medium supports the concrete until curing strength is achieved, as depicted in Figure 2.4. This method allows for the creation of porous lightweight designs that would not be self-supporting until hardened. I3DCP is among the newest fabrication methods in the field of 3DCP with ongoing research challenges related to surface quality, reinforcement, and material strength (Hack et al., 2020). Currently, injection printing has limited technology readiness, with applications currently limited to laboratory proof-of-concepts (Figure 2.5). However, it has been the subject of speculative applications such as the creation of artificial reef structures (Figure 2.6).

Figure 2.3 3D Concrete Printing through extrusion of concrete (left), Spray-based “Shotcrete” 3D Concrete Printing through spraying of concrete (right)

(Hack & Kloft, 2020; Kloft et al., 2021b)

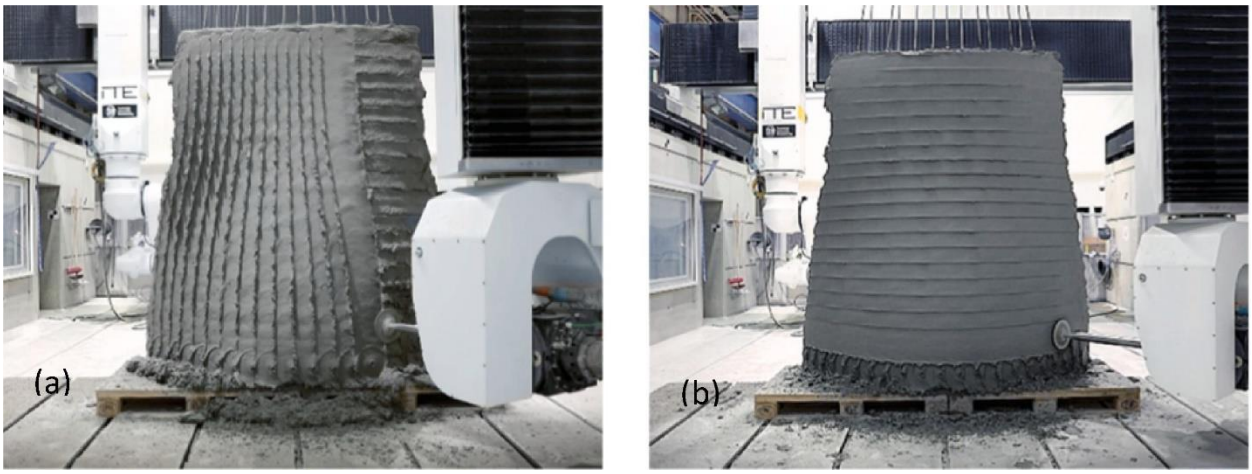

Figure 2.4 Post-print processing of Spray-based “Shotcrete” 3D Concrete Printing

(Hack & Kloft, 2020)

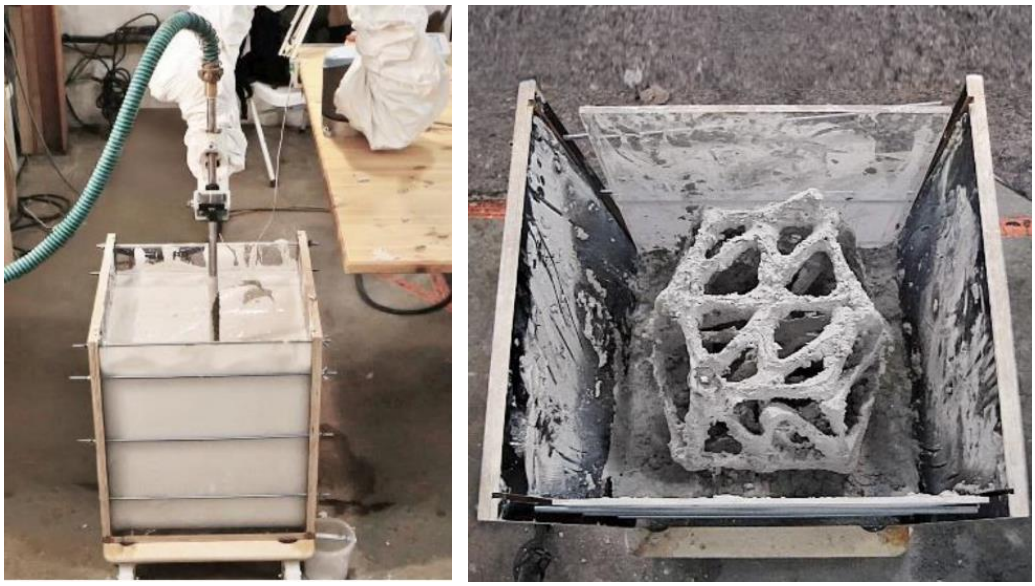

Figure 2.5 Injection 3D Concrete Printing in a limestone sand suspension: setup (left) and result (right)

(Hack et al., 2020)

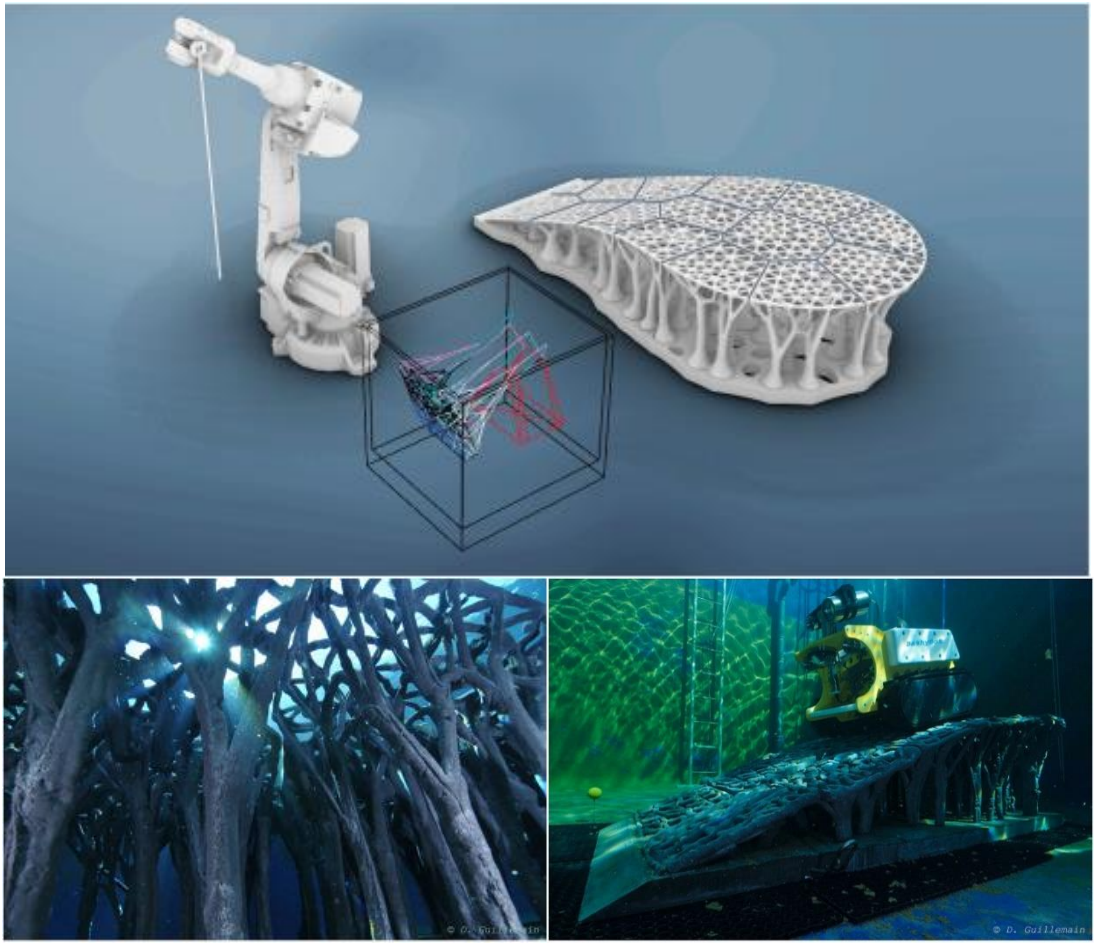

Figure 2.6 Visualization of artificial reef module and printing setup: Module is printed in carrier bed and banded together into a slab.

(image credits: D. Guillemain, Vicat, Soliquid, Tangram Architects, MIO, CRNS), (Lowke et al., 2021)

The last DFC formwork system to note is the use of sand binder jetting. Sand binder jetting, which is widely adopted for metal casting, has also been demonstrated as stay-in-place formwork for concrete casting. This method was demonstrated through a smart slab prototype (Figure 2.7). The composite of concrete and sand formwork allows for higher compressive strengths through ultra-high performance fiber reinforcement concrete. However, the process of filling the sand printed formwork has geometric limitations, due to the need to remove excess

sand. Likewise, the filling of concrete is limited to channels larger than 20 mm and bending radii of 10 mm (Meibodi et al., 2019). Similar processes have been documented with the use of clay formwork filled with concrete (Dielemans et al., 2022).

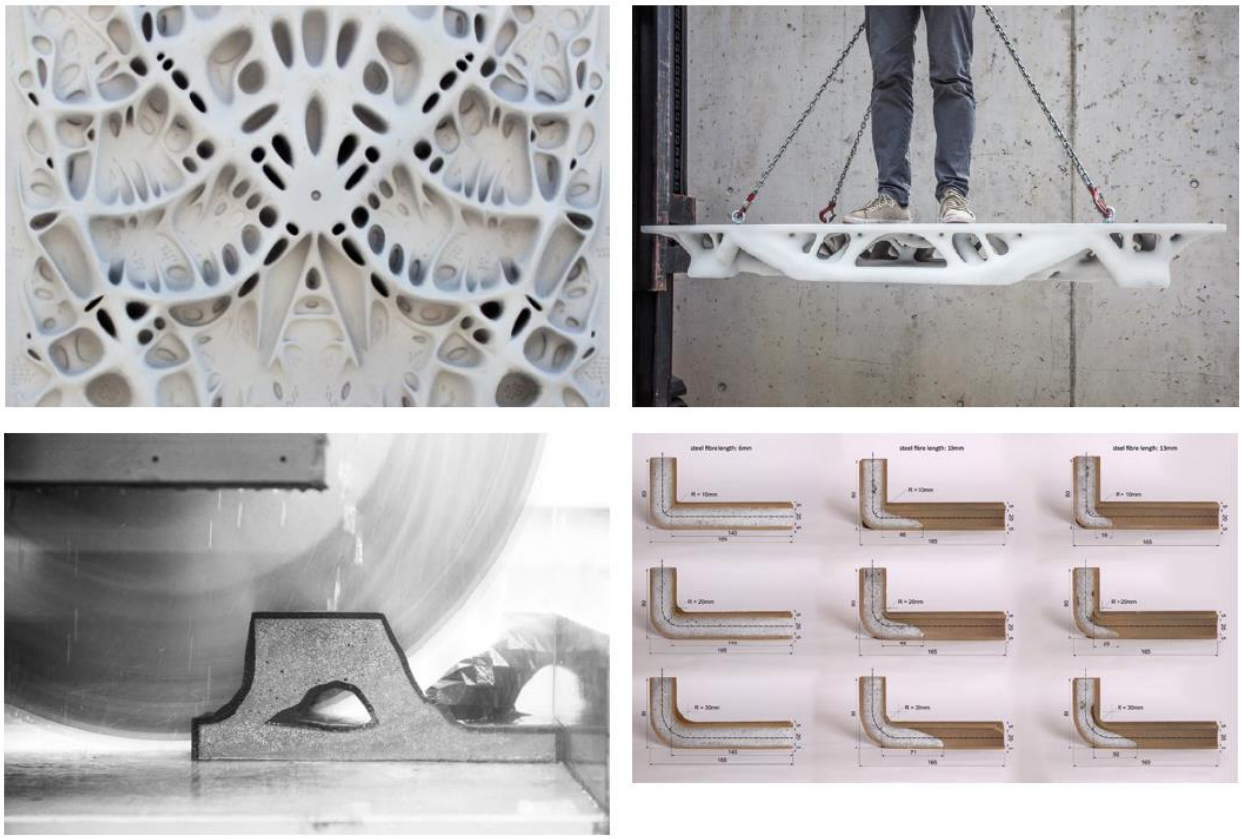

Figure 2.7 Formwork fabricated by binder jetting sand for a material efficient slab (Meibodi et al., 2019)

2.1.2 Particle bed-based systems

Particle bed-based systems in DFC are distinct from deposition-based DFC in their use of layered dry materials to form 3D geometries. Instead of extruding wet concrete or spraying it onto a surface, particle bed-based systems involve the mechanically layering of dry materials, with areas that are selectively activated or cemented to form a 2D shape with each layer. There

are two common approaches within particle bed-based systems: selective cement activation and selective paste intrusion. Selective cement activation is the use of layers of cement that have water applied to desired areas to activate the cement (Figure 2.8). Selective paste intrusion relies on a layer of aggregate into which cement paste is precisely inserted to bind the intended geometries (Figure 2.9). By stacking successive layers of these 2D shapes vertically, the final 3D form is created (Lowke et al., 2018).

Figure 2.8 Selective cement activation where desired geometries are activated by precise application of cement to water, depowdering of final product

(*Project A 01 - Additive Manufacturing in Construction TRR277*, n.d.)

Figure 2.9 Selective paste intrusion where an aggregate layer has cement paste applied in areas to be hardened

(*Project A 02 - Additive Manufacturing in Construction TRR277*, n.d.)

2.1.3 Formwork-based systems

One of the advantages of DFC is the potential reduction or total elimination of traditional formwork. With 3DCP, concrete is extruded and hardens in its final form without any formwork. However, formwork-based systems can still minimize waste and labor while producing highly individualized geometries. Formwork-based systems in DFC follow two strategies, either a smart adaptive formwork that is reused across changing designs or a minimal lightweight machine-fabricated formwork for a single complex design. Other formwork-based systems use digital fabrication to manufacture a thin lightweight formwork for a single design, such as the KnitCrete technology by UTH Zurich Block Group. The KnitCrete system uses standard industrial knitting machines to knit a textile formwork from a 3D model. The knitting pattern is generated automatically from a digital model, an algorithmic approach that vastly reduces effort for complex geometries (Popescu et al., 2018). This knitted textile formwork reduces physical labor by eliminating the need for welding, gluing, or sewing typically associated with fabric formworks for concrete (Rippmann et al., 2016). This textile is tensioned and primed in the final intended location of the concrete. The concrete is cast into the textile which can remain in place

permanently for aesthetic benefits (Popescu et al., 2021). The KnitCrete system produces “an ultra-lightweight knitted formwork that was carried from Switzerland to Mexico in a suitcase” (*Block Research Group*, n.d.). KnitCrete produces a single-use formwork specific to a single design. An example of this system is the KnitCandela, illustrated in (Figure 2.10). The technology still achieves labor reductions in a fully machine fabricated formwork with lightweight materials that do not incur transport costs. Further research could establish fabric formworks with integrated reinforcement for irregular concrete geometries, enhancing the structural performance and design possibilities of DFC (Rippmann et al., 2016).

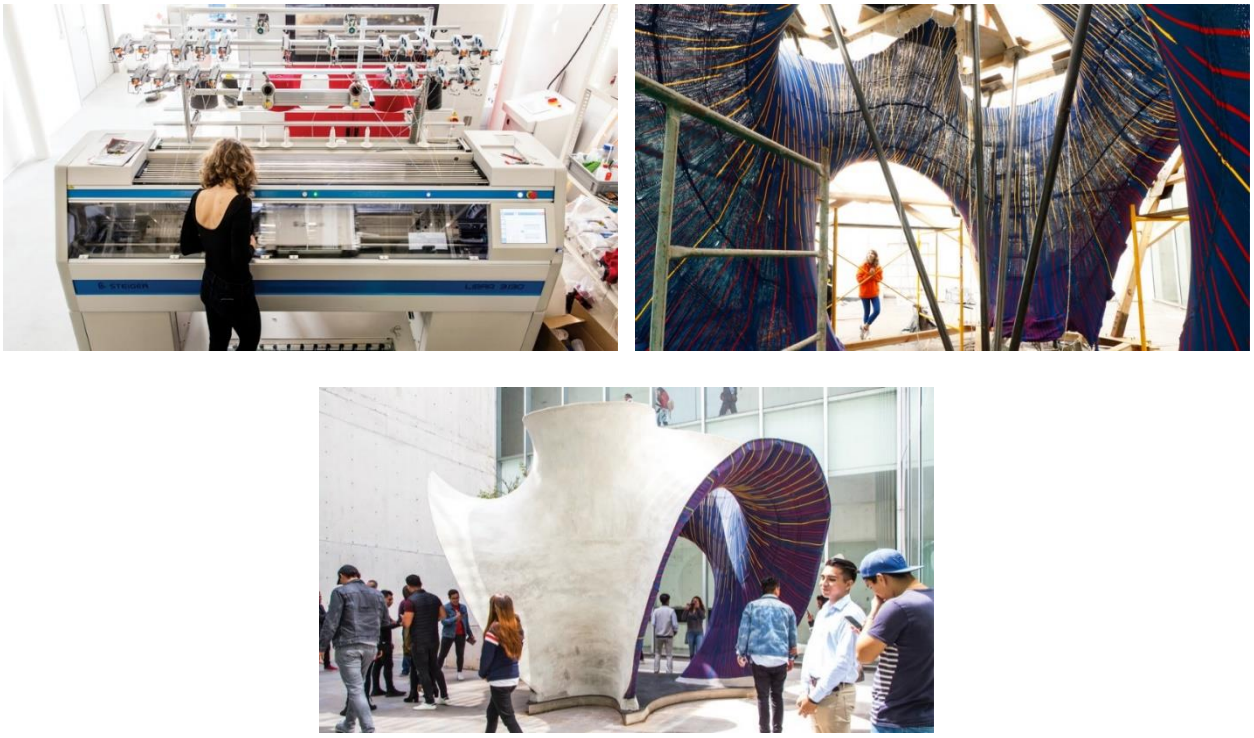

Figure 2.10 KnitCandela, Mexico City, 2018, Product of KnitCrete flexible knitted textile formwork

Left: Knitting machine that produces the formwork, Right: Formwork suspended pre-casting, Bottom: Final product after casting (*KnitCandela - A Flexibly Formed Thin Concrete Shell at MUAC, Mexico City, 2018*, n.d.; Popescu et al., 2021)

Another branch of DFC through formwork is the use of tensioned weak materials as formwork that is pulled into the desired shape using mechanical or robotic means. This method takes advantage of precise set-on demand hydration of concrete, allowing for the use of weak and thin materials such as foil sheets as formwork. These materials are pulled into tension with concrete poured rapidly at the vertical rate of 2.5 meters per hour (8.2 feet per hour). The tensioned foil concrete casting has been only demonstrated in a laboratory environment at UTH Zurich with their In-Tense formwork research (Figure 2.11). However, the foil systems have the potentials to be one of the least expensive methods with possibilities of accessible and recyclable materials (Lloret-Fritschi et al., 2020).

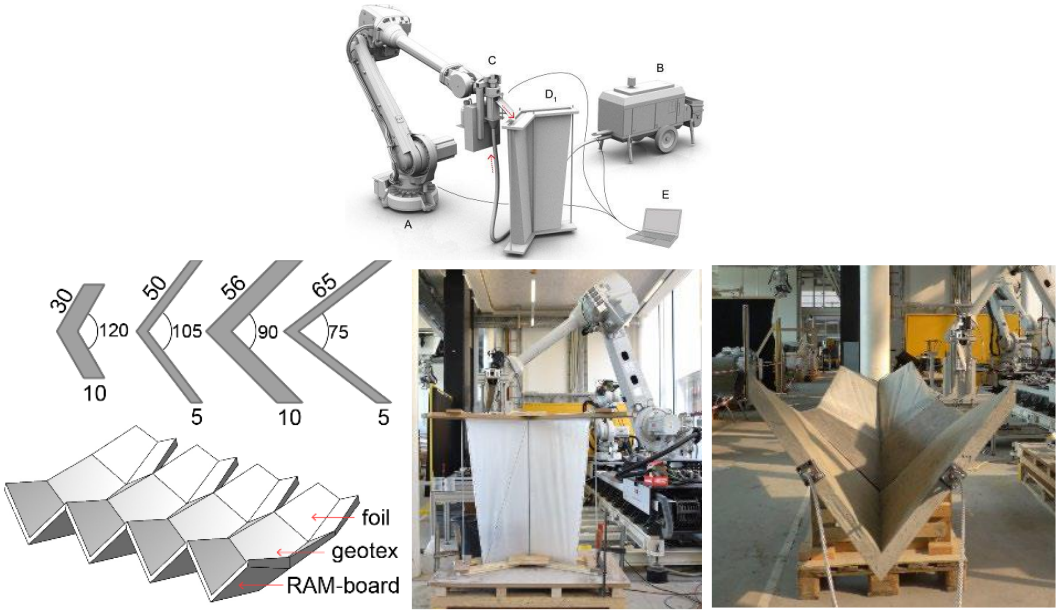

Figure 2.11 Diagram of a foil-based robotic concrete casting setup and lab demonstration of roof section with a changing cross-section

(Lloret-Fritschi et al., 2020)

Instead of using single-use formworks, another approach to digital fabrication of concrete involves the use of adaptive formworks that continuously reshape throughout a single design and

across multiple designs. These adaptive formworks use robotics and other mechanics to pull and manipulate flexible materials into a shape-shifting formwork (Figure 2.12). UTH Zurich Block group describes these technologies as “Smart Casting Systems” (Lloret-Fritschi et al., 2020). These smart, flexible, reusable formworks depend on the precise control of the hydration and setting of concrete. The systems harden concrete on-demand, removing the pressure the concrete would impose on the weak and flexible formwork. This precise control of the setting of concrete is a recent innovation that enables these new digital fabrication systems. One such system is based on the slip-form processes commonly used in traditional concrete construction. In traditional slip forming, a single formwork is pulled vertically as concrete is continuously casted into the form. Slipforms are used for vertical continuous elements such as elevator shafts. In Smart Dynamic Casting systems, a sheet metal cross section is robotically pushed and deformed to form varying cross-sections as the concrete is being cast. Current variations of this slipform system are based on column, wall, and folded V shapes (Figure 2.13). While the geometry types demonstrated are currently limited, there is potential for a wide range of outputs within these geometry types. For example, the experimenters created a canoe using a changing V cross-section (Lloret-Fritschi et al., 2020).

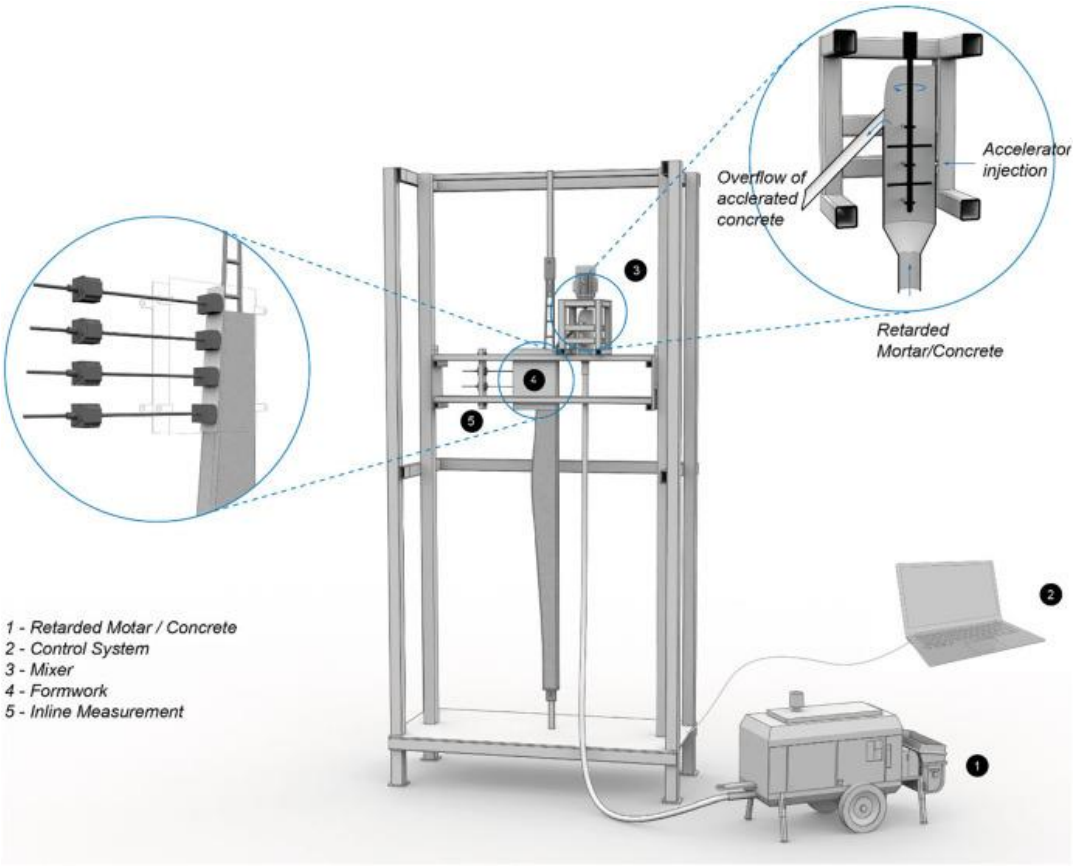

Figure 2.12 Diagram of Smart Casting System by UTH Zurich Block group

On the left, formwork is depressed in multiple points to reshape the cross-section area for a "global deformation" with a large cross section geometry change. Other variations of digital slipform deform only at the concrete exit point of the formwork for a small cross section change as a "local deformation" (Lloret-Fritschi et al., 2020)

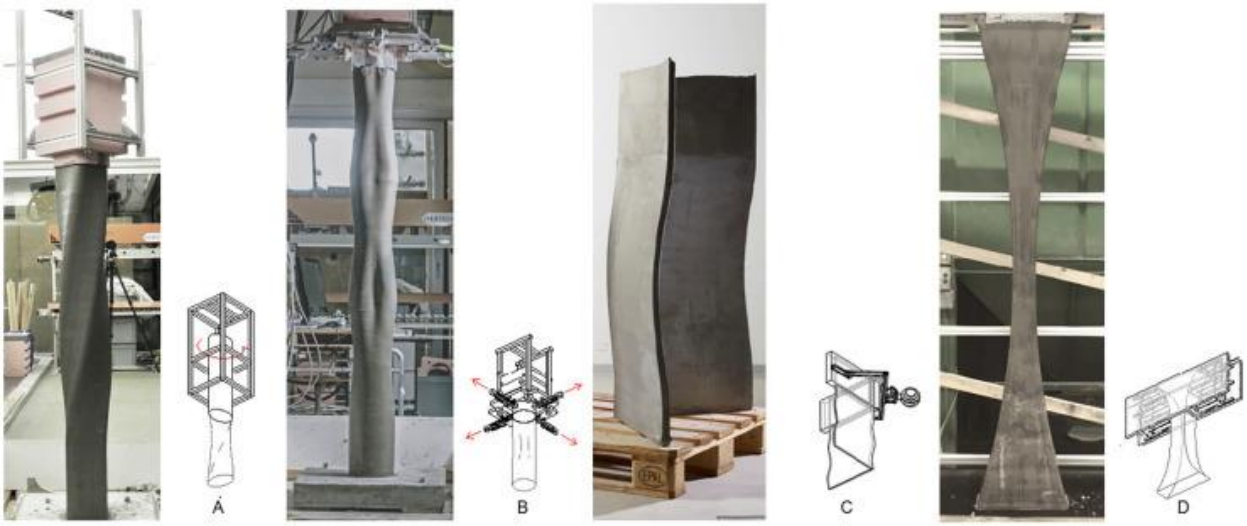

Figure 2.13 Different geometry typologies demonstrated to date by UTH Zurich Block group

From left to right, rigid ellipsoidal formwork, flexible formwork, thin folded formwork, globally deformed formwork with significant cross-section changes (Lloret-Fritschi et al., 2020)

Formwork-based systems in DFC can reduce labor and material waste through three innovative reconsiderations of concrete formwork:

1. Lightweight formwork that remains permanently in place with added value to the final concrete product
2. Lightweight, disposable, and recyclable formworks that rely on precise chemical hydration of concrete: Formwork can be fragile and malleable instead of rigid bulky formwork that resists pressure from concrete.
3. Adaptive formworks that are not spent with a single design: Formwork can be continuously reusable for new designs.

These formwork-based DFC technologies can achieve individualized, one-off designs or simple repetitive designs without increasing cost or time. With typical construction methods, labor and time costs are at a premium. Moreover, formwork can typically cost up to 50% of the overall construction cost or up to 90% for non-standard formwork (Lloret-Fritschi et al., 2020; Schipper & Grünewald, 2014). In the previous demonstrated projects such as the KnitCandela, concrete use was reduced through elaborate thin but strong geometries where material is used only where

structurally necessary. With reductions of concrete, formwork waste, labor and transportation costs, formwork-based DFC could have positive environmental impacts alongside liberative design geometries.

2.2 Process Factors for DFC

Additive manufacturing processes, such as DFC, are defined by a complex system of parameters between the mechanical systems, material properties, structural requirements, and the context (Dörfler et al., 2022). A prerequisite for designing for DFC is a thorough understanding of process factors and their limitations. These factors define the range of printable geometries as well as identify unachievable geometric characteristics. These process factors can derive from the physical properties of the mechanical system or the material properties of the concrete mix design(Dörfler et al., 2022). These physical factors are supplemented with an understanding of the operating processes and factors from the perspective of manufacturer or machine operator. Mechanical, material, and operational factors often overlap and can be indistinguishable during production. This elementary categorization is only used for the sake of clarity, to lend structure to a diverse range of considerations.

2.2.1 Mechanical factors for DFC

Digital fabrication systems for concrete have diverse ranges of abilities and limitations based on their unique mechanical systems. The mechanical factors include the ranges of mobility within a fabrication system (Dörfler et al., 2022). Likewise, in the absence of formwork, it is crucial to account for the effects of gravity on the wet concrete in DFC. The adaptations and advantages for mobility and gravity factors vary broadly across DFC technologies. In particle

bed systems, mechanical issues tend to recede where material issues predominate. The following mechanical factors pertain mostly to deposition systems.

2.2.1.1 Large-scale mobility factors

Large-scale mobility describes the movement capabilities of the entire machine, such as how far a machine can reach and print. Large-scale mobility factors can also describe the ability to maneuver through the site. Small-scale mobility is the ability of the mechanical system to make fine-grained movements during the application of concrete. This includes feasible nozzle movements and the resulting constructible geometric characteristics. An analogous comparison would be the overlapping movement potential of the human body, where the arm can position the hand within reach, and the hand and fingers can move in specific directions to perform tasks like writing. Similarly, in DFC systems, there are separate but interconnected ranges of movement at both large and small scales. The primary large-scale mobility factors addressed in this chapter are (1) print volume, (2) workspace, and (3) material delivery limitations. Small-scale mobility factors described below include (1) changes in direction and (2) changes in printing plane (Dörfler et al., 2022).

The initial consideration for large-scale mobility is the print volume, also referred to as build volume or machine reach. A print volume describes the volume of space the concrete printer can reach without stopping and resetting its operations. Outside this volume, the printer would have to start a new and separate printed piece to continue fabricating a design larger than its print volume. For example, in Figure 2.1, the CyBe concrete printing robot crawler has a donut-shaped print volume around the robot.

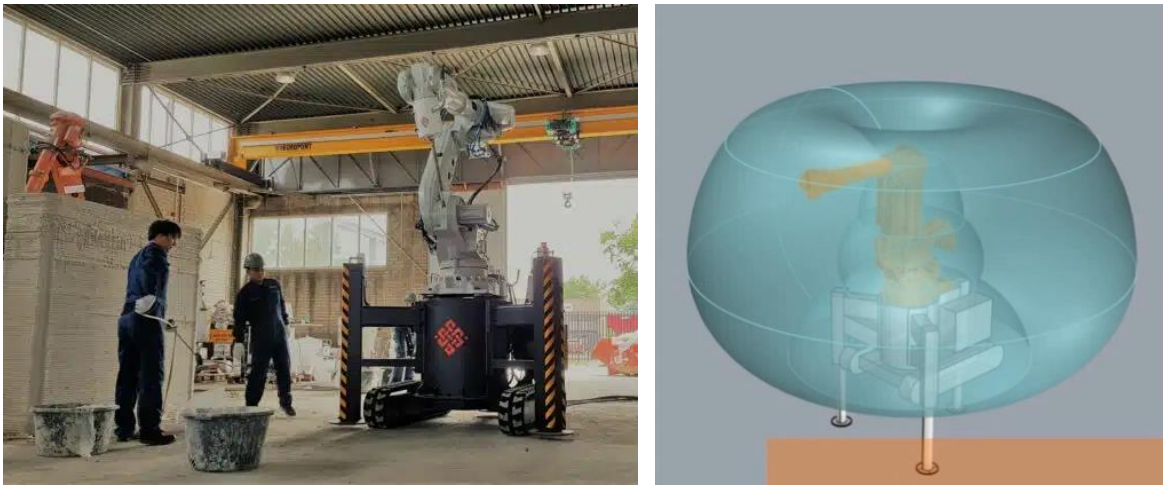

Figure 2.14 Photograph of Cybe RC, diagram of the printing volume inside which the Cybe robot crawler can reach while printing concrete

(CyBe Construction, 2022; *CyBe RC (Robot Crawler) — CyBe Construction*, n.d.)

The relationship between scale and mobility in mobile additive manufacturing has been previously studied through a review of precedent technologies by Dörfler et al., 2022. This research investigated the relationship between the mobility of the machine and the scale of its production, from which the following concepts are adopted. An individual printing system has a defined print volume, which refers to the designated workspace where the printing process occurs. In the case of a single frame-based printing system, it can only print within the boundaries of its frame before needing to be disassembled or otherwise relocated to work in new areas. However, a collection of cooperative mobile robots have small printing volumes and limited individual workspaces but gain the freedom of large collective working area as described in Figure 2.15. When multiple simultaneous on-site actors are involved, the technological and operational complexity increases compared to a single stationary system, which is discussed in more detail later in this chapter. The working area can be further expanded by systems that print continuously while in motion, such as the MiniBuilders by IIIAC (Dörfler et al., 2022). The

system utilizes a series of distinct mobile robots that operate as sequential stages within the construction of one printed object (*Minibuilders - Institute for Advanced Architecture of Cataloni*, n.d.). The process begins with the Base Robot, which drives on the ground and prints the first ten foundational layers. Subsequently, the Grip Robot climbs onto the structure and begins to print and continuously drives along the perimeter, building up the vertical shell of the print. Lastly, the Vacuum Robot uses vacuum suction to attach to the previously printed surface and deposits more material. In this setup, a large structure is produced by relatively small robots. Likewise, the print volume is infinitely expandable if the robots can continuously climb the structure they produce.

When considering the workspace for DFC, the delivery method of the material is an additional limitation and can impact where the machine can print (Dörfler et al., 2022). Possible means for delivering concrete to the machine include: a tethered connection between the machine and the concrete mixer, an on-board tank for storing pre-mixed concrete, or an on-board concrete mixer with the robot carrying a limited amount of raw material as it prints. Each of these methods can have its own limitations on production volume and workspace for the robot, such as a limited length of tethering, a limited time frame to use up premixed concrete, or a limited volume of material. Previous research has made a comparison of these material delivery methods, as depicted in Figure 2.17.

The mobility of a DFC system greatly influences design possibilities and operations on construction sites. The machine print volume determines the need for splicing a larger design into printable parts. Moreover, the movement of a printing system across a site creates novel challenges for construction planning. A mobile system also relies on increased technological sophistication in both the machine and its operators.

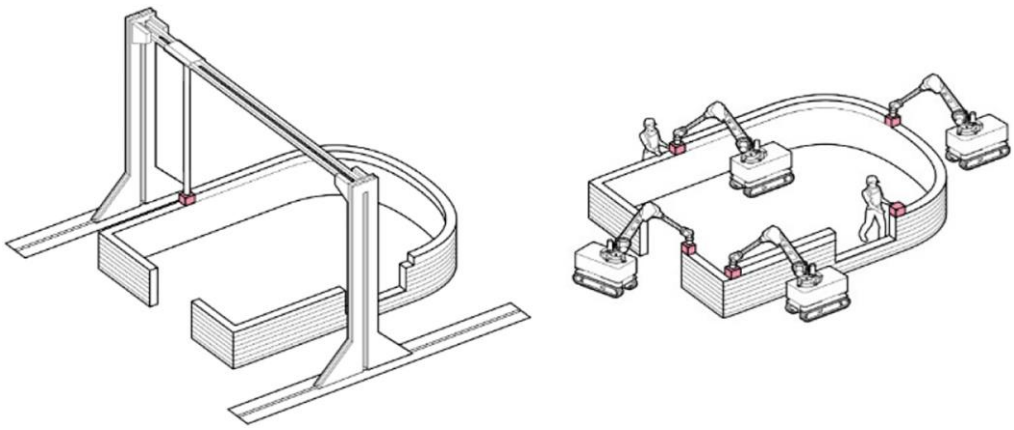

Figure 2.15 Single gantry frame printing setup (left) versus collaboration between multiple robots printing simultaneously (right)

(Dörfler et al., 2022)

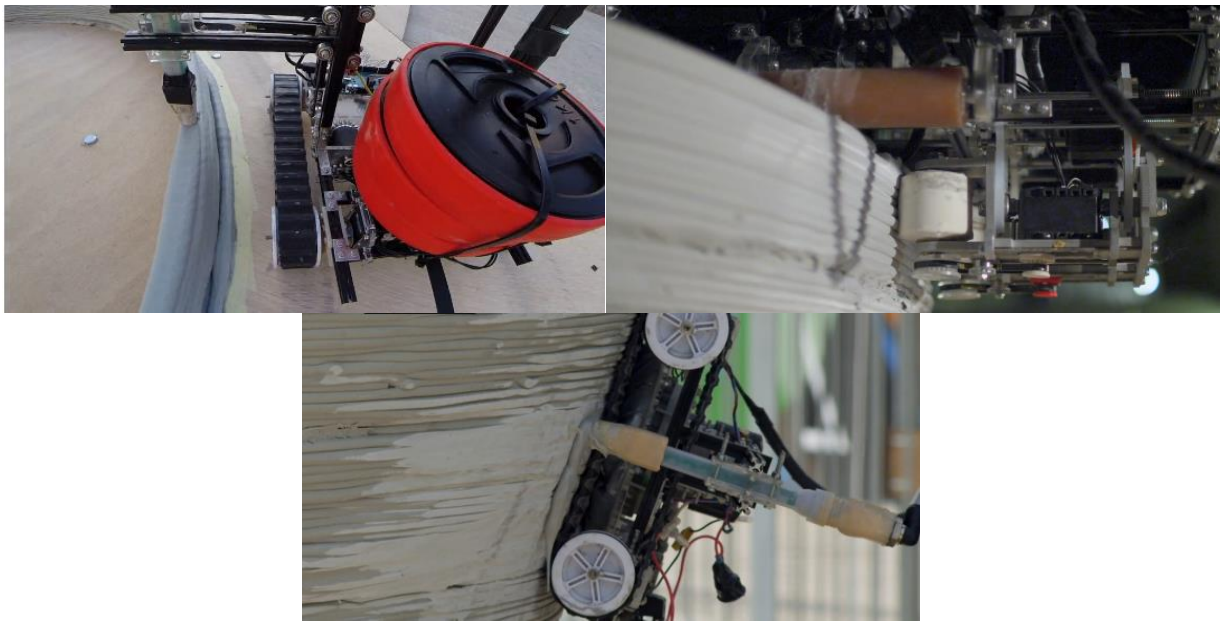

Figure 2.16 Fabrication with partnering robots: a robot that builds the foundation, a robot that increases the wall height and a robot that refinishes the surface

(*Minibuilders - Institute for Advanced Architecture of Cataloni*, n.d.)

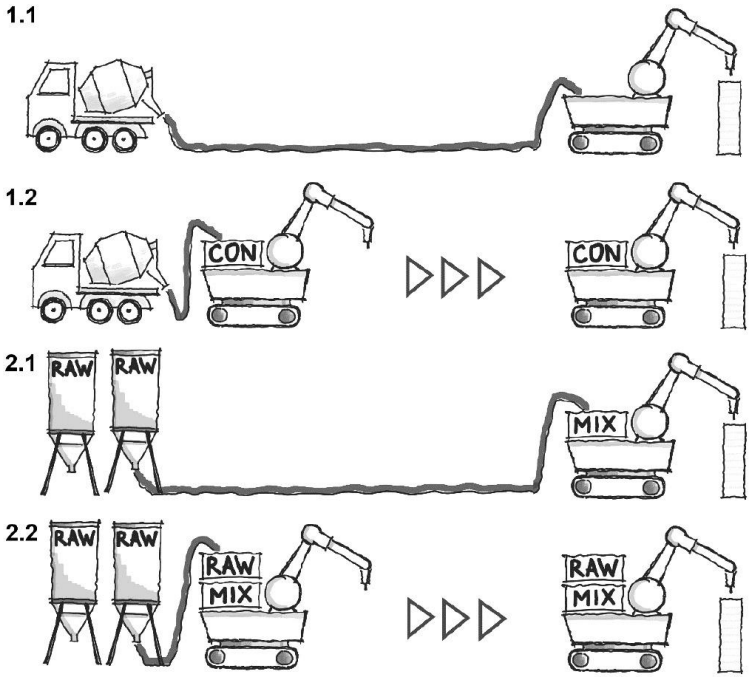

Figure 2.17 Various material supply strategies for in-situ mobile robotic concrete printing (Dörfler et al., 2022)

2.2.1.2 Small-scale mobility factors

Small-scale mobility defines printable geometries within printed objects rather than the size of the objects themselves. Particle bed systems can be modeled after 2D paper and ink printing systems. They have a greater ease of achieving higher degrees of geometric or design freedoms compared to typical deposition-based systems such as extrusion-based 3DCP. The following mechanical factors mainly apply to deposition-based concrete printing systems.

Concrete printing is dependent on nozzle movements where the concrete can be applied precisely. Nozzle movements are termed “tool paths”, which are instructions for the movement of the print head as it deposits material in 3D space. The manufacturer processes of generating these tool paths to control the mechanical systems are referred to as slicing. A prerequisite for a

designer is understanding what movements are difficult for the mechanical system to perform and how these movements can impact printable geometries.

One primary challenge is changes in direction for the print head. This can be described as a minimum turning radius or minimum fillet radius. Some systems have more nimble movement abilities with small turning radii as seen in the "Concrete Choreography" printed columns and printing tests in Figure 2.18. These designs were produced by a robotic arm with a wider range of movement freedom. In contrast, some DFC systems utilize wide concrete filaments that require more gradual changes in direction to avoid inconsistencies with sharp nozzle directional changes. Other systems may have a high amount of inertia in their mechanical movements, making it difficult to perform sharp, nimble, or small movements (Roussel, 2018). The turning radius is dependent on not only the mechanical system but also the ductility of the concrete (Roussel, 2018). Tight bends can cause a discrepancy in the amount of material deposited inside and outside the curvature, causing tearing or a "Shark-skin" texture on the outer curve (Figure 2.19). Figure 2.20 illustrates the difference of printing a 90 degree and a 180 degree turn with a small and large turning radius. Rapid changes in direction would need to be analyzed for every printed layer whereas Figure 2.20 only shows changes in direction in a single printed layer for visual clarity. These changes in direction pertain to a plan view (parallel to the printing bed and perpendicular to the nozzle), as shown in the 3D representation in Figure 2.5c, rather than a section or elevation view. The Living Room benches designed by Mississippi State University utilize a four-inch turning radius (Figure 2.21). The benches were printed in a vertical orientation rather than their final horizontal orientation. Thus, a plan view of each printed layer is a cross-section drawing of the bench in its final orientation. The turning radius is incorporated into each print layer as shown in the diagram in Figure 2.21.

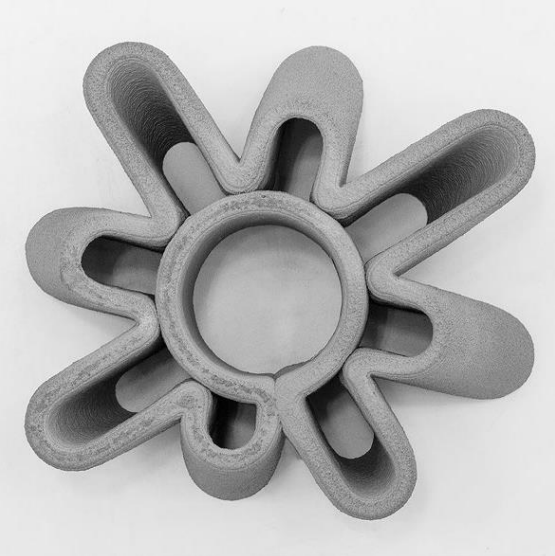

Figure 2.18 Tight bends and curvatures produced by a robotic arm (Anton et al., 2020)

Figure 2.19 Tearing and texture issues with tight curvatures in 3DCP (Roussel, 2018)

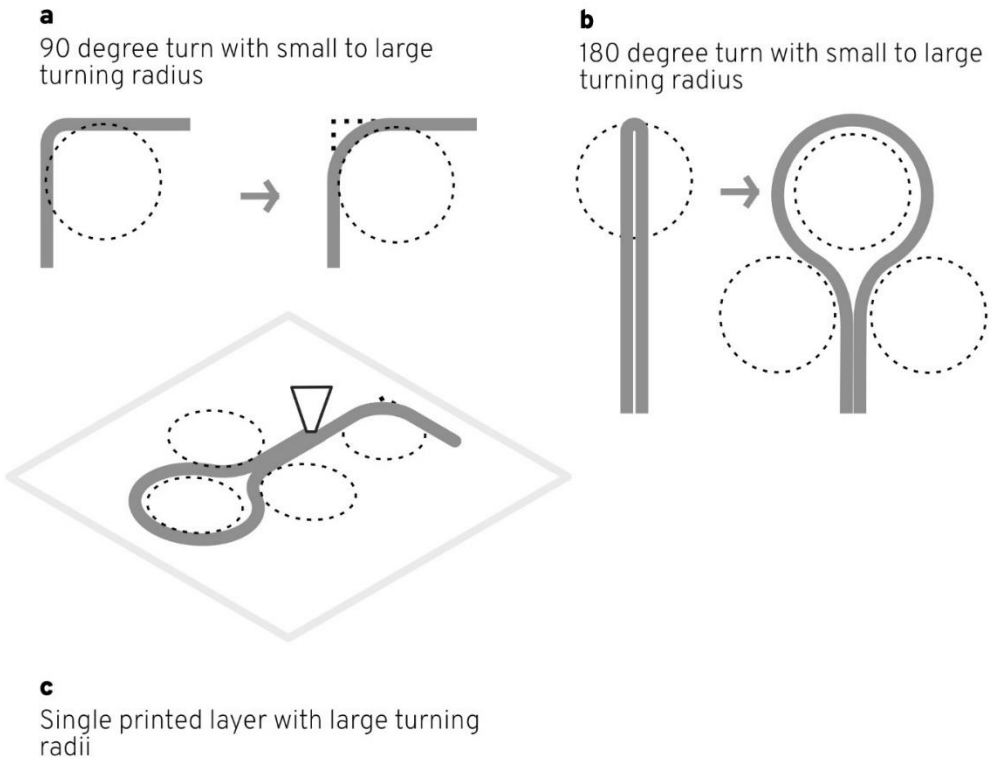

Figure 2.20 Effects of machine turning radius on printable geometries, not to scale

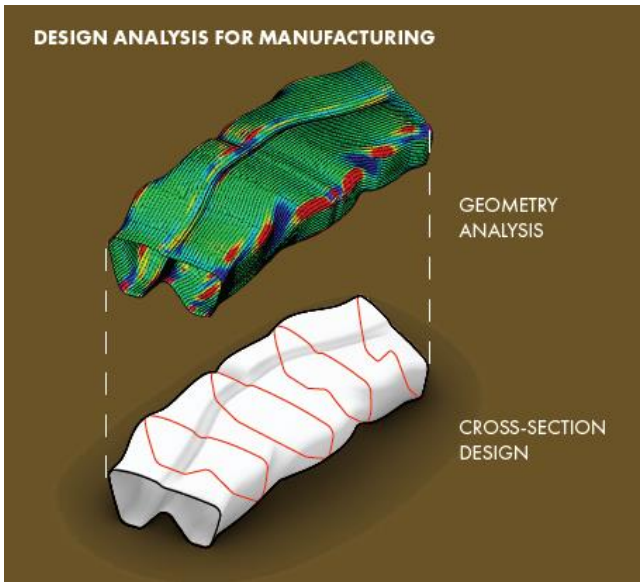

Figure 2.21 3D printed benches with gradual, loose curvatures with diagram of sectional design to meet turning radius requirement.

The second consideration for small-scale mobility is the orientation of the printing plane and the resulting orientation of the printed layers. Many DFC systems are based on 3 directions of movement, moving horizontally in the X+Y directions, and vertically in the Z direction. These systems typically utilize a “gantry” frame system where the print head moves within the frame. This is similar to the setup of widely available plastic fused deposition modeling (FDM) 3D printers. These systems typically utilize a single printing plane that is oriented parallel to the ground plane. The nozzle remains in a fixed orientation and is perpendicular to the ground plane and the printed layers. However, alternative inclined printing planes are possible for DFC systems with limited degrees of movement freedom, such as an inclined sloped base shown in Figure 2.22. This technique of inclined printing with a fixed nozzle orientation is infrequently used, and is mostly seen in FDM plastic printing with narrow feasible geometric ranges compared to systems with unfixed nozzle orientations. Other systems utilize robotic arms with multiple degrees of freedom, such as the printing setup depicted in Figures 2.23, 2.25, 2.26. The robotic arm can change the orientation of the nozzle, thus changing the printing plane. For example, in Figure 2.23, the printing plane starts parallel to the ground, and the printed layers gradually incline as the printing plane is made progressively steeper. This variable printing angle was used to produce a bridge module where the layer striations were orthogonal to the expected force as well as give the module sectional curvature. Changing the printing plane allows for steeper overhangs and slopes as demonstrated by a 40 cm overhang in S3DCP (Kloft & Hack, n.d.) In systems with uniform printing planes, slopes or overhangs are formed by stepping each printed layer past its previous supporting layer, resulting in a narrow range of feasible slopes for deposition-based printing of concrete (Figure 2.26). However, angling the printing plane allows

each successive layer to be oriented for maximum contact between layers, allowing steeper overhangs and slopes.

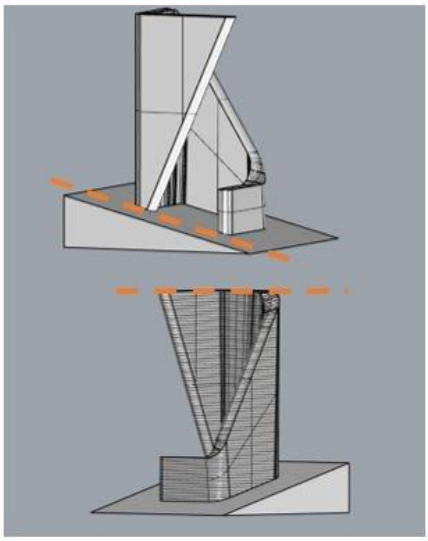

Figure 2.22 Printing bench on sloped base with a fixed nozzle orientation

(Baniasadi, 2021)

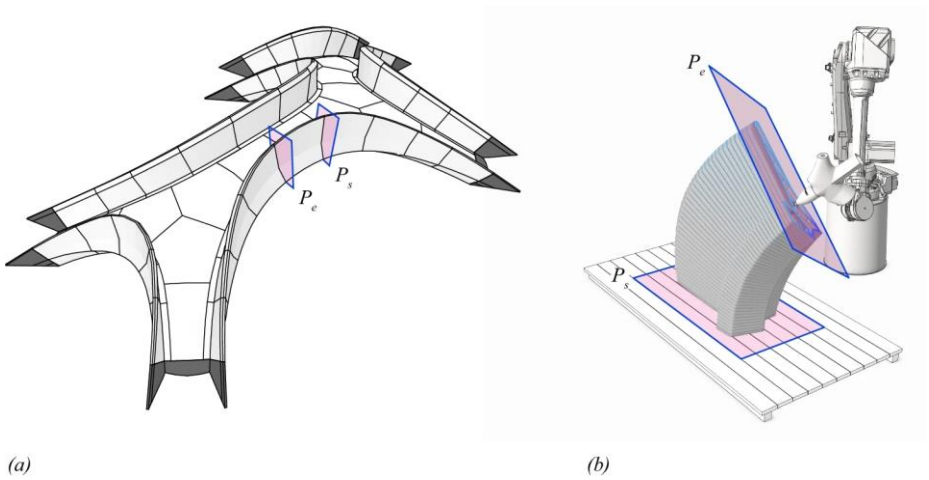

Figure 2.23 Diagram of printing planes for a bridge module utilizing successive variable inclined printing planes

(Bhooshan et al., 2022)

Figure 2.24 A typical robotic arm set up with incremental3D, printing modules for the Striatus bridge

Image courtesy of press package (*Striatus 3D Concrete Printed Masonry Bridge*, n.d.)

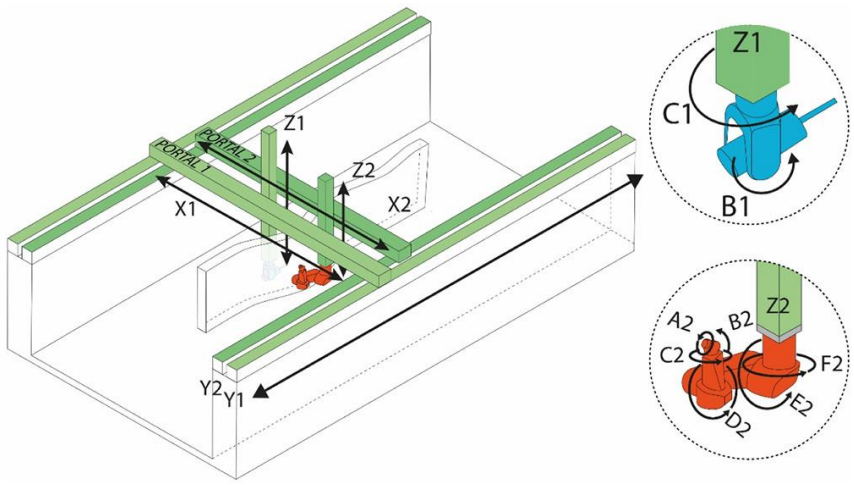

Figure 2.25 A robotic arm mounted within a gantry frame system

(Freund & Lowke, 2022)

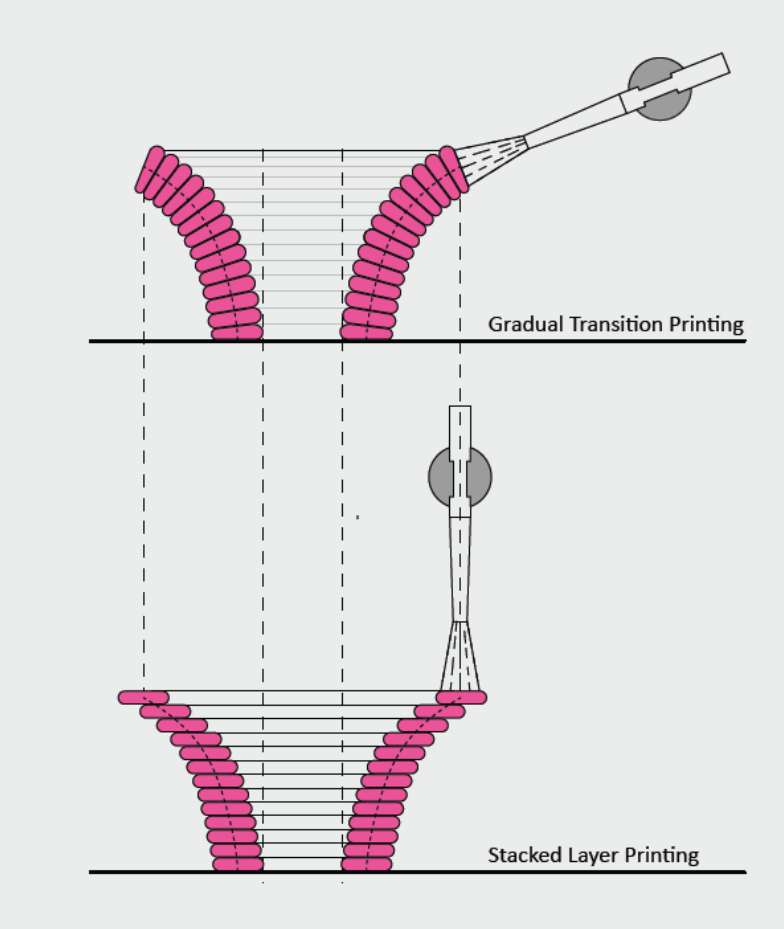

Figure 2.26 Overhang produced by a uniform layer angle versus a variable layer angle (Kloft & Hack, n.d.)

2.2.1.3 Effects of mechanical factors on printable design resolution

For deposition-based systems, the range of plausible nozzle movements defines the possible design geometries. For example, Figure 2.27 describes the various effects of changes in nozzle movement on the printed object in the context of S3DCP. In this example, the printing speed controls the layer thickness, the nozzle standoff distance effects the layer width and the printing plane effects the possible angles. These factors contribute to the possible design resolution or the "minimum feature size" that can be accurately printed (Roussel, 2018). If a design feature is smaller than the minimum feature size or layer dimensions, it will be

approximated. This is depicted in Figure 2.28, where changes in layer height allow increased or decreased design fidelity. This can fail to meet tolerances expected by typical construction. Likewise, the minimum turning radius is a limitation against producing small geometries with tighter curvatures as shown in Figure 2.29.

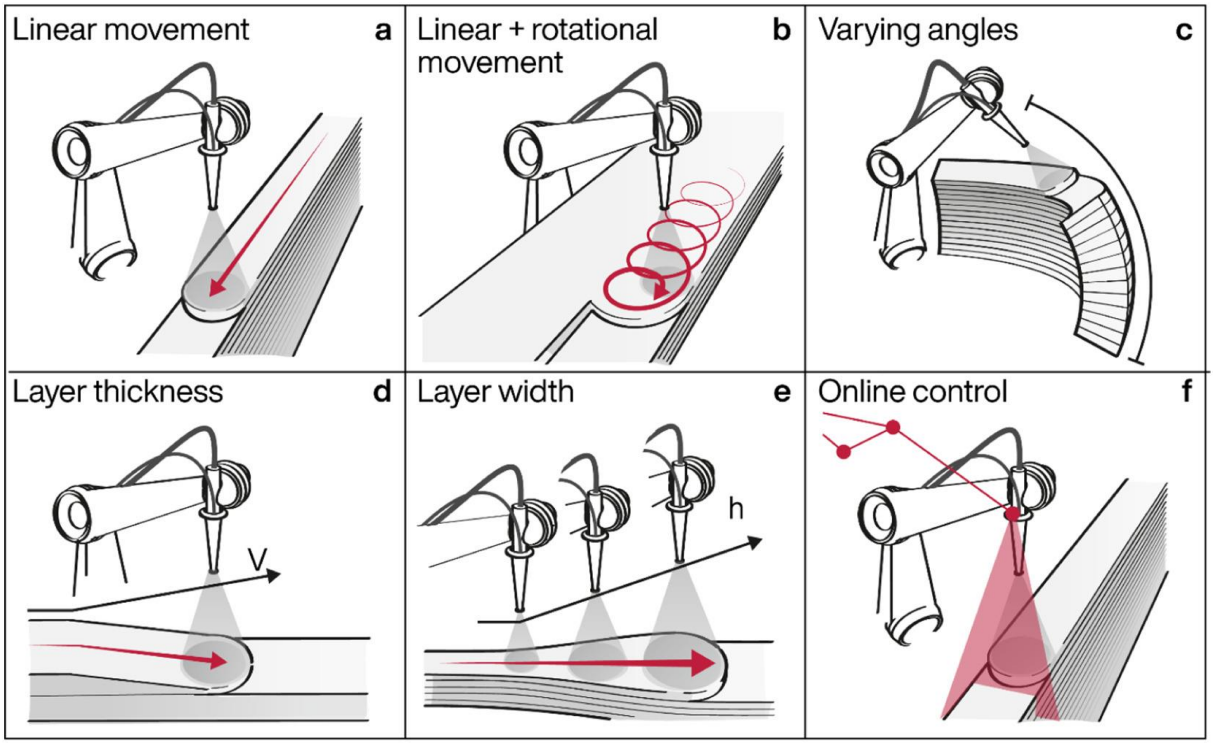

Figure 2.27 Nozzle movement and their effects on layer dimensions for S3DCP (Kloft, Krauss, et al., 2020)

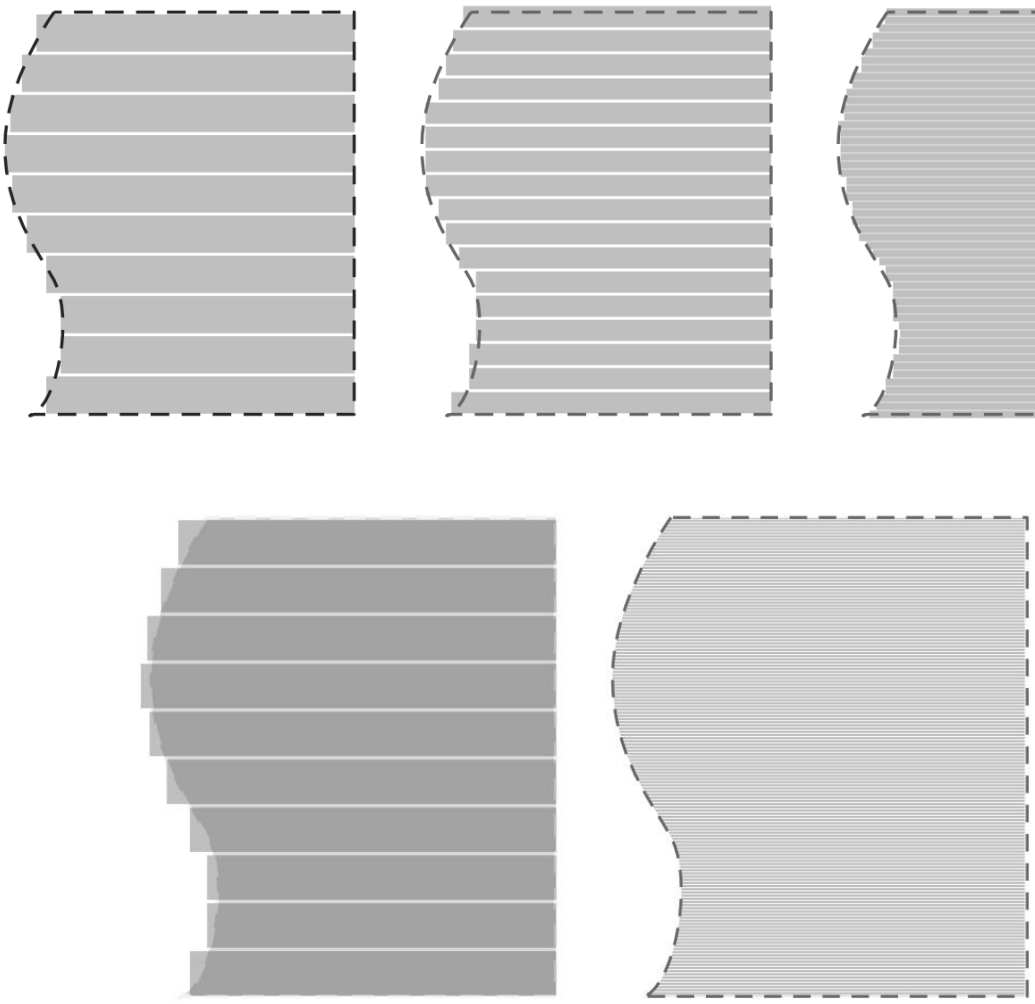

Figure 2.28 Effects of layer height on fidelity of printed object to desired geometry

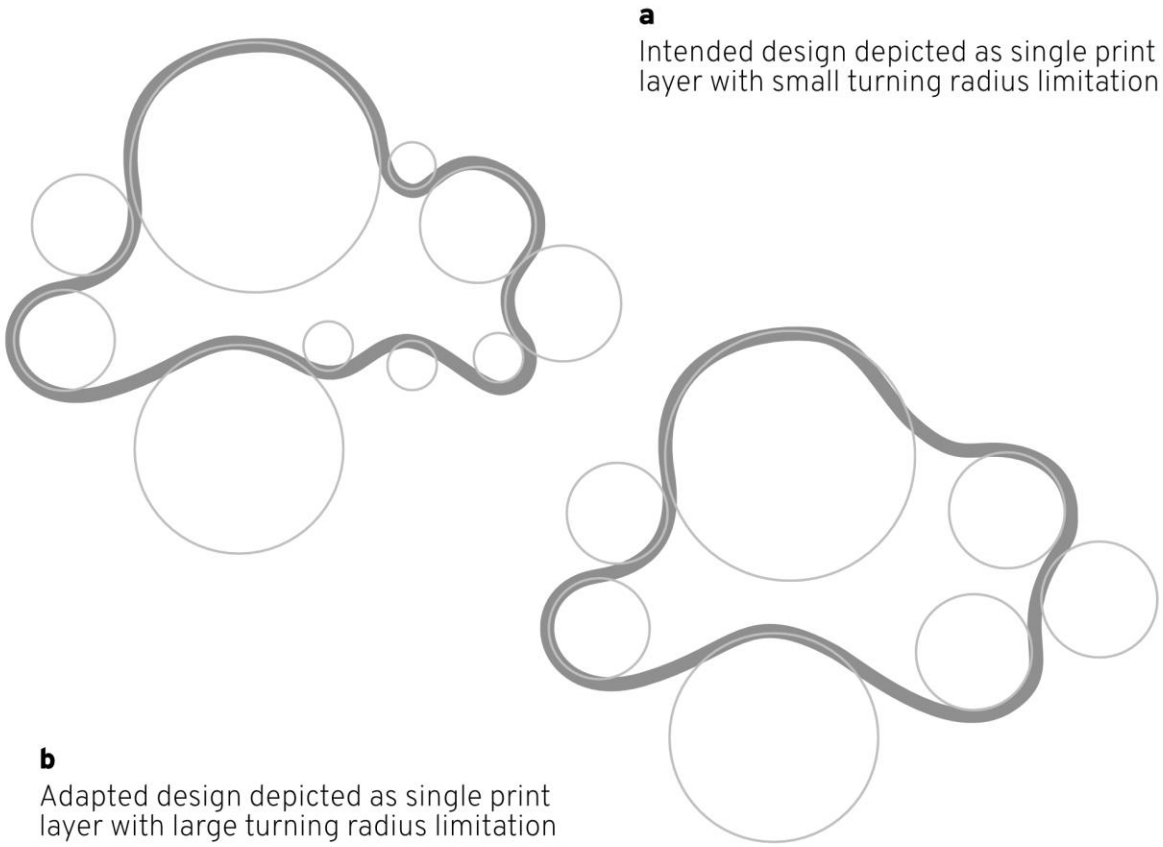

Figure 2.29 Effects of minimum turning radius on fidelity of printed object to desired geometry

Particle bed systems have an advantage when producing high fidelity concrete printed objects. Particle bed systems such as selective cement activation can utilize layer heights as small as 0.14mm (Lowke et al., 2020). The design resolution is defined by the precise application of an individual water drop. However, there is a strong trade-off between resolution and production rate. Deposition-based systems print rapidly by building up successive micro layers in comparison to particle bed systems, which have been demonstrated with large aggregates and thicker layers. Large-scale particle bed printing systems are exceptions as they have higher production speeds and lower geometric resolutions due to the larger aggregate sizing

(Mai et al., 2021). Generally, deposition-based systems prevail in higher production speeds whereas particle bed systems excel in design freedom and resolution (*Project A 03 - Additive Manufacturing in Construction TRR277*, n.d.)

2.2.2 Material factors for DFC

The following sections summarize the pertinent material factors for DFC. Deposition-based systems have distinct factors since the concrete is self-supporting while wet, leading to challenges of layer bonding, stability and curing issues. Particle bed systems are defined by the adequate penetration and hydration of cement, creating an opposing tension between compressive strength and geometric fidelity. Lastly, innovations in the digital control of concrete acceleration are discussed with their impacts on DFC methods.

2.2.2.1 Material factors for deposition-based systems

There at two major factors to consider while the material is wet, cycle-time and deformation under self-weight. The concrete mixture maintains an appropriate viscosity and yield stress for a finite amount of time, which creates a limit on how long each layer can be printed, which is called “cycle-time”. Increased print speed allows longer layer lengths, but print speed is decreased by direction changes and limits of the mechanical system (Buswell et al., 2018). As a result, there is a limit on how long a perimeter can be easily printed without manipulating accelerants. With successive layers, the printed object can buckle with self-weight, which is remedied by accelerant usage to harden lower layers. With slender and tall objects, such as a column, the shorter layer lengths and rapid layering of new materials can be challenging to print without buckling, decreasing print speed, or increasing accelerants (Buswell et al., 2018) (Figure 2.30).

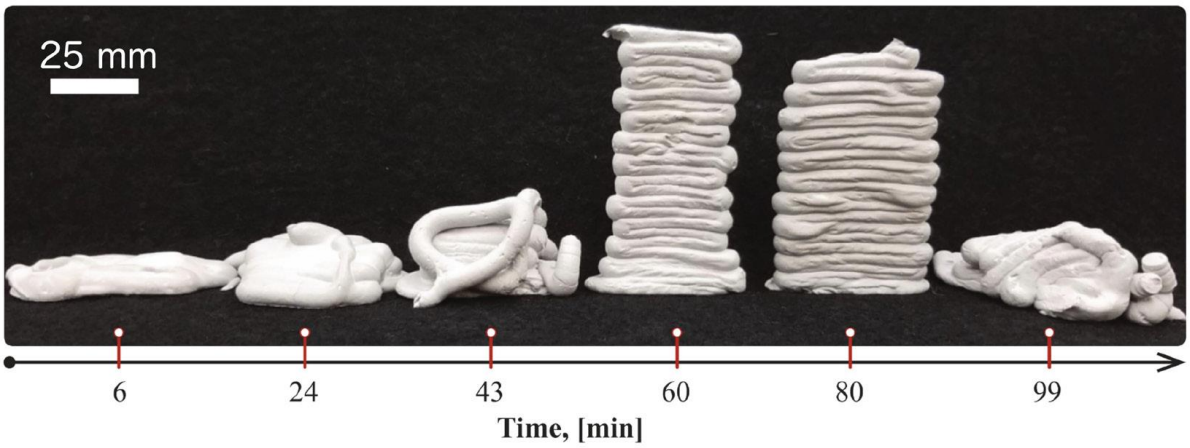

Figure 2.30 Effect of time delay after concrete mixing

(Buswell et al., 2018)

Other material factors describe behavior of the material while drying, including interlayer bonding strength and curing issues. For the rapid hardening of concrete to be self-supporting, an elongated time between layers can cause cold joints, especially in 3DCP (Figure 2.31). S3DCP was designed in response to this issue, where delays under 30 minutes between layers can be tolerated. Likewise, S3DCP has a longer drying time window, allowing surface refinishing, compared to 3DCP where a layer dries with 3-5 minutes of being extruded. Humidity can also affect the bonding between layers, where an on-site humidity condition can cause interlayer bonding strength to decrease by 35% (Freund & Lowke, 2022). Deposition-based printing methods typically utilize a high cement ratio with small particle sizes which creates a high susceptibility to cracking during drying (Buswell, 2018). A case study review found curing control methods such as foil wrapping were necessary for multiple printed applications (Bos et al., 2022).

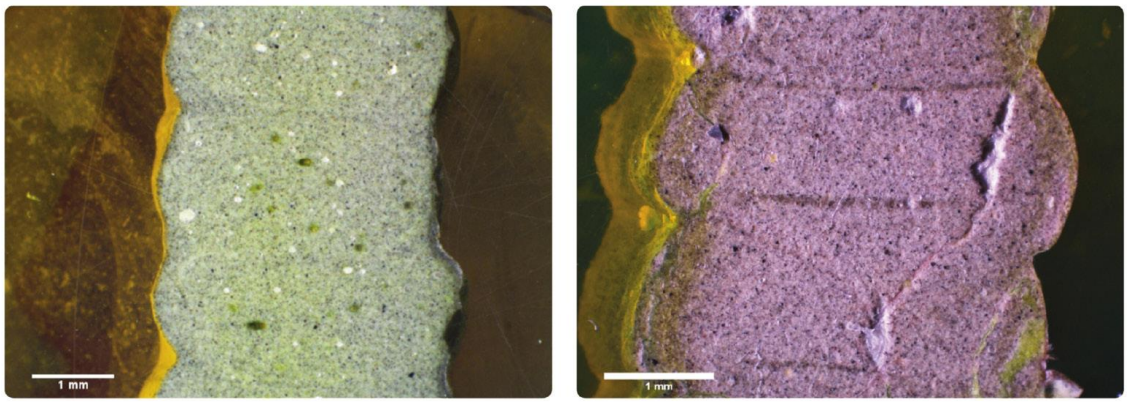

Figure 2.31 Defects between printed layers built after initial setting time of concrete (Buswell et al., 2018)

2.2.2.2 Material factors for particle bed-based systems

Selective cement activation (SCA) has its distinct material considerations. The resolution of SCA is determined by high precision control of water drop size during the application onto layers of dry cement. However, more sparse water applications leave unintended, under-hydrated areas, leading to a decrease in the strength of the print. On the other hand, increased water penetration increases compressive strength but decreases geometric accuracy as more areas are unintentionally wetted. This is illustrated in Figures 2.32 and 2.33 (Lowke et al, 2020). Compressive strength also increases as particle size increases, as shown in Figure 2.34 (Lowke et al., 2020). SCA is among the DFC methods with the lowest compressive strengths but with the finest design resolution.

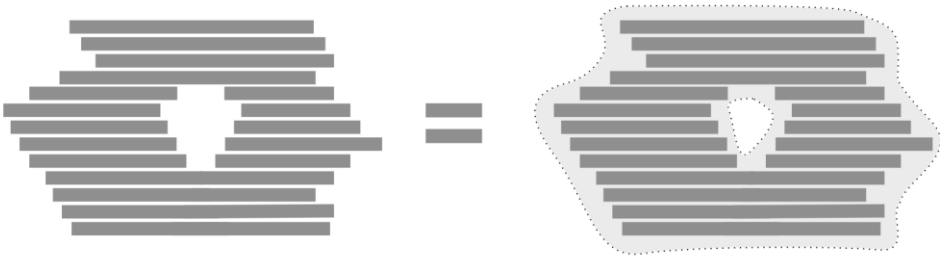

Figure 2.32 Effects of water penetration on geometric fidelity

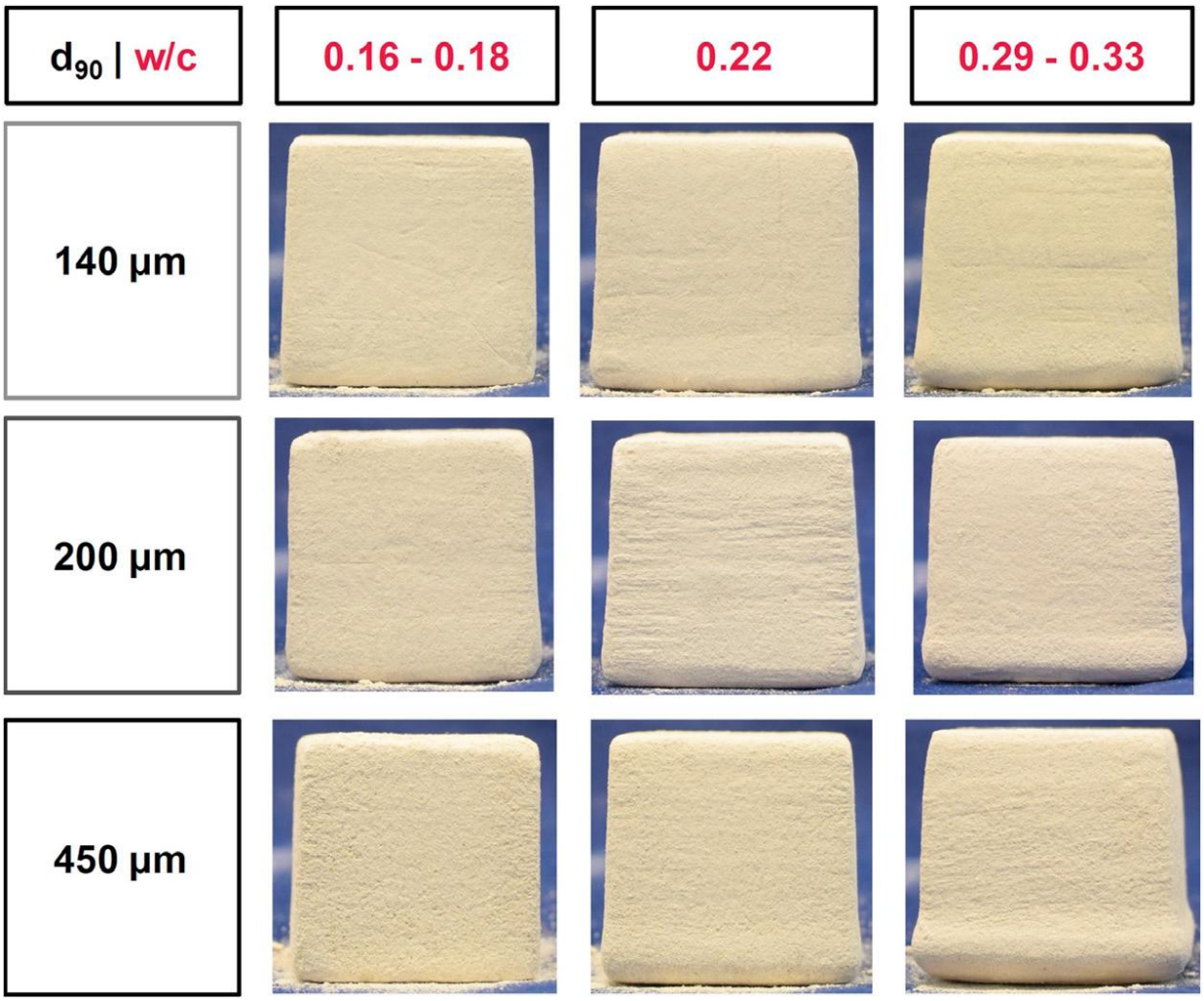

Figure 2.33 Effects of water penetration and particle size on geometric fidelity

(Lowke et al., 2020)

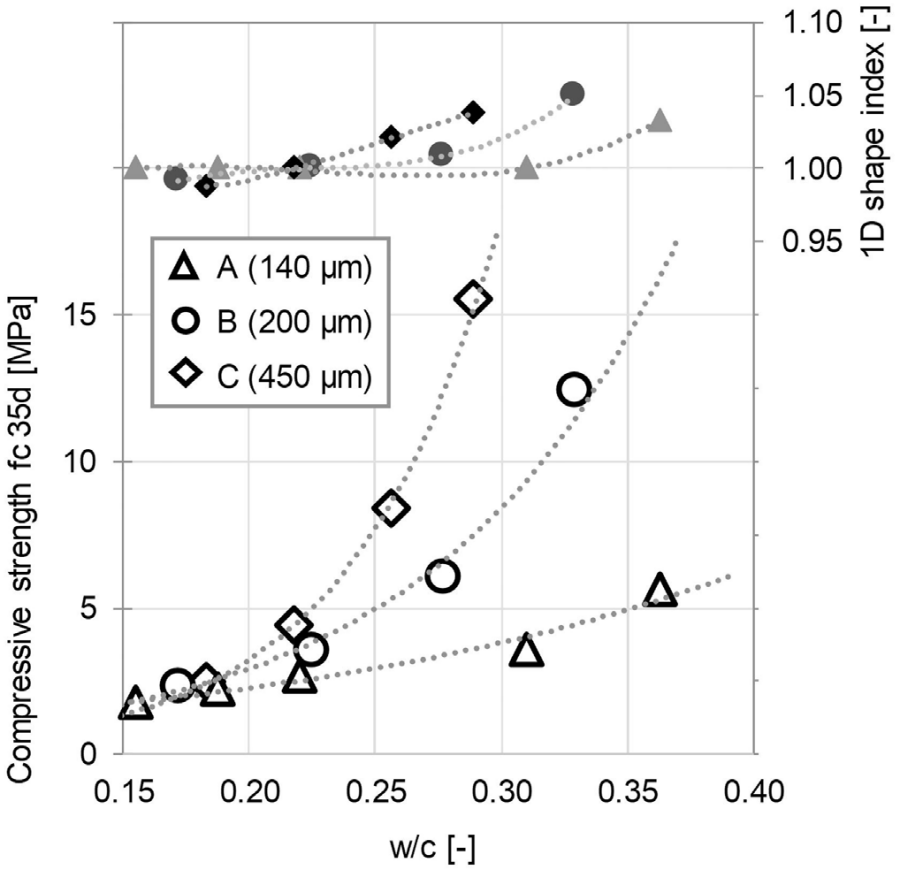

Figure 2.34 Effects of water penetration and particle size on compressive strength (Lowke et al., 2020)

For selective paste intrusion (SPI), there are two major factors that impact design resolution and compressive strength. Critically, there must be a sufficient coverage of cement paste in and between aggregate layers (Figure 2.35). Incomplete penetration of the cement paste within and between layers results in inadequate bonding of the material and subsequently lowers strength. A paste with a low yield stress allows the cement to increasingly fill the gaps between aggregate particles, thus increasing strength. However, when cement paste has a more fluid ease in moving across aggregate particles, it can be moved further than intended by capillary action resulting in decreased geometric accuracy, as shown in Figure 2.35 (Weger & Gehlen, 2021)

Increased particle size allows for greater compressive strength but lower geometric accuracy for SPI (Mai et al., 2021). Figures 2.36 and 2.37 provide examples of SPI with different particle sizes and the subsequent level of geometric detail.

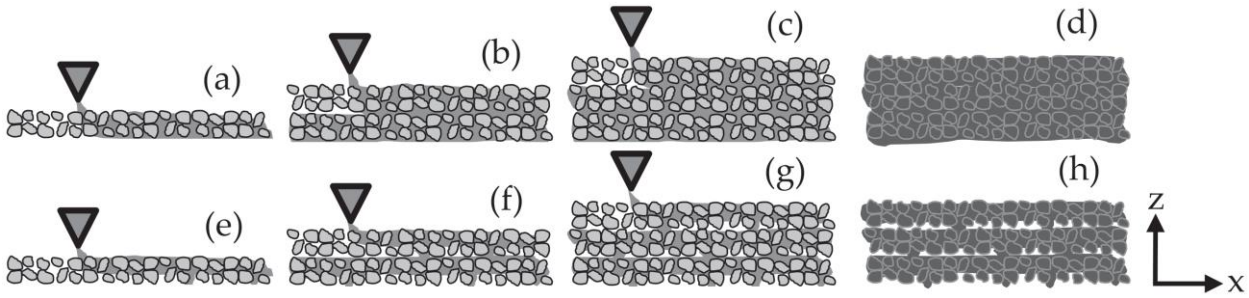

Figure 2.35 Levels of penetration of cement paste into aggregate bed

(Weger & Gehlen, 2021)

Figure 2.36 SPI with small scale particles

(Weger & Gehlen, 2021)

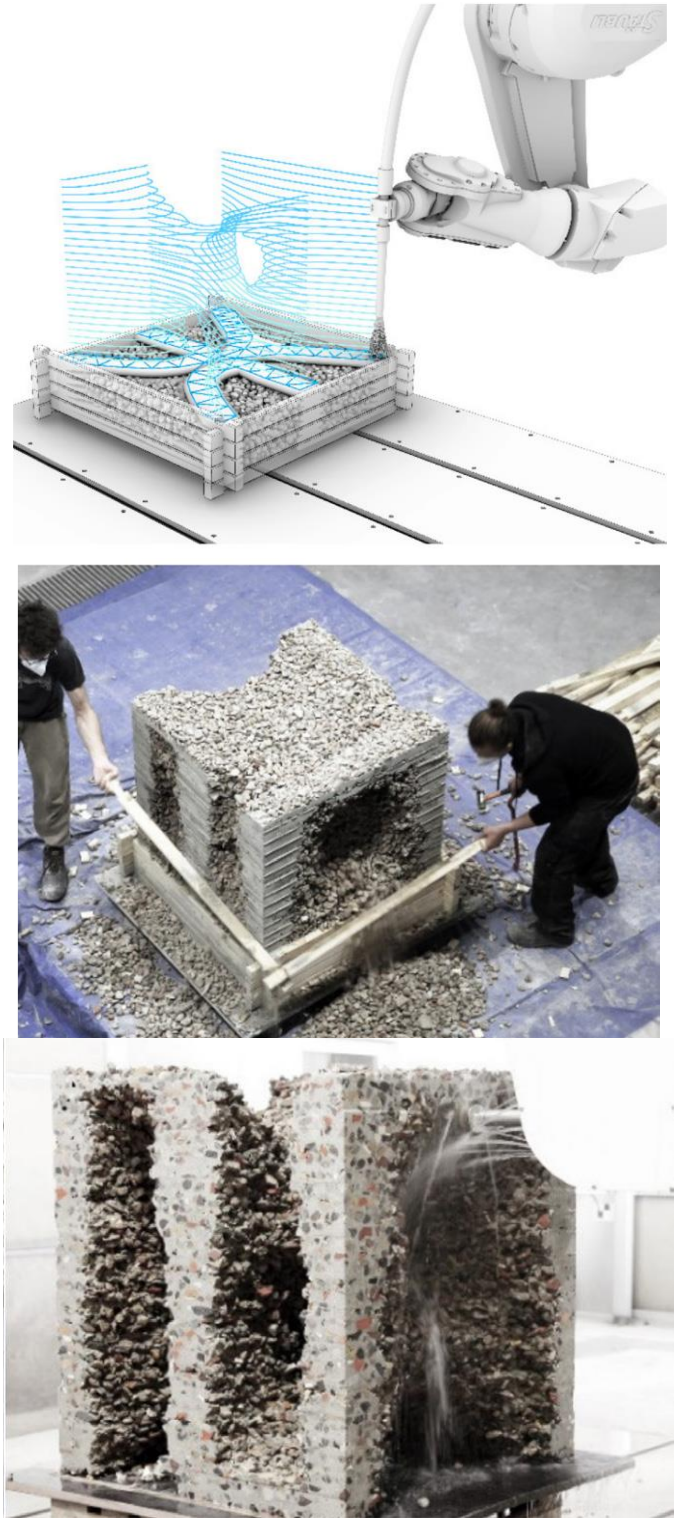

Figure 2.37 SPI with large scale particles

(Mai et al., 2021)

2.2.2.3 Processes for "setting on demand" activation of concrete

The hardening of concrete has been controlled to a high degree of precision using accelerant dosing at the nozzle (Reiter et al., 2020). The concrete is mixed with a retardant to maintain viscosity and yield stress until it reaches the nozzle. At the nozzle, the accelerant is mixed with the material immediately before application (Figure 2.38). There are different timing variations and applications of "setting on-demand". For a plastic formwork, concrete is set immediately after exiting the nozzle to alleviate pressure on formwork. For smart dynamic casting (slip forming), concrete setting is timed to harden after leaving the slipform formwork (Szabo et al., 2020). Setting on demand is a recent innovation and has seen less deployment across DFC methods.

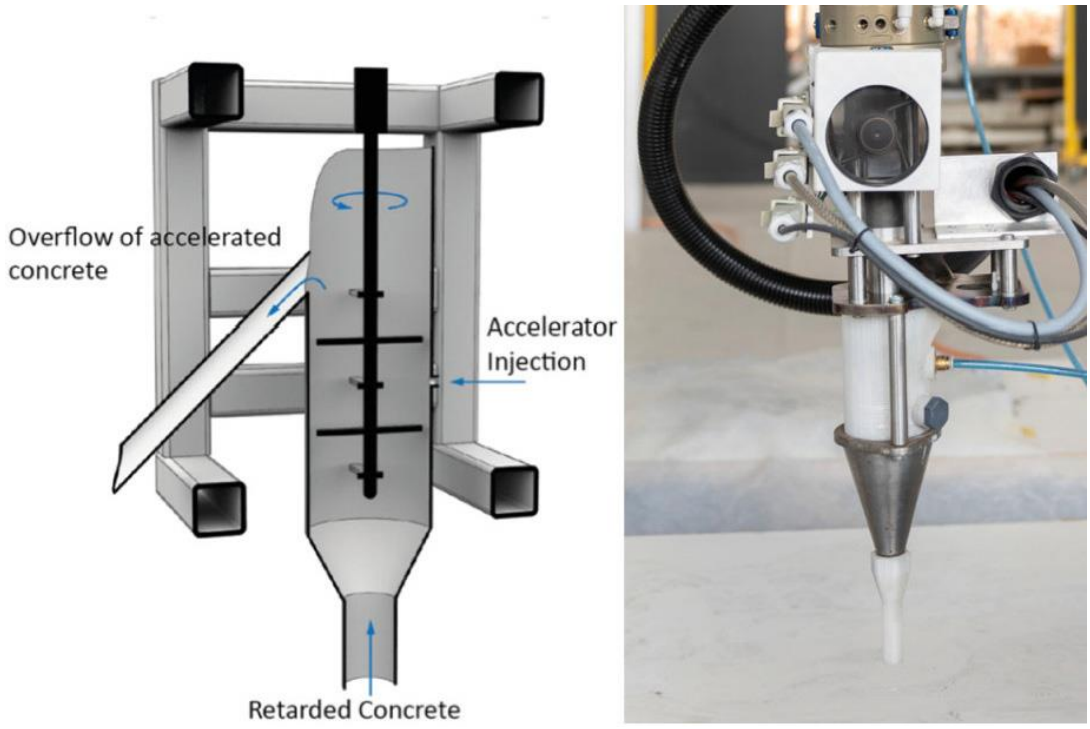

Figure 2.38 An example of mixing chambers for setting on demand (Reiter et al., 2020)

2.3 Robotic construction processes in relation to site and terrain conditions

With in-situ construction, there are additional considerations for additive manufacturing. For instance, when using mobile robots, the movement and printing locations of the robot needs to be sequenced. If multiple robots are involved, their tasks can be managed centrally, with a planned approach, or decentralized where each robot responds to the site conditions (Dörfler et al., 2022) . Likewise, how robots collaborate and print in tandem can be complex, such as the example illustrated in Figure 2.39. To operate on a construction site, mobile additive manufacturing uses localization and sensing for awareness at two scales. Localization could include point cloud mapping of the site. Small scale sensing is used by mobile robots to evaluate the task at hand such as the 3D laser scans shown in Figure 2.40 (Dörfler et al., 2022). Similarly, additional sensing capacities can accommodate for variations in the printing surface, as depicted in Figure 2.41 (Wolfs et al., 2018). The attachment arm of the printing system allows it to perceive changes in the ground surface, and the printer adjusts the layer material to compensate for deviation and create level print layers.

Most in-situ DFC projects rely on leveled, prepared ground. However, there are examples where mobile robotic construction carried out on unlevel terrain, particularly excavation and embankment tasks. The HEAP robot automates earth-moving tasks, providing a precedent for how mobile 3DCP robots might navigate and interact with complex terrain. Figure 2.43 depicts the various processes HEAP relies on to iteratively sense and alter the terrain (Jud et al., 2021). An initial drone survey provides a 3D model of the site condition before the work commences. This model is used in Rhino and Docofossor, a Grasshopper plugin for manipulating terrain, to describe the terrain changes to be constructed. HEAP plans their course of attack, performs excavation and/or dumping, and then senses the current state and replans the next course of

action. Through iterative sensing, HEAP iteratively responds to fallen soil movements and other changes.

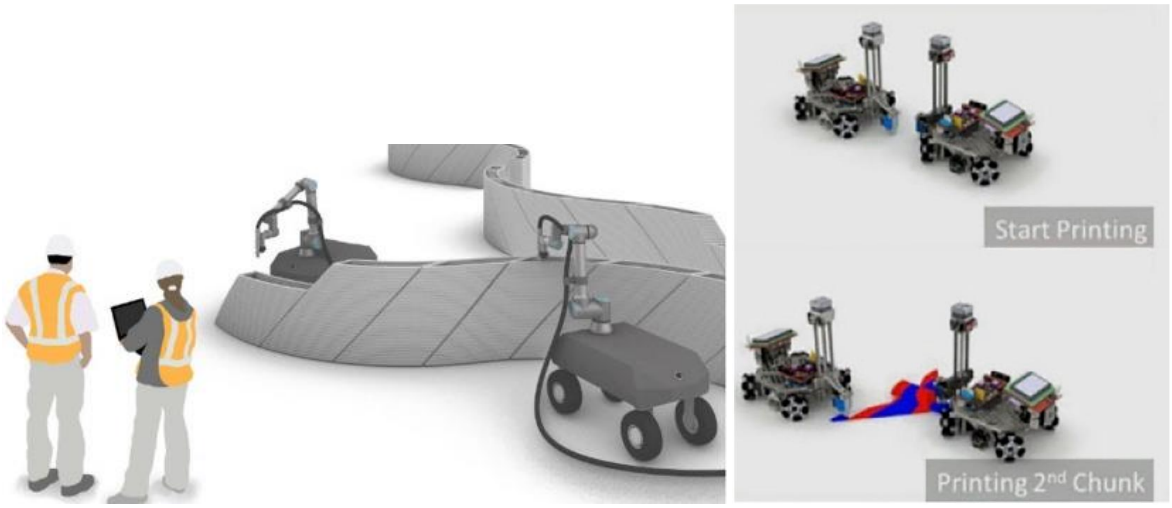

Figure 2.39 Examples of collaborative printing between two robots

(Dörfler et al., 2022)

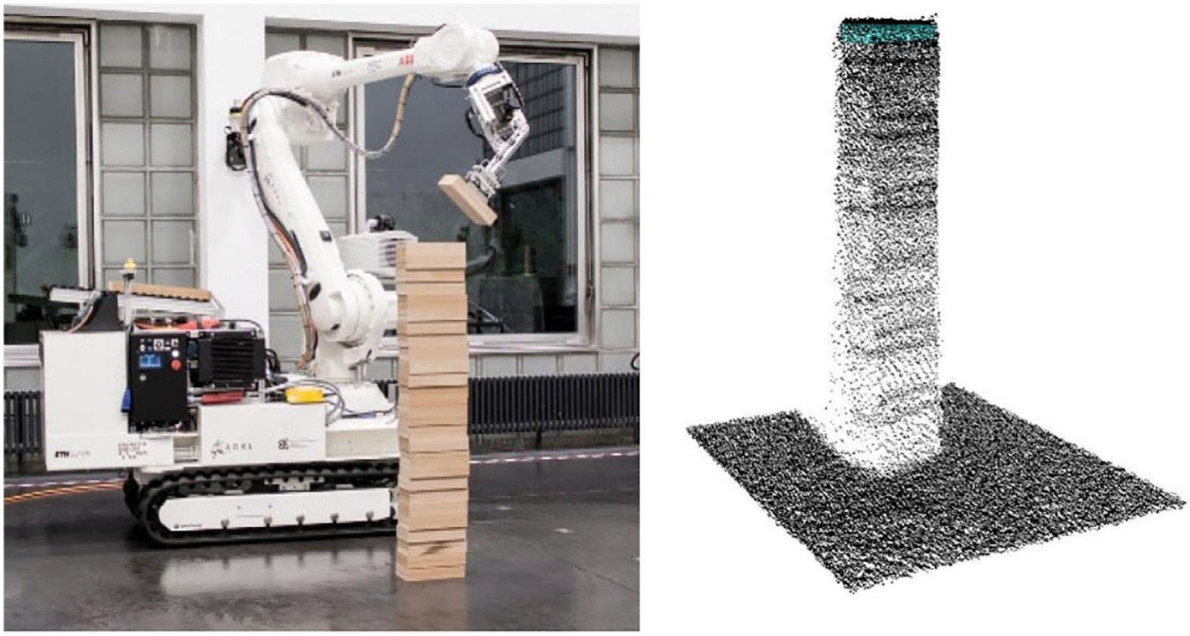

Figure 2.40 In-Situ Fabricator using 3D laser scan to guide task

(Dörfler et al., 2022)

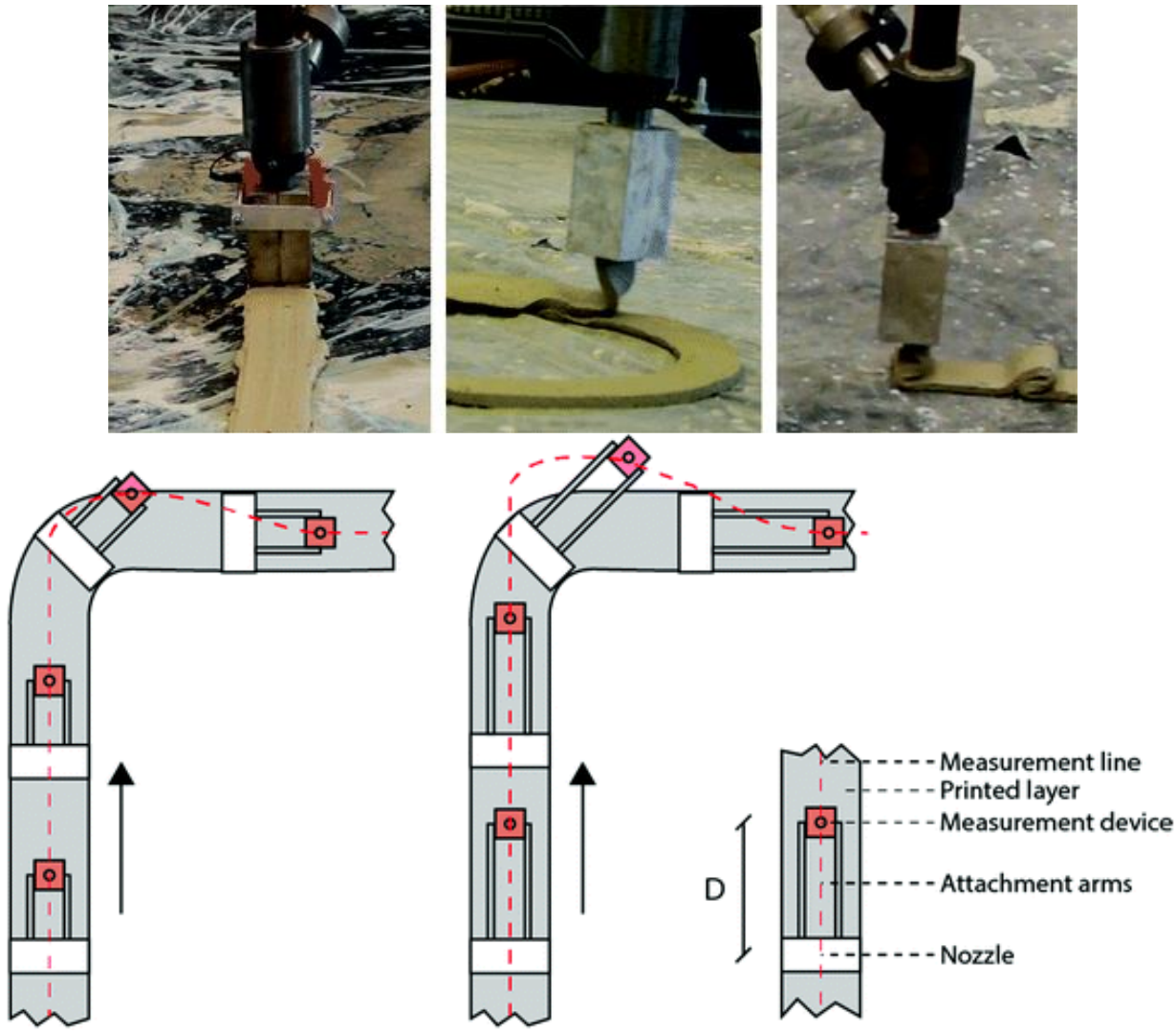

Figure 2.41 Real time height adjustment to accommodate ground plane deviations

(Wolfs et al., 2018)

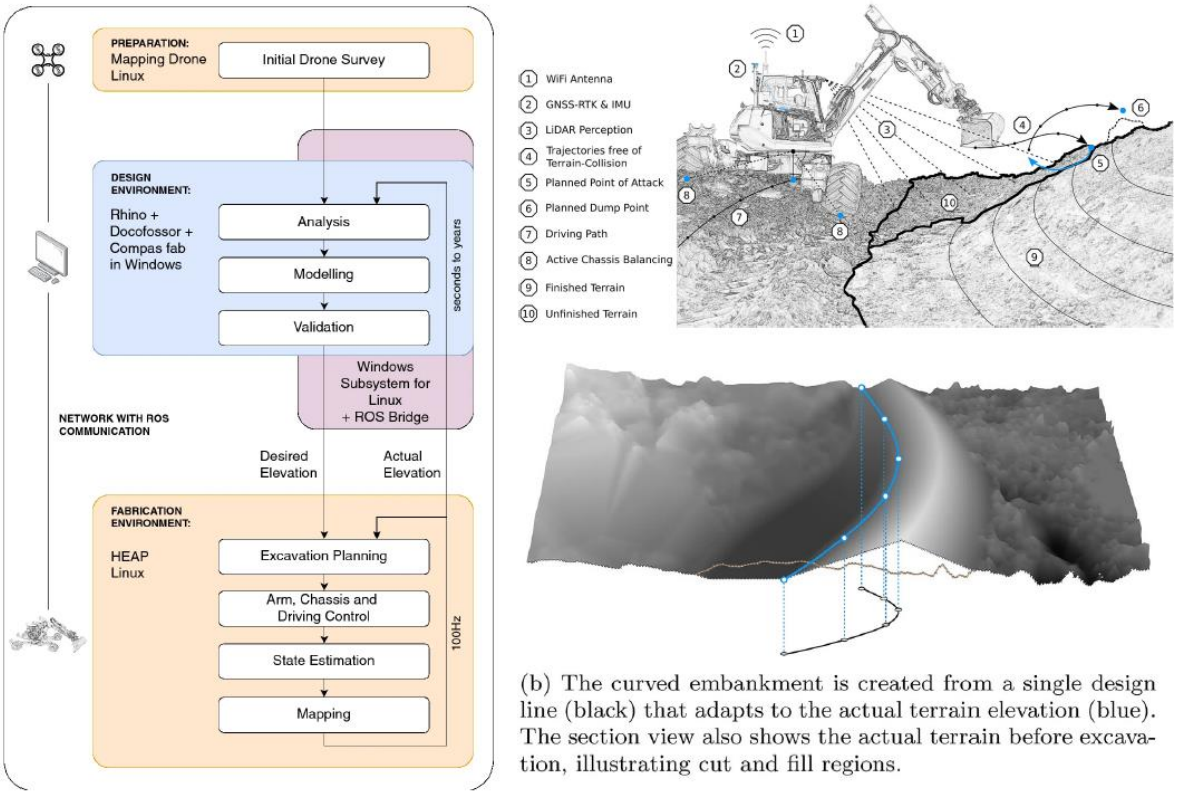

(b) The curved embankment is created from a single design line (black) that adapts to the actual terrain elevation (blue). The section view also shows the actual terrain before excavation, illustrating cut and fill regions.

Figure 2.42 Processes for robotic embankment undertaken by “HEAP”, the robotic excavator (Jud et al., 2021)

Mobile robots provide new challenges for construction planning and construction detailing. One example is a farmhouse designed and constructed by Tsinghua University, aiming to decrease labor and increase 3DCP participation in the construction process (Xu et al., 2022). This project was thoroughly detailed and scheduled to reduce time and labor. However, the trench wall details show the complexity of deploying 3DCP in-situ. A trench is preprinted in a factory environment with fiber reinforcement placed in the x direction. The concrete trench is then placed in the ground with y direction horizontal rebars installed on site. The installation of vertical rebar poses a challenge because they would collide with the printer head as it produces the wall sitting atop the foundation. To address this issue, hollow conduits are placed within the

trench with concrete cast in place to fill the trench. This forms the flat surface on which the wall is printed. After printing 300 mm to 400 mm of the vertical wall height, the vertical rebar is placed into the wall. Then, mortar is poured to cover the vertical rebar.

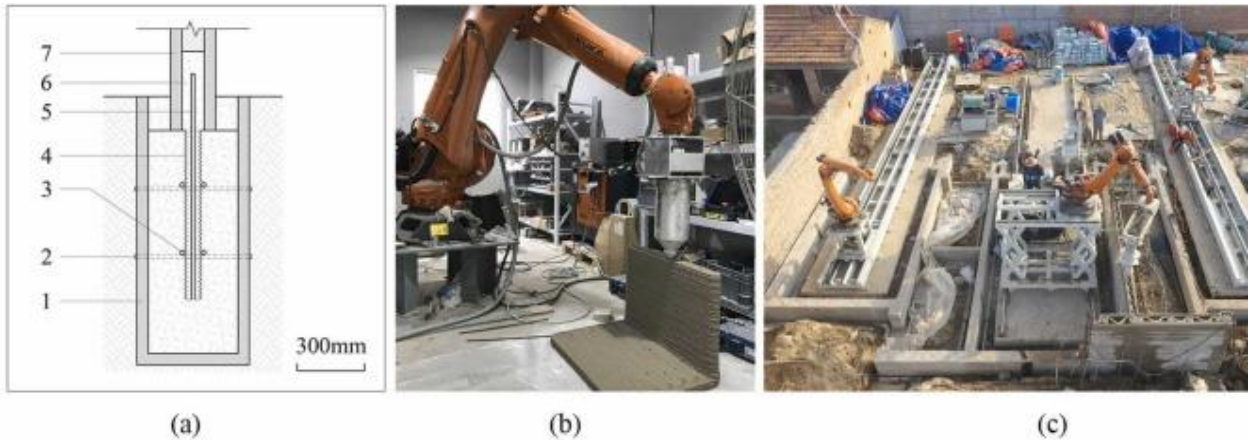

Figure 2.43 Trench detail from Tsinghua University's farmhouse prototype

"(a) The connection details of foundations and walls (section); (a1) 3D printed concrete trench; (a2) X-directions FRP rebar; (a3) Y-direction FRP rebar; (a4) Flexible metallic conduit; (a5) Z-direction FRP rebar; (a6) Filled-in 3D printing mortar; (a7) 3D printed concrete wall; (b) The 3D printing process of the foundation trench; (c) The construction site after the walls' bottom were poured." (Xu et al., 2022)

CHAPTER III

PROBLEM STATEMENT: RECIPROCAL PROCESSES BETWEEN DESIGN INTENT AND MACHINE SELECTION

3.1 Introduction

This research addresses the unmet needs for designer implementation of DFC with a focus on challenges unique to landscape architecture applications. This focus was a response to identified research gaps found in the literature review, precedent studies, and prior 3DCP experiences as demonstrated by the Galloway learning garden described in Figure 1.3. These research gaps were translated into the following objectives:

1. Communicate the "design space" of DFC to describe the feasible geometries for fabrication and identify the limiting process factors. The research proposes an adaptive and didactic system that allows a designer to explore their ideas and see the implications of the fabrication system.

2. Demonstrate a process for machine selection to match design intent. Currently, there is a lack of comparison between fabrication systems, particularly describing current technology readiness, feasible geometries, and relative advantages. This chapter demonstrates the process for selecting a fabrication system for terrain responsive retaining walls, followed by a process for adapting the design intent to the fabrication system.

3. Manage the complexity of meeting fabrication requirements to improve the feasibility of implementing DFC. Meeting complex requirements can prolong or consume design timelines for non-expert designers. Chapter IV describes an interactive design environment that gives continuous constructability feedback throughout the design process.

4. Respond to the lack of DFC applications integrated into landscapes. There are disparate technologies that could impact landscape architecture, particularly in-situ 3DCP and robotic construction with terrain discussed in the literature review. This research imagines a potential application for DFC not yet exhibited: to create landscape structures that respond to their terrain. A demonstration can indicate new potential for landscape architecture. A speculative application for terrain responsive design is applied to an amphitheater in Chapter V, showcasing the value of further technological development for DFC in unlevel terrains.

These objectives inform and structure for the interactive design toolkit and amphitheater application presented in the following chapters. However, the prerequisite to these research activities is envisioning and defining a potential landscape application for DFC, understanding the appropriate fabrication system for that design intent, and reassessing the design intent to fully take advantage of the machine. Terrain variables and wall attributes were used to create alternate scenarios that lend definition to the concept of terrain responsive design. This definition was used to select a machine for the design concept. Multiple precedent projects were reviewed to establish a framework for understanding differences between DFC technologies. This framework was used to select the fabrication methods most appropriate for a retaining wall. The capabilities and limitations of the fabrication methods were described and used to define the rules, variables, and agenda for the research methodology.

3.2 Research context and designer challenges identified for DFC

3.2.1 Understanding of design space for DFC

To successfully incorporate DFC in landscape architecture, it is crucial to first understand the mechanical and material factors that define the chosen fabrication method. Designers are often guided by observations of construction practices and rules of thumb to guide their understanding of constructability. The range of possible constructible geometries and strategies can be termed as a "design space" (Dörfler et al., 2022). This term is similar to the more familiar

term of “color space”, where standards describe the range of colors that can by produced by a typical computer display monitor. Often graphic design software alerts a user if their chosen color is inside or outside the color space suitable for the internet. Similarly, the design space of traditional concrete construction is defined by understanding labor, formwork, and the material properties of concrete such as slump and workability. However, in the case of DFC, the design space is defined by new processes and parameters based on robotics and other mechanical systems and the properties of concrete that hardens in minutes instead of days. For designers, becoming acclimated to these new factors can be challenging. For example, one designer spent several weeks on a bench design, learning the process factors, then hours on a second design (Baniasadi, 2021). Research in process factors have been studied extensively in the fields of engineering and material science, particularly for 3DCP (Strohle et al., 2023). This research is generally focused on improving materials and mechanics. There exists a research gap when it comes to understanding how to design specifically for DFC construction. In the following sections, fabrication process and parameters are explained from the perspective of a designer.

3.2.2 Complexity of design process for DFC

There is a need for a visual framework to describe a means for designing for the machine and for understanding the factors related to mechanical and material systems. However, these parameters can be complex and interdependent, making it challenging to even well-informed designers to meet all fabrication requirements. Figures 3.1 and 3.2 illustrate a critical difference between designing for DFC and traditional construction. When designing a typical retaining wall, a designer might draw one or two cross-sections that describe the wall geometry. In these cross-sections, the designer considers the limits of the construction process and whether the cross-section meets the structural needs. However, DFC projects tend to be motivated to fully

utilize the technology by incorporating non-uniform geometries. When designing for DFC, even if the designer only needs to draw a few cross-sections to form a 3D model of the wall, the design has a much more thorough evaluation process compared to traditional construction. Figure 3.1 depicts a segment of a wall to be 3D printed in concrete. The wall can be printed in its final horizontal orientation or printed vertically. In either situation, the wall must be evaluated for its adherence to the fabrication limitations such as minimum radii (red circles) or maximum slopes (red angled lines). The difficulty arises in that the wall needs to be continuously evaluated against the fabrication limitations not just in a few cross-sections as shown in Figure 3.2. The example provided in the figures is fairly uniform. However, rapidly changing areas can have geometries that fail to meet print parameters in between successfully designed cross-sections.

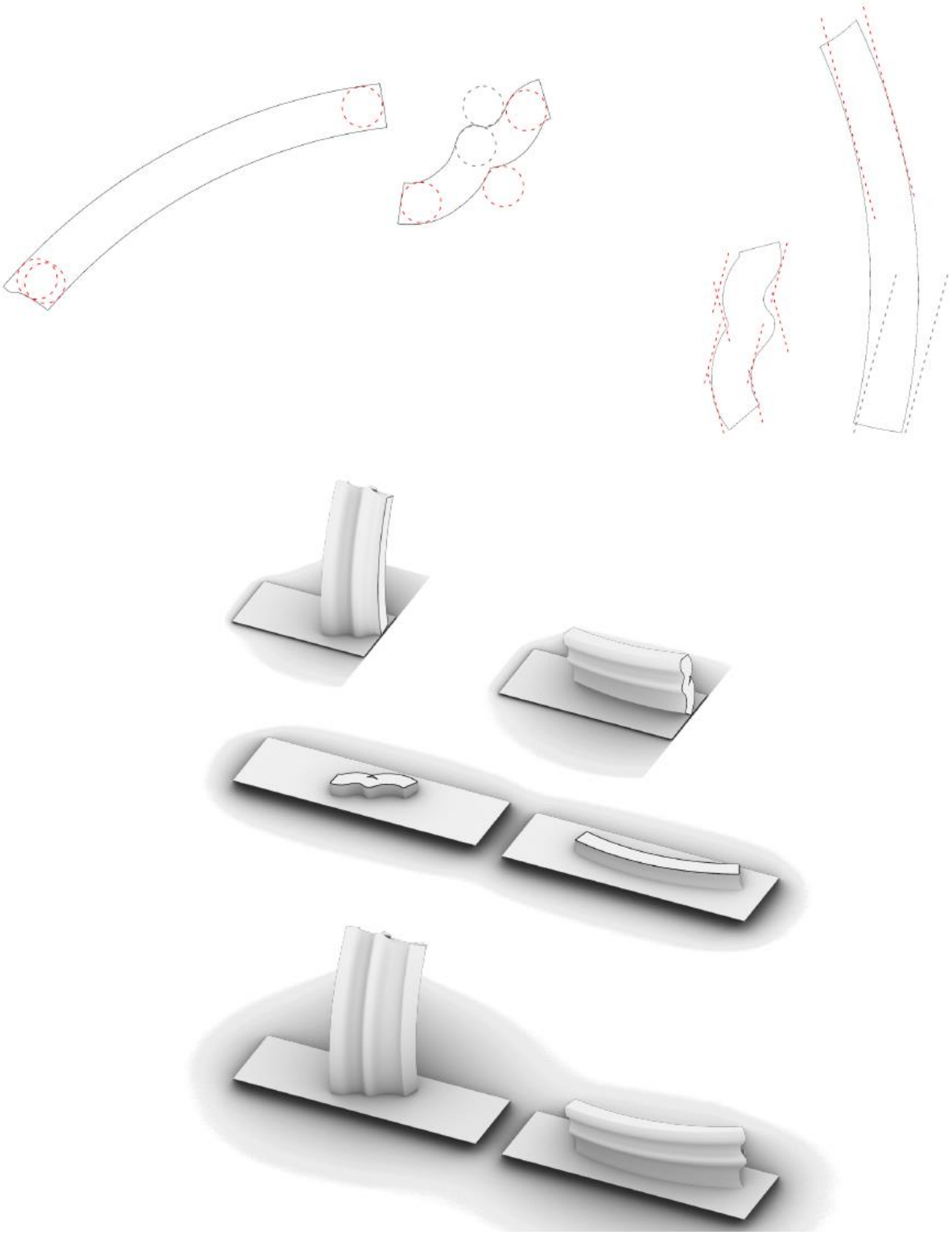

Figure 3.1 Cross-sections of a wall design are evaluated for printability

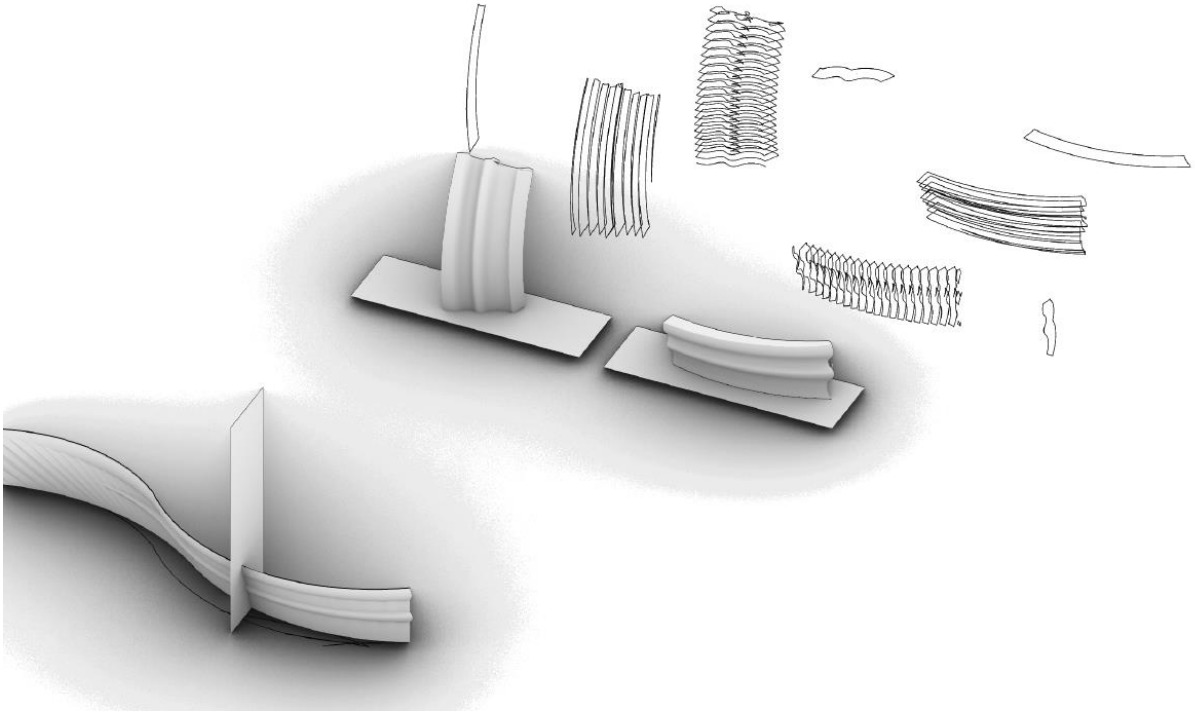

Figure 3.2 Complex geometries require evaluation of serial sections throughout the wall.

3.2.3 Print method suitability evaluation and comparisons

There are diverse DFC methods with varying degrees of technological development and readiness. However, there appears to be little evaluation or comparison between fabrication methods. It is not the authors' intent to question differences between manufacturers, but rather to compare the limitations and advantages between disparate technologies, such as comparing spray-based concrete printing to extrusion-based concrete printing or "inkjet" printing water onto cement. Existing research on DFC methods describe mechanical or material factors for individual methods. These factors are generally not compared across methods to describe best-uses, applications, or printable geometries for each technology. Comparative studies between fabrication methods are scarce with one exception. One notable study conducted a systematic review of 3DCP projects and identified differences in the typical applications and printable

geometries between in-situ fabrication and factory prefabrication. The authors also identified best use cases for different mechanical systems and fabrication environments (Huang et al., 2022). However, this study focused solely on variations within extrusion-based 3DCP. For the field to transition into routine manufacturing, there is a need for a standardized approach to evaluate fabrication processes, particularly in identifying factors that affect mechanical and material performance (Buswell et al., 2020). The RILEM DFC process classification system establishes a framework for a shared vocabulary to describe and categorize methods of shaping concrete and post-production operations. However, the authors did not include applications or printable geometries for each method; it only defines the current fabrication methods.

While case studies and manufacturer demonstrations can assist designers in providing examples of geometries and strategies that can be fabricated, they do not necessarily inform a designer if their concept or strategy can be fabricated. Most completed DFC projects are designed as showcases for the technology with heavy manufacturer support and feedback (Bos et al., 2022). While manufacturer support is critical, demonstration projects inherently avoid the limitations of the fabrication method. There is no current benchmark or sample design test that clarifies the limits and strengths of different fabrication methods. Having various fabrication methods produce the same test would objectively reveal what cannot be produced and what falls within their capacity. This would enable designers to decide which fabrication method would meet the design intent. A designer-oriented DFC toolkit should facilitate “designing for the machine” and “choosing the machine for the design”.

3.2.4 Application to landscape architecture and terrain responsive design

The previous chapter summarized the large body of research describing the material science and engineering research behind DFC technologies. In contrast, research on design and

construction implementation has received less attention (Figure 3.3). There are additional challenges in the implementation of DFC specific to landscape designers. Typical completed projects lie in the domains of architecture and engineering, such as floor slabs, columns, houses, and pedestrian bridges. Applications for landscape architecture have been limited to site furniture such as benches. DFC has primarily been used for objects that are placed on level ground like benches rather than structures that engage the terrain. One notable exception is a park in Shenzhen, China where various elements like retaining walls, sculptures, paving, and flower beds were 3D printed in concrete inside factory conditions and then transported to the site for installation (Williams, 2021). There appear to be no instances of on-site DFC within the field of landscape architecture. On site robotic concrete construction has been successfully deployed on level ground to produce small buildings, particularly houses. There are existing robotic processes and technologies for construction on unlevel or changing terrain, including drone monitoring, iterative adaptive robot control, and robot senses. With these strategies, HEAP, a mobile robot excavator, navigates and sculpts terrain with both cut and fill operations (Jud et al., 2021). Architectural applications have the advantage of a growing body of research on construction planning and processes with in-situ 3DCP (Xu et al., 2022). For landscape design, in-situ DFC involves understanding both the processes of robotic in-situ 3DCP as well as strategies for robotic construction in complex terrain. However, the development of these young technologies is ongoing and incomplete, and there is a lack of research at the intersection of these emergent technologies that could potentially impact landscape architecture (Figure 3.4).

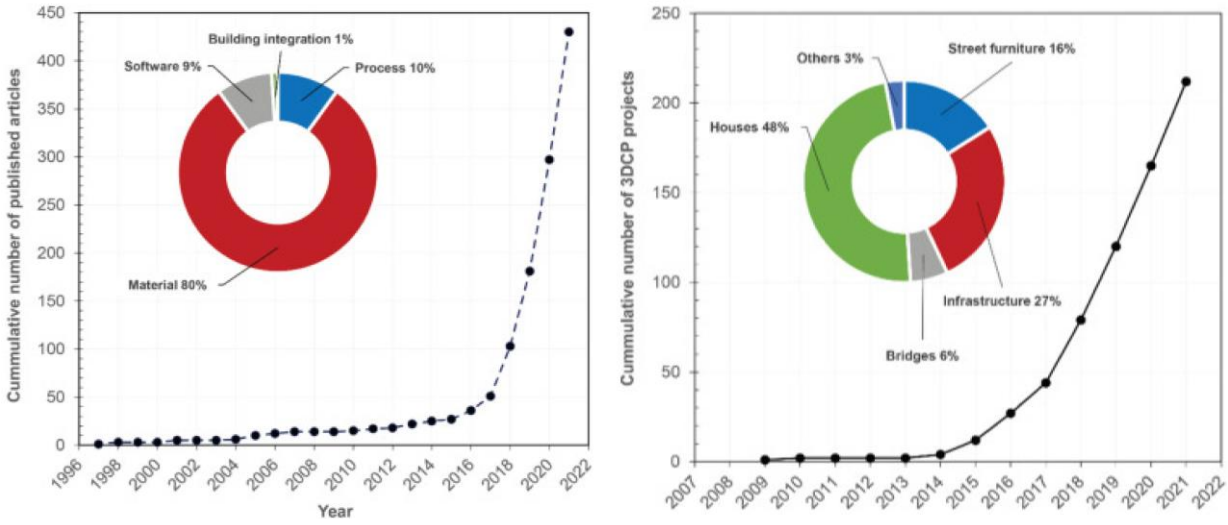

Figure 3.3 Bibliographic statistics concerning extrusion-based 3D concrete printing with the disciplines of published articles and the project type

(Strohle et al., 2023)

Figure 3.4 Diagram of research gaps that drive the study agenda

3.3 Defining terrain responsive design

Technology can be a homogenizing force, such as the spread of mass-produced site furniture without any relation to the site. On the impacts of global technology and culture, the French philosopher Paul Ricoeur observed:

> Everywhere throughout the world, one finds the same bad movie, the same slot machines, *the same plastic or aluminum atrocities* [emphasis added], the same twisting of language by propaganda.(1961)

However, as discussed in Chapter I, existing applications of DFC successfully demonstrate highly individualized complex geometries (Figure 1.2). Similarly, previous precedents demonstrate the potential of DFC to construct designs where "form follows force", reducing material use for more sustainable designs (Bhooshan et al., 2022). In response, this research investigates whether DFC can be adapted for site-specific landscape designs and in doing so possibly reduce material use. Terrain can serve as a source of data from which geometries can be generated. For instance, in the case of a retaining wall, the geometry could be adapted to accommodate not only structural loads of the terrain but also visually respond to shifts in the terrain. Precedent works such as Richard Serra's sculptures, *Shift* and *Pulitzer Piece*, exemplify this concept (Figure 3.5). These sculptures are hard lines of steel against which the imperceptible gentle rolling character of the terrain is made visible. In an interview with Hal Foster, Serra observes that land art is often a shape painted on the landscape, like Robert Smithson's *Spiral Jetty*:

> For the most part earthworks are graphic ideas imposed on the landscape. I was interested in a different penetration into the land, one that would open up the field and bring you into it bodily through movement, not just draw you in visually. The rhythm of the body

> moving through space has been the motivating source of most of my work… I didn't want to make a sign or a symbol in the landscape as earthworks do; I wanted to work with its topography… How do you cut into the land, gather it in a volume, and hold that volume? (Serra & Foster, 2018)

Figure 3.5 *Pulitzer Piece*, a sculpture inserted into the landscape to draw attention to the gentle terrain slope

Pulitzer Residence, Saint Louis. Photo Shunk-Kender. © Roy Lichtenstein Foundation (Serra & Foster, 2018)

Similarly, in landscape architecture, two dimensional symbols and shapes are often applied to landscape as a way of lending meaning and familiarity to designed spaces. But when freeform, shifting geometries can be created as easily as 2D shapes, what would be the impact on design and experience? Serra uses a contrasting element to bring about an intimate and clear perception of a terrain aspect that might go unnoticed. In doing so, he turns the terrain into the main experience for the visitor. With DFC's unique capacities for freeform geometries, designs could describe or respond to an aspect of the terrain. Walls could bulge, bend, or otherwise dance in response to any data derived from the context.

The following scenarios explore how terrain responsive design might reduce material while taking visual form from the landscape. First, attributes of the terrain are identified as data points to influence the wall geometry (Figure 3.6). Second, wall attributes are also defined as possible variables to be modulated based on terrain conditions. Case 0 describes typical construction as a baseline scenario, depicting typical retaining wall proportioning, where an entire wall is sized to meet its maximum load. Cases 1, 2 and 3 bulge and narrow in response to their location in the hill and the increasing soil loads on the wall. Case 4 takes an alternate approach where the wall radii increase and become concave in response to higher loads. In these scenarios, the wall simultaneously adapts to its varying structural loads and visually translates the terrain into a new wall form. This adaptative behavior becomes the design intent by which the fabrication method is selected.

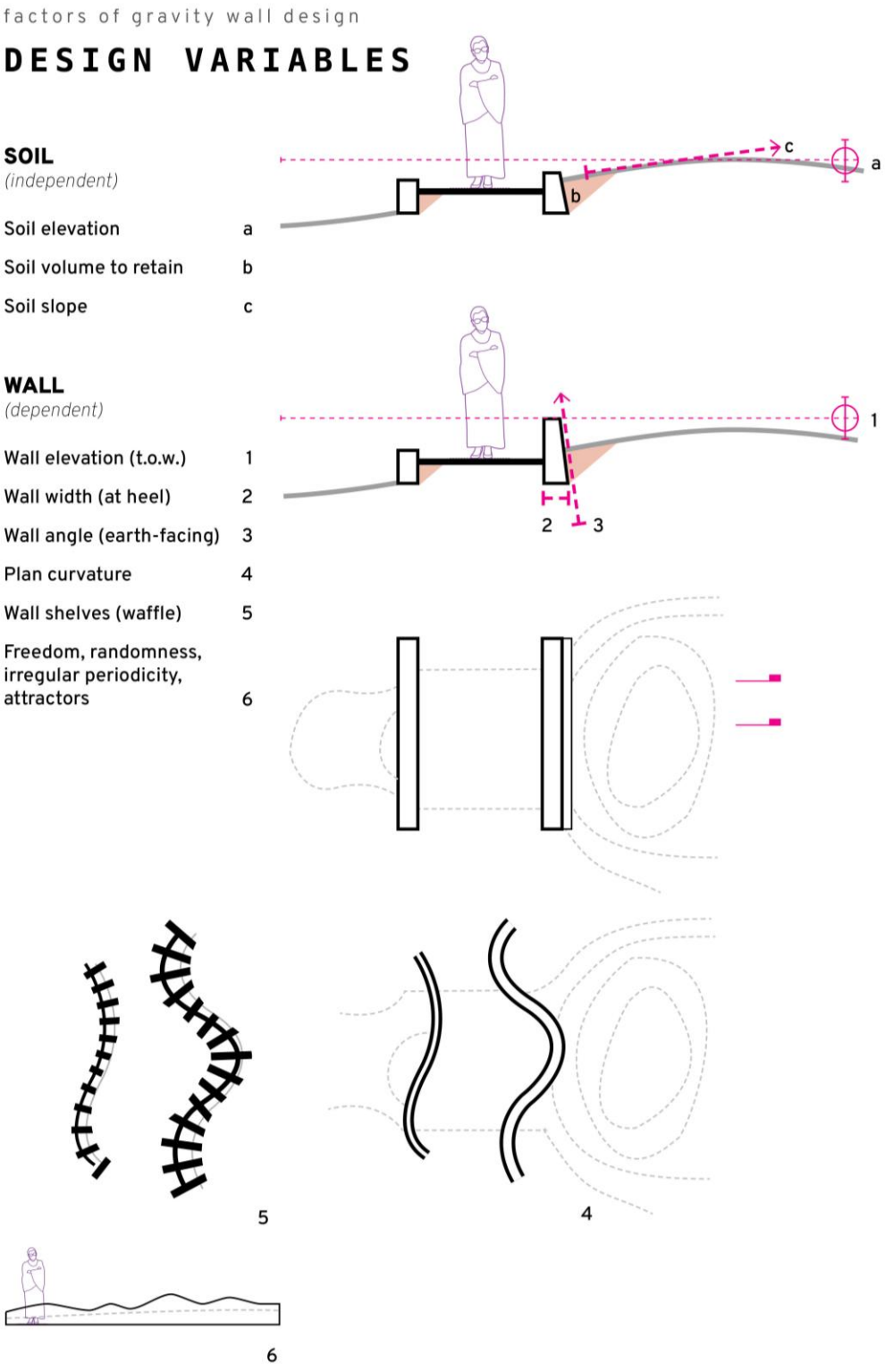

Figure 3.6 Retaining wall variables identified for material reduction

Scale figure of Ruth Bader Ginsberg courtesy of dimensions.com

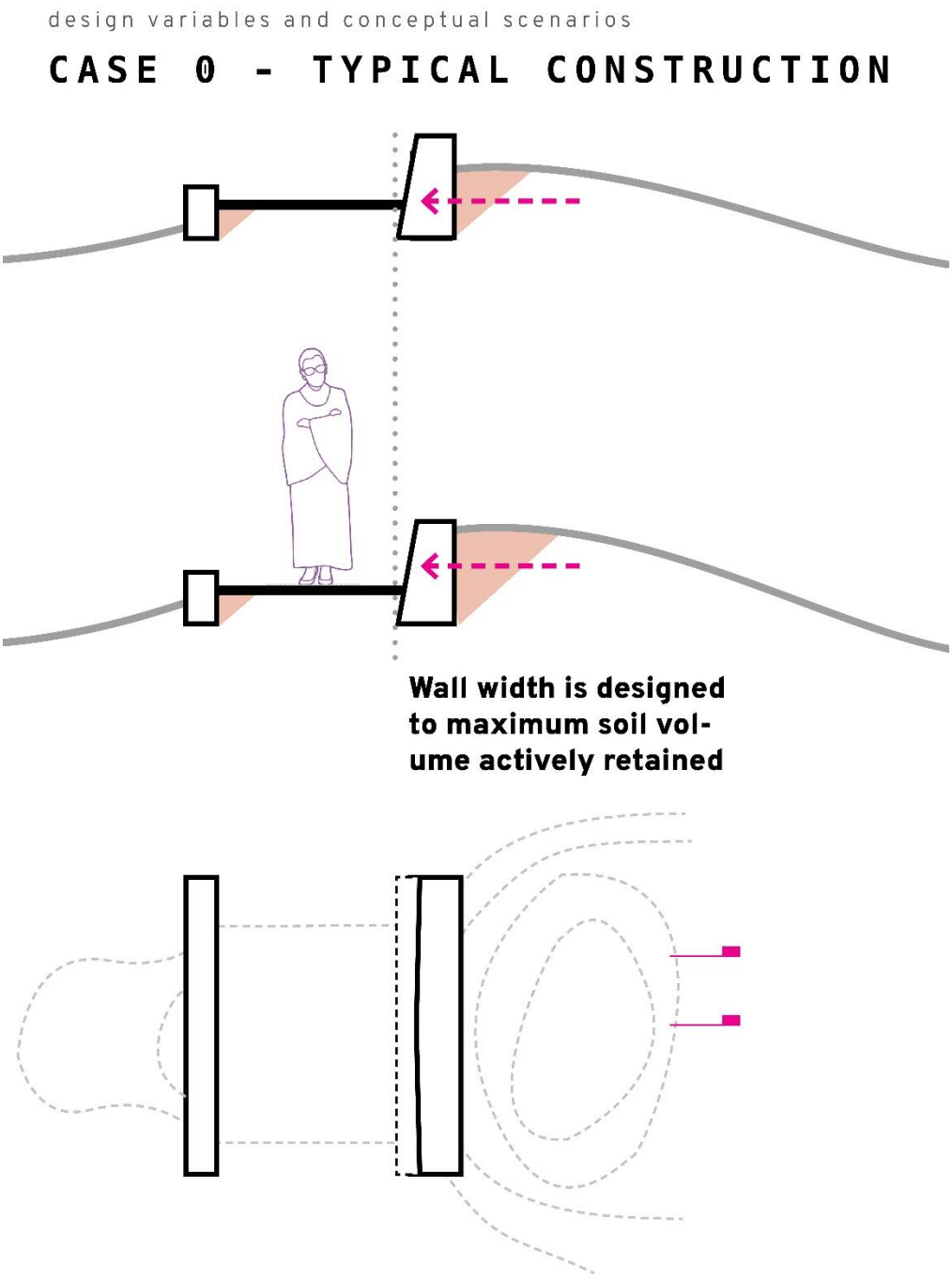

Figure 3.7 Baseline scenario where wall dimensions are consistent irrespective of location within terrain

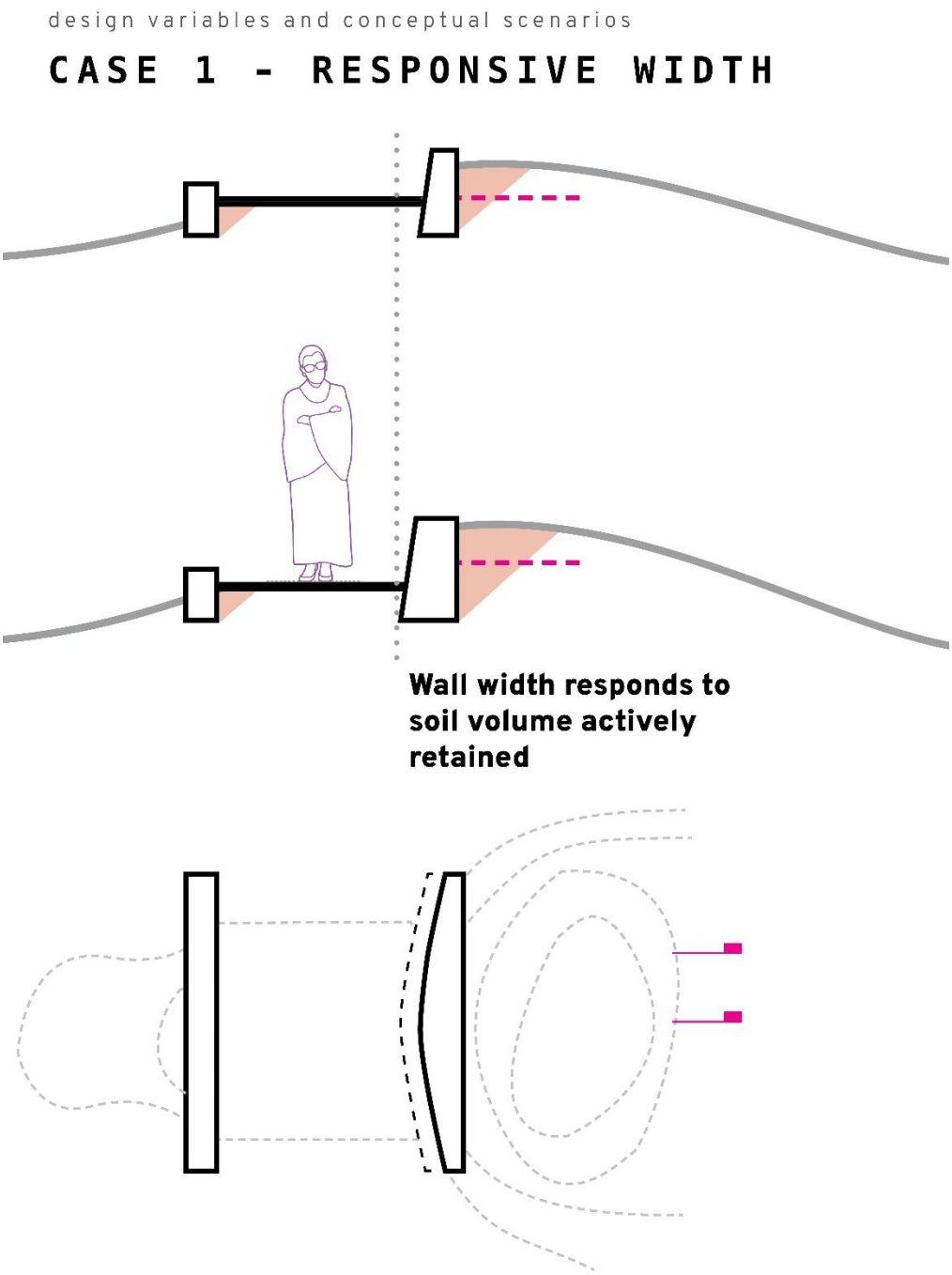

Figure 3.8 First scenario where wall width changes relative to location within terrain

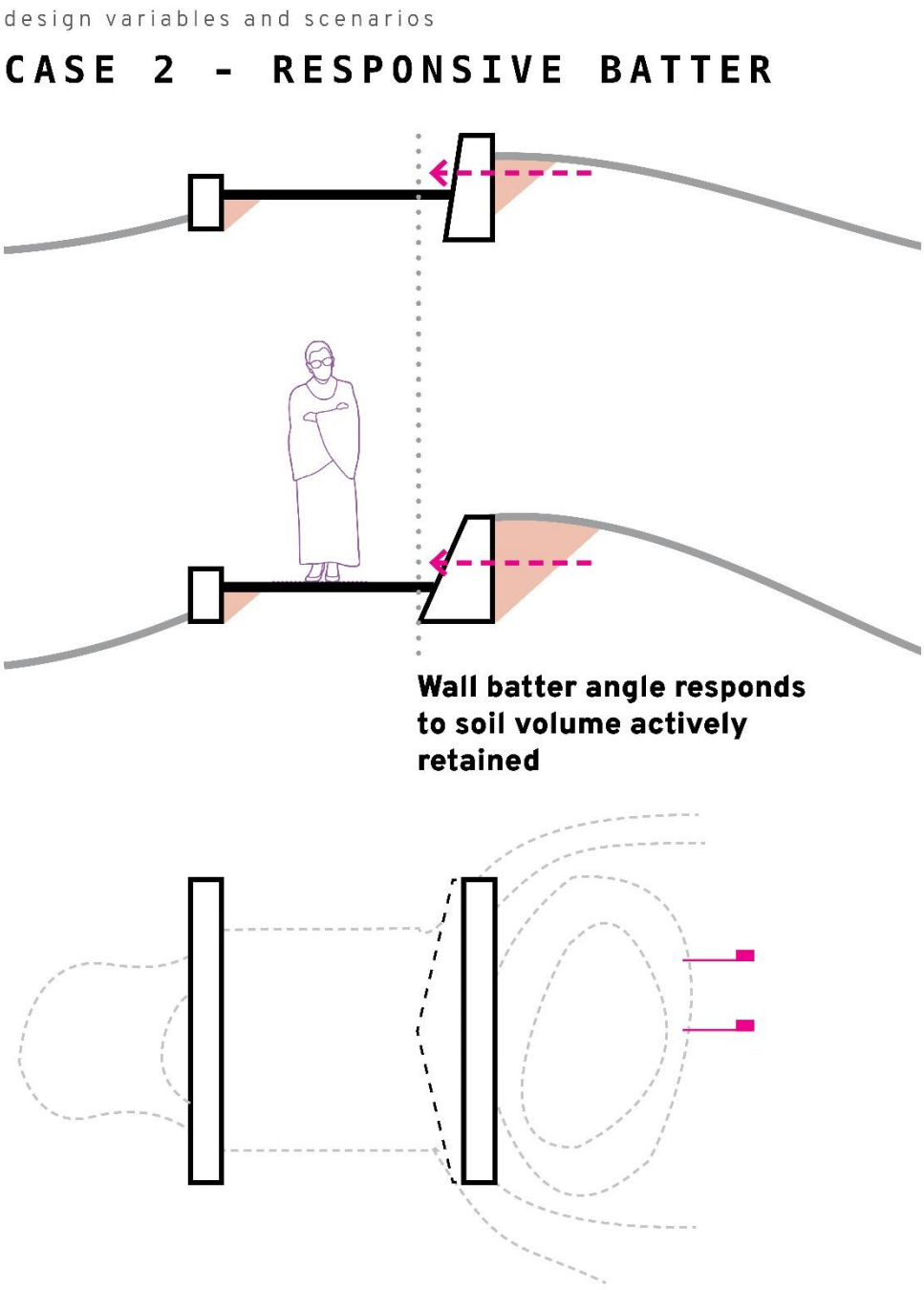

Figure 3.9 Second scenario where wall batter changes relative to location within terrain

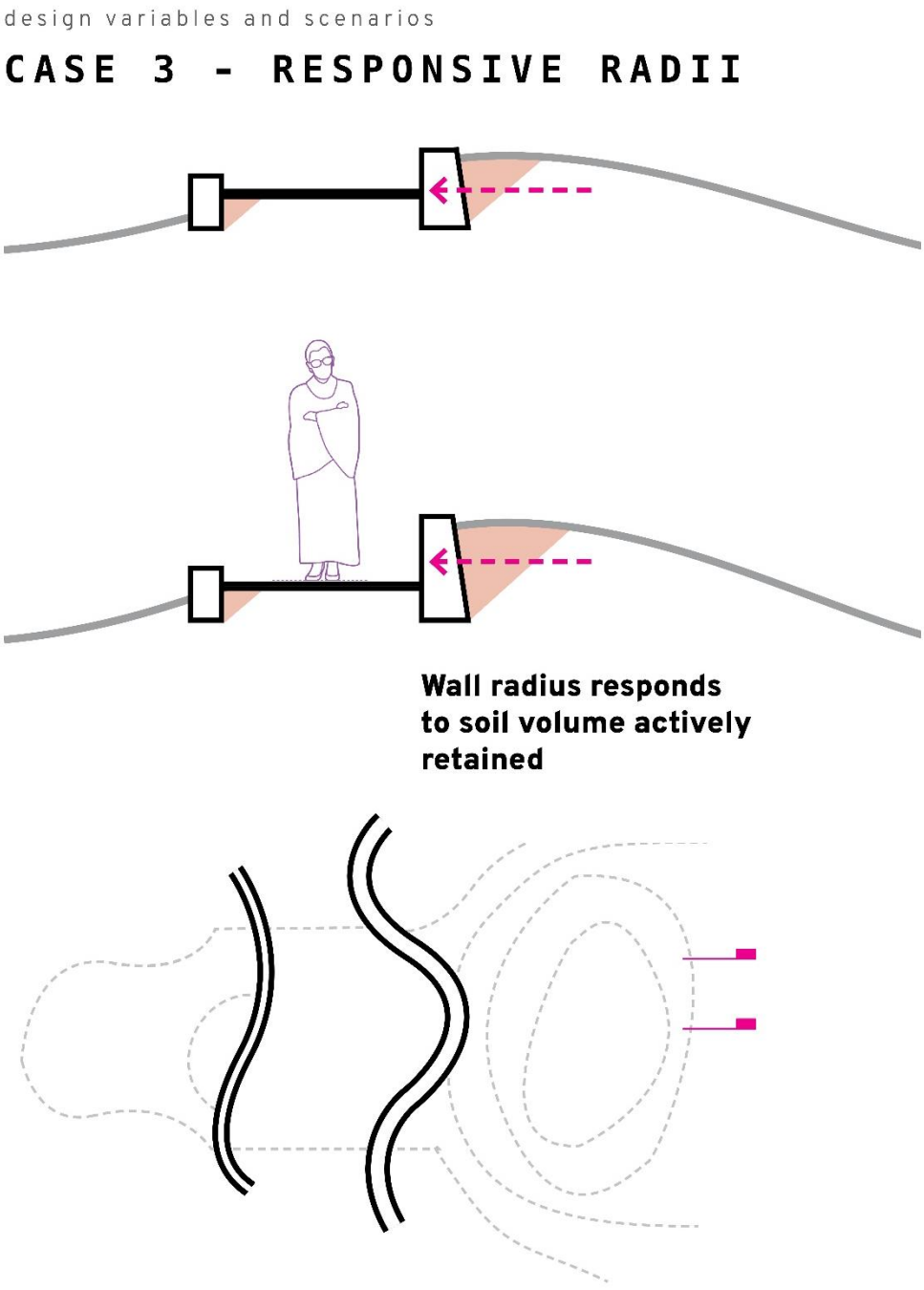

Figure 3.10 Third scenario where wall radii become more concave relative to location within terrain

3.4 Print method comparisons and selection process

This research defines a four-step process that provides a systematic approach for selecting the suitable fabrication method for a DFC retaining wall in landscape architecture:

1. Review of 27 precedent studies across 3 major DFC classifications and 17 fabrication systems (limited to publicly available data)

2. Translation of precedent studies into a framework of factors describing technology readiness to date and extent of current applications: Fabrication systems are analyzed in terms of the scale of producible objects, the presence of implementation in real-world environments with ongoing continuous use, and the production environments where technology has been deployed, such as factory conditions or construction sites.

3. Comparison of fabrication methods with regards to their relative strengths in terms of production speed, size of possible products, and geometric freedoms

4. Examination of known and unknown parameters for fabrication methods determined to be most suitable for design intent and implementation

This process describes a breadth of fabrication methods with an understanding of their current viability outside laboratory conditions. Likewise, for each fabrication method, this process identifies the attributes best suited to each method.

Table 3.1 lists the precedent projects reviewed to investigate a diverse range of fabrication methods. The fabrication systems of the precedents spanned the three major classifications of deposition-based, particle bed-based systems, and formwork-based systems. Multiple variations of a fabrication type were considered such as mechanical systems variations (3DCP with robotic arm versus 3DCP with gantry frame with 3DCP with cable systems). Material system variations within each method were also considered such as selective paste intrusion with large-scale particles and small-scale particles (Figure 3.11). Larger and smaller particles vary the compressive strength and geometric resolutions within selective paste intrusion methods as discussed in Section 2.2.2. Table 3.1 also documents each precedent study in terms

of its production environment (prefabrication or in-situ construction) and the final product type, from columns to bridges.

Table 3.1 Commercial and academic case studies referenced for systematic discussion of digital fabrication of concrete (DFC)

	Method	Environment	Case Study	Product
Extrusion Based DFC				
1.	3DCP with Robotic Arm	Factory Prefabrication	Striatus Bridge (Bhooshan et al., 2022)	Pedestrian bridge
2.	3DCP with Robotic Arm	Factory Prefabrication	Concrete Choreography (Anton et al., 2020)	Columns
3.	3DCP with Robotic Arm	Academic Experiment	(Gebhard et al., 2023)	Reinforced water tanks
4.	3DCP with Robotic Arm	Academic Experiment	(Gebhard et al., 2021)	Beams w/ various reinforcements
5.	3DCP with XYZ frame	Commercial Factory Prefabrication	(*The LivingRoom: A Freeware Learning Garden Focused on Health, Food, and Nutrition Education | ASLA 2020 Student Awards*, n.d.)	Galloway learning garden, benches and pipe stem covers (Mississippi State Univ. + Pikus3D Concrete)
6.	3DCP with Robotic Arm	In-Situ Construction	(Xu et al., 2022)	Single family house
7.	3DCP with mobile robots	In-Situ Construction	(*Minibuilders - Institute for Advanced Architecture of Cataloni*, n.d.)	Curvilinear wall
8.	3DCP with gantry frame	In-Situ Construction	US Army (Bos et al., 2022; Jagoda et al., 2020)	Military barracks
9.	3DCP with gantry frame	In-Situ Construction	US Army (Jagoda et al., 2020)	“Dragon tooth” for anti-tank defenses
10.	Shotcrete 3DCP	Academic Experiment	(Lachmayer et al., 2021)	Column capital
11.	Shotcrete 3DCP	Academic Experiment	(Hack & Kloft, 2020)	Slender curved wall
12.	Shotcrete 3DCP	Academic Experiment	(Dörrie et al., 2022)	Adaptive coastline protection, proof of concept
13.	Aerocrete (Spray) 3DCP	Academic Experiment	(Taha et al., 2019)	Freeform wall for bus shelter
14.	Cable-Based 3DCP	Academic Experiment	(Walker et al., 2023)	Proof of concept
15.	Injection 3DCP	Academic Experiment	(Hack et al., 2020)	Space frame (3D truss) modules

Table 3.1 (continued)

Particle Bed Based DFC				
16.	Selective Cement Activation	Commercial Factory Prefabrication	(*Facade - Additive Tectonics*, n.d.)	Façade module
17.	Selective Cement Activation	Academic Experiment	(Talke et al., 2019)	Proof of concept objects
18.	Selective Paste Intrusion w/ Large Particle	Academic Experiment	(Mai et al., 2021)	Proof of concept objects
19.	Selective Paste Intrusion	Academic Experiment	(Weger et al., 2020; Weger & Gehlen, 2021)	Proof of concept objects
Digital Formwork Systems				
20.	Knitted Textile Formwork	Factory Prefabrication of formwork, on-site casting	KnitCandela, (Popescu et al., 2021)	Pavilion
21.	Binder jetting sand printed formwork	Academic Experiment	(Meibodi et al., 2019)	Smart slab for DFAB House
22.	Plastic 3D Printed Formwork	Factory Prefabrication	(Burger et al., 2020)	Column
23.	Adaptive Slipform Casting	Factory Prefabrication	(Lloret-Fritschi et al., 2020)	Column, wall, canoe
24.	Digitally Tensioned Formwork	Academic Experiment	(Lloret-Fritschi et al., 2020)	Proof of concept
25.	Mesh Mould wall	Academic Experiment	(Dörfler et al., 2019; Hack & Lauer, 2014)	Wall in DFAB House, (Robotically fabricated reinforcement with manual concrete application)
26.	Clay formwork with mobile robots	Academic Experiment for In-situ construction	(Dielemans et al., 2022)	Column formwork

This precedent research was distilled into two frameworks that classify the current applications and advantages. To describe the current range of applications, each DFC method was evaluated in terms of product scale, technology implementation level and production environment (Figures 3.12, 3.13, and 3.14). Particle bed methods have been used to produce small artifacts due to their slower production rates but high geometric precision (Kloft et al., 2021b). Commercial exemptions include the manufacturers *FIT* and *at-additive tectonics*. Deposition-based DFC methods have faster production speeds and are used for large objects from columns to single-family houses (Figure 3.12).

Technologies varied widely in their level of development. Previous studies have applied NASA's technology readiness level (TRL) qualifications and similar scales to quantify the current level of technology development for 3DCP (Ma et al., 2022). Similar research has yet to be undertaken for other DFC methods. In this framework, technology readiness is simplified to describe if the DFC method has been used to create a product or structure in typical conditions with continuous use (Figure 3.13). For example, 3DCP has been used to fabricate pedestrian bridges currently in active use in urban environments (Bos et al., 2019). To date, KnitCrete has only been used for a pavilion-like structure for a museum (*KnitCandela - A Flexibly Formed Thin Concrete Shell at MUAC, Mexico City, 2018*, n.d.). Smart Dynamic Casting (digital slipforming) has been used to produce mullions, an architectural glazing product, for the DFAB demonstration house (Lloret-Fritschi et al., 2020). Other methods have been limited to proof of concepts in laboratory settings.

3DCP has been the main fabrication method used on-site with the others being predominantly used in factory conditions (Figure 3.14). However, two formwork methods have been deployed on construction sites. KnitCrete produces the formwork off-site, but the formwork

is light and easily transported. The knitted formwork is erected and cast on-site (Popescu et al., 2021). Mobile robots that print formwork in clay have likewise been studied for deployment on construction sites (Dielemans et al., 2022).

Critically, 3DCP has a long development period with publications dating back to 1997 (Pegna, 1997). For this reason, comparing 3DCP to other DFC methods is similar to comparing the abilities of a teenager to a toddler. These observations merely reflect the present state of the technologies without speculation on future increase of capacities in the realm of production scales, product applications and printing environments.

Figure 3.11 Variations within one fabrication method

(Mai et al., 2021; *Project A 02 - Additive Manufacturing in Construction TRR277*, n.d.)

Figure 3.12 Various scales of products made by DFC

(Lloret-Fritschi et al., 2020; Xu et al., 2020, 2022)

Figure 3.13 Levels of technology implementation

(Anton et al., 2020; Dörfler et al., 2019; Popescu et al., 2021)

Figure 3.14 Production environments from factory conditions to in-situ printing (Bhooshan et al., 2022; Dörfler et al., 2022; Xu et al., 2022)

After the precedent review, it was determined that evaluating formwork-based systems would not be feasible or accurate. Each formwork-based system had unique limitations too distinct from deposition-based and selective binding methods to be a fair comparison. Likewise, there were numerous methods within formwork-based systems, but few precedent projects per fabrication methods. This caused limited information for fair comparison.

The following evaluation was limited to deposition-based and particle bed systems, i.e., DFC without the use of a secondary material (Figure 3.15). Each method was plotted on an axis depicting its relative speed, design resolution and compressive strength. The term "porosity" was used to describe whether the fabrication method could print a non-continuous surface, an object with holes or gaps. Geometric accuracy and resolution are limited by layer dimensions and particle sizes for 3DCP and SCA (Buswell et al., 2018; Lowke et al., 2020). However, there is a lack of research quantifying or comparing the level of geometric accuracy for some methods. The range of geometric precision can be visually compared in Figure 3.16. Both geometric resolution and porosity would allow more design freedoms.

Production speed and compressive strength were determined to be more critical for a retaining wall, especially considering the large volume of concrete to be fabricated. Large particle printing with SPI exhibits higher compressive strengths and is more suitable than printing with smaller aggregate. SPI with large particles can exhibit compressive strengths up to 64 MPa, with loads perpendicular to layers (Mai et al., 2021). S3DCP and 3DCP similarly can reach 71 MPa and 58 MPa respectively. The higher production speeds and compressive strength led 3DCP, S3DCP, and SPI with large particle sizes to be the primary choices. However, there is more information available on the fabrication limitations of 3DCP than S3DCP and SPI.

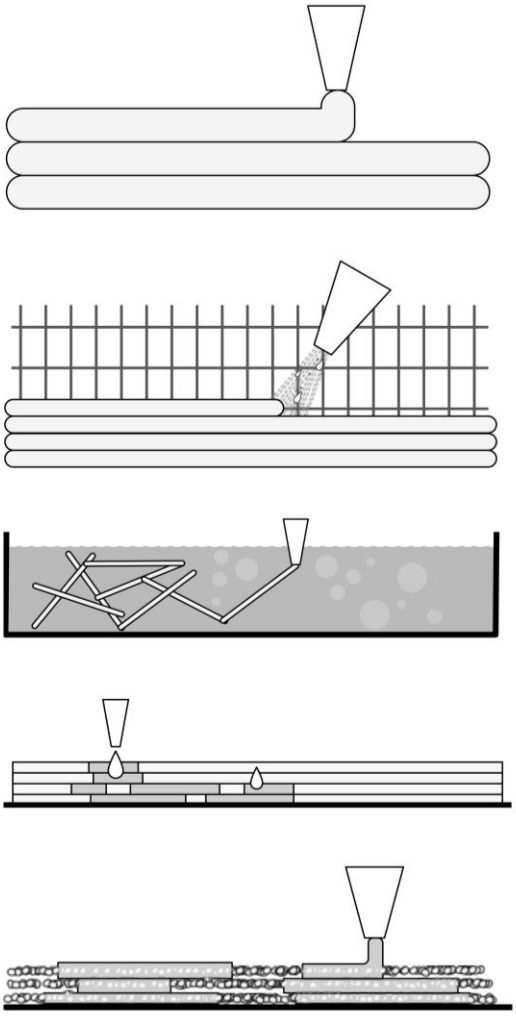

Figure 3.15 Diagram of DFC methods considered (listed from top to bottom): 3D Concrete Printing (3DCP), Spray-based 3D Concrete Printing (S3DCP), Injection-based 3D Concrete Printing (I3DCP), Selective Cement Activation (SCA) and Selective Paste Intrusion (SPI)

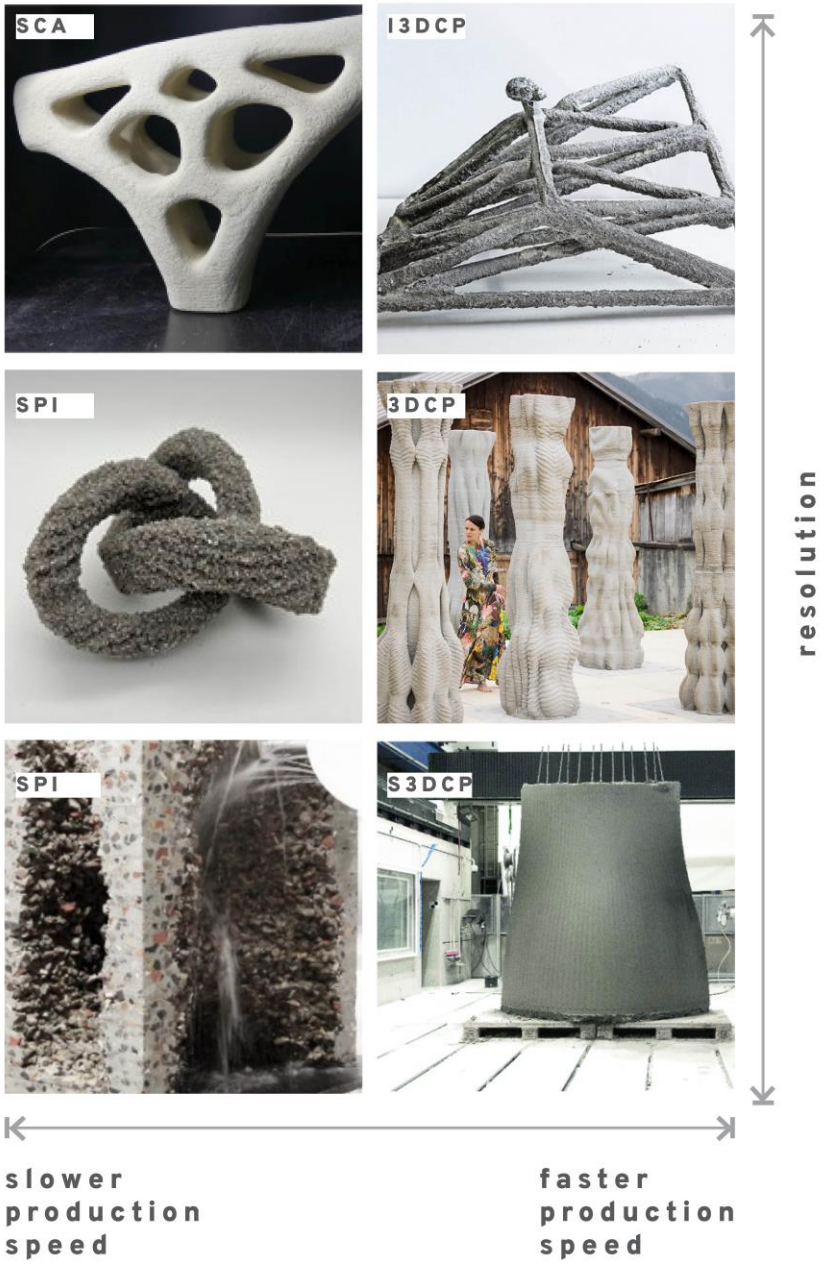

Figure 3.16 Range of geometric precision

(Anton et al., 2020; Hack et al., 2020; Hack & Kloft, 2020; Mai et al., 2021; *Project A 01 - Additive Manufacturing in Construction TRR277*, n.d.; *Project A 02 - Additive Manufacturing in Construction TRR277*, n.d.)

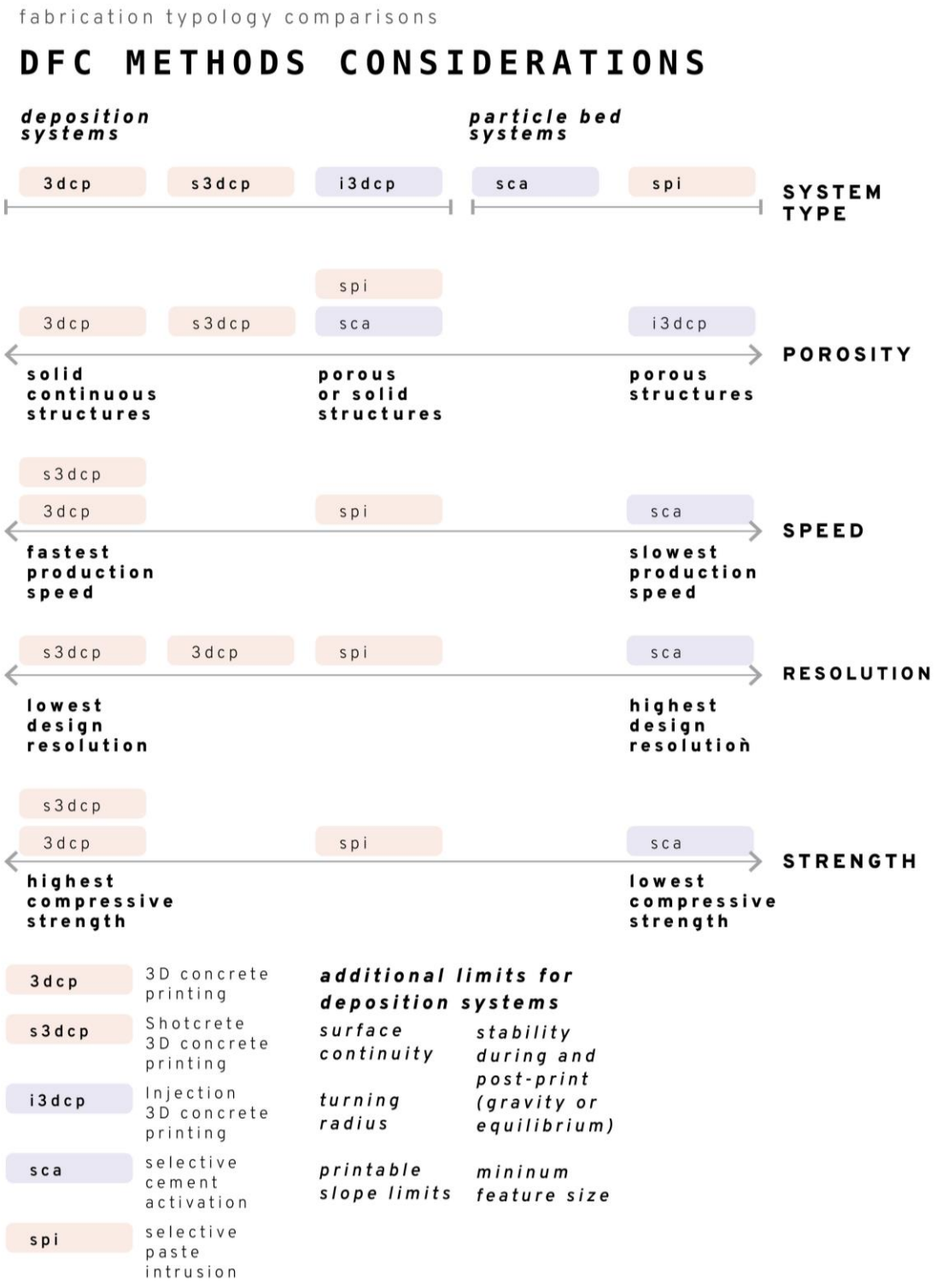

Figure 3.17 Relative advantages of each digital concrete fabrication method considered

Based on the literature review and precedent studies, the following fabrication parameters were selected for further analysis to establish limitations for each of the selected fabrication method:

1. Production environment
2. Print volume
3. Minimum feature size
4. Surface slope
5. Perimeter lengths (open-time or cycle time)
6. Surface continuity
7. Self-Intersection (whether print material can overlap or intersect in one area)

3.4.1 Production environment

To date, S3DCP and SPI have not been deployed outside of indoor factory or laboratory conditions. Uncontrolled climate conditions do impose restrictions on 3DCP. Environmental conditions with higher evaporative rates can cause decreases in the interlayer bonding strength up to 35% percent compared to an indoor condition (Moelich et al., 2022). On-site 3DCP tends to have simpler geometries with shallow or no slopes to reduce the likelihood of cracking and subsequent rework challenges (Huang et al., 2022). However, there are examples of in-situ printing with sloped surfaces (Figure 3.18). The US military experiment, *B-Hut*, has undulating thin walls that might gain rigidity from their geometry. The US military also uses 3DCP for pyramidal “dragon teeth” for tank determents. The R&Drone laboratory is a commercial building in Dubai that was printed in-situ with sloped wall faces. In the case of a desert climate, a tent structure was used to control the climate for printing (*CyBe Construction 3D Prints Concrete Drone Laboratory On-Site in Dubai - 3D Printing Industry*, n.d.).

Figure 3.18 Examples of sloped surfaces in military experiments (precedent studies #8 and #9) with commercial example by CyBe Construction

(Bos et al., 2022; Jagoda et al., 2020; *R&Drone Laboratory — CyBe Construction*, n.d.)

3.4.2 Print volume

Print volume is critical in that it limits the maximum dimensions of a printed object and thus requires splicing of larger objects. However, print volume is affected by individual manufacturers and laboratories rather than a total reflection of physical limitations. Large particle SPI has demonstrated to produce a 1m by 1m by 1m cubic object (Mai et al., 2021). It is not necessarily limited to that print volume, considering academic studies do not need larger print volumes for their experiments. However, further research is needed to investigate further physical limitations on increasing print volume for SPI.

Another consideration is the effect of the mechanical system on the shape of the print volume. Both robotic arms and gantry (XYZ) frames are limited to the volume of space in which they can extend their nozzle or other material applicator. Figure 3.19 depicts two different print volume shapes. A mobile printer can have a donut shaped print volume describing the volume the robotic arm can extend to. In the second example, a robotic arm is attached to a gantry frame that defines a rectangular volume in which the machine can print. The examples provided are a 3DCP and S3DCP setup respectively but neither method is limited to a particular set-up.

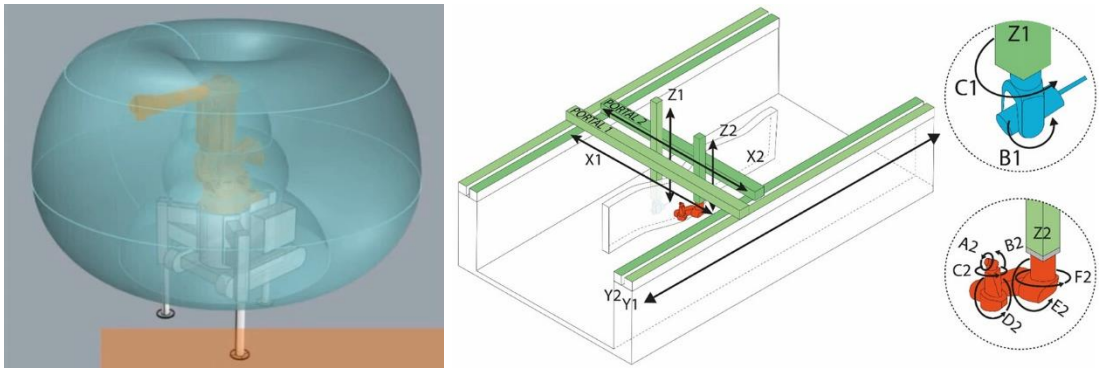

Figure 3.19 Varying print volume forms

(*CyBe RC (Robot Crawler) — CyBe Construction*, n.d.; Kloft, Krauss, et al., 2020)

3.4.3 Minimum feature size

The size of the minimum printable features for 3DCP is defined by the limits of the mechanical system and material application (Buswell et al., 2018). A large strand width can prevent smaller geometries from being printed as well as require more gradual curvatures to prevent tearing of the material (Roussel, 2018). A mechanical system with a large amount of inertia or otherwise limited mobility can require similar limitations. Layer or strand dimensions across DFC methods act as a "pixel size" where geometric details similar than the layer size cannot be printed and will be approximated similar to a reduction in image resolution. For 3DCP, the turning radius is used as a quantifiable metric to describe unfeasible geometries (Baniasadi, 2021). The machine can not apply material at tight curvatures below the minimum turning radius.

For S3DCP and SPI, further research is needed to establish a metric for describing geometric limitations. Both are similarly restricted by their layer dimensions; neither method can print details smaller than their layer size or particle size. For S3DCP, it is unclear to date what geometric limitations exist for adequate, consistent, spray application of concrete without under or overspray. Generally, S3DCP has been used for large geometries without small details as seen in Figure 3.16. Research on other particle bed systems such as SCA has measured the geometric precision and fidelity as a tolerance (+/- mm) difference in width or height. However, it is worth considering layer curvatures and turning radii as an adaptable, descriptive metric for S3DCP and SPI. Evaluating geometry for minimum radii identifies tight bends and small geometries (Figure 3.21). For example, the geometry curvature must be at least larger than the strand width of the print material (Figure 3.20). A higher minimum radius would describe more gradual and large geometries, reducing small details and tight corners.

Figure 3.20 Examples of layer sizes and layer curvatures

(Anton et al., 2020; Lachmayer et al., 2021; Mai et al., 2021)

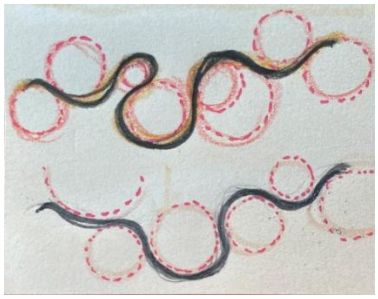

Figure 3.21 High versus low curvature as an approximation for minimum feature size

3.4.4 Surface Slope

Deposition-based systems like 3DCP and S3DCP are limited in their printable slopes due to the need for the concrete to be self-supporting. This results in limited “2.5D” geometry with no undercuts or overhangs compared to the freeform geometry produced by particle bed systems

that fully support the print object as it cures (Mai et al., 2021). Slope is not a consideration for SPI other than typical considerations for the structural integrity of an overhang. For 3DCP with a fixed level printing plane, twenty and thirty degrees have been the maximum slope for precedent studies #2 and #5. Higher slopes have been demonstrated by inclines of the printing plane for 3DCP and S3DCP (Figure 3.22). The printing plane is incrementally angled which maintains contact between layers. An overhang with a fixed printing plane is created by stepping the layers outward which decreases the surface contact between layers and limits the plausible stable slope (Carneau et al., 2020; Kloft & Hack, n.d.).

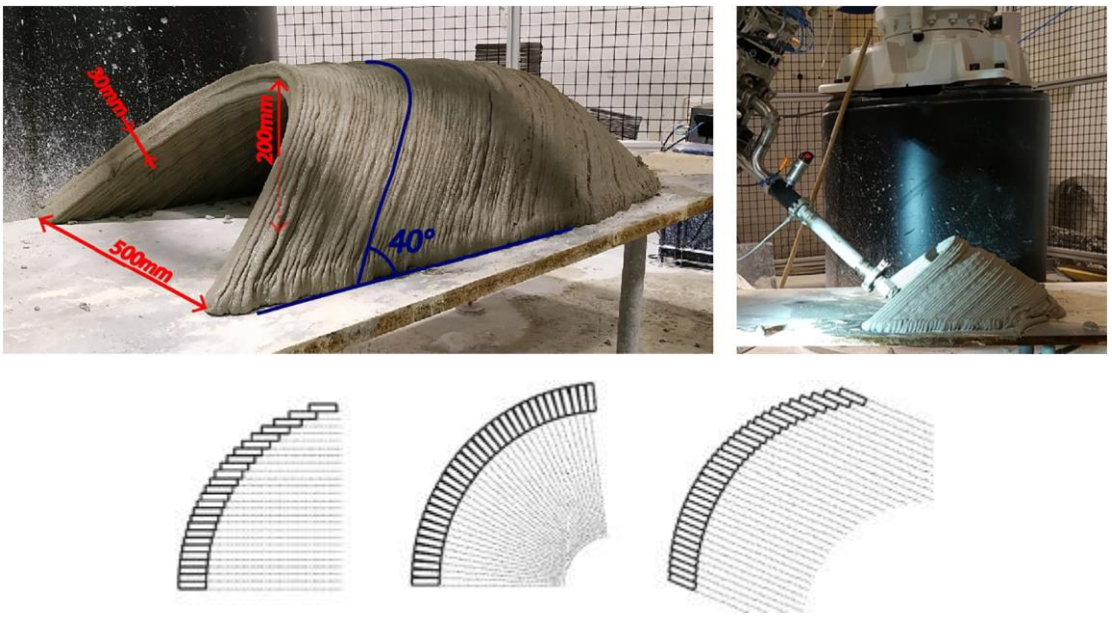

Figure 3.22 Inclined plane printing strategies

(Carneau et al., 2020)

3.4.5 Perimeter lengths

3DCP has a narrow “rheological window” in which the material is printable without deforming or forming cold joints (Roussel, 2018). The question of how much material and how

long of a layer length can be printed in a single layer is highly dependent on mix design and print speed. Long layer lengths can be challenging to print for the risk of time delays between layers and the resulting effect on bonding strength as depicted in Figure 3.23 (Babafemi et al., 2021; Roussel, 2018; Tay et al., 2018). Rheological challenges dictate that mix design and print speed should be adapted to each product and fabrication process (Roussel, 2018). This creates challenges in identifying general guidelines for designers. Instead, this research relies on existing literature, sample manufacturers and laboratories to provide typical examples. The following are various representations of intolerable time delays or concrete setting times compared to the print speed of the fabrication method.

- For S3DCP, a time delay of 15 min between layers did affect flexural strength parallel to the layer orientation (Kloft, Krauss, et al., 2020). The print speed was 6 m/min with an 18.6mm by 140-149mm layer cross-section. This research established longer tolerances for time delays for S3DCP than 3DCP but did not define the maximum delay time for S3DCP.

- A review of four interlayer bonding experiments found lower tensile strength for 3DCP with a time delay of 5 minutes between layers (Babafemi et al., 2021).

- 3DCP print speeds and layer dimensions vary widely. A review of eight 3DCP case studies found layer dimensions from 200 to 2000 mm^2 and print speeds from 50 to 250mm/s.

- The CyBe Robot Crawler, a mobile 3DCP set-up with a robotic arm can print 500 mm/sec with material setting between 3-5 minutes. Layer heights range from 10mm to 20mm depending on the layer width of 40/35mm (CyBe Construction, 2022). The CyBe mortar only needs 5 seconds to print onto the previous layer (*CyBe Mortar — CyBe Construction*, n.d.).

- For large particle SPI, an object that printed in 4 minutes per layer maintained comparable strength to traditional concrete (Mai et al., 2021). Particle bed systems do not rapidly harden like 3DCP, thus cold joints are not as large of a concern.

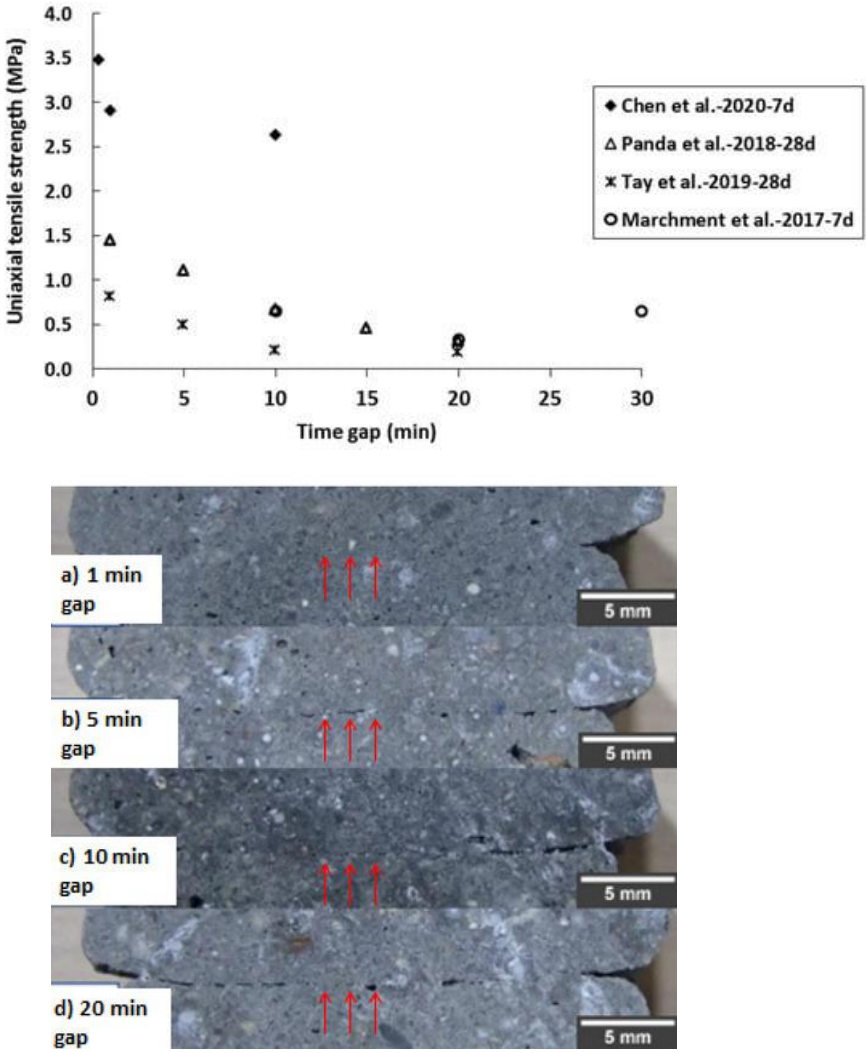

Figure 3.23 Effect of time delays between layers

(Babafemi et al., 2021; Tay et al., 2018)

3.4.6 Surface Continuity and self-intersection

Particle bed systems can start and stop printing, allowing for voids in the printed object. 3DCP is generally deployed as a continuous spiral of printed material that does not intersect itself. S3DCP is also applied continuously without interruption. Unlike 3DCP, the tool path for S3DCP can overlap material to ensure coverage. Likewise, there is ongoing research on expanding the ability of S3DCP to start and stop printing without overspray and excess material.

Table 3.2 Parameter comparison for 3DCP, S3DCP and SPI

Parameters	*3D Concrete Printing*	*Spray-Based 3D Concrete Printing*	*Selective Paste Intrusion*
Production Environment	Deployed in factory conditions with few geometric limitations but has more restrictive limitations on-site such as surface slope limits	Confined to laboratory conditions to date	Confined to laboratory conditions to date
Print volume	Dependent on manufacturer	Dependent on laboratory	Dependent on manufacturer, typically used for smaller objects than 3DCP/ S3DCP
Minimum feature size and design resolution	Defined by turning radii and layer dimensions; resolution tends to be lower than particle bed systems.	Defined by layer dimensions with further research needed to further measure and describe geometric limitations: Has not been demonstrated to produce smaller-scale geometric details to date.	Has been demonstrated to produce smaller-scale geometric details with the particle size of the aggregate affecting scale of produced geometries; Further research is needed to describe and measure minimum feature size.
Maximum Slope	Dependent on manufacturer but 30 degrees is typical for a fixed printing plane. Also, slope is highly limited in outdoor environments.	Has been demonstrated up to with inclined print planes.	Not applicable, printed object is fully supported while in production, so slopes are a nonissue.

Table 3.2 (continued)

Parameters	*3D Concrete Printing*	*Spray-Based 3D Concrete Printing*	*Selective Paste Intrusion*
Layer Length	Highly dependent on manufacturer, print speed and mix design.	Further research is needed, but S3DCP is less susceptible to cold joints which is the primary concern with layer lengths.	Further research is need on time-related factors for paste penetration. Current research is limited to the yield stress of the mix design rather than quantity of material possible to deposit before time affects material bonding. May be noncritical for SPI with its longer curing times compared to 3DCP.
*Surface Continui*ty	Objects are printed in continuous spiral without interruption	S3DCP may be able to start and stop printing based on current research, however there are issues with overspray and keeping openings clear of excess material.	Designs can be as porous as desired. Printed material is fully supported while wet so structural integrity in final fully cured state is the primary limitation.
Self-Intersection	Each layer is generally a continuous loop, without intersections.	S3DCP material can overlap and its often intentionally printed with overlapping layers for coverage.	Not applicable with system of with layered beds of aggregate.

3.5 Retaining wall considerations and variables

A major consideration for this research is fully utilizing the advantages of the fabrication method while respecting its current limitations. This study assumes traditional excavation and backfill processes as well as typical drainage systems behind the wall. The major evaluation

metric for the study is minimizing material use, rather than attempting to subjectively measure aesthetic qualities. The design intent of a terrain responsive retaining wall was analyzed for opportunities to adapt to the capacities to the fabrication method. These considerations are diagrammed in Figure 3.24.

As discussed in the literature review, reinforcing 3DCP can be challenging due to the fast curing times. There is ongoing research on various reinforcement strategies for DFC, such as incorporating wire arc additive manufacturing to digitally fabricate steel reinforcement for S3DCP and SPI. However, this research is still limited by the high welding temperatures and required cooling time for the robotically welded product. Section 2.3 describes a multi-step labor intensive process for reinforcing a 3DCP trench foundation. Thus, this study focuses on designing retaining walls without the need for traditional reinforcement labor. That consideration eliminates the possibility of designing cantilever retaining walls. This research focuses on retaining walls over other slope stabilization strategies.

For 3DCP, objects are printed as hollow shells. The inner fill of the wall is a major consideration. This study assumes the wall will be filled with cast-in-place concrete after the outer wall surface is printed. An alternate approach would begin to use the printed shell as a crenellated 3D pattern to form some of the inner fill of the wall. Other possibilities could include filling the wall with other materials such as gravel aggregate or recycled construction waste or designing a shelf-like retaining wall with no inner fill. There are many potential variations of a retaining wall that could be explored through DFC with just considering wall type and wall fill.

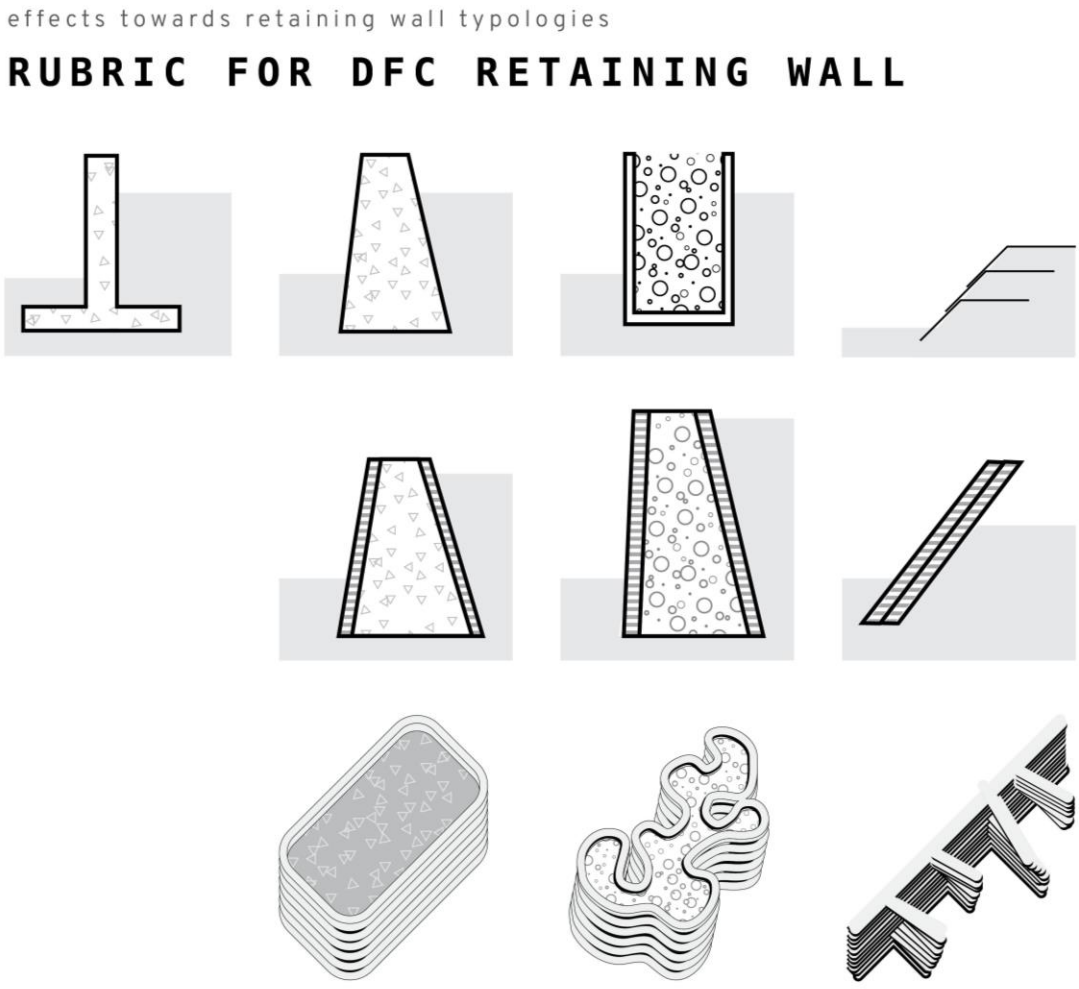

Figure 3.24 Initial considerations for a digitally fabricated concrete retaining wall

Exploring DFC as a means of site-specific design or sustainability is greatly aided by easing the implementation challenges of non-expert designers. This research proposes an interactive design experience as an alternative to the limitations of a case study approach. This would provide designers with a means to explore own solutions and ideas for DFC while visually discovering the impacts of the fabrication methods. Imagining new uses for DFC in landscape architecture can reflect theoretical and conceptual questions in the discipline, for example bringing new light to questions of site specificity and landform experiences. This chapter proposed a process for selecting the fabrication method through reviewing technology readiness and physical strengths of each technology. The fabrication parameters were reviewed to find opportunities for DFC innovations within the typology of a retaining wall. This formed a new design intent and collection of fabrication parameters used in the following design toolkit and demonstration.

CHAPTER IV

METHODOLOGY: PARAMETRIC SCRIPTING APPLIED TO AN INTERACTIVE DESIGN TOOLKIT FOR AESTHETICS, STRUCTURE, AND FABRICATION

4.1 Introduction

The previous chapter established the research agenda for creating an interactive design environment where users can iterate solutions to aesthetic, structural, and fabrication requirements. The design toolkit is focused on the design of a 3DCP gravity retaining wall. This chapter describes the user experience and technical processes underpinning the interactive design environment. The design environment is a toolkit consisting of modular scripts that can utilize any terrain and any intended path and can give live design feedback. Updates in landform and path are allowed at all phases of the user's design process within the toolkit. The toolkit analyzes soil volume actively retained. In response, users can iteratively test different ratios to relate the wall proportions to the soil loads on the retaining wall. The toolkit provides immediate structural feedback based on rules of thumb, allowing for quick risk identification as a precursor to more time-consuming rigorous structural analysis further down the project timeline. Similarly, the toolkit provides immediate printability feedback to designs as they are generated, supplementing slower time-consuming manufacturer communications on feasibility. The toolkit is organized into modules for different process phases that can be reused outside the context of designing a 3DCP gravity wall. Users can use the modules individually or in sync with the entire toolkit. Lastly, the toolkit provides live visual previews of wall geometry, structural risks, printability

concerns, as well as exportable data and geometries for use outside of the toolkit. The goals identified in the previous section are translated into these objectives:

1. Generate terrain responsive designs that provide opportunities for reductions in concrete usage.
    a. Create a geometric language from material and structural constraints as well as generate geometries that are influenced by the context, in this case, the landform.
2. Allow design processes to shift from a traditional preconception to exploratory approaches.
    a. Design a tool to rapidly explore options for meeting aesthetic, structural and fabrication requirements. Instead of requiring a designer to preconceive a solution that fulfills all the requirements through typical design processes, the toolkit serves as an environment to discover plausible geometries.

The first objective is met by analyzing the terrain conditions and then allowing users to design geometric responses to that terrain data. The second objective requires prioritizing rapid processes that allow for easy iteration rather than resource-intensive accurate computations. Designed artifacts will receive more thorough structural and manufacturer reviews further in the design-fabrication process. The intent of this toolkit is to facilitate rapid generation of designs that can be further analyzed structurally and by manufacturers, saving time in the design process. The toolkit is developed using Grasshopper, a parametric scripting plug-in for the modeling software Rhinoceros (*Grasshopper - Algorithmic Modeling for Rhino*, n.d.). Grasshopper allows users without programming experience to create algorithms that generate forms and designs. By utilizing Grasshopper, designers can create flexible and customizable design solutions that can be easily modified and optimized based on various criteria and constraints.

4.2 Preparation of inputs

This toolkit is designed to generate a multi-segment retaining wall for a walking path with varying surface elevations. Only non-surcharged gravity retaining walls can be designed. The structural calculations employed in this toolkit are not applicable to surcharged walls where the soil elevation is higher than the top of wall elevations. This toolkit cannot accommodate a flat walking path with no elevation change nor create a single continuous retaining wall with no vertical seams. The script can utilize diverse path geometries. However, path geometry should not contain tight kinks or corners. To overcome this limitation, square corners can be divided into two separate single lines, or a fillet radius can be employed. The toolkit was designed using two test scenarios:

1. the amphitheater path and retaining walls at Mississippi State University with tight curvatures in the path and changing path elevations
2. a fictionalized serpentine wall with gradual concave and convex bends

The amphitheater complex serves as the primary test subject. The fictional wall is utilized exclusively to test and to describe the script validity for geometric and terrain conditions not present in the amphitheater. It is important to note that the toolkit is designed only for numeric data and geometries using metric units.

4.3 Toolkit phases and modules

The toolkit processes terrain conditions into retaining walls in four major process phases:

1. Initial Conditions: This phase involves an initial module where users input data on terrain conditions, desired wall conditions, and material properties.
2. Terrain Analysis: Modules process the user's terrain, path, and wall conditions to determine the soil loads acting on the retaining walls to be designed.

3. Form Generation: Modules translate soil loads into geometries with adjustable proportions and other aesthetic decisions throughout the retaining wall.
4. Structural Evaluation: Modules rapidly test the retaining wall against “rule of thumb” structural formulas, providing live design feedback.
5. Printability Evaluation: Modules test for possible constructability issues during the design process, such as self-intersection, layer lengths, continuity, turning radii, and printable slopes.
6. Geometry and Data Export: Modules export the wall design, its parameters, and data to convenient file formats for use outside of the Grasshopper script.
7. Each phase has multiple color-coded modules in the Grasshopper script for ease of use and navigation. Each module is identified by labels that are used across the toolkit and this document (Figure 4.1 and Table 4.1).

Table 4.1 All toolkit modules with identifier and short functional descriptions

1 - Initial Conditions – White Modules
1.1 - Initial terrain and path conditions
1.2 - Frost depth and base elevation parameters
1.3 - Wall attributes for segmentation
1.4 - Soil and concrete material data
1.5 - Determining wall direction versus soil direction
2 - Terrain Analysis – Green Modules
2.1 - Creating preview of path excavations for unaltered terrains
2.2 - Accommodating frost depth
2.3 - Determining segmentation of path for multiple printed walls
2.4 - Generating a series of elevations for leveled bases
2.5 - Determining respective base elevation for each wall
2.6 - Determining actively retained soil volume for each wall

Table 4.1 (continued)

3 - Form Generation – Blue Modules
3.1 - Subdividing each wall and respective retained soil volume into sub-pieces for more detailed analysis
3.2 - Generating points along walls for cross section design
3.3 - Assigning retained soil volumes to each cross-section point
3.4 - Generating heights of each cross sections relative to soil elevation and as a ratio to sub-piece retained soil volume
3.5 - Generating wall width of cross sections as a ratio to sub-piece retained soil volume
3.6 - Generating toe batter of cross sections as a ratio to sub-piece retained soil volume
3.7 - Generating front toe batter of cross sections as a ratio to sub-piece retained soil volume
3.8 - Drawing random cross section points along each wall to protrude or subside a distance in proportion to the retained soil volume of the sub-piece
3.9 - Generating cross section lines that describe front and back sloped faces
3.10 - Generating cross section lines for individual wall starting shape to match neighboring wall ending shape.
3.11 - Generating solid wall forms from cross section lines.
3.12 - Generating hollow wall forms from cross section lines.
4 - Structural Evaluation – Yellow Modules
4.1 - Determining wall height variables
4.2 - Analyzing wall base to generate necessary variables for structural evaluation
4.3 - Preparing locations to display text notifications of structural risks and issues
4.4 - Calculating lateral soil pressure
4.5 - Calculating concrete wall variables by each sub-piece: centroid, volume, and weight
4.6 - Calculating total concrete usage for whole path and each wall segment
4.7 - Determining supportive soil volume, then calculating variables by each sub-piece: centroid, volume, and weight
4.8 - Determining weighted center of gravity between concrete wall and supportive soil volume by sub-piece
4.9 - Generating point where lateral pressure acts and finding the moment arm for lateral pressure
4.10 - Graphically generating gravity force, lateral force, and resultant force.
4.11 - Evaluating the intersection of the resultant force with the wall base.
4.12 - Finding eccentricity of each wall sub-piece (distance of resultant force base point to base centerline)
4.13 - Evaluating overturning risk ratio
4.14 - Evaluating sliding risk ratio
4.15 - Evaluating crushing risk against soil bearing capacity

Table 4.1 (continued)

5 - Printability Evaluation – Purple Modules
5.1 - Generating layer contours from wall geometries
5.2 - Checking layer contours for continuity
5.3 - Checking layer contours for self-intersection
5.4 - Checking layer contours to be within bounds of minimum and maximum layer perimeter length
5.5 - Evaluating turning radii in layer contours to be above minimum turning radius.
5.6 - Evaluating slopes of printed surfaces
5.7 - Automatic evaluation of rectangular print volumes
5.8 - Manual evaluation of non-rectangular print volumes and on-site robot station points
6 - Geometry and Data Export – Orange Modules
6.0 - Remote Control Panel
6.1 - Exporting multiple iterations with Colibri plug-in
6.2 - Baking geometry to file layer
6.3 - Collecting numeric data

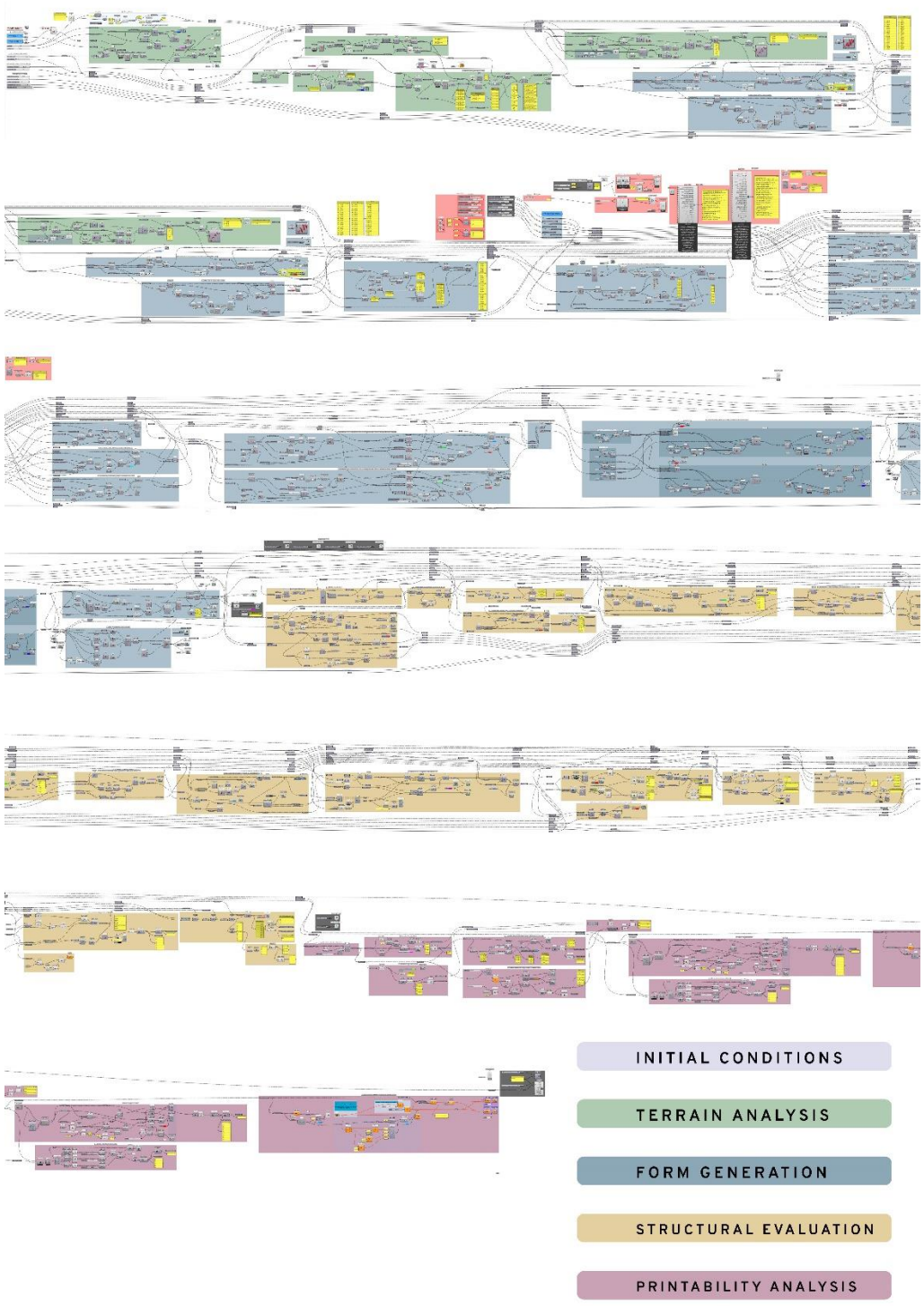

Figure 4.1 Zoomed out perspective of Grasshopper script

4.4 Initial conditions processes

4.4.1 Terrain preparations and inputs

The first module allows users to input their terrain, path, and material data. The script can be used with post-construction terrain or unaltered terrain. This script was tested with both scenarios, the post-construction terrain of the MSU amphitheater (Figure 4.2) and a fictional hill pre-excavation (Figure 4.4). For the MSU amphitheater, the site was documented through a drone survey. This drone survey generated a point cloud model that was converted into a site model in ".fbx" or ".obj" file formats through the Pix4D software. The site model documents the terrain as it is currently constructed. The script only accepts terrain geometries in the format of a single NURBS surface. This site model was converted from a mesh to a NURBS surface in Rhino with some intentional reduction in data size and fidelity for faster computation times (Figure 4.3). For unaltered terrains, the script can be used to create a 3D model of the post-construction terrain with an excavated path in module 2.1 (Figure 4.4).

Figure 4.2 Drone point cloud model of existing conditions at MSU amphitheater

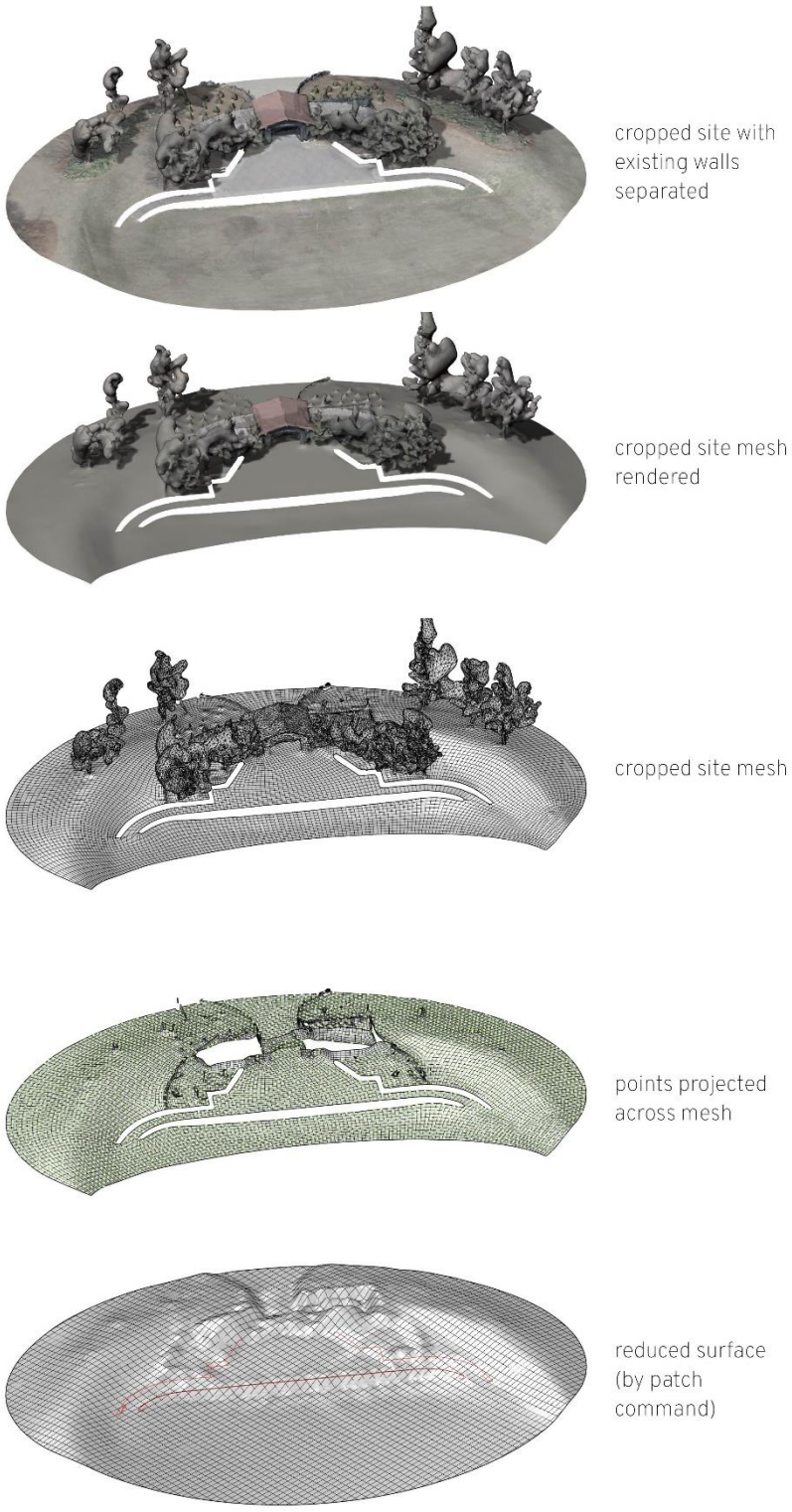

Figure 4.3 Preparations for input into the Grasshopper script; removal of existing retaining walls, a point grid projected onto the mesh, a reduced detail single surface approximating the existing terrain

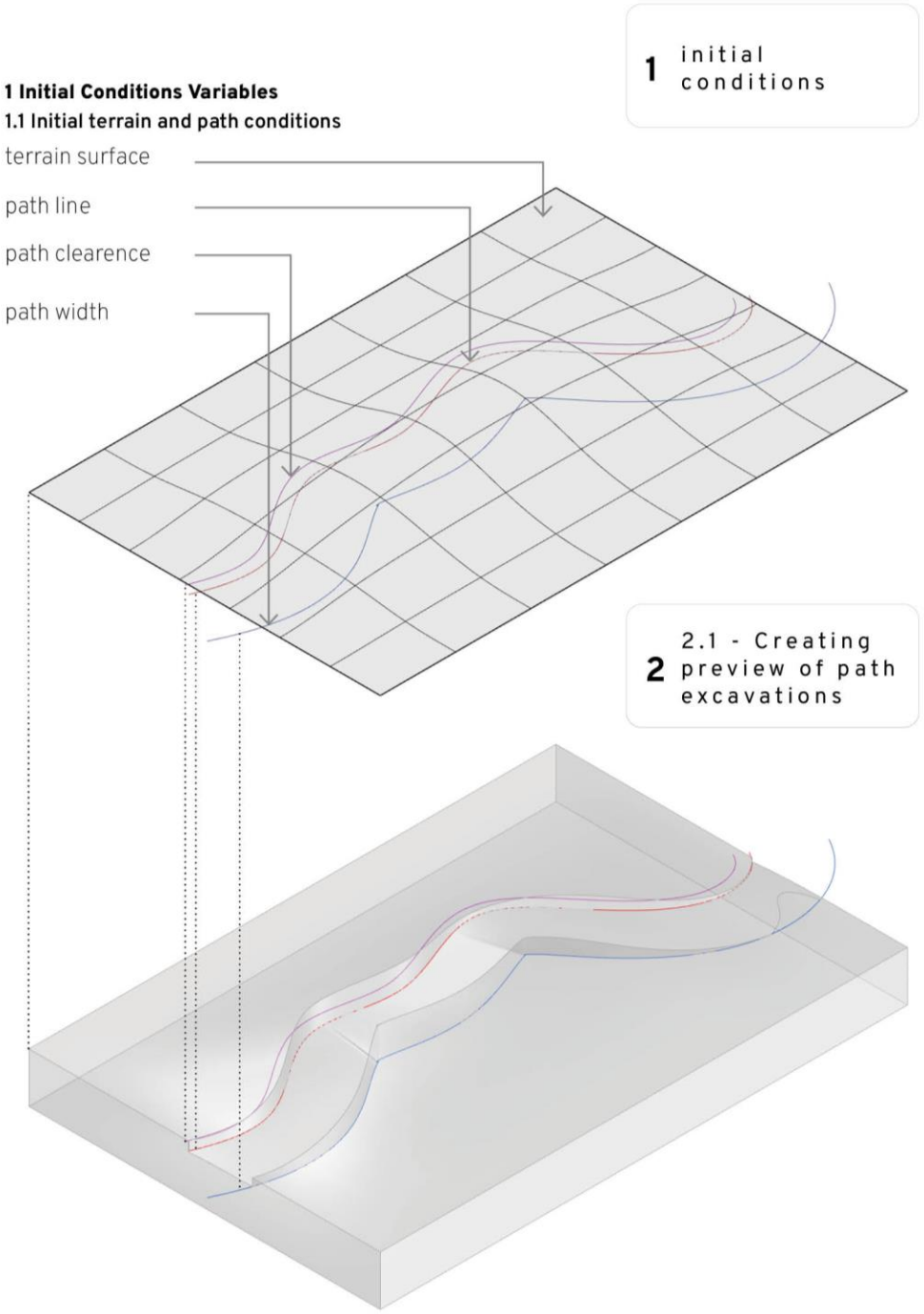

Figure 4.4 Initial condition variables in the case of an unaltered terrain pre-construction

4.4.2 Path inputs

The user provides a line as input into the “Path Line” variable to define the edge of the path along which the retaining wall will be located. The “Path Width” variable is used to create a visual of the path area post-construction. The absolute value of the path width is used to set the wall orientation. This determines which side of the path line will house the excavated path and retaining wall, and which side will retain the soil. To avoid conflicts with the path walking area, the wall can be offset away from the path using the “Path Clearance” variable in the initial setup. These path variables and their effects are depicted in Figure 4.4 in the previous section.

In module 1.2, users can control the variables describing the elevations of the retaining wall’s base, such as frost depth. For instance, in the case of a sloped path with changing surface elevations, a leveled base for each segment would be necessary for construction. The wall can be terraced into different excavation levels onto which different wall bases sit. For example, a path that climbs 2 meters in height may have two separate leveled bases for where the retaining wall can be placed. This is illustrated in Figure 4.5 where the user’s path (red line) is offset by the frost depth variable (blue line) which is then divided into the green lines describing the leveled bases of the retaining wall. Multiple retaining wall segments can lie on the same leveled base if the base step height variable is increased, as seen in the difference between image A and B in Figure 4.5.

In module 1.3, users can determine parameters describing the division of the retaining wall length into shorter segments for printability. The “Desired Seam Length” variable determines an actual seam length that would split the wall into even lengths without a shorter wall as a remainder. For instance, a 36-meter path with a 5-meter desired seam length would have an actual seam length of 6 meters to create 6 equal segments instead of 5 equal segments

with a short 1-meter leftover wall. The corners of the wall segments can also be rounded with the "Fillet Radius" variable for aesthetic decisions and to meet the fabrication limitation of minimum turning radii discussed in Section 2.2.1.2.

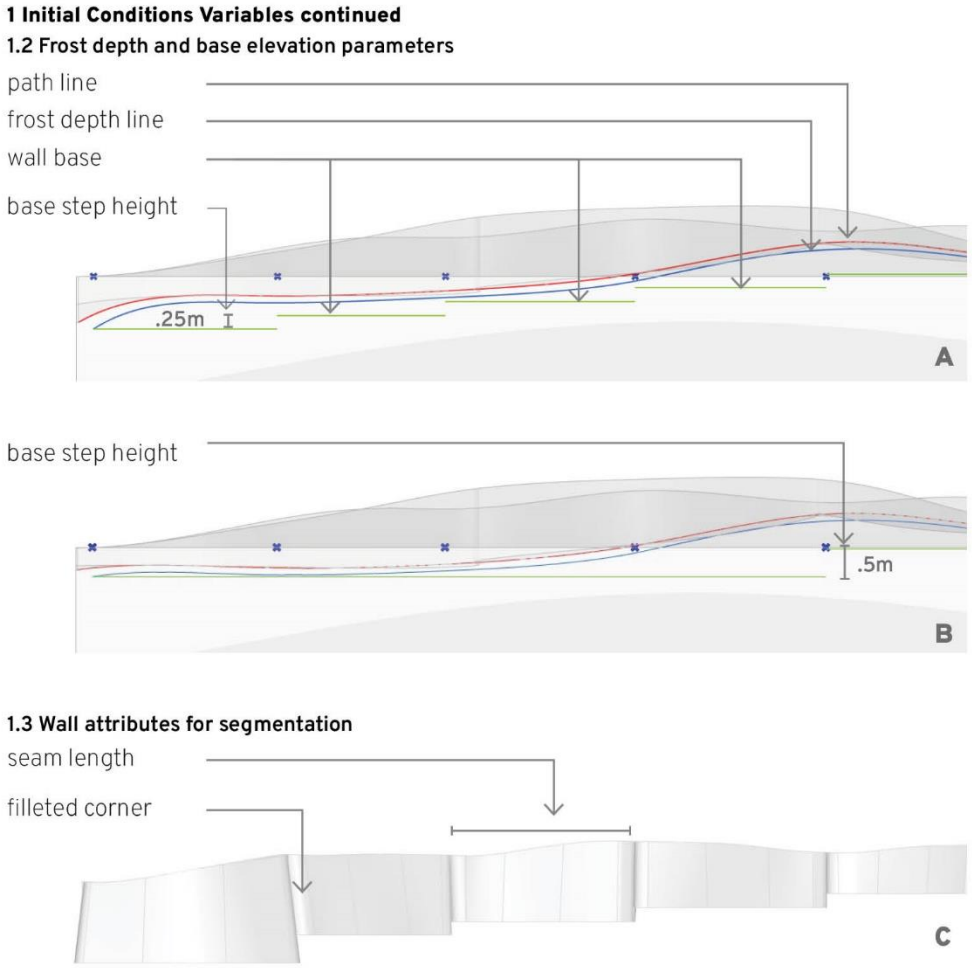

Figure 4.5 Initial condition variables determining attributes related to the base of the retaining wall and the splitting of the retaining wall into multiple segments

Material data for soil and concrete is determined in module 1.4. All units are metric and specified in the Grasshopper script as well as this document. This module allows the setup of the

soil bearing capacity (kilonewton per square meter), concrete density (kilonewton per cubic meter), soil density (kilonewton per cubic meter) and expected angle of repose for the soil. The angle of repose is the highest angle where a sloped soil surface will pile without slumping or further movement.

Table 4.2 List of user inputs and their definitions for the Initial Conditions modules variable

Module #	User Input Variables	Definition
1.1	Path	A line describing the inner edge of the path closest to the retaining wall
1.1	Terrain Surface	A single surface describing terrain
1.1	Path Width	An offset distance to determine width of path area
1.1	Path Clearance	An offset to locate retaining wall out of path area
1.2	Frost Depth Offset	An offset to describe wall depth below the path line
1.2	Base Step Height	A distance by which the total change in path elevation is divided and rounded to the nearest lowest integer to generate a series of level planes for the wall bases; A path with a 1.9m change in elevation would have 3 bases if the base step height is .5. The number of base levels is rounded downwards to the nearest integer to minimize excessive levels for small elevation deviations.
1.3	Fillet Radius for Wall Corners	An optional radius for rounding the vertical edges of the wall segments
1.3	Desired Seam Length	An approximate seam distance that is used to find the actual seam length that splits the path into evenly sized segments without generating a shorter wall segment as a remainder
1.4	Angle of Repose	Angle that describes the range of soil at risk of moving.
1.4	Soil Density	Density of soil as kilonewtons per cubic meter
1.4	Concrete Density	Density of concrete as kilonewtons per cubic meter
1.4	Soil Bearing Capacity	Bearing capacity of subgrade in kilonewtons per square meter

4.5 Terrain analysis processes

4.5.1 Brief process summary

The terrain analysis modules process the path edge to locate the wall base and calculate the soil volume actively retained. The wall toe location is a prerequisite to deriving the retained soil volume which is later used to generate the wall geometries (Figure 4.6). This causes the wall

toe to be the initial starting point for the script processes and designer experiences, despite it being hidden completely underground. The terrain analysis modules begin with a visual preview of the post-construction terrain in module 2.1 (Figure 4.4). The script then offsets the line describing wall location downwards for the frost depth in module 2.1 (Figure 4.8a). At this stage, the splicing and placement of vertical seams along the wall is determined. This is done as a prerequisite to locating the final placement of each wall segment. As the path surface is sloped, the retaining wall base may be terraced, where wall segments lie on different levels of prepared sub-grade (Figure 4.8b). From these terraced wall bases, the script uses the angle of repose to find the soil volume actively retained in each segment. This soil volume is further divided for a finer grain of control and fidelity in the subsequent form generation modules (Figure 4.11).

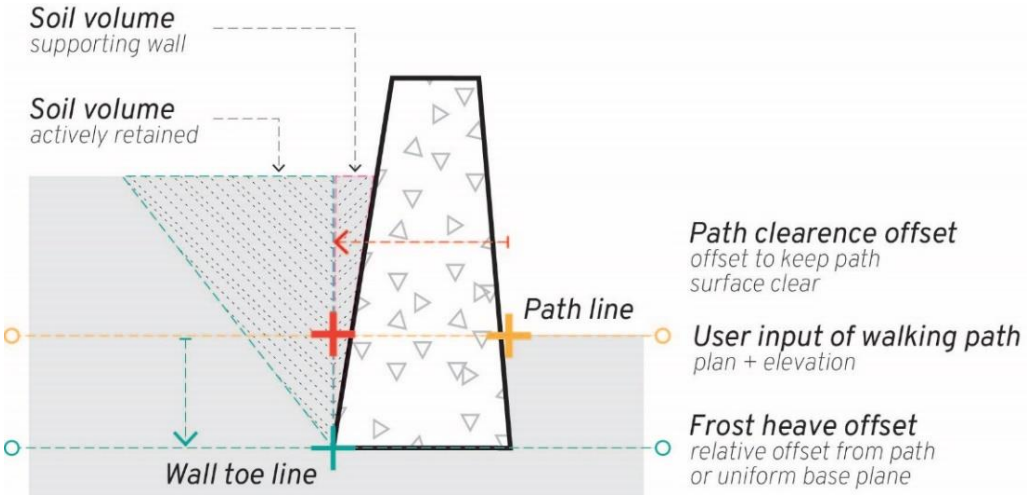

Figure 4.6 Major variables for terrain analysis modules

4.5.2 Sectional versus volumetric approaches

In traditionally constructed retaining walls, there are few cross-sectional changes in the wall form. Thus, retaining walls may be designed using a 2D sectional approach. The cross-

sectional area and volume are interchangeable for a uniform wall. However, with non-uniform walls a sectional approach can be an oversimplification, such as the varying soil volumes between equidistant sections in Figure 4.7c. Thus, the script processes prioritize the utilization of volumes over sectional areas when possible. Similarly, the frequency and size of sub-division has a design impact, acting as a determiner of design resolution. In the form generation modules, wall cross-sections change across a single wall. In the following examples, the wall is divided into thirds that respond to a sub-section of the soil volume of one wall segment. This is an alternative to the entire wall having a single geometry that averages out the deviations of the terrain. Each sub-piece of a wall is affected by a respective sub-piece of soil volume. This allows gradual changes between sub-pieces to be articulated rather than describing more general terrain changes between walls. This is similar to changing the level of detail by reducing the rectangle size in Figure 4.7. The frequency of subdivision can be reduced for a smoother, less jittery, less responsive wall design whose geometry averages out more subtle terrain changes.

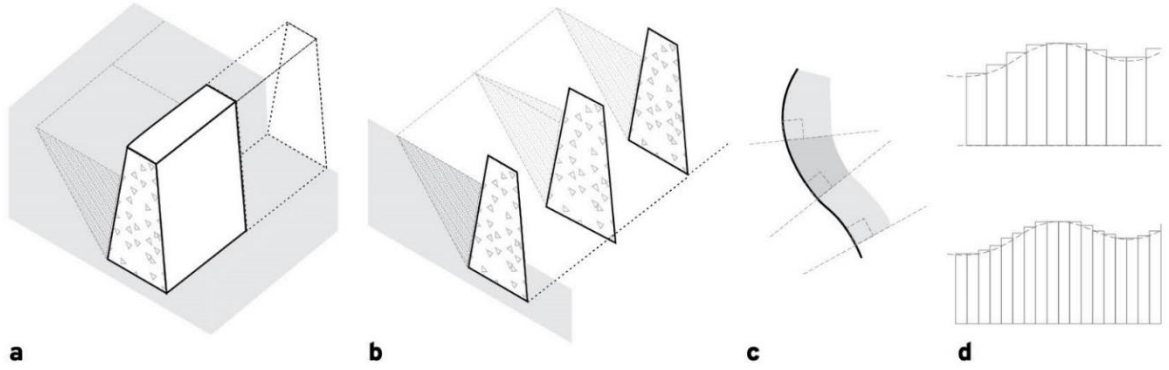

Figure 4.7 Conceptual considerations for sectional and volumetric approaches to terrain analysis and wall design

4.7a and 4.7b – a uniform wall whose cross section comprehensively describes its 3D volume
4.7c – a plan view of a non-uniform wall whose serial cross sections may not account for its 3D volume variations4.7d – an abstraction depicting the effect of an increased vs decreased analysis resolution

4.5.3 Process considerations for terrain analysis

Figures 4.8, 4.9 and 4.10 summarize the terrain analysis modules and their variables in the case of the fictional hill. In this stage, the path line input by the user is adjusted by the "Path Clearance" variable to avoid the retaining wall from protruding into the path walking surface. Adding a negative vertical offset produces a toe line that matches the original slope of the path line. However, it is preferable for the wall base to be level, i.e., flat bottom to allow for 3D concrete printing on a level surface and to simplify subgrade preparations. This research assumes that a leveled, compacted aggregate base is a suitable printing surface. Otherwise, there may be a need for a cast-in-place concrete base, which is the printing surface typically seen across in-situ 3DCP projects. As described previously in section 2.3, existing research indicates imperfect printing surfaces can be tolerated using supplementary sensors. However, further research is required to determine acceptable printing surfaces, which falls outside the scope of this toolkit.

Likewise, it is not feasible to print the entire length of the path as a single continuous wall. Vertical seams are necessary to split the path length into wall segments small enough to be contained within the printable volume described in Section 2.2.1.1. In this toolkit, the vertical seams are equidistant in a plan projection, rather than being evenly spaced along the actual sloped path. This was an aesthetic decision for the appearance of uniformity in the seam spacing. In Figure 4.8a, the magenta line is the projected (flattened into a plan projection) toe line. The vertical planes and blue points are equally spaced and perpendicular to the path, ensuring that the seams correspond with the curvature of the path line. These vertical planes are used to divide the toe line into segments for each wall.

Each wall segment is intended to sit on a leveled and prepared base at varying elevations along the path length. The user sets the "Base Step Height" variable which determines the

elevation change between leveled bases. This allows the user to quickly create a series of base levels and decide the frequency of stepping. A larger base step height decreases the number of base levels for a more expedient site preparation process. The below example in Figure 4.8a uses a smaller base step height only for visual clarity. Figure 4.8b depicts a larger base step height where multiple walls reside on the same level. The toe line of each wall segment is analyzed to find the lowest elevation point. This lowest elevation is used to identify the base level elevation directly below the toe line, even if the toe line is closer to the base level directly above. The toe line segment is projected down to the base level plane, creating a flat toe line.

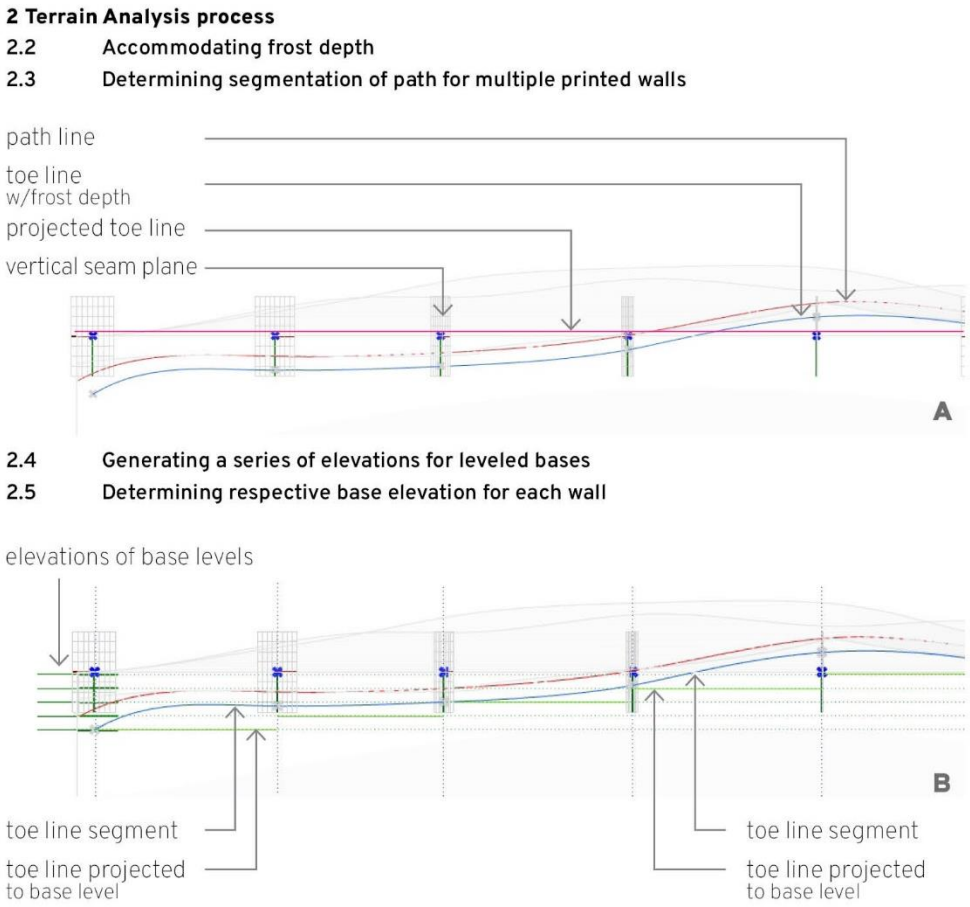

Figure 4.8 Creation of a terraced toe line and vertical wall seams in terrain analysis phase

These projected toe lines are extruded vertically and outwards at the angle of repose in module 2.6 (Figure 4.9). These extrusions serve the purpose of cutting the retaining soil volume out of the terrain polysurface created in module 2.1 (Figure 4.10). Each wall segment is evenly divided later in the script, creating the soil volume sub-pieces referred to throughout the script. Each toe segment is roughly equal in length, allowing each sub-piece to be similarly sized across the path length.

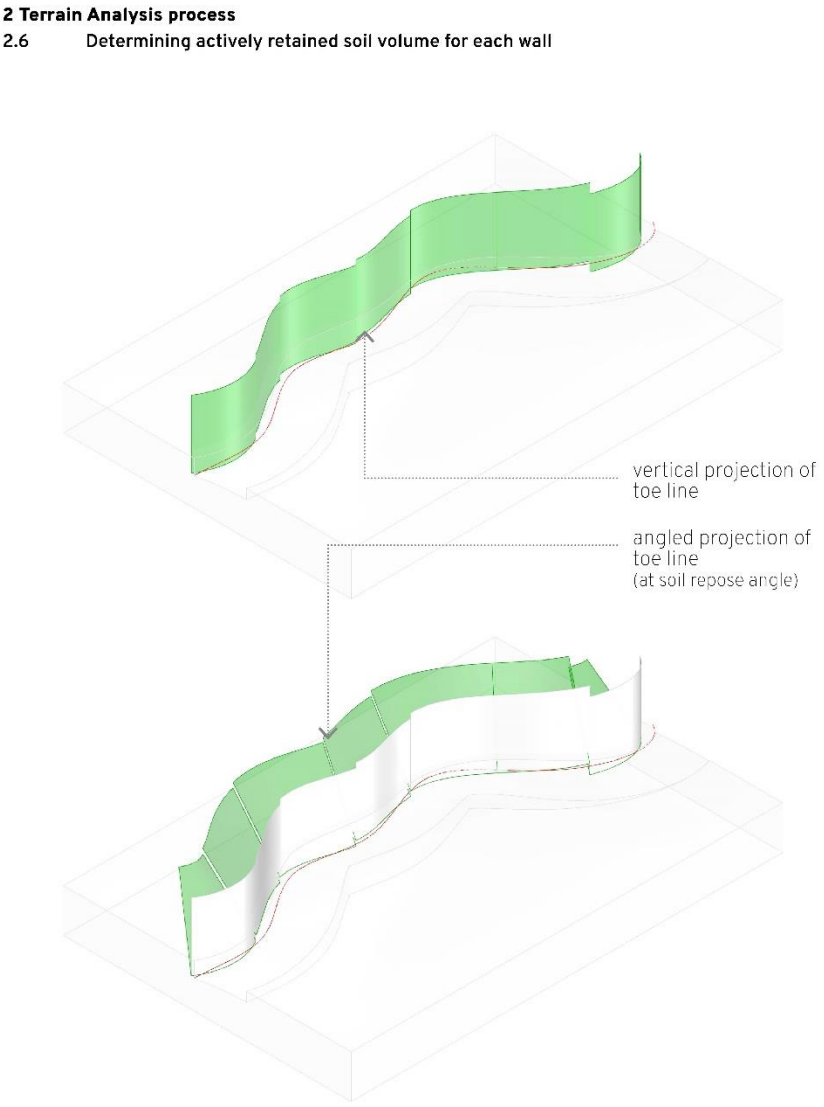

Figure 4.9 Vertical and angled extrusions used to find the soil volume actively retained

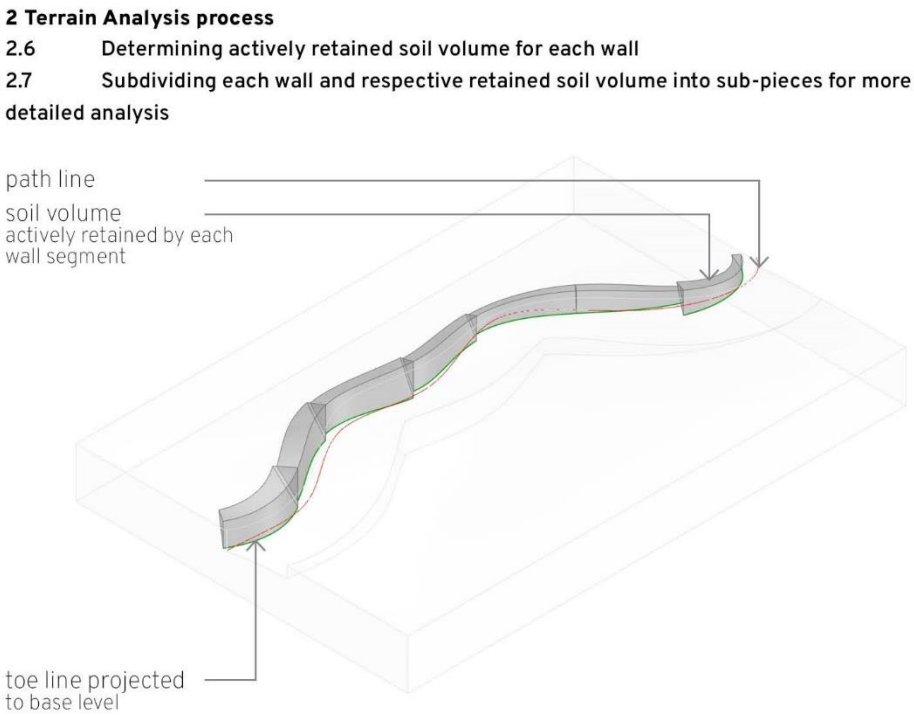

Figure 4.10 Determination of soil volume actively retained

4.6 Form generation processes

4.6.1 Cross section distribution

Each wall segment is designed as a series of cross-sections that derive their geometry from a fragment of the soil volume to be retained. The user multiplies the soil volume is by chosen ratios to determine the wall width and face batters, allowing the derivation of a wall from the terrain conditions. To control the level of detail and fidelity to terrain, the soil volume and wall segments are divided into sub-pieces using an “analysis fraction” variable. In Figure 4.11, the wall segments and soil volumes are divided into thirds, marking the points, vectors, and soil volumes used to create the wall forms. The volumes of each soil piece are then used to design cross sections for each respective wall segment.

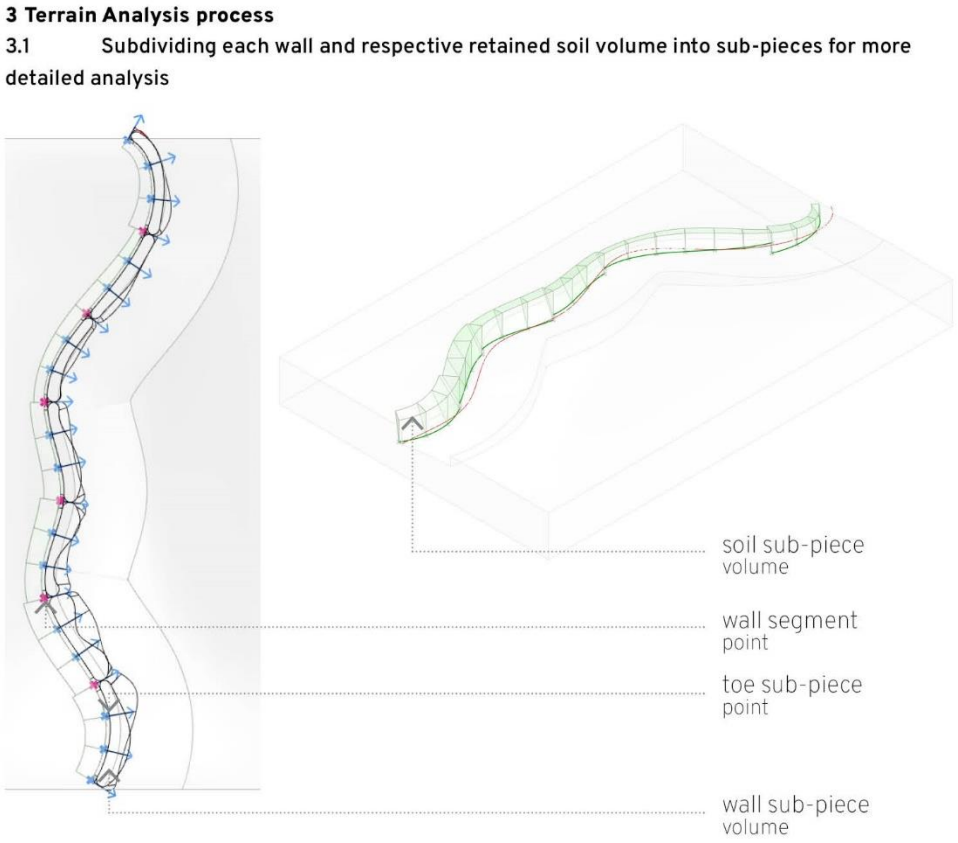

Figure 4.11 Subdivision of wall and soil

One major consideration is the relationship between wall cross-sections and soil volumes described in Figure 4.12. Each sub-piece of soil has a bisecting wall cross-section. Additionally, the starting point of the wall segment also has a cross-section. The end point of the wall segment inherits the initial geometry of its neighboring wall to maintain visual continuity. Thus, a wall segment divided by the analysis fraction (*f*) would have f+1 cross sections initially. In the script, these cross-section points are generated by dividing each wall segment (*W*) by 2*f*, resulting in 2*f*+1 points, depicted in Figure 2.14. The initial point of the wall segment (W^0) and all odd-numbered points (W^1, W^3, W^5, etc.) are the required cross-section points. The even-numbered

points, including the wall end point (W^{end}), are culled except for the final terminus point of the path (N^{end}). The path end point does not need to imitate a neighboring wall, so it is not culled.

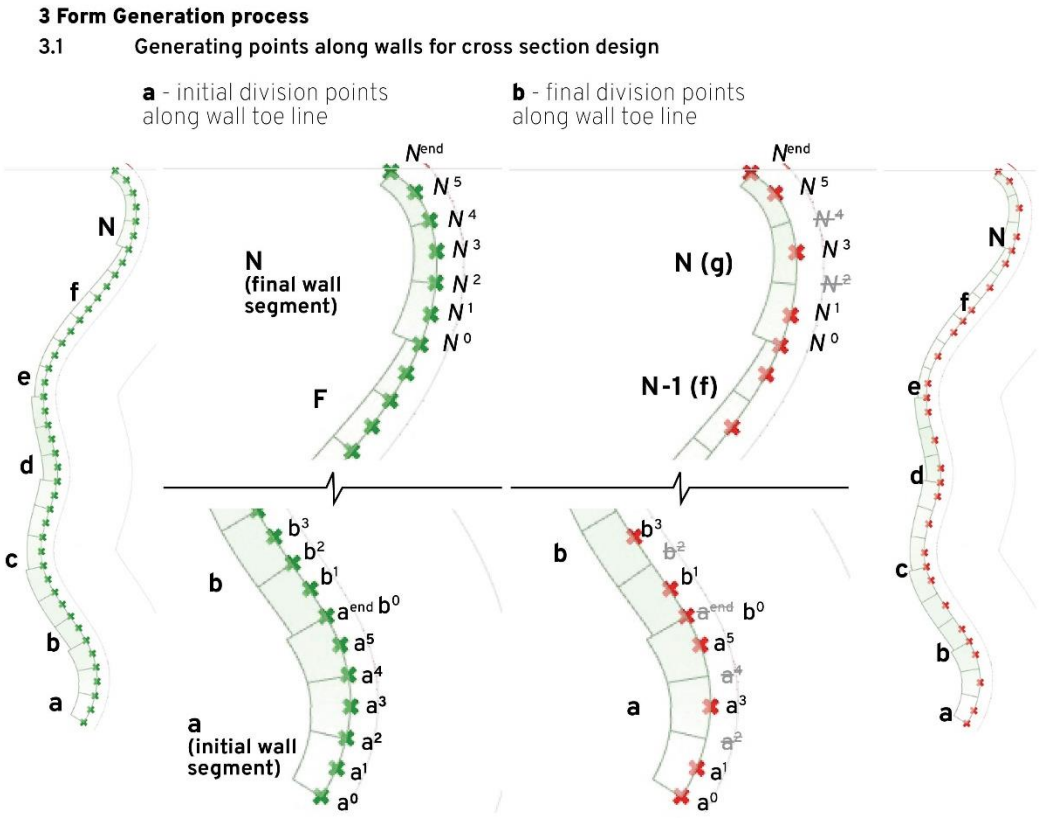

Figure 4.12 Generation of cross-section points for the wall segments

Table 4.3 Cross-section organization

Abbrev.	
f	Analysis fraction
W	Wall segment
W^0	Start point of wall segment
W^{end}	End point of wall segment
N	Final wall segment in path line
N^{end}	Final terminus point of path line, i.e. end point of final wall segment

Each wall cross-section is matched to a soil sub piece. Notice that there are *f* number of soil pieces but *f*+1 cross-sections for typical walls (*W*) and *f*+2 cross-sections for the final wall

segment (N). This results in the following matching process described in Figure 4.13: The odd-numbered cross-section points respond to the data of the soil sub-piece they bisect. The W^0 cross section responds to the initial soil sub-piece in each wall segment. The N^{end} cross-section responds to the final soil sub-piece of the final wall segment.

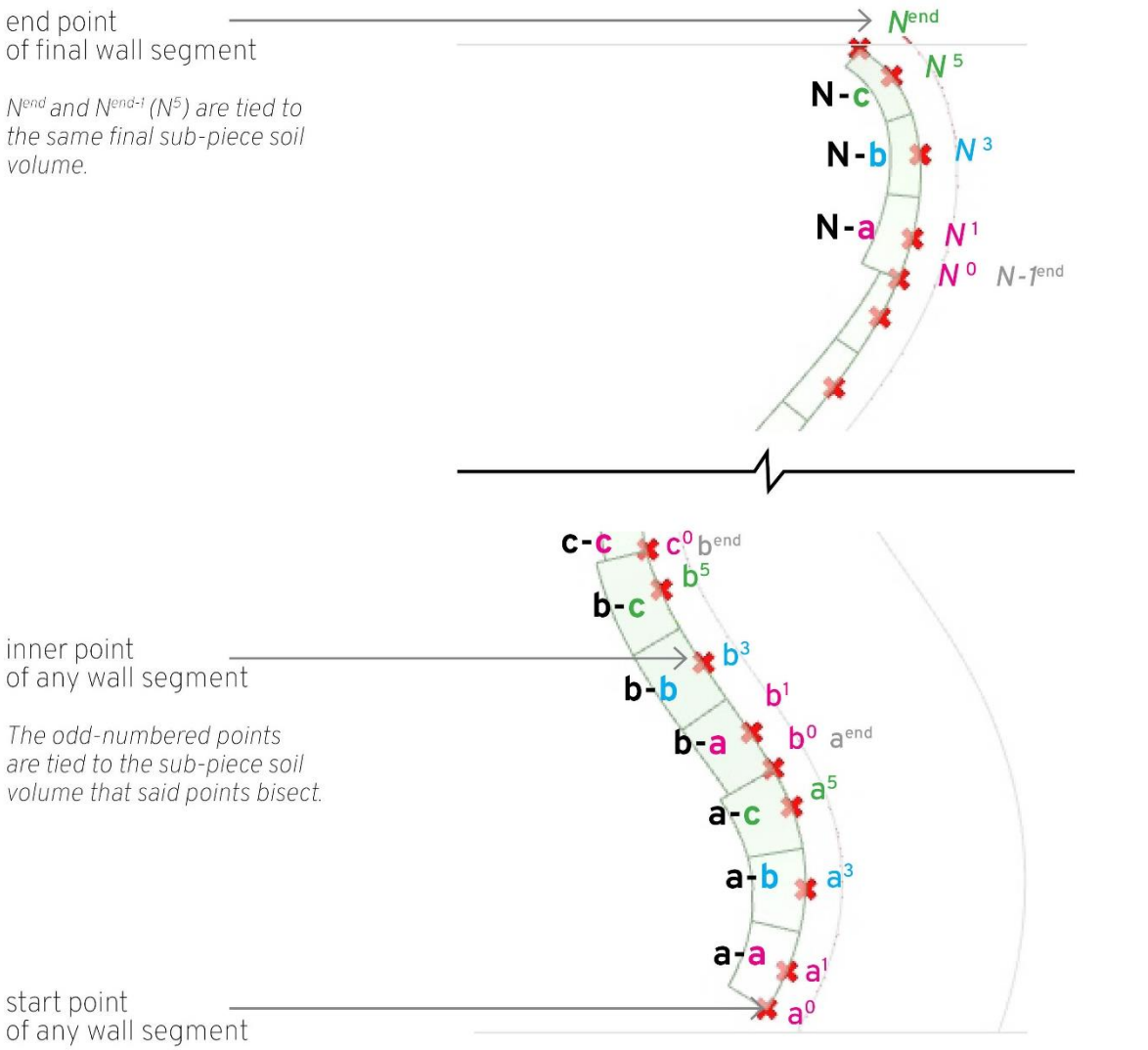

Figure 4.13 Matching process between soil sub-pieces and cross-sections

4.6.2 Cross-section design

The generation of the wall form involves applying ratios to the volume of the soil sub-piece. For example, a soil volume of 4 m^3 and a wall width ratio of 0.125 will generate a width of 0.5m plus the minimum wall width set by the user. This script utilizes soil volume ratios and minimum dimensions to determine the wall height, width, and batters as shown in Figure 4.14. The wall batters are described by their distance from the wall toe rather than an angular dimension. The wall height is designed as a vertical offset of the highest elevation of each soil sub-piece. Users define the "Soil Height Offset" variable which sets the minimum height above the soil. Then, the wall elevation can be further raised in proportion to the volume of the soil sub-piece by the ratio variable "Wall Height - Soil Volume Multiplier" (Figure 4.15).

The previously generated cross-section points become the toe points for the wall cross-section. These toe points are translated along the perpendicular vector of the projected toe line segments of module 2.5. To determine the wall width, a minimum dimension is added to an additional distance, proportional to the soil sub-piece volume. This cumulative distance becomes the amplitude of the vector, setting the bottom point of the front face of the wall. Both the front and toe batter are translated on the same vector and projected upwards to the top of wall elevation (Figure 4.16).

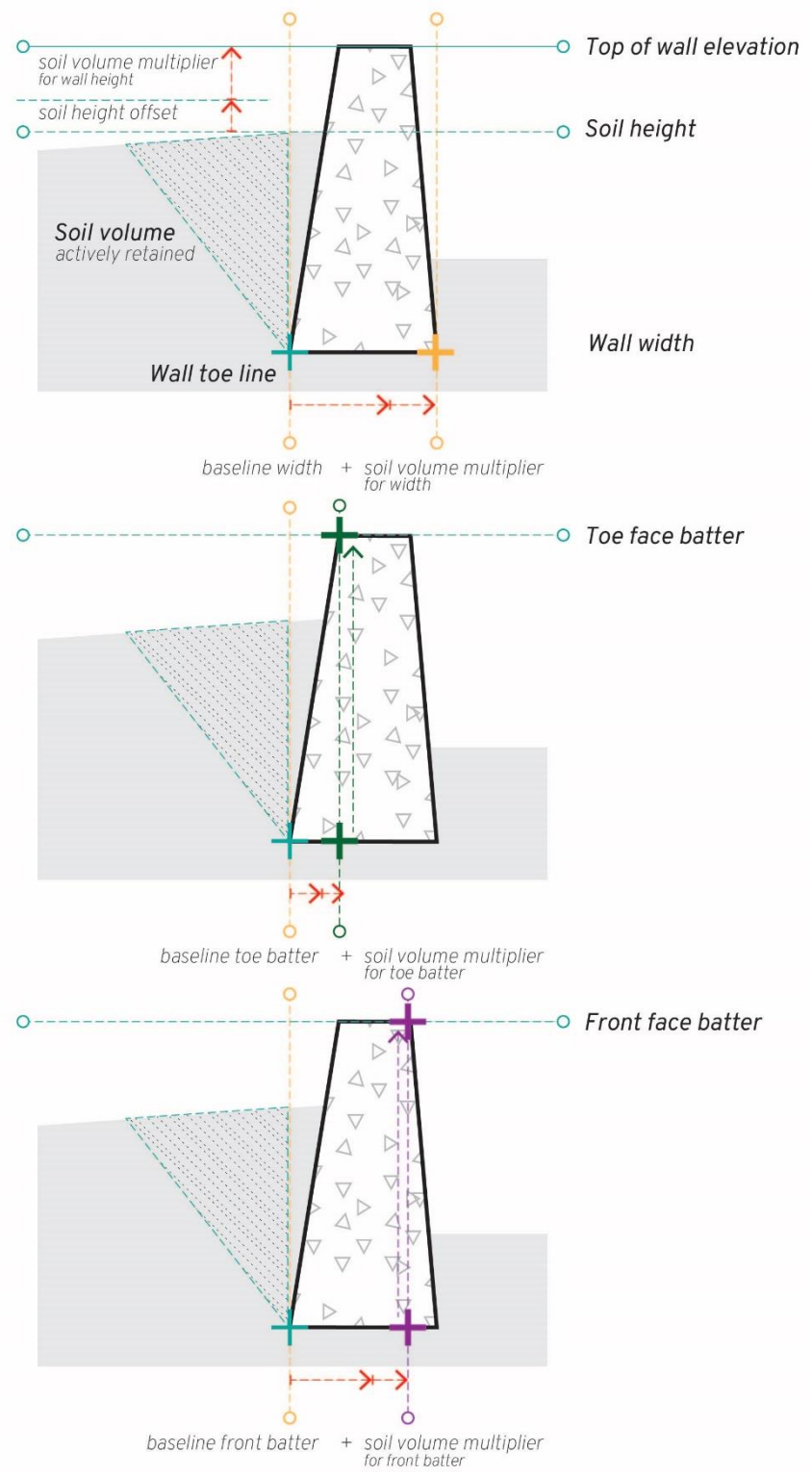

Figure 4.14 Diagram of variables determining wall proportions

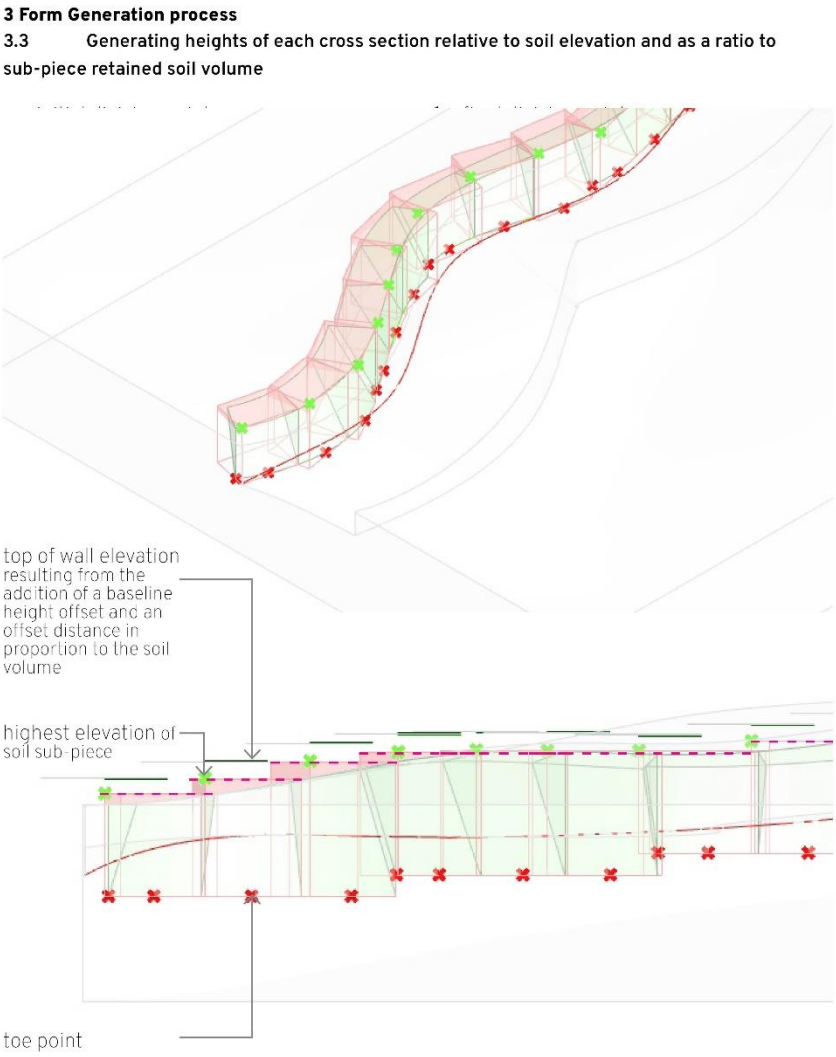

Figure 4.15 Process for setting top of wall elevation

Table 4.4 User inputs for wall proportions

Module #	User Input Variables	Definition
3.1	Analysis fraction	Number used to divide each wall segment into sub-pieces
3.4	Wall Height - Soil Height Offset	Distance used to offset wall height above soil elevation
3.4	Wall Height - Soil Volume Multiplier	Ratio multiplied by soil volume to create a distance that increases the wall height
3.5	Wall Width -Baseline	Minimum wall width across all cross-sections
3.5	Wall Width - Soil Volume Multiplier	Ratio multiplied by soil volume to create a distance that increases the wall width
3.6	Toe Batter -Baseline	Minimum toe batter distance across all cross-sections
3.6	Toe Batter - Soil Volume Multiplier	Ratio multiplied by soil volume to create a distance that increases the toe batter
3.7	Front Batter -Baseline	Minimum front batter distance across all cross-sections
3.7	Front Batter - Soil Volume Multiplier	Ratio multiplied by soil volume to create a distance that increases the front batter

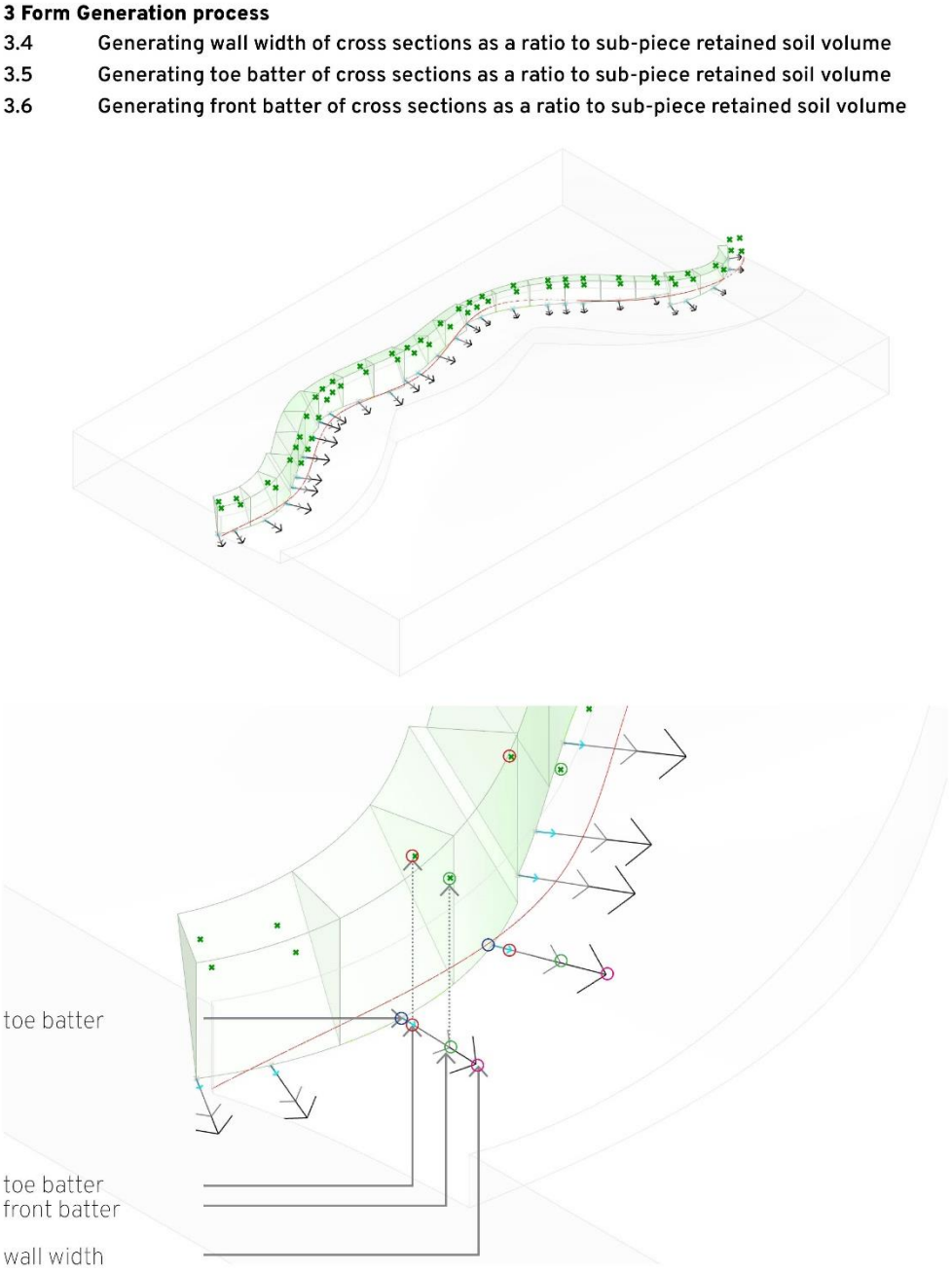

Figure 4.16 Generation of wall proportions by perpendicular vectors

4.6.3 Random manipulation process

The geometry randomizer module allows users to experiment with geometric variations and observe their effects on aesthetics, structural issues, and printability. The randomization is based on altering a few cross-sections across each wall segment, particularly the locations of the top front and bottom front points of the wall cross-section. Each wall segment has a number of total cross-section points previously generated, denoted as n^w. The user sets the number of points to be randomly selected and deviated, represented as n^r. The total points (n^w) subtracted from the number of random points (n^r) results in the number of points to be unaltered (n^{w-r}). The list of cross-section points of each wall segment is randomly shuffled with a seed number variable. If n^w is 5, n^r is 2, and n^{w-r} is 3, the script culls the first 3 (n^{w-r}) values, leaving 2 (n^r) points remaining. This randomization process behaves more like choosing from a shuffled deck of playing cards than a coin toss. This is an intentional alternative to the script selecting a random point three (n^{w-r}) independent times. This would have the possibility of repeat selection of the same individual. Instead, choosing the first three (n^{w-r}) items out of a shuffled list does not allow for any repetition. Disallowing repeat selection prevents the creation of duplicate cross-sections that cause issues when generating the final wall forms. After the random points in each wall segment are chosen, they are pushed outwards or inwards by a similar set of variables to the width and batter proportions (Figure 4.17). Table 4.5 lists the user inputs for the randomization module, including a minimum distance and a distance derived from the soil sub-piece volume. The randomization module has an additional user input variable called a “MixerUpper”, which represents the seed number used to shuffle the points for random selection. Altering the seed number changes the shuffling and determines which points are randomly selected. After the movement of the random points is translated, they must be inserted into the data tree that

contains all the cross-section points for each wall segment. The original list of random points pre-alteration is found within the original list of all cross-section points and replaced with the new altered random points.

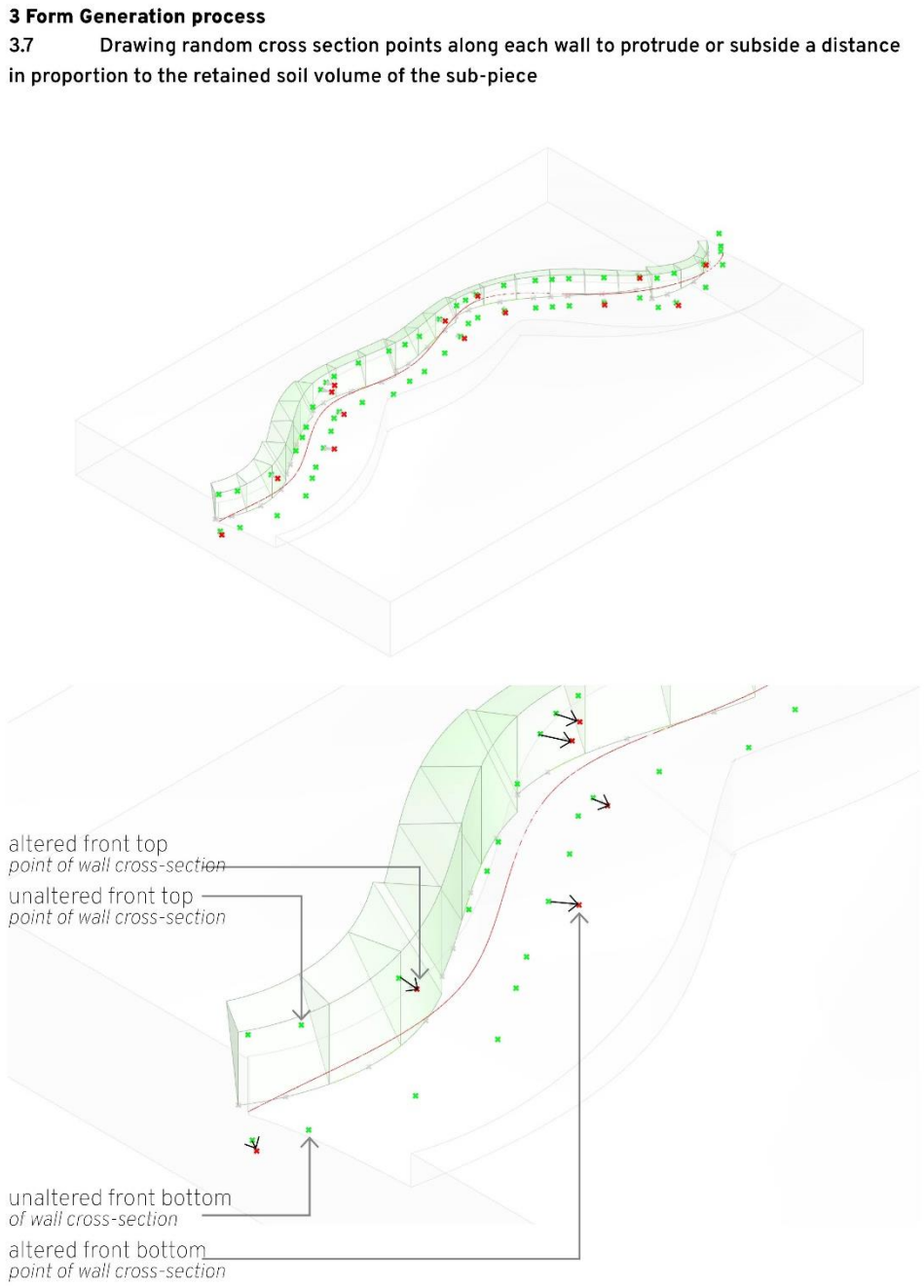

Figure 4.17 Translation of randomly chosen cross-section points

Table 4.5 User inputs for randomizing wall proportions

Module #	User Input Variables	Definition
3.8	Top - # of Random Points	Number of front top points per wall segment randomly selected to be deviated
3.8	Top Random Pts – Soil Volume Multiplier	Ratio multiplied by soil volume to create a distance that increases the front batter for randomly selected points
3.8	Top – Mixer Upper	Seed number used to randomly draw front top points
3.8	Bottom - # of Random Points	Number of front top points per wall segment randomly selected to be deviated
3.8	Bottom Random Pts – Soil Volume Multiplier	Ratio multiplied by soil volume to create a distance that increases the front batter for randomly selected points
3.8	Toe Face – Mixer Upper	Seed number used to randomly draw front top points

4.6.4 Resulting forms

The points generated in the previous modules form the wall cross-sections that create the final wall form (Figures 4.18 and 4.19). To maintain geometric continuity between wall segments, the end point of each wall inherits the initial cross-section of its neighboring wall in module 3.9 (Figure 4.18). For this reason, the end point of each wall segment was ignored and removed from module 3.1 processes. Note that neighboring wall segments may lie on different base levels. Thus, the neighboring initial cross-section is extended or retracted to the base level of the recipient wall segment. These new end cross-sections are merged into the list of cross-sections for each wall segment. Then the merged list becomes the solid and hollow geometries of the final wall form. The solid geometries are used to determine weight and volume data for structural calculations. The hollow geometries approximate the actual printed object. Thus, they are used for printability analysis. The sloped lines depicted in Figure 4.18 are used to form the hollow geometries while the closed polylines shown in Figure 4.19 are used for the solid geometries.

3 Form Generation process

3.8 Generating cross section lines that describe front and back sloped faces

3.9 Generating cross section lines for individual wall starting shape to match neighboring wall ending shape.

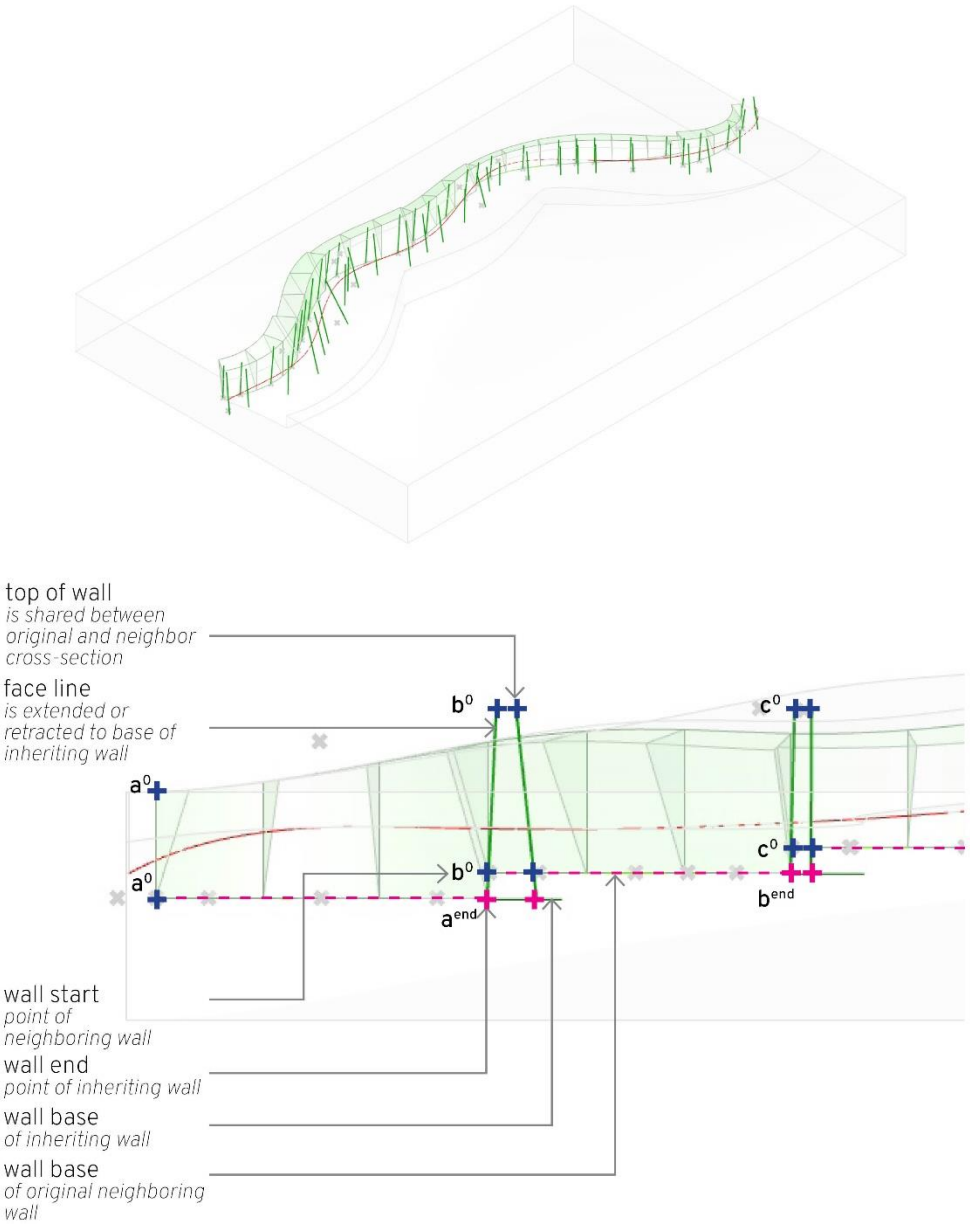

Figure 4.18 Creation of sloped lines that describe the final wall form and adjustment process to match geometries between wall segments

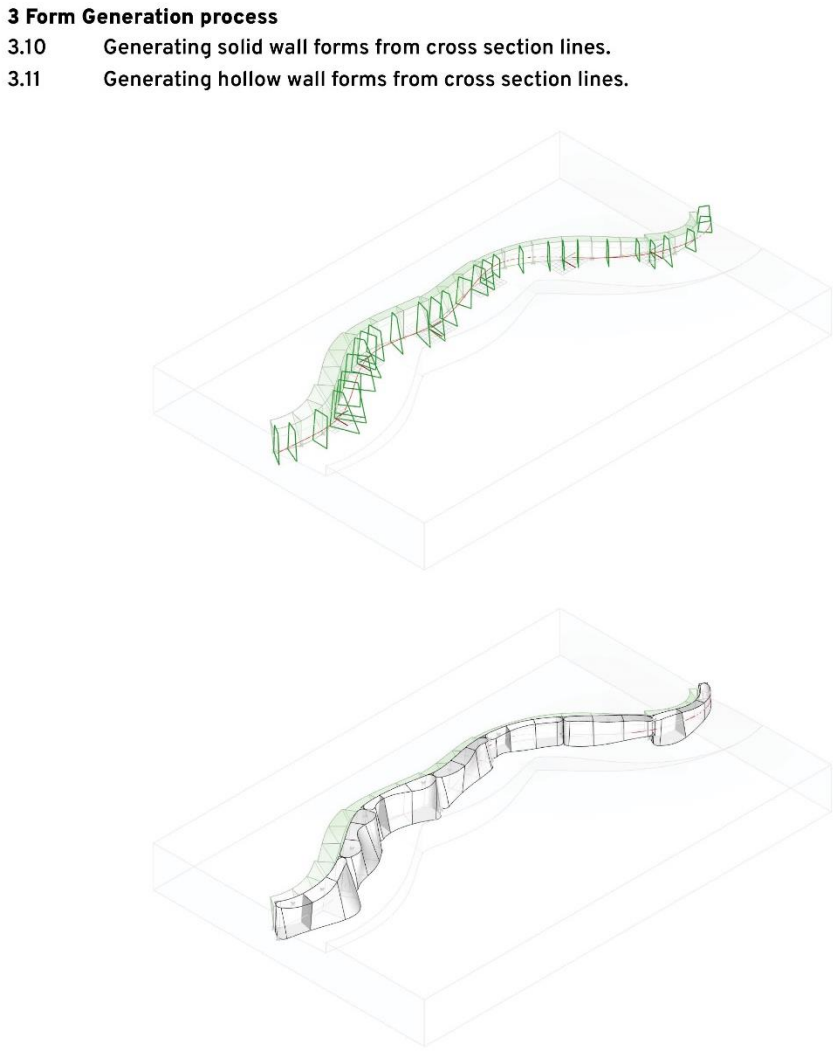

Figure 4.19 Closed cross-section polylines that create the solid geometries

4.7 Structural evaluation

4.7.1 Formulas and processes

The structural evaluation modules test the wall against “rule of thumb” structural formulas. This analysis is intended as a precursor to more rigorous evaluation further in the design process. The structural evaluation modules are adapted from Time Saver Standards for Landscape Architecture (Harris & Dines, 1998). All structural calculations are performed per

sub-piece within each wall segment. The lateral load on the wall is a function of the soil volume that exceeds the angle of repose (Figure 4.20). The wall weight is sum of both the concrete weight and a proportion of the soil depicted in blue in Figure 4.20. The soil directly above the wall adds to the weight of the wall. This supporting soil volume and the concrete volume have a combined center of gravity onto which the resultant force acts at the third of the wall height. The resultant force is found by calculating the diagonal of the forces of the wall weight and lateral load (Figure 4.21). The extension of the resultant force must intersect the base at its middle third for wall stability. The ratio between the vertical force of the wall weight and the horizontal force of the soil pressure describes the overturning risk of the wall (Figure 4.22). An eccentric loading of the wall can concentrate pressure and can cause settlement at the toe. The eccentricity, base width and area are factors that determine the crushing risk of the wall. The final parameter is evaluating the risk of sliding if the friction between the soil and wall is inadequate.

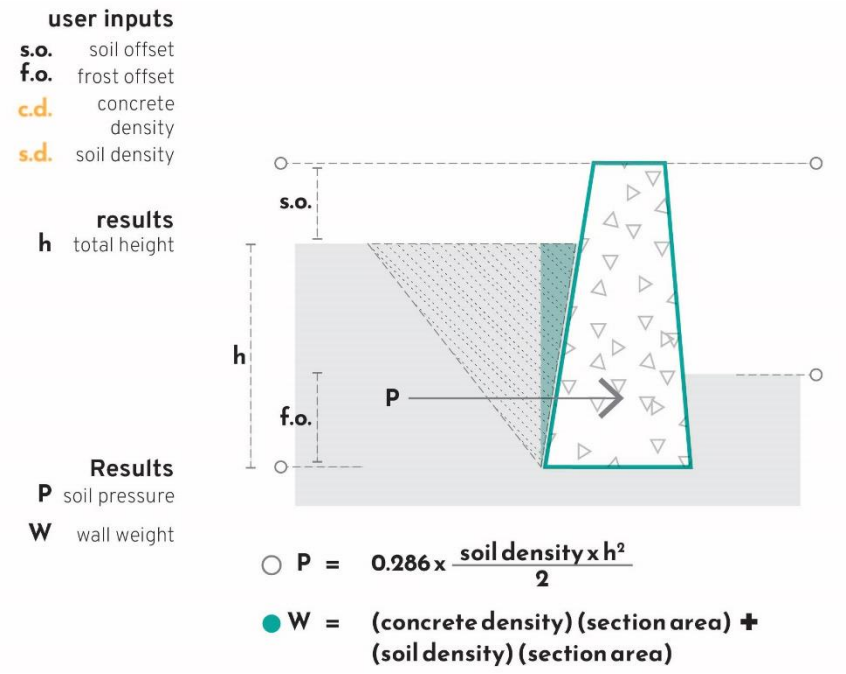

Figure 4.20 Lateral pressure and wall weight definition

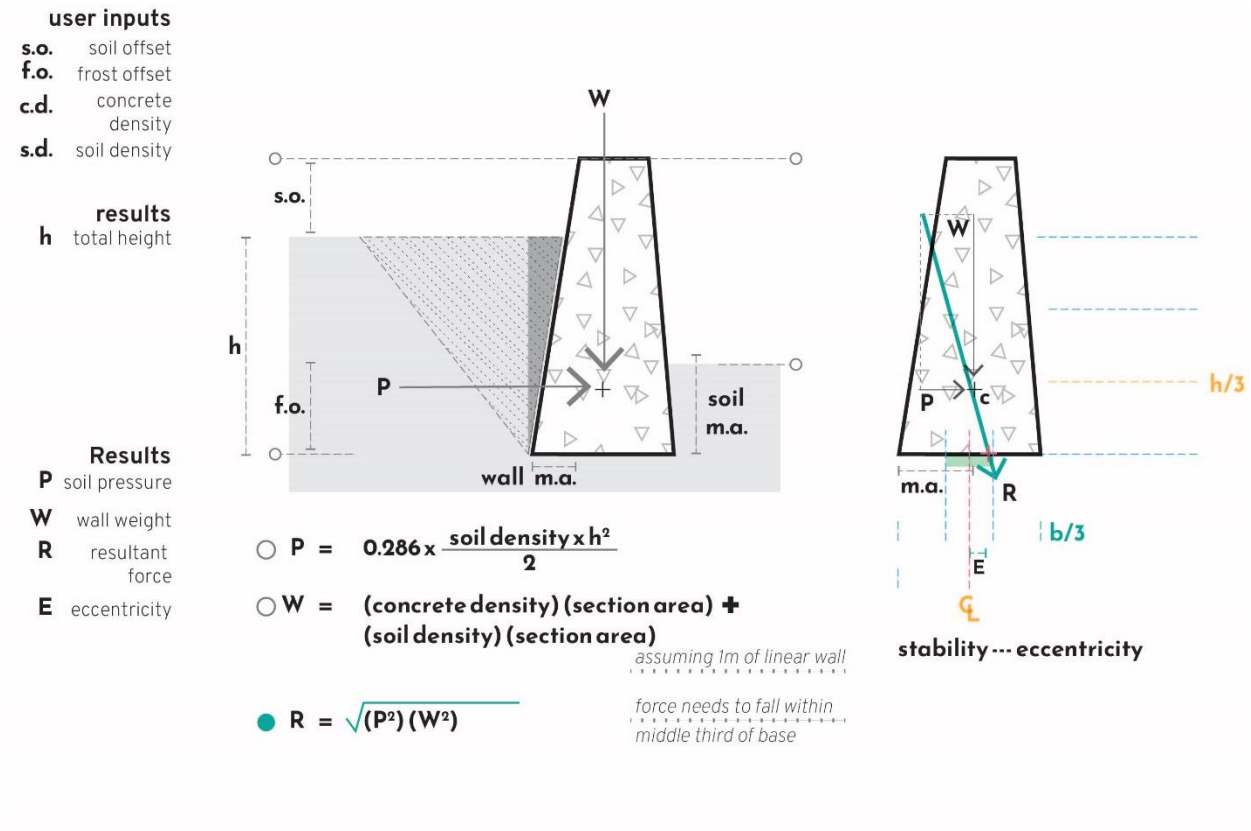

Figure 4.21 Resultant force definition

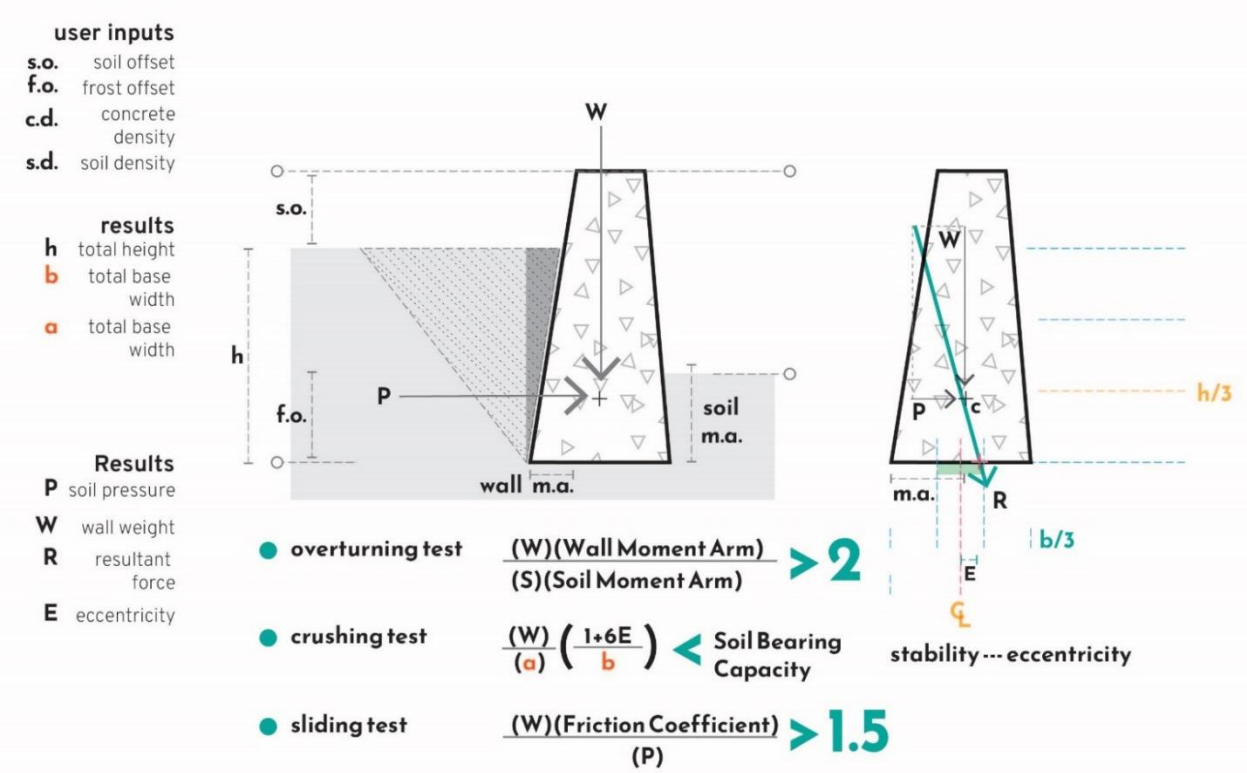

Figure 4.22 Definition of overturning, crushing, and sliding risk.

4.7.2 Data preparations

The wall geometry, such as the height and width, needs to be further processed to find the relevant data for structural calculations. The analysis of wall sub-pieces involves determining the base area and base width (at center) of each sub-piece. The fillet radius is accounted for when calculating the base area. The base centerline is found for each wall segment. The wall base surface is divided into thirds for the resultant force calculations. This division helps in assessing the distribution of forces across the base. These base variables are illustrated in Figure 4.23. Furthermore, the total height of each wall sub-piece (*h*) is found. This allows for the generation of two elevation levels: the wall bottom and the elevation level for one-third of the wall height (*h/3*).

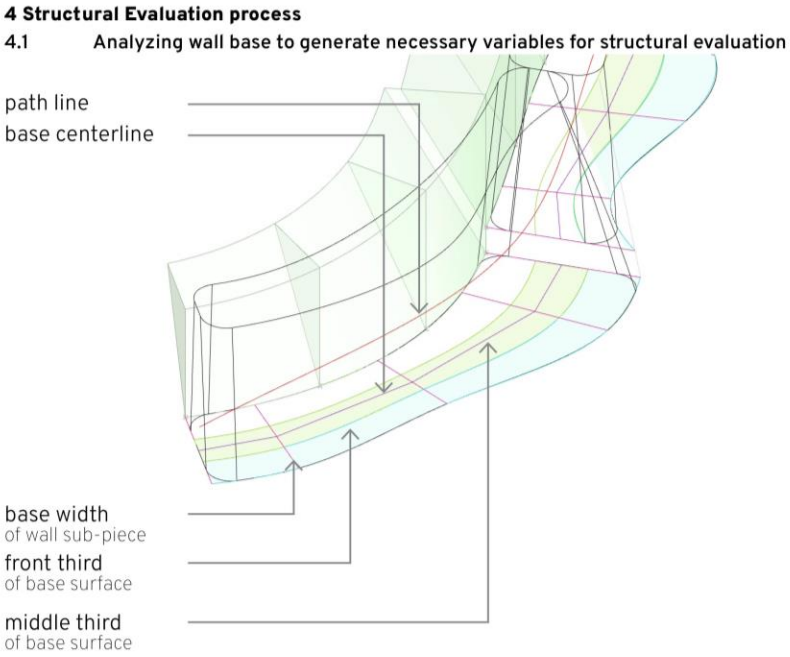

Figure 4.23 Variables describing the wall base for structural evaluation

4.7.3 Lateral pressure and weight

The script calculates the lateral pressure exerted by the soil onto the wall and the vertical forces of the wall weight. The following equation is used to calculate the lateral soil pressure (P) with soil density (d^S) and the wall sub piece height (h) found in module 4.2:

$$P = (0.286)(d^S h^2/2) \tag{4.1}$$

Previous modules generated the wall sub-pieces and the corresponding sub-pieces for the actively retained soil volume. At this stage, it is necessary to find the volume of soil that adds to the weight of the wall, which is referred to as the supportive soil volume. To accomplish this, the script calculates the centroid and volume (in cubic meters) of both the concrete wall sub-piece

and the supportive soil sub-piece (Figure 4.24). The supportive soil volume is found using the dimensions for the wall toe batter.

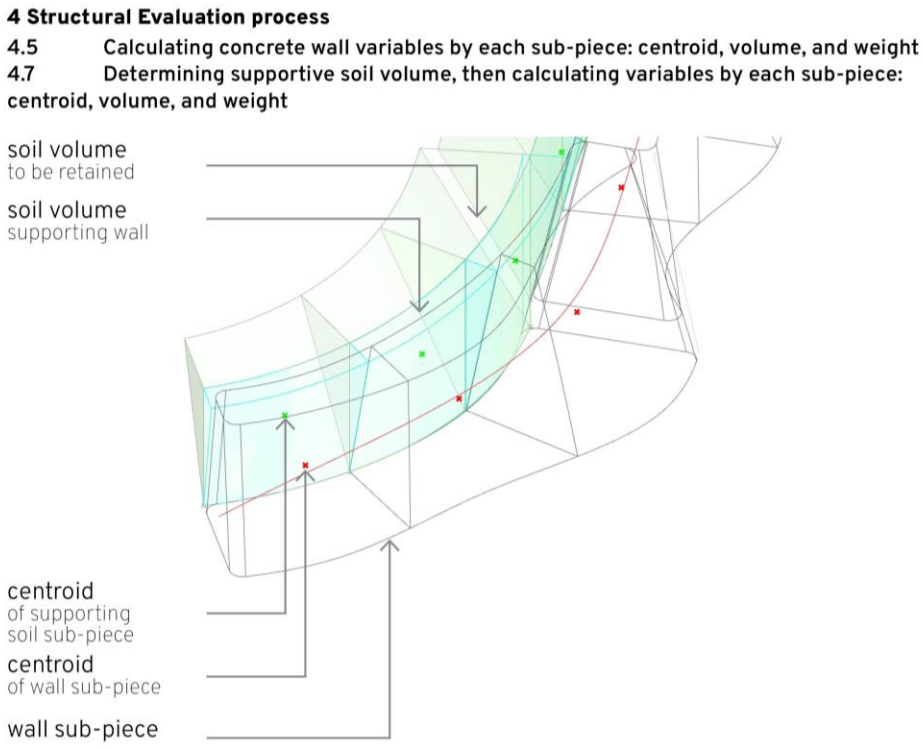

Figure 4.24 Volume variables for structural calculations

To calculate the total weight of the wall (W^T), the script considers both the supporting soil weight (W^S) and the concrete weight (W^C) for each sub-piece. The supporting soil weight is calculated by the soil volume (v^S) multiplied with soil density (d^S) for each sub-piece. The concrete weight is calculated by the concrete volume (v^C) multiplied by the concrete density of (d^C) for each sub-piece. The wall weight (W^T) is the sum of the supporting soil weight (W^S) and concrete weight (W^C) for each sub-piece.

$$W^T = W^S + W^C \tag{4.2}$$

$$W^S = (v^S)(d^S) \tag{4.3}$$

$$W^C = (v^C)(d^C) \tag{4.4}$$

Table 4.6 Structural variables

Module #	Abbrev	Definition
4.4	P	Lateral pressure for single sub-piece (kN)
4.1	B^A	Base area for single wall sub-piece (square meters)
4.1	B^W	Base width at center of single wall sub-piece (meters)
4.4	H	Total height for single sub-piece (meters)
4.4	h/3	One-third of base height, used for resultant force calculations (meters)
1.4	d^S	Soil density in kN per cubic meter
1.4	d^C	Concrete density in kN per cubic meter
4.5	v^C	Concrete volume per soil sub-piece (cubic meter)
4.6	$\sum v^C$	Concrete volume of entire path length (cubic meter)
4.7	v^S	Soil volume per soil sub-piece (cubic meter)
4.7	W^S	Supportive soil weight for single sub-piece
4.5	W^C	Concrete weight for single sub-piece
4.8	W^T	Total wall weight for single sub-piece (W^S+W^C)
4.8	c.o.g	Weighted center of gravity for supportive soil and concrete sub-piece
4.9	M^W	Moment arm for wall weight
4.12	e	Eccentricity, distance between base centerline and base intersection point of resultant force
1.4	c^f	Soil friction coefficient

4.7.4 Resultant force and eccentricity

The 3D volumetric process involves finding the center of gravity, also known as the volume centroid, of both the supportive soil and concrete volume. This is necessary to determine the resultant force point location onto which the lateral soil pressure and gravity act on the wall.

The center of gravity uses an arbitrary reference point. The distance between each centroid and the reference point is *a* and *b* respectively. The script uses the centroid of the concrete wall sub-piece as the reference point to where *b* equals zero. The distance from the supporting soil centroid to the concrete centroid becomes *a*. The soil weight (W^S) is multiplied by *a*, then divided by the total weight of supporting soil and concrete (W^T). This results in *c*, the distance between the concrete centroid and the weighted center of gravity. This process of determining the weighted center of gravity. is diagrammed in Figure 4.25. The projected distance between the wall toe and weighted center of gravity is the moment arm for the wall weight. The projected distance would be the distance between the two points if they were in the same plane, i.e., the distance if measuring a plan view drawing. The lateral soil pressure acts at a third of the wall height (h/3), so the weighted center of gravity is projected to the h/3 elevation. The toe line is projected to the h/3 elevation as well. To find the wall weight moment arm (M^W), the script finds the distance between the closest point on the toe line to the weighted center of gravity. This process of deriving the moment arm and projected weighted center of gravity is depicted in Figure 4.26.

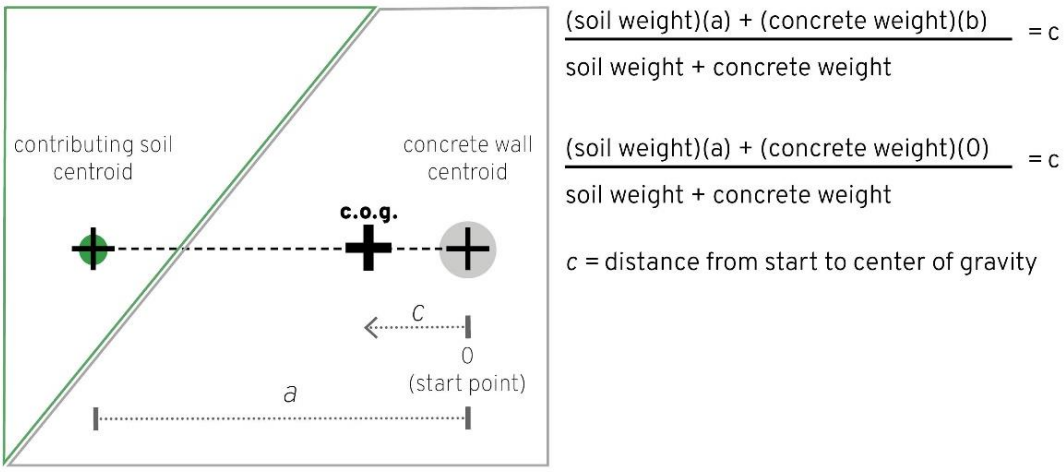

Figure 4.25 Diagram of process for finding weighted center of gravity

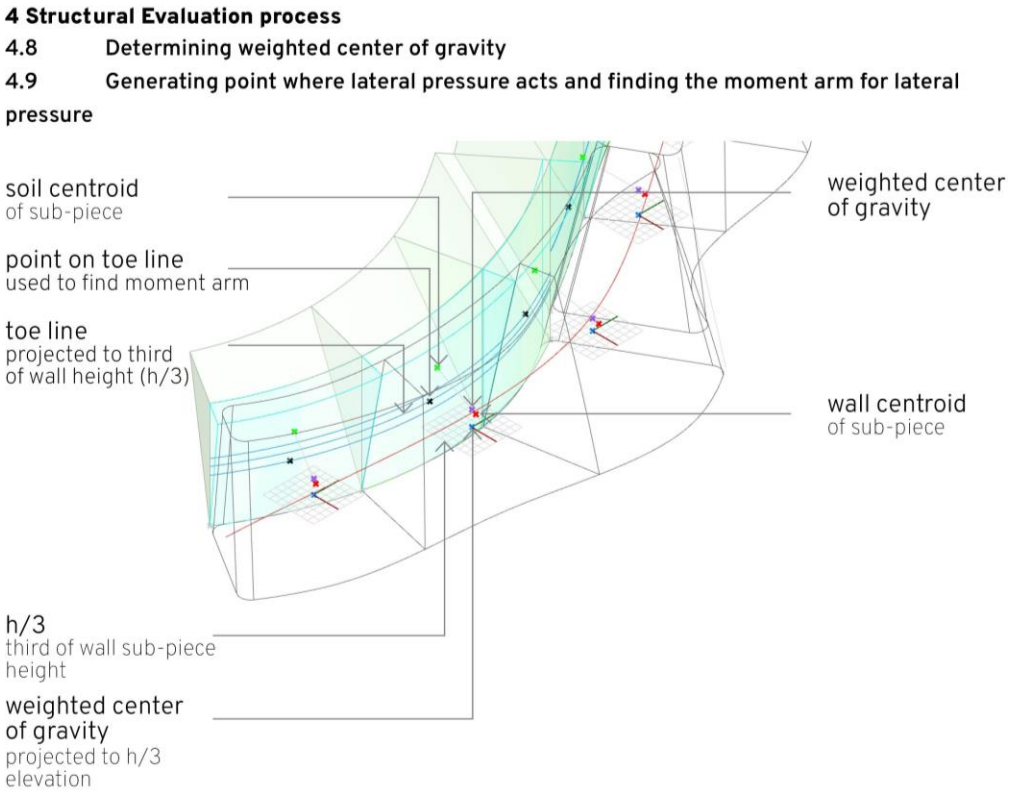

Figure 4.26 Preparations for resultant force calculations

After projecting the weighted center of gravity to the h/3 elevation, it becomes the point onto which forces of the lateral soil pressure and wall weight act. The lateral pressure (P) and wall weight (W^T) are graphically depicted at a 1:100 scale in the grasshopper preview (Figure 4.27). For example, if the wall weight is 30 kN per sub-piece, then the force would be a .3m line in the graphic preview. The lateral pressure requires the use of a perpendicular vector from the toe line to set the XY direction of the force. The wall weight is simply an upright vector with a negative Z direction. The value of the resultant force is $(W^T)^2 + (P)^2$. The script constructs a rectangle from the P and W^T vectors to generate the resultant force graphically. The diagonal of this rectangle is the scaled resultant force with the correct amplitude and direction. This resultant force line is extended to intersect with the wall base surface. For the wall to be stable, the intersection point must be within the middle third of the base. The distance from the intersection point to the base centerline line is the eccentricity of each wall sub-piece. The eccentricity variable is used in later modules to calculate the risk of crushing. Figure 4.24 depicts the graphical solution of the resultant force.

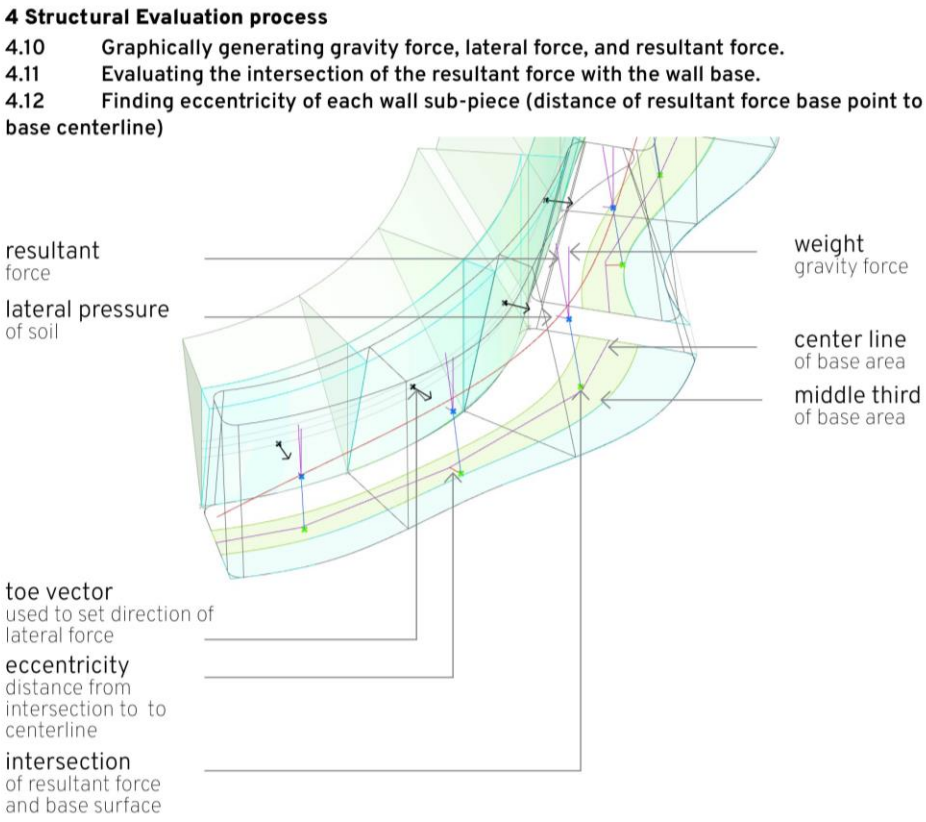

Figure 4.27 Resultant force variables

4.7.5 Sliding, crushing, and overturning risks

The script tests each sub-piece for its risk for overturning, crushing (i.e. settlement at toe) and sliding. These tests are primarily numerical calculations with geometry data generated in previous modules.

For the risk of overturning equation, the variables used are W^T (wall weight), M^W (moment arm for the wall weight), P (lateral pressure) and h (wall height), each variable is for a single sub-piece. The result must be larger than 2:

$$((W^T)(M^W)) / (P)(h/3) \quad > 2 \tag{4.5}$$

The test for crushing uses W^T (wall weight), B^A (base area), e (eccentricity), and B^W (base width). All variables are for a single sub-piece. The result of the crushing test must not exceed the soil bearing capacity in kN per square meters.

$$f = (W^T/B^A)(1+(6e/B^W)) \quad (4.6)$$

The test for sliding uses W^T (wall weight), c^f (a coefficient of friction) and P (lateral pressure). The result must be greater than 1.5.

$$((W^T)(c^f))/P > 1.5 \quad (4.7)$$

4.8 Printability evaluation processes

The fabrication parameters from Section 3.3 are incorporated into the toolkit as metrics the user can use to input their own manufacturer's limitations. In the next chapter, a composite sketch of different manufacturers is used to set the machine limitations for the amphitheater application. In this chapter, no particular manufacturer is used as the demonstration and parameters values are fictional for illustration purposes. The printability analysis in the script follows three processes: analyzing individual print layers for issues such as turning radii, evaluating surface slopes, and determining if the object fits within the print volume of the machine. All of these are automatic processes except for evaluating wall segments with a non-rectilinear print volume. In that process, the user must manually find a station point within the terrain for the 3D concrete printer. The script then evaluates where the wall object can be printed from selected station point. The script does not find plausible station points for the user, only

confirms feasibility. In this process, the user designs the movement sequence across the site for the printer.

4.8.1 Layer contour analysis

3D concrete printing uses a spiralized tool path derived from a continuous hollow surface. However, the print analysis modules use a simpler approximation with “layer contours”, section curves created by serial slicing of the wall segment. The script utilizes a default print orientation parallel to the ground, assuming the intent is in-situ concrete printing. The slicing orientation could be manually substituted in the script if the intent is off-site printing. The script is set to generate layer contours at 0.2m apart for faster computation times and legibility. However, this spacing value can be decreased as the wall’s geometric complexity increases. In addition, the layer contours could be generated at every layer height. However, this creates a density of error data that can be challenging to read.

Surface continuity allows the printer to extrude the entire object without stopping. Each layer contour is analyzed for its continuity by two parameters: closure and number of contours per layer height. Each layer contour is determined to be closed or open as a true/false value. An open contour curve would indicate a high point that prevents a full layer perimeter. Each layer height should only have one layer contour. Two layer contours at the same elevation would indicate that the top area of the wall has two hills or valleys preventing a single continuous layer contour. High and low points in the top surface could be accommodated by a manufacturer with variable layer heights if the height deviation is minor. Nonetheless, the script provides a clear visual reading of areas where continuity might be a concern. The number of contours per layer height is evaluated as equal or not equal to 1 as a true/false value. If both tests are true, then the layer contours at that particular layer height pass the test for surface continuity. Each layer

contour is also evaluated for self-intersection, so that the printer would not collide with its previously printed material.

As discussed in Section 2.2.2, there is a limited time frame in which a 3D concrete printer may deposit a layer of material to avoid issues with interlayer bonding. Essentially, a layer that takes too long to print will cause previous print material to dry out before adhering to the next layer. There is also the challenge with printing successive layers too quickly. If the layer is too short, the previous layers have inadequate time to develop self-supporting strength. However, these variables range between printing methods, print material and manufacturers. A complication is that print speed can be manipulated by the operator to alleviate these issues at least in part. The script tests each layer contour against a minimum and maximum perimeter length. The script allows the user to set their manufacturer specific recommended range. Layer contours that do not fall within the range are identified.

The layer contours are also evaluated for curvatures below the minimum turning radius of the 3D concrete printer. This evaluation assumes the print layer orientation is fixed parallel to the printing plane and does not account for inclined plane printing. Each contour is divided by a testing length of 0.05m to create a series of points. The curvature is evaluated at each point to be larger or smaller than the minimum turning radius. Areas that are straight will have a curvature radius of infinity and thus will prompt an error message. However, straight areas do not need to be evaluated when searching for tight bends.

4.8.2 Surface slopes

The steepness or slope of the surface is a critical factor in determining the printability of the object. A steep surface may fail mid-print as the concrete must be self-supporting while wet. The slope of the surface is defined for the user as the angle in degrees from the vertical direction.

The script generates a grid of points across the surface at which the surface normal direction is evaluated. This grid is generated from the existing UV grid of the surface. The UV grid is a coordinate system relative to the surface. An unaltered UV grid is denser in areas with geometric complexity. For this reason, using the UV grid points allows an adaptive level of testing precision where complex areas have more testing points. The angle between the surface normal and the XY plane is used to evaluate surface slope. The data is converted from radians to degrees for ease of use. If the maximum slope from vertical is 30 degrees (a^S), then the angle from XY plane (a^{act}) must be between 60 degrees and 120 degrees:

$$90-a^S \leq a^{act} \leq 90+a^S \tag{4.8}$$

This accounts for negative and positive surface normal vectors as well as surface orientation (Figure 4.28).

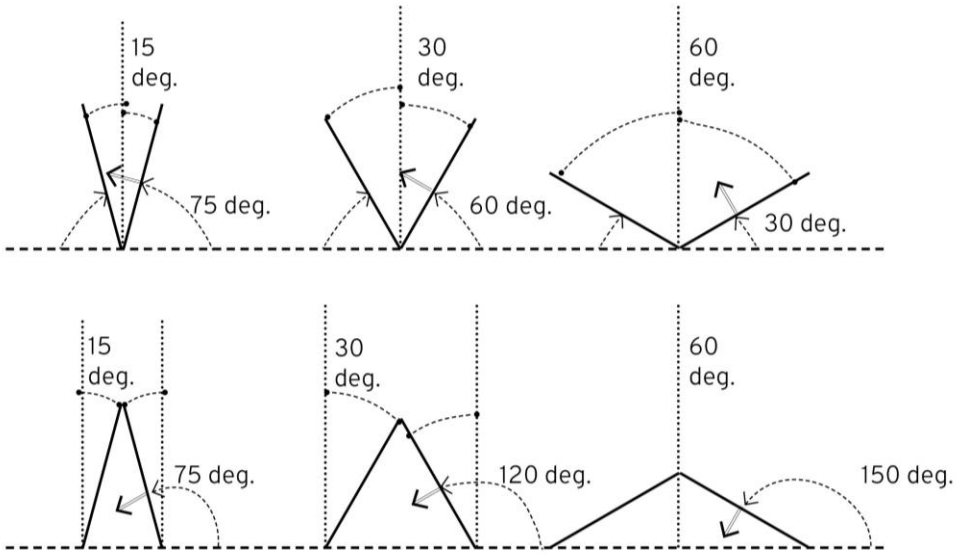

Figure 4.28 Relationship of surface normal vectors, angle from vertical and angle from XY plane

4.8.3 Print volume

Generally, 3D printers have a limited volume in which printing is feasible, with some exceptions discussed in Chapter II. Gantry frame printers are defined by a rectangular print volume. Other printing methods may have a donut-shaped or non-rectilinear print volume. The script evaluates each wall segment with a user-defined rectilinear print volume (Figure 4.29). To assess if a wall segment can fit within a print volume extents, a bounding box is created around each segment.

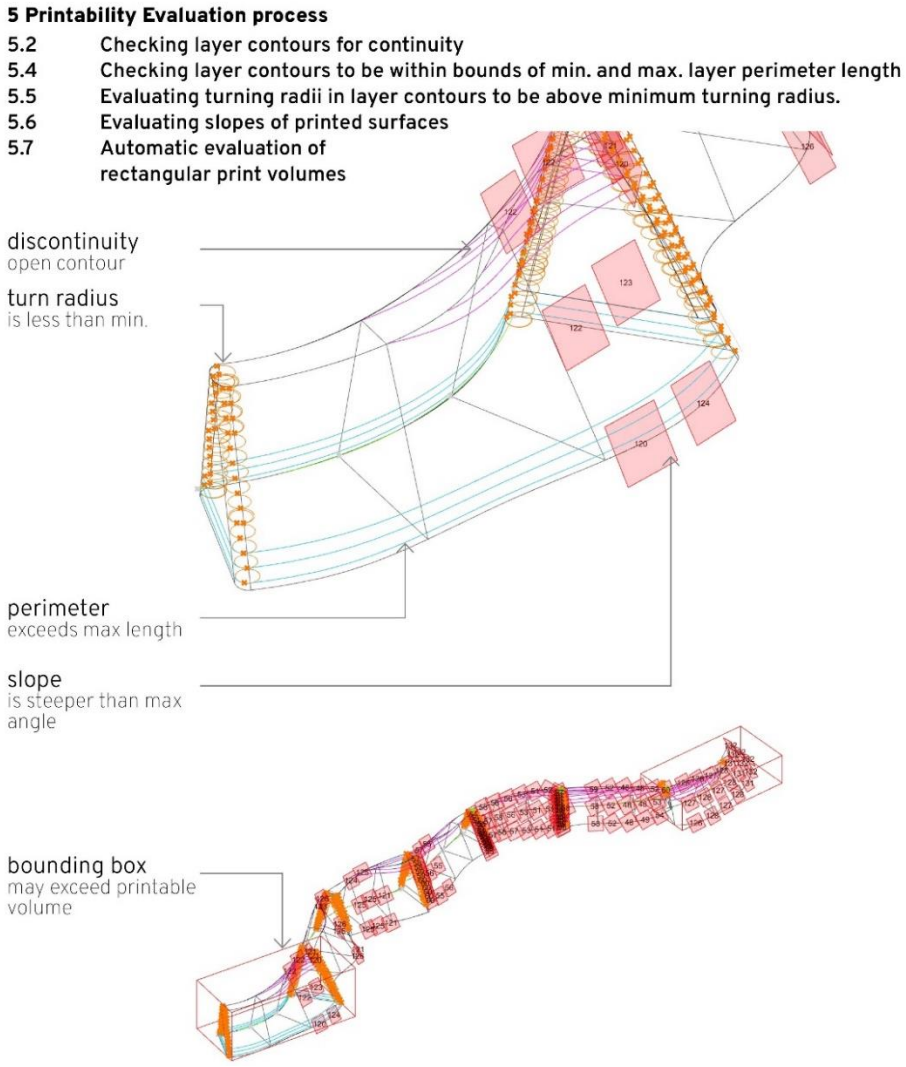

Figure 4.29 Live feedback on printability issues during design process

For non-rectilinear print volumes, module 5.8 allows the user to define the shape of the print volume and its station point (Figure 4.30). The script then evaluates whether the wall segment can be printed from that station point within the defined print volume. This becomes a process of manually shifting the station points to find the optimal location for each wall segment.

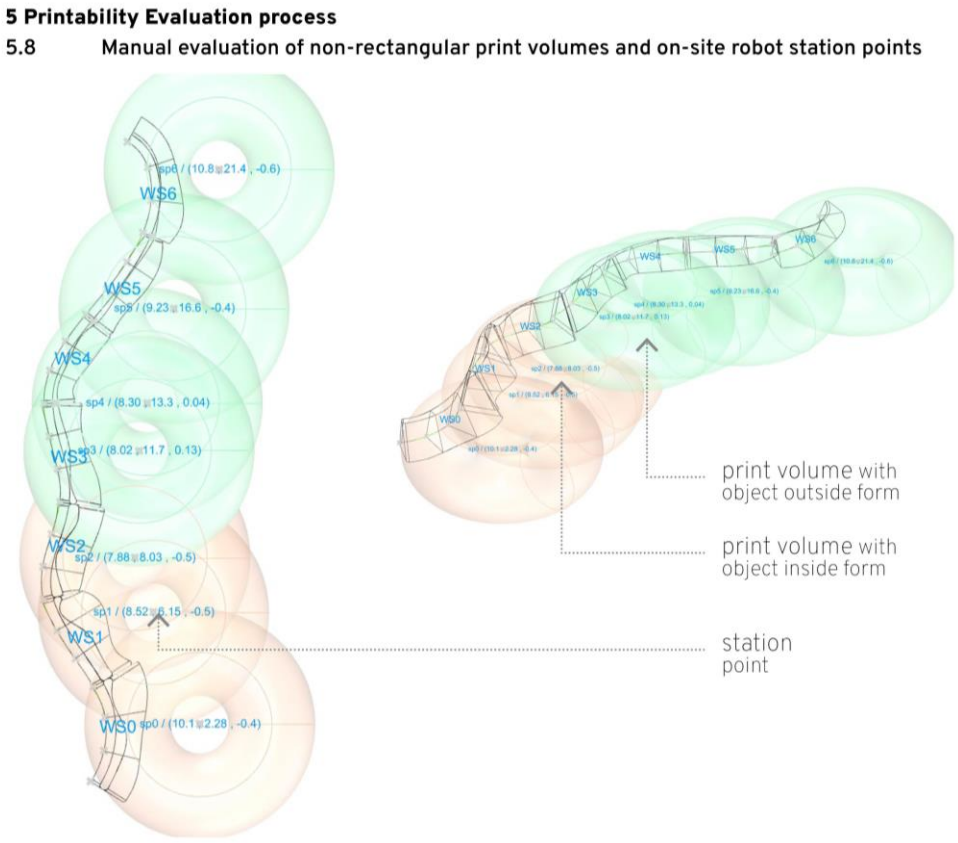

Figure 4.30 Iterative design of station points for printer

4.9 Remote control panel and export options

The script has a few features to ease the user experience within the tool and to facilitate further design work further outside the tool. The script is equipped with a remote control panel that allows convenient access to input variables while in the modeling environment (Figure 4.31). The script also has modules for baking geometry into a permanent form and exporting the wall's numerical data as comma separated value files. Baked geometry can be further edited, analyzed, or integrated into other design workflows. Numerical data can be further used to extract and analyze the data for structural and printability analysis. The script is also setup with the Colibri plug-in to process multiple design iterations and automatically export the visual and

numerical data. Colibri 2 is a plug-in for Grasshopper that aids in creating batch iterations of multiple variables. This plug-in allows for batch processing of numerous variable options, offering designers the ability to quickly explore different scenarios and evaluate their designs.

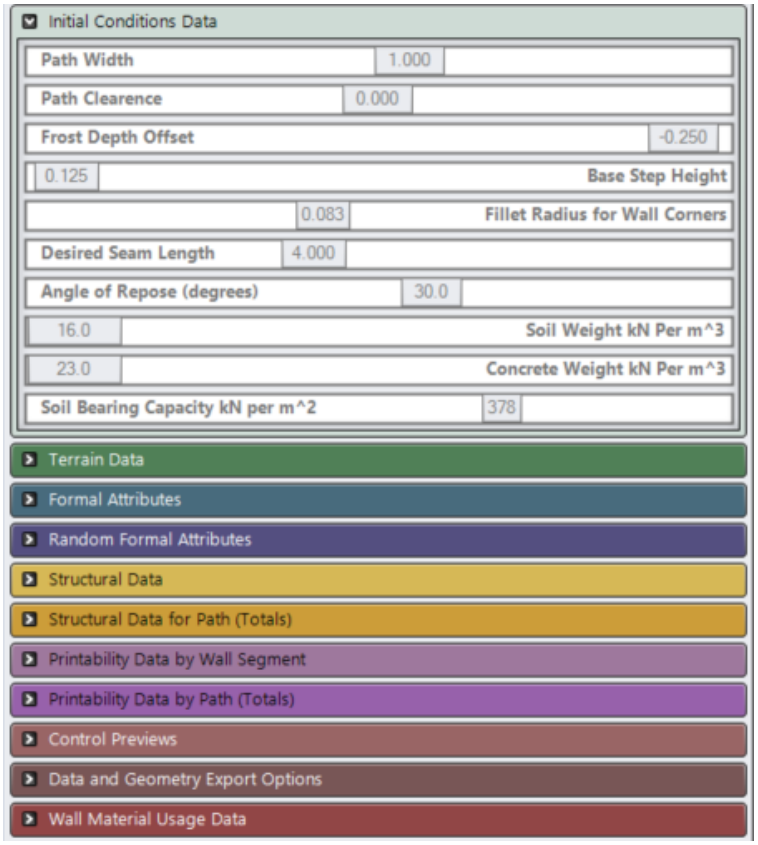

Figure 4.31 Remote Control Panel interface

CHAPTER V

RESULTS AND DISCUSSIONS: DEMONSTRATION OF DFC PROCESSES AND POTENTIALS WITH AN AMPHITHEATER APPLICATION

5.1 Experimental applications and purpose

The aim of this research and the toolkit is to inform and assist in the design process for DFC. The main question addressed is how DFC might facilitate terrain responsive design. Another motivation was to provide a demonstration case that serves as an initial starting point for speculations and critiques on the value of DFC in landscape architecture. The intent is not to contribute knowledge to the civil engineering discipline about retaining walls.

To explore the different avenues of the toolkit as a design aid, two different experiment series were conducted. The first series explores wall proportions that changed individually and incrementally. This intention was to quantify and visually demonstrate the impact of individual parameters on printability and structural stability. For example, by increasing and isolating the soil height multiplier, it was found to increase layer continuity issues: The increase in the undulation of the top wall edge resulted in more high and low points thus forming discontinuous layers. Afterwards, the design toolkit was used as a freeform design tool to investigate aesthetics and geometries within the concept of terrain responsive design. This series of results was undertaken in part to demonstrate an iterative exploratory process where design tools alleviate the burdens of meeting complex and wide-ranging requirements. This series of results is also intended to provide speculative examples of DFC in landscape architecture.

5.2 Existing conditions of test case - MSU Amphitheater

The amphitheater at Mississippi State University was chosen as the test case for its variety of terrain and wall geometry conditions (Figures 5.1 and 5.2) . The amphitheater wall geometry is composed of arcs connected to straight line segments, and it has different relationships to the terrain. On occasions, the wall is flush with the terrain. In other moments, the wall rises above the terrain without actively retaining much soil. The wall is paired with a sloped path. The wall also has relatively flat areas with the stage and lawn area immediately in front of the amphitheater.

The toolkit can accommodate tight square corners by either splitting the wall into two perpendicular segments or by filleting the corner to a large radius. In the following results, the strategy of rounding the corner was chosen, as seen in Figure 5.3. The amphitheater has three retaining walls: a long linear wall along the stage edge and two mirrored side walls. Since the script only processes one path at a time, the linear and left wall were executed separately. The right wall is usually ignored or mirrored from the left to avoid repeat computation. Table 5.1 describes the soil volume loads across each wall. There are some areas on each wall with higher volumes of soil to be retained. The following soil and material variables were used within the structural evaluation modules:

- Frost depth – 0.3m
- Angle of repose – 30 degrees
- Soil weight - 16 kN per cubic meter
- Concrete weight – 23 kN per cubic meter
- Soil bearing capacity – 378 kN per cubic meter
- Soil friction coefficient – 0.5

Figure 5.1 Front view of Mississippi State Univ. amphitheater with long linear wall framing stage

Figure 5.2 Side walls and path of Mississippi State Univ. amphitheater

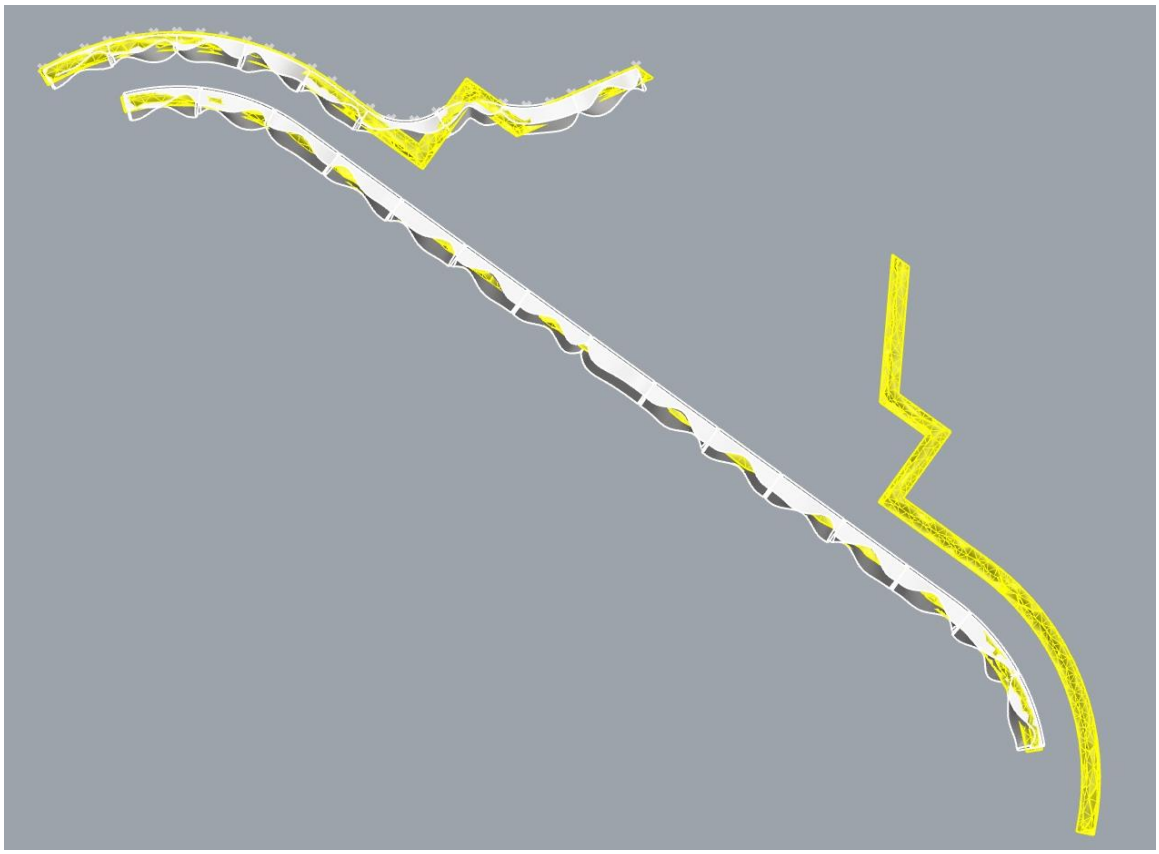

Figure 5.3 Footprint of existing walls (yellow) versus altered wall corners

Table 5.1 Soil volume, length, and height for each sub-piece within each wall

V	L	H		V	L	H	
0.25	1.32	1.37	0.19	0.12	1.20	1.23	0.10
0.29	1.32	1.38	0.22	0.15	1.20	1.23	0.13
0.32	1.32	1.38	0.24	0.19	1.20	1.23	0.16
0.42	1.32	1.39	0.32	0.23	1.20	1.24	0.19
0.41	1.32	1.39	0.31	0.28	1.20	1.24	0.23
0.42	1.32	1.39	0.31	0.31	1.20	1.25	0.26
0.65	1.32	1.41	0.49	0.33	1.20	1.25	0.27
0.67	1.32	1.34	0.51	0.33	1.20	1.25	0.28
0.63	1.32	1.32	0.48	0.34	1.20	1.25	0.28
0.74	1.32	1.32	0.56	0.27	1.20	1.24	0.23
0.74	1.32	1.32	0.56	0.28	1.20	1.24	0.23
0.82	1.32	1.32	0.62	0.26	1.20	1.24	0.22
1.05	1.32	1.32	0.80	0.25	1.20	1.24	0.20
0.98	1.32	1.32	0.74	0.23	1.20	1.20	0.19
0.96	1.32	1.32	0.73	0.26	1.20	1.20	0.22
0.96	1.32	1.32	0.73	0.23	1.20	1.17	0.19
1.07	1.32	1.32	0.81	0.25	1.20	1.17	0.21
1.08	1.32	1.32	0.81	0.24	1.20	1.27	0.20
1.01	1.32	1.32	0.77	0.24	1.20	1.30	0.20
0.99	1.32	1.32	0.75	0.21	1.20	1.35	0.18
1.05	1.32	1.32	0.80	0.21	1.20	1.26	0.18
1.13	1.32	1.32	0.85	0.26	1.20	1.19	0.21
1.08	1.32	1.32	0.81	0.31	1.20	1.19	0.26
0.95	1.32	1.32	0.72	0.34	1.20	1.20	0.28
1.03	1.32	1.32	0.78	0.35	1.20	1.20	0.29
1.14	1.32	1.32	0.86	0.33	1.20	1.20	0.27
1.20	1.32	1.32	0.90	0.36	1.20	1.20	0.30
1.06	1.32	1.32	0.80				
1.00	1.32	1.32	0.75				
1.12	1.32	1.32	0.85				
1.21	1.32	1.32	0.91				
1.18	1.32	1.32	0.90				
1.04	1.32	1.32	0.79				
0.91	1.32	1.32	0.69				
0.96	1.32	1.32	0.73				
1.03	1.32	1.32	0.78				
0.80	1.32	1.32	0.60				
0.73	1.32	1.32	0.55				
0.78	1.32	1.32	0.59				
0.58	1.32	1.32	0.44				
0.63	1.32	1.57	0.48				
0.64	1.32	1.49	0.48				
0.42	1.32	1.38	0.32				
0.41	1.32	1.35	0.31				
0.36	1.32	1.34	0.27				

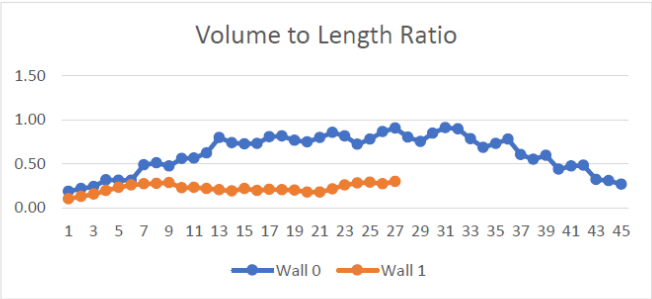

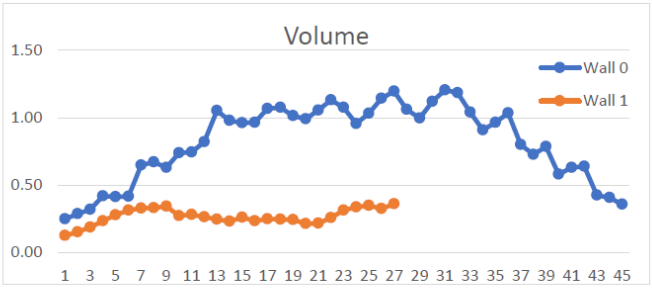

5.3 Fabrication parameters

For the amphitheater demonstration, the toolkit was set to parameters for a mobile robotic arm printer like the *Cybe Robot Crawler*. The following parameters were created as a composite of multiple manufacturer systems:

- Production environment – In-situ printing
- Print volume – 5m wide donut and 4.5m max height (CyBe Construction, 2022)
- Minimum turning radius - 17.5mm (Baniasadi, 2021)

- Slope – 30 degrees (Baniasadi, 2021)
- Perimeter length – Lengths below 2.5m and above 90m were identified, but further manufacturer consultation would be required to deem these lengths unprintable. These lengths were derived from a 5-second and 3-minute print length at 500mm/s.
- Surface continuity – Geometry is evaluated for continuity and lack of self-intersection.

5.4 Series I: inventory stage

5.4.1 Series objectives and definitions

In this iteration series, one variable of the wall proportions changed while all other dimensions were constant. There were four variables that received four iterations each, which were performed on both walls resulting in a total of eight wall forms per variable. The variables studied were the "soil volume multiplier", which define the ratio between the wall proportions and the soil volume actively retained. Each multiplier was studied at the following ratios: 0.1, 0.2, 0.3, and 0.4. Each wall aspect had a "baseline" that defined the minimum dimension across all variations. Table 5.1 outlines the inputs for each iteration. Since the soil volume multipliers increase the wall dimensions, each experiment had the focus variable reduced to a lower baseline dimensions to prevent excessive wall growth. The wall base had a slight adjustment, being set at .7m, except when testing the effect of the wall width multiplier. In that case, the minimum wall base dimension was lowered to .5m. Otherwise, the width multiplier would cause the wall to grow excessively huge. However, lowering the wall base to 0.5m caused the other experiments to have excessive structural risks and skewed the data. Similarly, the toe batter was lowered to a baseline of 0 m only in the iterations focused on the toe batter soil volume multiplier. The front batter baseline dimension was lowered to .2 m for the front batter soil volume multiplier

iterations. One critical observation from the previous chapters is the definition of front batter. The front batter is defined as the projected distance between the top front edge of the wall and the back toe edge. An increase in the toe batter dimension is an increase in the distance away from the back toe and a decrease in the angle of the front face. In other words, increases in the front batter reflect the front face becoming more vertical, with the top edge becoming closer in line with the wall width. This reflects an increase in material as well. The toe batter increase is also an increase in the projected distance from the back toe. However, the increase in toe batter angles the back face further and decreases concrete material, while increasing the supporting soil volume. An increase in batter dimension has distinctly different effects depending on which batter is altered.

Table 5.2 Inputs for the formal variables for each iteration of the first series

DV	Series		FORMAL Height Baseline (m)	Height Multiplier	Width Baseline (m)	Width Multiplier	Toe Batter Baseline (m)	Toe Batter Multiplier	Front Batter Baseline (m)	Front Batter Multiplier
Height	1	a	0	**0.1**	0.70	0	0.03	0	0.40	0
Height	1	b	0	**0.2**	0.70	0	0.03	0	0.40	0
Height	1	c	0	**0.3**	0.70	0	0.03	0	0.40	0
Height	1	d	0	**0.4**	0.70	0	0.03	0	0.40	0
Width	2	a	0	0	0.50	**0.1**	0.03	0	0.40	0
Width	2	b	0	0	0.50	**0.2**	0.03	0	0.40	0
Width	2	c	0	0	0.50	**0.3**	0.03	0	0.40	0
Width	2	d	0	0	0.50	**0.4**	0.03	0	0.40	0
ToeBatter	3	a	0	0	0.70	0	0.00	**0.1**	0.50	0
ToeBatter	3	b	0	0	0.70	0	0.00	**0.2**	0.50	0
ToeBatter	3	c	0	0	0.70	0	0.00	**0.3**	0.50	0
ToeBatter	3	d	0	0	0.70	0	0.00	**0.4**	0.50	0
FrontBatter	4	a	0	0	0.70	0	0.03	0	0.20	**0.1**
FrontBatter	4	b	0	0	0.70	0	0.03	0	0.20	**0.2**
FrontBatter	4	c	0	0	0.70	0	0.03	0	0.20	**0.3**
FrontBatter	4	d	0	0	0.70	0	0.03	0	0.20	**0.4**

Table 5.3 Definitions of dependent variables for structural analysis (output data)

Variable	Definition
Lateral pressure	The lateral pressure (kN) for each sub-piece was calculated. This metric is the sum of all sub-pieces.
# of Eccentricity Issues	This counts the total number of sub-pieces whose resultant force does not intersect with the middle third area of the base.
# of Overturning Issues	This counts the total number of sub-pieces with a risk of overturning as defined in the previous chapter.
# of Sliding Risks	This counts the total number of sub-pieces with a risk of sliding as defined in the previous chapter.
# of Crushing Risks	This counts the total number of sub-pieces with a risk of crushing as defined in the previous chapter.
# of SubPieces w/Struct Issue	This tallies the number of sub-pieces with at least one structural risk, but not the total number of structural risks. A wall with two possible risks would only be counted once.
Total # of SubPieces	This is the total number of sub-pieces in the path across wall segments.
% of SP w/StructIssue	The total of unique sub-pieces with at least one structural risk is divided over the total number of sub-pieces in the path.

Table 5.4 Definitions of dependent variables for printability analysis (output data)

Variable	Definition
# of Discontinuous Layers	This counts the number of horizontal analysis planes with layer contours that are discontinuous rather than a count of all fragmented layers.
# of Self-Intersection points	This totals all self-intersecting points on the layer contours generated across the entire path.
# of Contour Length Issues	This totals all layer contours that do not fall within the user's min/max perimeter length across the entire path.
# of Small Turning Radii	This totals all analysis points where the curvature radius has been found to be under the minimum turning radius.
# of Steep Slope points	This is the total of all UV grid points found to exceed the maximum slope angle. This is a relative metric that will differ between different walls and iterations. A more complex geometry will be tested more densely and frequently, which may result in a higher count of failing slopes. This metric is supplemented by a visual inspection of the image output.
# of Print Volume Issues	This tallies the number of wall segments whose form may not fit within the extents of a rectangular print volume.

Table 5.5 Definitions of dependent variables for material usage analysis (output data)

Variables	Definitions
Total Concrete Volume	This is the sum of all concrete sub-pieces in the entire path using cubic meters.
Total Soil Volume	This is the sum of all actively retained soil sub-pieces in the entire path using cubic meters.
C:S Volume Ratio	Ratio between concrete volume and soil volume actively retained in the entire path.

5.4.2 First series data

Table 5.6 Input and output data for iteration series with wall elevation multiplier as unfixed variable

Wall Index	Formal	Height Baseline (m)	Height Multiplier	Width Baseline (m)	Width Multiplier	Toe Batter Baseline (m)	Toe Batter Multiplier	Front Batter Baseline (m)	Front Batter Multiplier	STRUCTURAL	Lateral Pressure	# of Eccentricity Issues	# of Overturning Risks	# of Sliding Risks	# of Crushing Risks	# of SubPieces w/Struct Issue	Total # of SubPieces	% of SP w/Structural Issues	PRINT EVAL	# of Discontinous Layers	# of Self-Intersection points	# of Contour Length Issues	# of Small Turning Radii	# of Steep Slope points	# of Print volume Issues	MATERIAL	Total Concrete Volume	Total Soil Volume	C:S Volume Ratio
0	1a	0	0.10	0.70	0	0.03	0	0.40	0		263.1	0	13	0	0	13	45	29%		16	0	9	0	0	15		52.0	36.9	1.41
0	1b	0	0.20	0.70	0	0.03	0	0.40	0		263.1	0	10	0	0	10	45	22%		19	0	12	6	0	15		54.6	36.9	1.48
0	1c	0	0.30	0.70	0	0.03	0	0.40	0		263.1	0	0	0	0	0	45	0%		19	0	11	0	0	15		57.2	36.9	1.55
0	1d	0	0.40	0.70	0	0.03	0	0.40	0		263.1	0	0	0	0	0	45	0%		27	0	19	0	0	15		59.8	36.9	1.62
1	1a	0	0.10	0.70	0	0.03	0	0.40	0		55.6	0	0	0	0	0	27	0%		12	0	6	0	0	9		16.7	7.2	2.34
1	1b	0	0.20	0.70	0	0.03	0	0.40	0		55.6	0	0	0	0	0	27	0%		12	0	6	0	0	9		17.2	7.2	2.40
1	1c	0	0.30	0.70	0	0.03	0	0.40	0		55.6	0	0	0	0	0	27	0%		15	0	8	0	0	9		17.6	7.2	2.46
1	1d	0	0.40	0.70	0	0.03	0	0.40	0		55.6	0	0	0	0	0	27	0%		11	0	6	0	0	9		18.1	7.2	2.53

Table 5.7 Input and output data for iteration series with wall width multiplier as unfixed variable

Wall Index	Formal	Height Baseline (m)	Height Multiplier	Width Baseline (m)	Width Multiplier	Toe Batter Baseline (m)	Toe Batter Multiplier	Front Batter Baseline (m)	Front Batter Multiplier	STRUCTURAL	Lateral Pressure	# of Eccentricity Issues	# of Overturning Risks	# of Sliding Risks	# of Crushing Risks	# of SubPieces w/Struct Issue	Total # of SubPieces	% of SP w/Structural Issues	PRINT EVAL	# of Discontinous Layers	# of Self-Intersection points	# of Contour Length Issues	# of Small Turning Radii	# of Steep Slope points	# of Print volume Issues	MATERIAL	Total Concrete Volume	Total Soil Volume	C:S Volume Ratio
0	2a	0	0	0.50	0.10	0.03	0	0.40	0		263.1	26	28	0	0	28	45	62%		16	0	9	0	0	15		44.3	36.9	1.20
0	2b	0	0	0.50	0.20	0.03	0	0.40	0		263.1	0	22	0	0	22	45	49%		16	0	9	0	0	15		48.3	36.9	1.31
0	2c	0	0	0.50	0.30	0.03	0	0.40	0		263.1	0	0	0	0	0	45	0%		16	0	9	0	0	15		52.4	36.9	1.42
0	2d	0	0	0.50	0.40	0.03	0	0.40	0		263.1	0	0	0	0	0	45	0%		16	0	9	0	0	15		56.4	36.9	1.53
1	2a	0	0	0.50	0.10	0.03	0	0.40	0		55.6	0	0	0	0	0	27	0%		12	0	7	0	0	9		13.6	7.2	1.90
1	2b	0	0	0.50	0.20	0.03	0	0.40	0		55.6	0	0	0	0	0	27	0%		12	0	7	0	0	9		14.1	7.2	1.96
1	2c	0	0	0.50	0.30	0.03	0	0.40	0		55.6	0	0	0	0	0	27	0%		12	0	7	0	0	9		14.5	7.2	2.02
1	2d	0	0	0.50	0.40	0.03	0	0.40	0		55.6	0	0	0	0	0	27	0%		12	0	7	0	0	9		14.9	7.2	2.08

Table 5.8 Input and output data for iteration series with wall toe batter multiplier as unfixed variable.

Wall Index	Formal	Height Baseline (m)	Height Multiplier	Width Baseline (m)	Width Multiplier	Toe Batter Baseline (m)	Toe Batter Multiplier	Front Batter Baseline (m)	Front Batter Multiplier	STRUCTURAL	Lateral Pressure	# of Eccentricity Issues	# of Overturning Risks	# of Sliding Risks	# of Crushing Risks	# of SubPieces w/Struct Issue	Total # of SubPieces	% of SP w/Structural Issues	PRINT EVAL	# of Discontinous Layers	# of Self-Intersection points	# of Contour Length Issues	# of Small Turning Radii	# of Steep Slope points	# of Print volume Issues	MATERIAL	Total Concrete Volume	Total Soil Volume	C : S Volume Ratio
0	3a	0	0	0.70	0	0.00	0.10	0.50	0		263.1	11	2	0	0	11	45	24%		16	0	8	0	0	15		51.3	36.9	1.39
0	3b	0	0	0.70	0	0.00	0.20	0.50	0		263.1	22	5	0	0	22	45	49%		16	0	9	0	0	15		47.3	36.9	1.28
0	3c	0	0	0.70	0	0.00	0.30	0.50	0		263.1	24	11	0	0	24	45	53%		16	6	9	0	0	15		43.2	36.9	1.17
0	3d	0	0	0.70	0	0.00	0.40	0.50	0		263.1	26	17	0	0	26	45	58%		16	20	9	0	0	15		39.2	36.9	1.06
1	3a	0	0	0.70	0	0.00	0.10	0.50	0		55.6	0	0	0	0	0	27	0%		12	0	7	0	0	9		17.8	7.2	2.49
1	3b	0	0	0.70	0	0.00	0.20	0.50	0		55.6	0	0	0	0	0	27	0%		12	0	7	0	0	9		17.4	7.2	2.43
1	3c	0	0	0.70	0	0.00	0.30	0.50	0		55.6	0	0	0	0	0	27	0%		12	0	7	0	0	9		17.0	7.2	2.38
1	3d	0	0	0.70	0	0.00	0.40	0.50	0		55.6	0	0	0	0	0	27	0%		12	0	7	0	0	9		16.6	7.2	2.32

Table 5.9 Input and output data for iteration series with wall front batter multiplier as unfixed variable.

Wall Index	Formal	Height Baseline (m)	Height Multiplier	Width Baseline (m)	Width Multiplier	Toe Batter Baseline (m)	Toe Batter Multiplier	Front Batter Baseline (m)	Front Batter Multiplier	STRUCTURAL	Lateral Pressure	# of Eccentricity Issues	# of Overturning Risks	# of Sliding Risks	# of Crushing Risks	# of SubPieces w/Struct Issue	Total # of SubPieces	% of SP w/Structural Issues	PRINT EVAL	# of Discontinous Layers	# of Self-Intersection points	# of Contour Length Issues	# of Small Turning Radii	# of Steep Slope points	# of Print volume Issues	MATERIAL	Total Concrete Volume	Total Soil Volume	C : S Volume Ratio
0	4a	0	0	0.70	0	0.03	0	0.20	0.10		263.1	0	26	0	0	26	45	58%		16	0	9	0	0	15		44.2	36.9	1.20
0	4b	0	0	0.70	0	0.03	0	0.20	0.20		263.1	0	22	0	0	22	45	49%		16	0	9	0	0	15		48.3	36.9	1.31
0	4c	0	0	0.70	0	0.03	0	0.20	0.30		263.1	0	0	0	0	0	45	0%		16	0	9	0	0	15		52.4	36.9	1.42
0	4d	0	0	0.70	0	0.03	0	0.20	0.40		263.1	11	0	0	0	11	45	24%		16	0	9	0	0	15		56.4	36.9	1.53
1	4a	0	0	0.70	0	0.03	0	0.20	0.10		55.6	0	1	1	0	1	27	4%		12	0	7	0	26	9		12.9	7.2	1.80
1	4b	0	0	0.70	0	0.03	0	0.20	0.20		55.6	0	0	0	0	0	27	0%		12	0	7	0	13	9		14.1	7.2	1.96
1	4c	0	0	0.70	0	0.03	0	0.20	0.30		55.6	0	0	0	0	0	27	0%		12	0	7	0	13	9		14.5	7.2	2.02
1	4d	0	0	0.70	0	0.03	0	0.20	0.40		55.6	0	0	0	0	0	27	0%		12	0	7	0	10	9		14.9	7.2	2.08

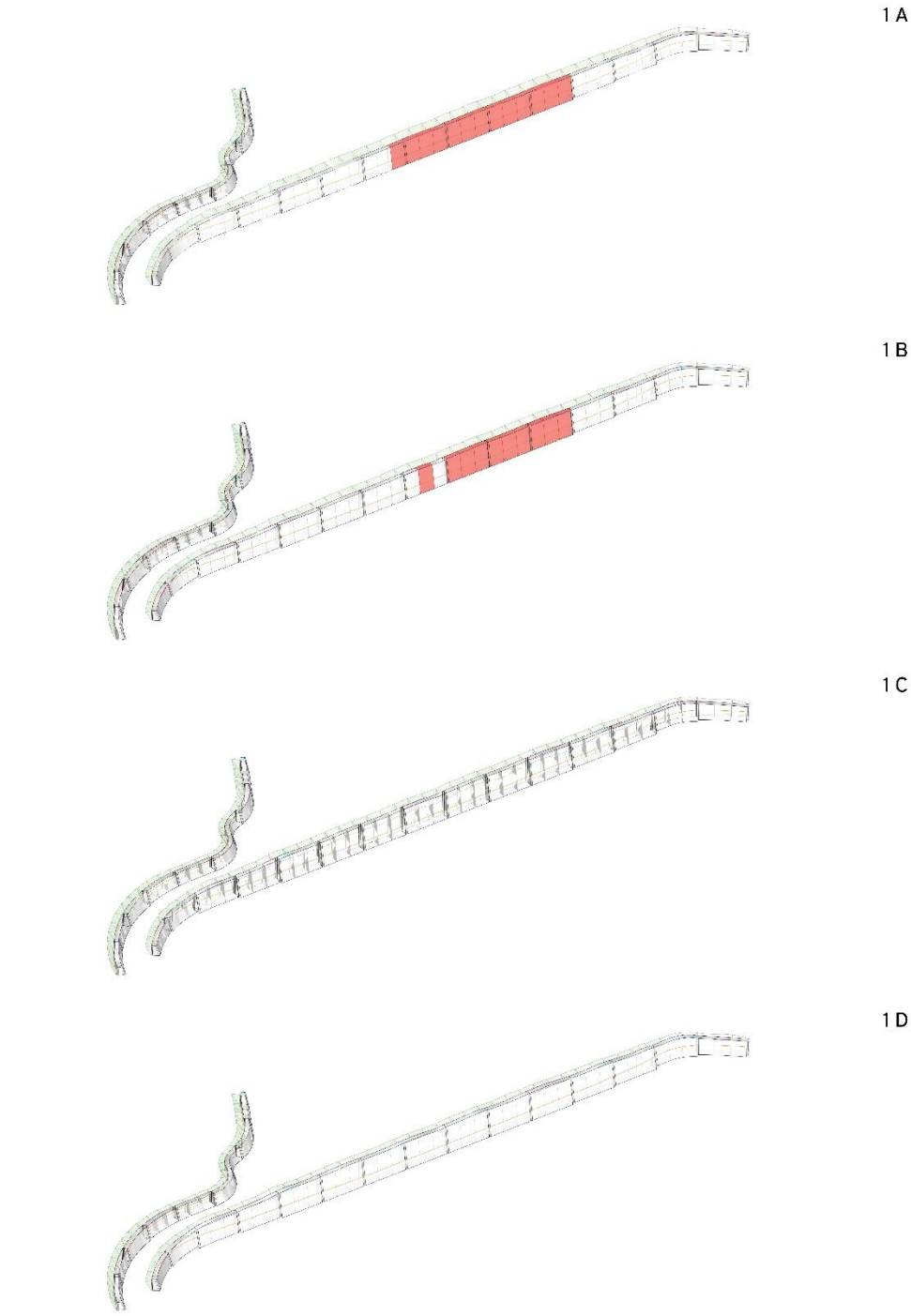

Figure 5.4 Wall forms with wall elevation multiplier as unfixed variable (Sub-pieces with structural risks are depicted in red.)

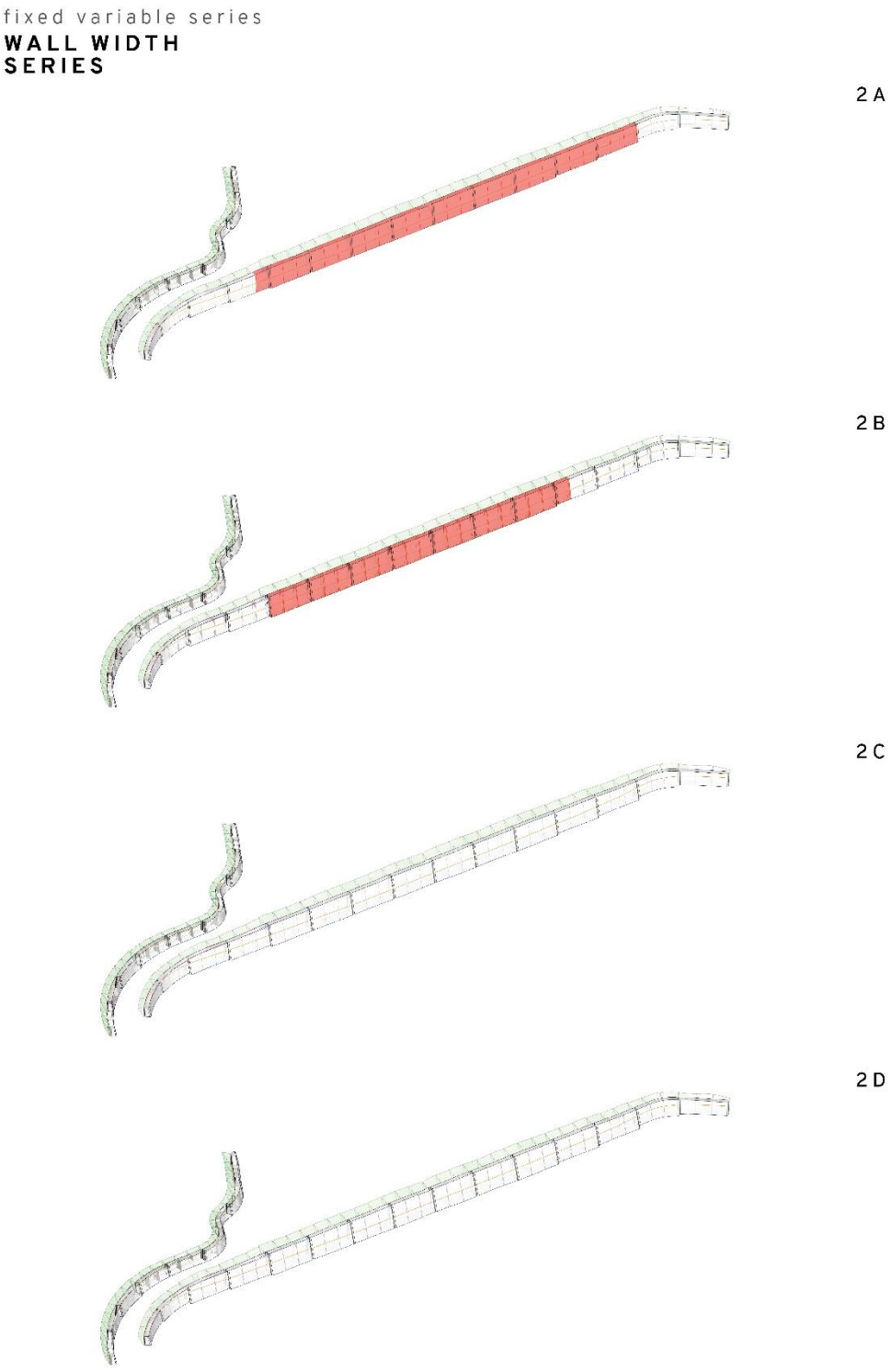

Figure 5.5 Wall width multiplier as unfixed variable (Sub-pieces with structural risks are depicted in red.)

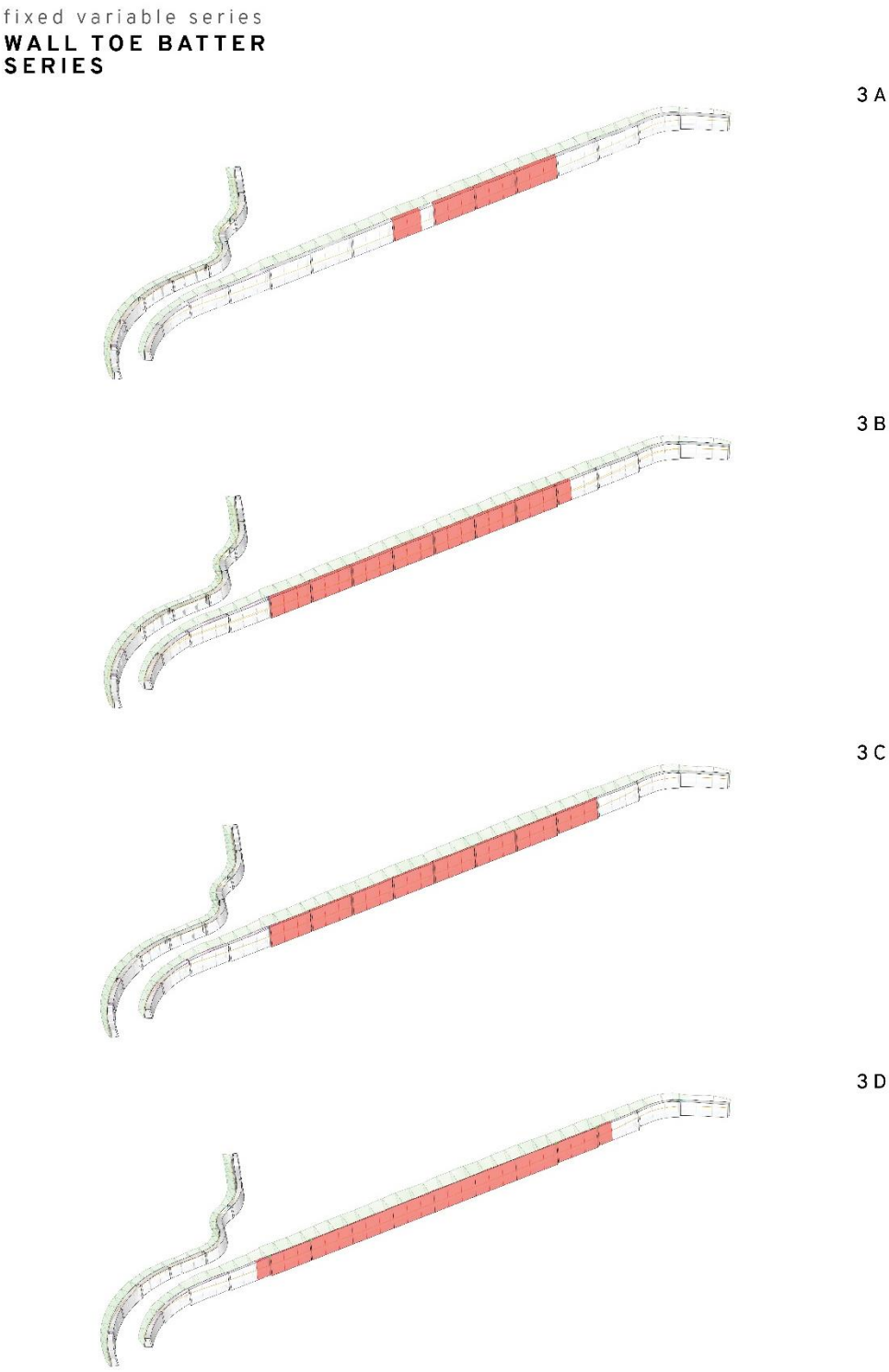

Figure 5.6 Wall toe batter multiplier as unfixed variable (Sub-pieces with structural risks are depicted in red.)

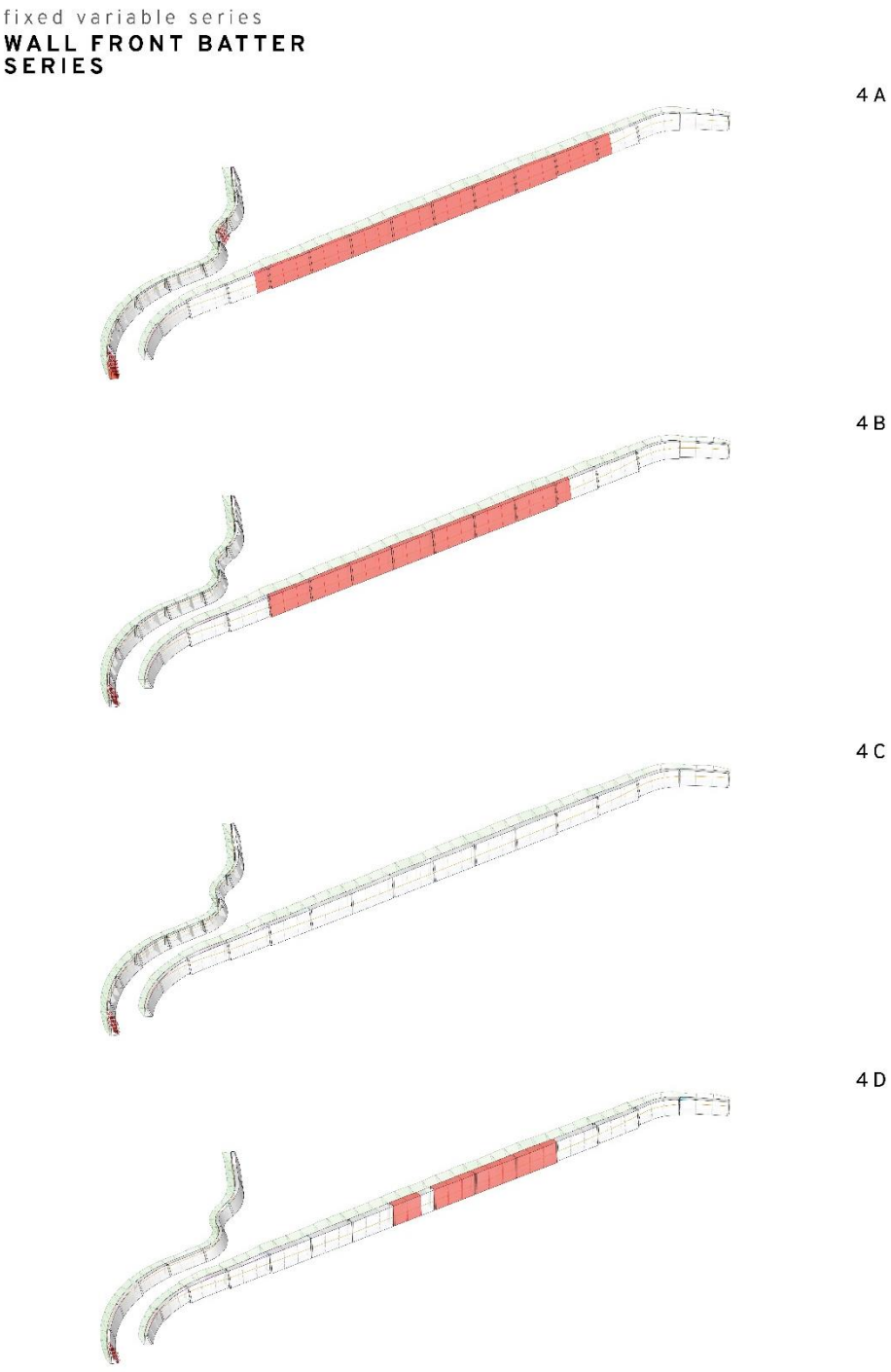

Figure 5.7 Wall front batter multiplier as unfixed variable (Sub-pieces with structural risks are depicted in red.)

5.4.3 Observations

There is value for a designer to see the impacts of isolated variables on a particular terrain and intended wall location. The intent of this series is not to state generalizable facts about how to successfully proportion any retaining wall in any site. Rather, this series is meant as a demonstration of processes, actions, and insights a designer can explore with the toolkit. This fixed series of manipulations articulates to the designer the different values and effects of each variable. Likewise, this allows the designer to see which permutations cause high and low material consumption across a mass of options. The following six insights were derived from the thirty-two wall iterations produced in this series.

Prior to the first series, the author was unaware of any major differences in structural needs between the different walls. Noticing the higher proportion of sub-pieces at risk of structural failure in wall 0 led to further investigation into the causes. The differences in the data led to an awareness that wall 0 could fail more easily and required more consideration for its proportions.

Increases in wall height increased the stability of the wall (Table 5.6). However, increasing the wall elevation multiplier led to more undulation in the top area of the wall which can be more complex to print, but not impossible for all manufacturers. This is evident in the increase of discontinuous layers with increases in the wall height multiplier in Table 5.6. For both the wall height and wall width soil multiplier, there is a point where the dimension is satisfactory and increases after that point have diminishing impacts on structural stability. In wall 0, the ratio of 0.3 seems to be a “sweet spot” for the wall width multiplier, including the 0.5m minimum wall width dimension. Similarly, 0.3 marks a sufficient wall height multiplier for wall 0. For Wall 1, increasing the toe batter is effective in trimming down material use, but for wall 0

this merely increases structural issues. Increasing the front batter (where the front face becomes less angled) increases material use but also wall stability (Table 5.8). There is a limit to how far the front batter can be increased without projecting the top edge of the wall past the wall bottom edge. Similarly, a low front batter dimension can cause steep slopes on the front face as seen in wall 1 (Table 5.8)

All permutations are primarily judged against the concrete volume to soil retained ratio and the percentage of wall sub-pieces with at least one structural risk. The concrete to soil retained volume ratio ranged from 1.06 to 1.62 for wall 0 and 1.80 to 2.53 for wall 1. The percentage of failing sub-pieces ranged from 0% to 62%. On average, wall permutations with a low concrete use have the higher percentages of structural issues. However, the large quantity of permutations makes it possible to find surprising successes with lower material use and positive structural qualities. For wall 0, iterations 2c and 4c had no structural risks and a concrete to soil volume ratio of 1.42. These iterations were highly efficient in comparison to the remaining 14 iterations. These iterations were used as the initial wall proportions for further design in Series II.

Note that this process can be used to inspire new tests and explore any proportion question the designer discovers. For example, one could explore setting the toe batter to be a negative ratio relative to the soil volume. In that case, the top back edge of the wall would progressively lean towards the soil retained as the soil loads increase. There would be a practical limitation on how far the top rear edge of the wall can recede without conflicting with the soil backfilling process. Another possibility could be paring opposing ratios, such as a ratio that increases material use combined with a ratio that trims material. A positive wall width soil volume multiplier would cause the bottom of the wall to kick out towards the path. This could be paired with a negative front batter ratio to where the wall leans in towards the soil as the soil load

increases. This would begin by setting the base dimension of front batter equal to the wall width baseline dimension making the front face vertical. Then as the soil volumes increase, the wall would both flare towards the path and lean back. The script allows the designer to quickly perceive the aesthetic and structural impact of such a decision without the time-consuming process of manually modelling the concept. Furthermore, the script would immediately clarify fabrication limitations such as excessive slopes in the previous example. The script, especially the use of Colibri to run series of permutations in a single batch, allows the user to run experiments effortlessly to inform their own design agenda.

5.5 Series II: exploratory stage of design process

5.5.1 Series objectives and definitions

The previous series is an inventory stage that equips the designer with possible wall proportion strategies and an understanding of soil loads across the wall. This second series is an initial exploration of design strategies and the resulting effects on aesthetics, printability, and wall stability. This stage quickly surveys the extents and range of the design qualities through studying the effects of the formal parameters. This is a deeper investigation of the findings from the first series as well as a preliminary stage to more detailed design.

5.5.2 Iteration stages and actions

Each wall was designed by the following three design stages. Initially, the basic wall proportions are set, which includes the baseline dimensions and the soil volume multiplier for the wall elevation, width, and batters. Next, the factors associated with random deviations in the wall were explored. There were three aspects to consider: the magnitude of the deviation, the frequency of deviant points, and then exploring multiple variations of the first two conditions.

The “seed number” variable allows the designer to reshuffle the design outcome and receive a different solution to the parameters set. Lastly, the “scale of detail” was manipulated to change the intensity or density of the geometry. The wall geometry ranged from intricate smaller undulations to sweeping large motions.

The information collected in the first stage became the starting point for the following four walls. Iteration 1 is treated as a baseline where there is no predetermined start point or intent. Iteration 2 begins with the series I proportions found to have the lowest concrete use relative to structural stability. In the first series, the front batter was found to increase stability as the slope increased while reducing material. Iteration 3 explores variations of a wall whose front batter leans more heavily as the soil volume increases. Iteration 3 is used as the start point for iteration 4 where the frequency of the cross-sections is manipulated, changing the level of detail. Each iteration had multiple stages and variations. In the following figures, wall sub-pieces with possible structural risks are highlighted in red.

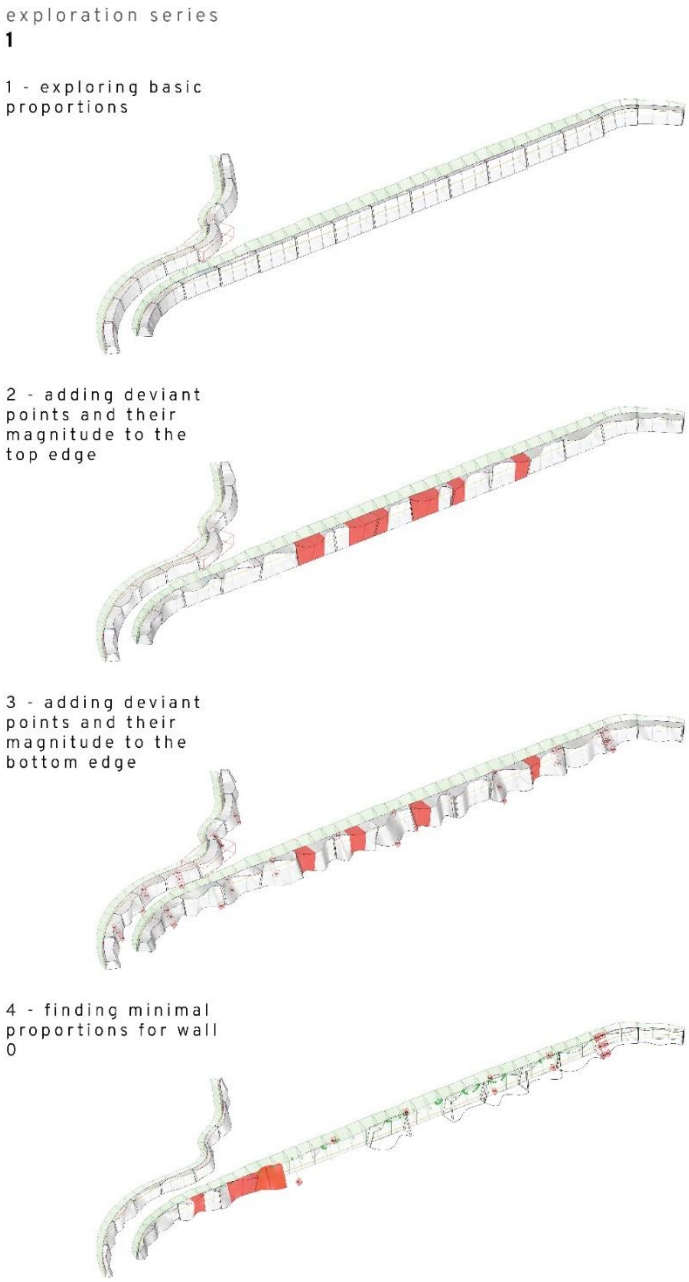

Figure 5.8 Design stages for iteration 1, which begins with no pre-determined agenda

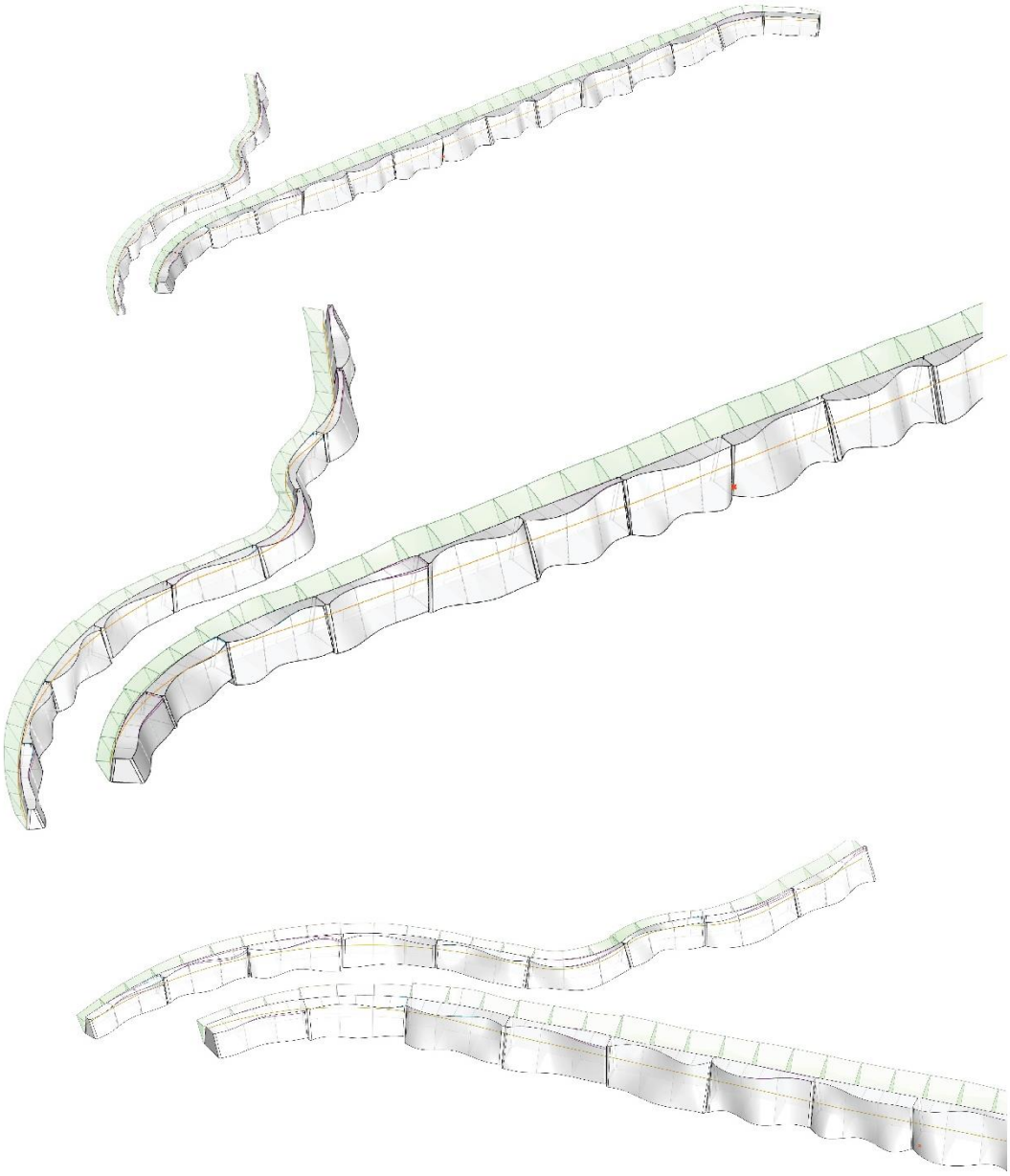

Figure 5.9 Design for iteration 1, which begins with no pre-determined agenda

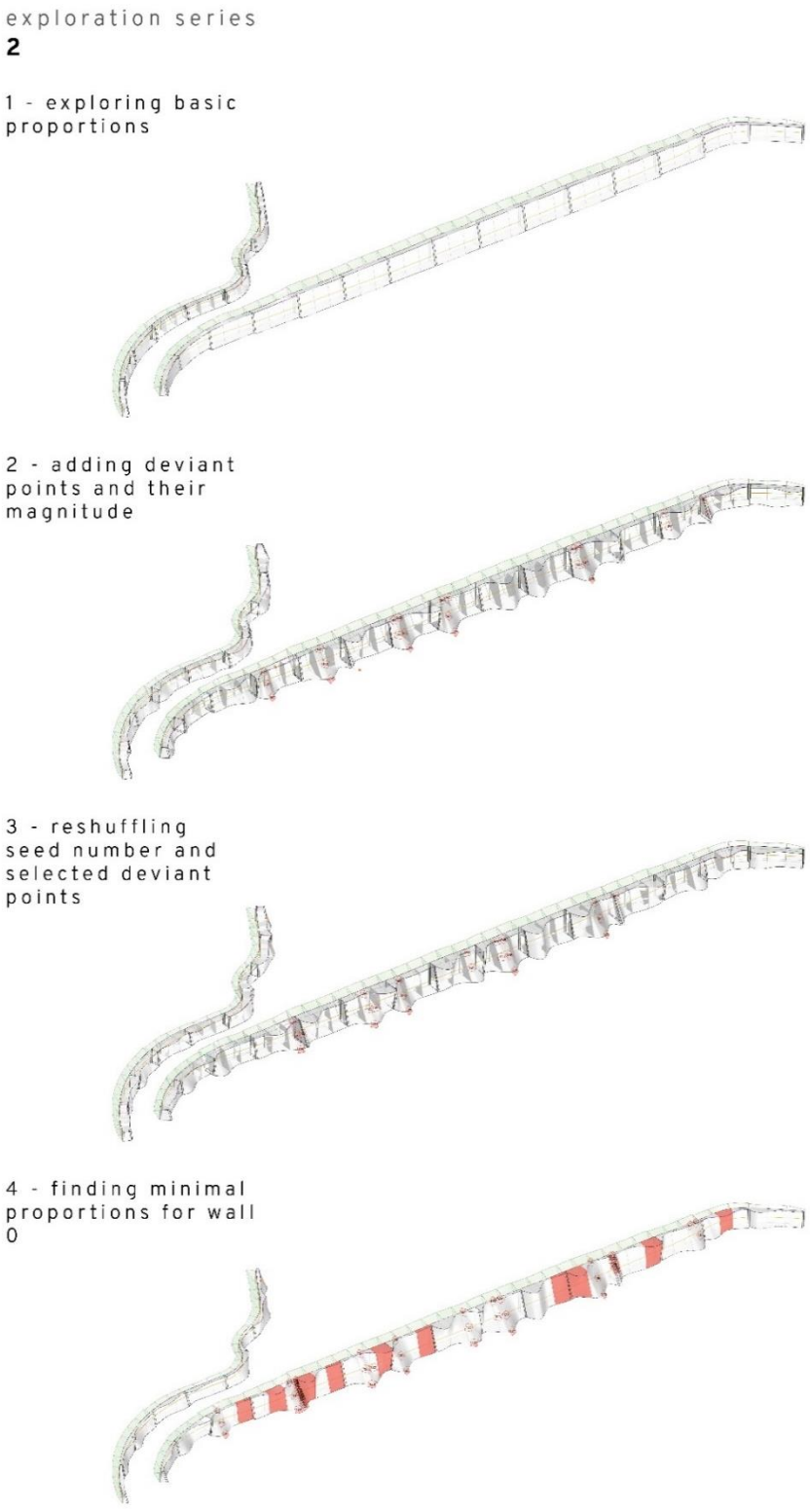

Figure 5.10 Design stages for iteration 2, which begins with successful wall proportions found in the first series

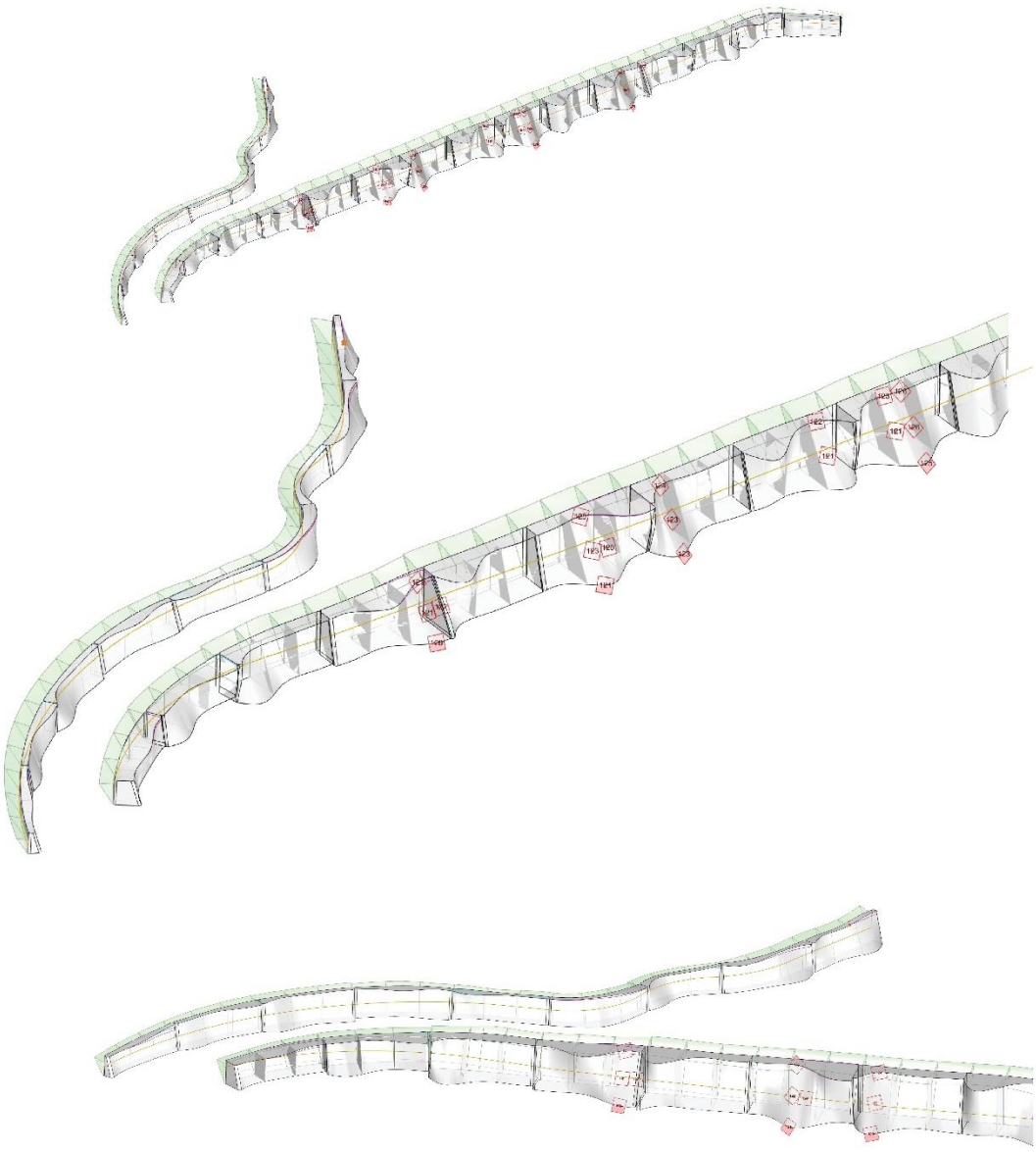

Figure 5.11 Design for iteration 2, which begins with successful wall proportions found in the first series

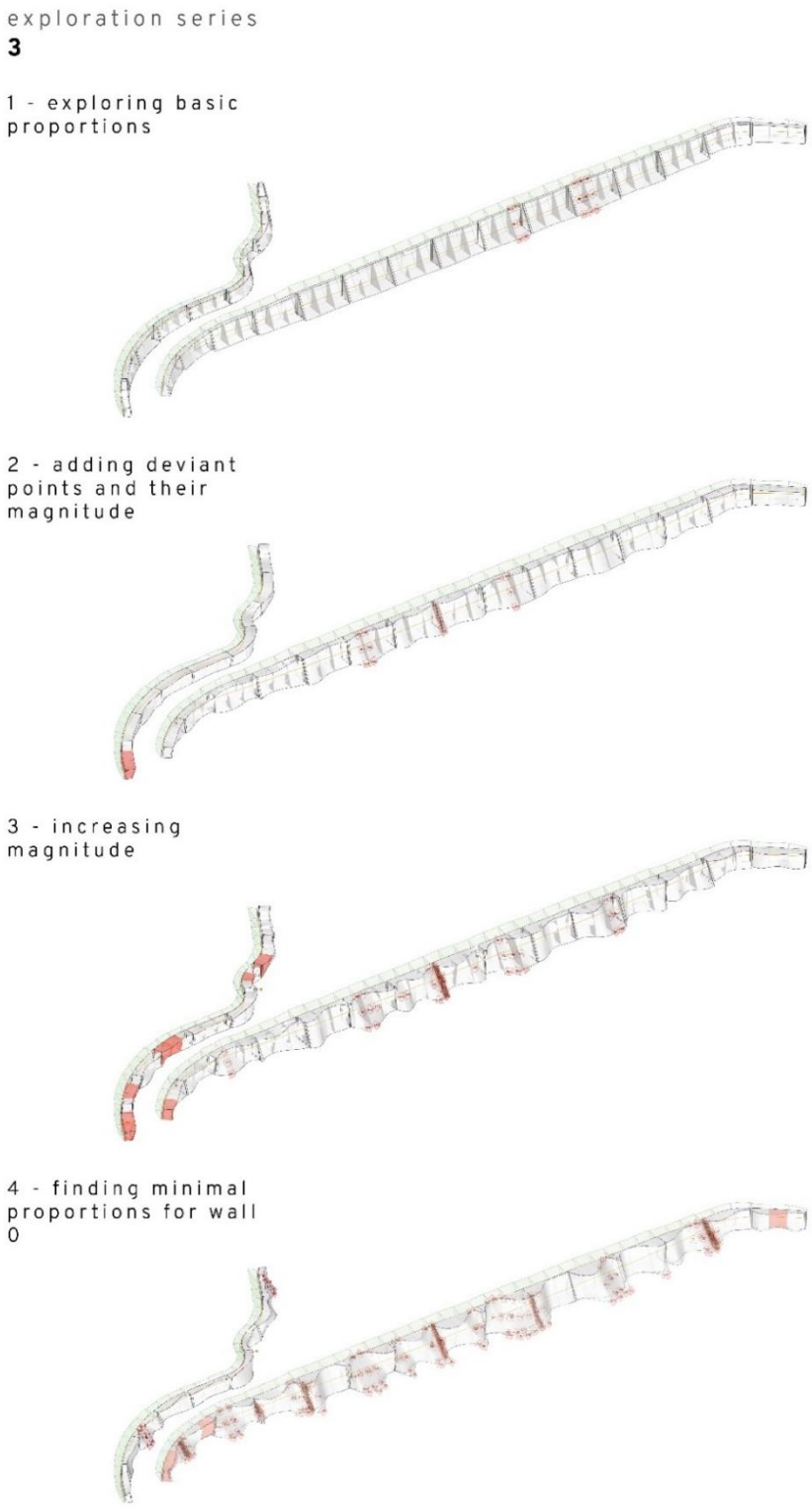

Figure 5.12 Initial design stages for iteration 3, which is based on manipulations of the front batter

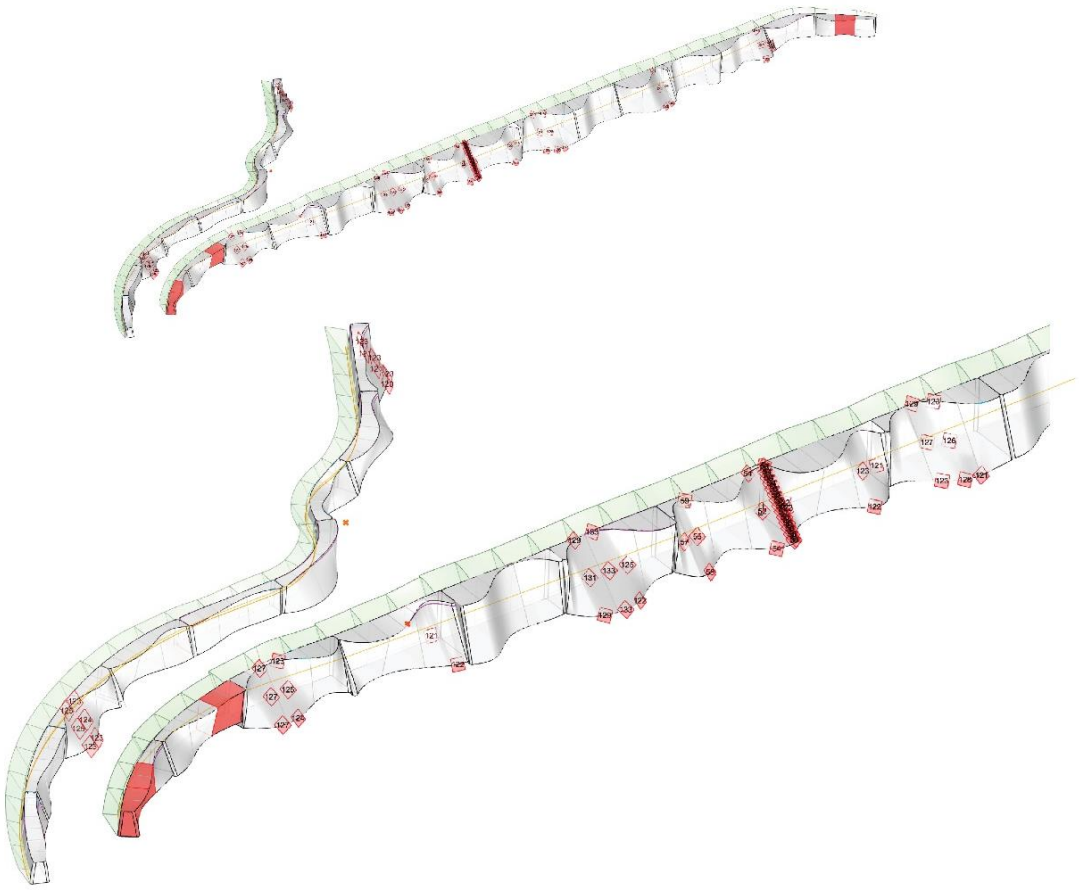

Figure 5.13 Design for iteration 3, which is based on manipulations of the front batter

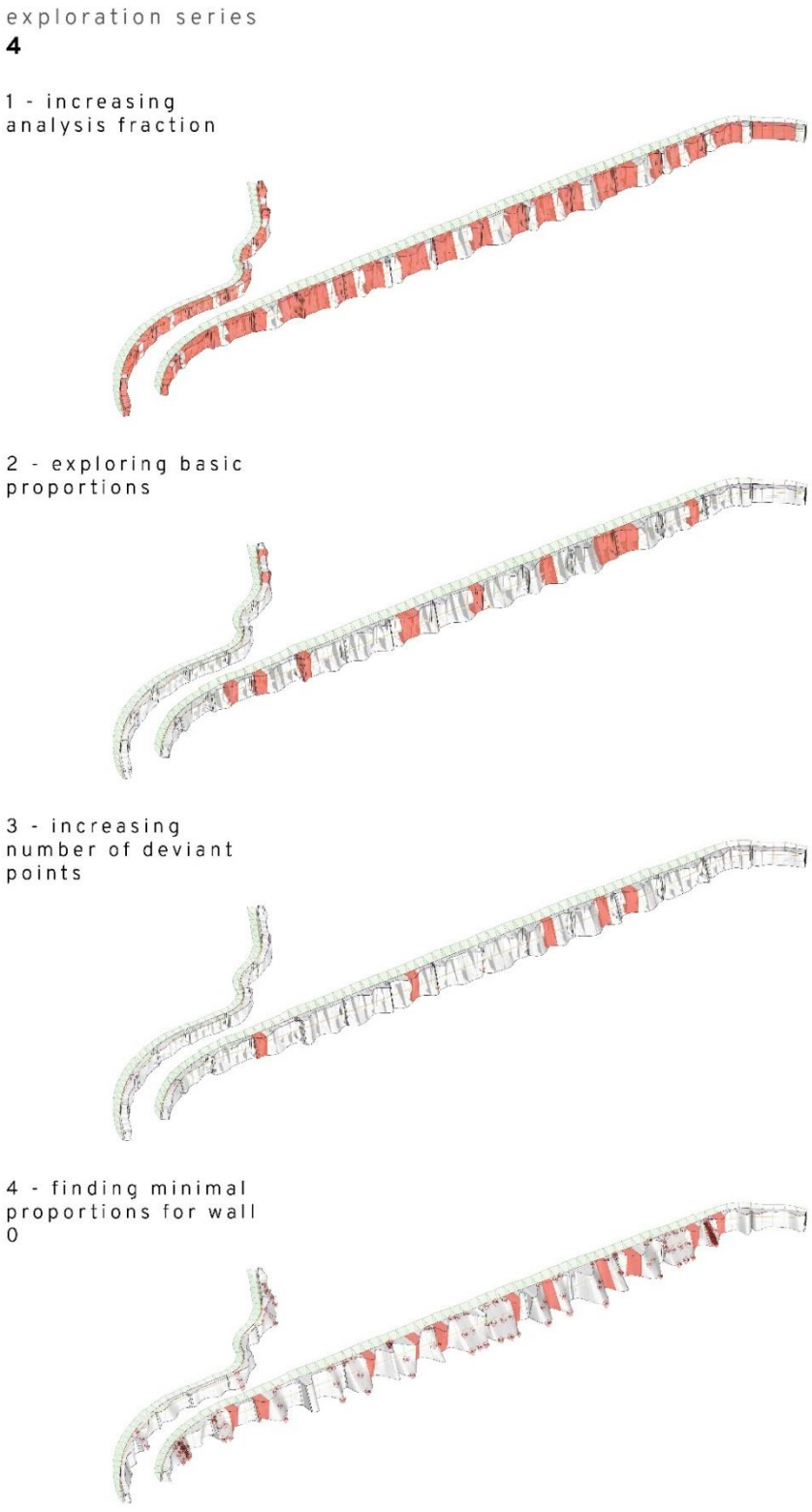

Figure 5.14 Design stages for iteration 4, which alters the level of detail of iteration 3

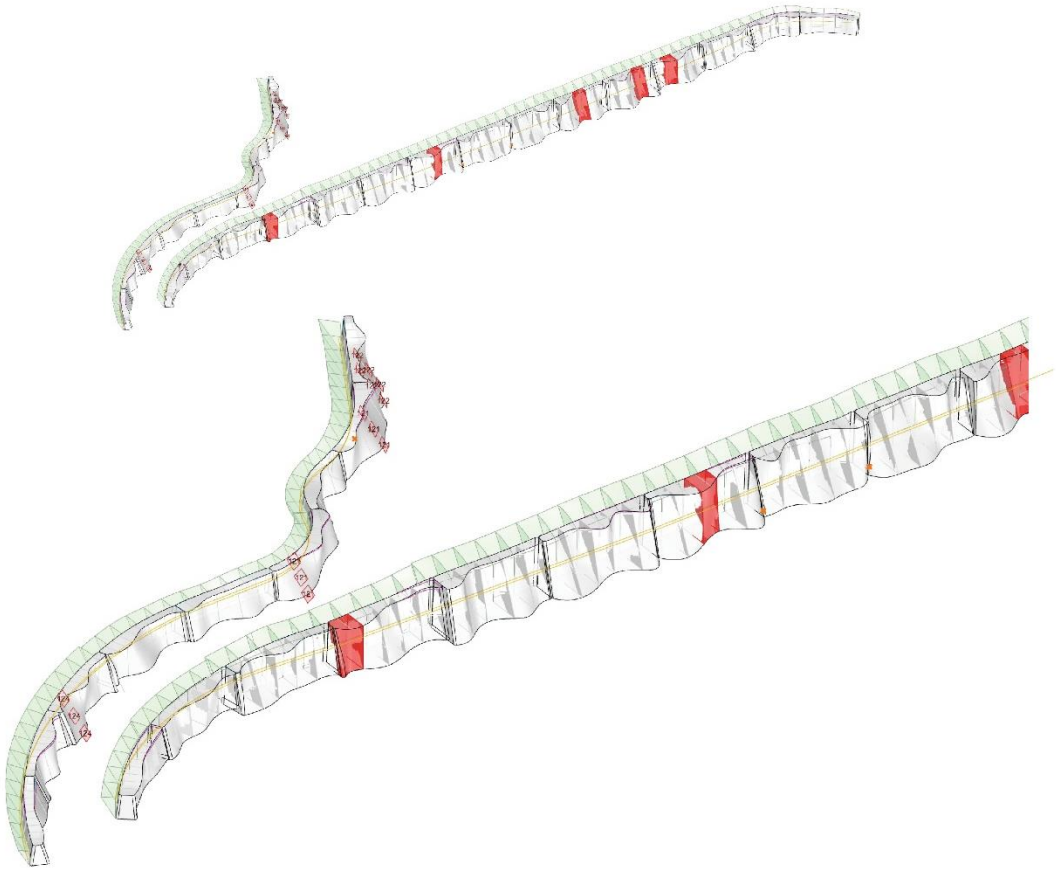

Figure 5.15 Design for iteration 4, which alters the level of detail of iteration 3

5.5.3 Observations

There are distinct values for this series. Strategies and concepts receive rapid evaluation and visualization without an investment of effort. It allows a strategy to be mocked up quickly as an alternative to manually creating a 3D model. This lowers the barrier to testing an idea such as the concept explored the first stage: What happens when wall leans back more in response to soil load? This stage can create rough early explorations of the intersection of aesthetics and structure. Similarly, the structural feedback of the toolkit caused the author to increase wall

proportions to the minimum required as well as reduce proportions to decrease excessive material use.

The last stage identified which areas had more challenging soil loads and unsuccessful wall proportions. This stage clarifies problematic geometries to avoid. In Figure 5.16, concave base edges can be formed in between protruding areas or the filleted edge of the wall segment. The middle has not been pushed inwards. Rather, the neighboring geometry is flared. This causes a concave base area that can be unstable. The number of deviant points or the magnitude of the deviation can be lowered to resolve this. Likewise, wall segments with randomized top edges can protrude over the base edge if the base width is low. Either the top deviation or baseline front batter can be lowered. Otherwise, an increase in the wall width would be necessary.

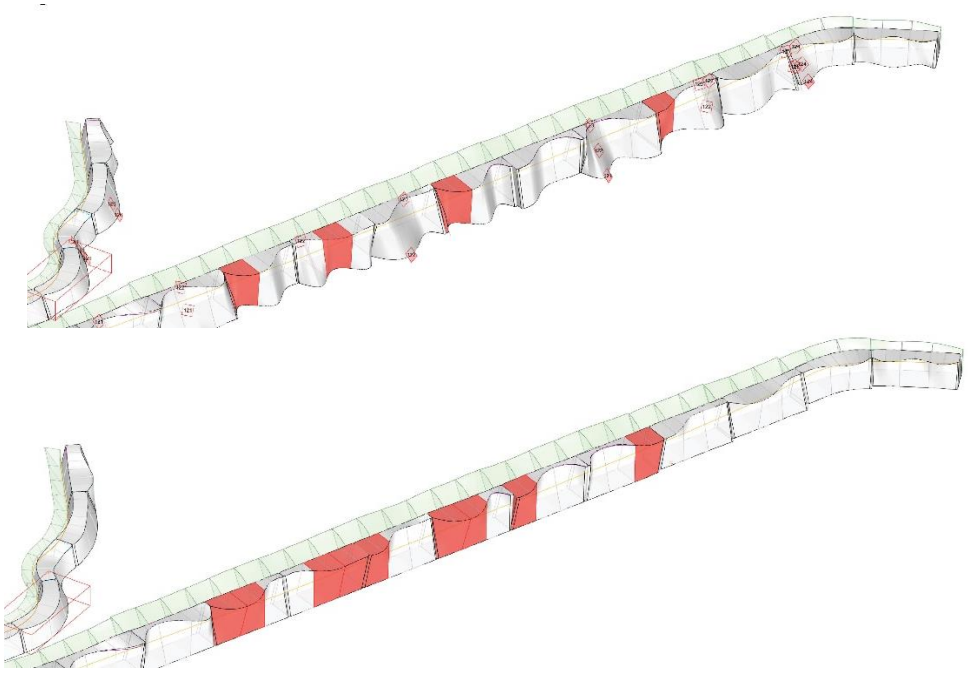

Figure 5.16 Challenging geometries across the second series of wall iterations

The second series also identified possible formal qualities resulting from each parameter. The quantity of deviant points affected how gradual or tight the movements across the wall surface were. The magnitude of the deviation created softer billowy forms on the low end and bursting, jutting forms on the high end. The frequency of cross-sections allowed changes in the scale of detail. The magnitude of the deviation can create soft or tight bends, but the frequency and density of cross-sections cause those forms to shrink or grow in size.

CHAPTER VI

CONCLUSIONS

6.1 Role of designer in emergent technology

This study was instigated in part by the need for further designer-oriented research to supplement the prevalence of material science and engineering research supporting DFC technology development. This research highlights two avenues by which designers can play a role in the development of emergent technologies. This toolkit illustrates the value of "tools for designers by designers". The modules are adaptive to where a designer can engage and evaluate their chosen strategies, concepts, with their specific manufacturer's limitations. This is a result of the prevalence of open variables across each stage for the user input. The live design feedback provides a didactic representation that increases the designer's comprehension of feasibility challenges. The short computation times allow for rapid design iterations as well as expedient batch processing of parameters.

There is another role for designers to contribute to emergent technology: to design is to give form and identity. Vernacular crafts and construction are defined by place, specifically the physical and structural limitations of the regional materials. Vernacular construction expresses the local craft strategies that accommodate their material limitations while reflecting local aesthetic values. These limits give vernacular construction a clear sense of identity through a bounded and defined visual language that is reflective of local conditions. This research is focused on generating forms adapted to the limitations and opportunities specific to 3DCP. Reinforcing 3DCP products can be a multi-step labor intensive process. The freeform capacities

of 3DCP provide the opportunity for geometries that adapt and respond to varying terrain conditions and structural needs. This research provides an illustration of a design language drawn from 3DCP limitations and structural agendas with a chosen aesthetic: The retaining wall geometries undulate in proportion to terrain soil loads. A different design language could be wall surface curvatures or scalloping fins in proportion to any data derived from the terrain or other context. These design languages could describe a “vernacular for 3D concrete printing”, a limited geometry that appropriately responds to the values and limits of the fabrication method. This research illustrates how design is an opportunity to define an identity through physical and visual forms.

6.2 Realized potentials of toolkit applications

Aside from clarifying fabrication limitations for designers, the results indicate the toolkit has significant applications. The toolkit allows designers to translate structural risk and fabrication data into actionable insights. The first series identified challenging terrain areas with larger loads. The first series also highlighted a basic wall proportion with the most efficient material use out of 16 iterations generated without excessive effort from the designer. The second series illustrated unsuccessful wall geometries from a structure and fabrication standpoint. Challenging geometries included concave base areas, protruding top edges, and the steep slopes and tight bends formed by large narrow protrusions and folds.

6.3 Future potentials for toolkit applications

This research detailed the toolkit application from the perspective of replicating an existing project. However, the toolkit was also tested with a path in a fictional hill. The toolkit allows the path and terrain to be changed during the design process. This would allow a designer

to design terrain, path, and wall in tandem, seeing the effect of changing the terrain and path on the wall. Similarly, the toolkit allows the user to easily input a 3D concrete printer's specific limitations. Having a fixed design but substituting the fabrication method would utilize the toolkit as an adaptive benchmark that allows comparison between extrusion-based 3DCP methods.

6.4 Research limitations

This research is inherently a snapshot in time regarding the state of 3DCP technology. There are limited standards for materials, processes or testing requirements unlike traditional concrete construction with its slump tests, testing cylinders and shared vocabulary. There could easily be more requirements that would need to be integrated into the toolkit. The toolkit is already a narrow set of considerations. For example, future toolkit developments could accommodate inclined plane printing or non-uniform print beds. Likewise, this toolkit is designed only for extrusion-based methods. This system has been focused on 3DCP but could be adapted to other DFC methods. The formwork-based systems have their own distinct criteria not considered or easily adapted within the toolkit. The principles of this interactive design environment could be deployed into new toolkits created for different DFC typologies. This research could also be further supported with FEM/FEA analysis of designs produced. The toolkit focuses on generating high quality candidates for further digital or physical structural testing.

6.5 Potentials for future research

The toolkit generates a wall in response to the terrain. It does not inform where the wall should be located within the terrain. The toolkit does not indicate terrain changes to

accommodate a desired wall design. These alternate perspectives could be investigated by future research. In this research, it is assumed that the wall would be filled with traditional concrete after printing the outer wall surface. Other research could explore printed hollow wall forms as gabion retaining walls filled with recycled construction riprap or other fill material. Future studies could consider 3D patterns as the inner fill of the wall. This study explored one defined geometric language of an undulating wall. Another study could compare multiple geometric responses to the terrain such as the earlier example of modulating the size of curves and fins.

6.6 Conclusions

As new construction technologies emerge, it is important to consider the implementation processes and challenges from the perspective of designers. The architecture, engineering, and construction industries have used DFC technologies to demonstrate new gains in sustainability through material reduction, novel project-specific geometries, and shortening of construction schedules through increases in automation. Thus, it is increasingly critical to investigate what values might DFC technologies bring to landscape architecture. In response to this need, this study proposes a novel toolkit to equip designers with rapidly exploring DFC in the case of an unreinforced retaining wall. This toolkit can help guide designers into understanding the limited "design space" of feasible geometries as well as facilitate the production of constructible designs. This toolkit has been based on the requirements of extrusion-based concrete printing, particularly in-situ robotic arm 3DCP. There is potential for future research to adapt the toolkit principles and processes to other DFC technologies.

As construction technologies grow more powerful and thus complicated, there is a value to tools that aid the designer in managing this newfound complex web of considerations. This study suggests that exploratory design processes facilitate rapid iteration. This can replace

traditional methods where a designer preconceives a solution that meets all fabrication, structural and aesthetic requirements. This research provides a working prototype of an interactive design environment. This toolkit illustrates the potential for new design processes that allow integration of structural, material, and fabrication agendas early in the project timeline. This research demonstrates that interactive design environments can be a replicable approach beyond retaining walls.

This research offers insight into major advantages of DFC for landscape applications. DFC has been found to be adaptable to generating site and project specific designs. This study provides an initial foray into the potential of DFC to construct terrain-responsive designs with complex geometries that respond to the site conditions. While the limits of 3DCP were found to have clear impacts on feasible geometries, the study results demonstrate new design freedoms and novel geometric qualities. These novel aesthetic qualities could add to the individuality of landscape architecture projects. This research also highlights the potentials of translating material and structural requirements into a design language that informs the project geometry. Further research could investigate the role of DFC in reducing the carbon impacts of landscape architecture. This study highlights the possibility of DFC as a vehicle for minimizing material use, reducing waste through the elimination of formwork, and constructing complex geometries adapted to their structural loads.

REFERENCES

Anton, A., Bedarf, P., Yoo, A., Dillenburger, B., Reiter, L., Wangler, T., & Flatt, R. J. (2020). Concrete Choreography. In *Fabricate 2020* (pp. 286–293). UCL Press. https://doi.org/10.2307/j.ctv13xpsvw.41

Asprone, D., Menna, C., Bos, F. P., Salet, T. A. M., Mata-Falcón, J., & Kaufmann, W. (2018). Rethinking reinforcement for digital fabrication with concrete. *Cement and Concrete Research*, *112*, 111–121. https://doi.org/10.1016/J.CEMCONRES.2018.05.020

Babafemi, A. J., Kolawole, J. T., Miah, M. J., Paul, S. C., & Panda, B. (2021). A Concise Review on Interlayer Bond Strength in 3D Concrete Printing. *Sustainability 2021, Vol. 13, Page 7137*, *13*(13), 7137. https://doi.org/10.3390/SU13137137

Baniasadi, S. (2021). *The Potential of 3D Concrete Printing Technology in Landscape Architecture*. https://www.proquest.com/openview/6af22e44955ae617f0067f05e2ec2d32/

Bhooshan, S., Bhooshan, V., Dell'Endice, A., Chu, J., Singer, P., Megens, J., Van Mele, T., & Block, P. (2022). The Striatus bridge. *Architecture, Structures and Construction 2022*, 1–23. https://doi.org/10.1007/S44150-022-00051-Y

Block Research Group. (n.d.). Retrieved December 5, 2022, from https://block.arch.ethz.ch/brg/project/knit-candela-muac-mexico-city

Bos, Menna, C., Pradena, M., Kreiger, E., da Silva, W. R. L., Rehman, A. U., Weger, D., Wolfs, R. J. M., Zhang, Y., Ferrara, L., & Mechtcherine, V. (2022). The realities of additively manufactured concrete structures in practice. *Cement and Concrete Research*, *156*, 106746. https://doi.org/10.1016/j.cemconres.2022.106746

Bos, F., Wolfs, R., Ahmed, Z., & Salet, T. (2019). Large Scale Testing of Digitally Fabricated Concrete (DFC) Elements. In *RILEM Bookseries* (Vol. 19, pp. 129–147). Springer Netherlands. https://doi.org/10.1007/978-3-319-99519-9_12

Burger, J., Lloret-Fritschi, E., Scotto, F., Demoulin, T., Gebhard, L., Mata-Falcón, J., Gramazio, F., Kohler, M., & Flatt, R. J. (2020). Eggshell: Ultra-thin three-dimensional printed formwork for concrete structures. *3D Printing and Additive Manufacturing*, *7*(2), 49–59. https://doi.org/10.1089/3DP.2019.0197

Buswell, R. A., da Silva, W. R. L., Bos, F. P., Schipper, H. R., Lowke, D., Hack, N., Kloft, H., Mechtcherine, V., Wangler, T., & Roussel, N. (2020). A process classification framework for defining and describing Digital Fabrication with Concrete. *Cement and Concrete Research*, *134*. https://doi.org/10.1016/J.CEMCONRES.2020.106068

Buswell, R. A., Leal de Silva, W. R., Jones, S. Z., & Dirrenberger, J. (2018). 3D printing using concrete extrusion: A roadmap for research. *Cement and Concrete Research*, *112*, 37–49. https://doi.org/10.1016/J.CEMCONRES.2018.05.006

Carneau, P., Mesnil, R., Roussel, N., & Baverel, O. (2020). Additive manufacturing of cantilever - From masonry to concrete 3D printing. *Automation in Construction*, *116*, 103184. https://doi.org/10.1016/j.autcon.2020.103184

CyBe Construction. (2022, June 22). *WEBINAR Crawler vs. Gantry - 3D printing*. https://www.youtube.com/watch?v=8fFzwAeE5Fc&t=1227s

CyBe Construction 3D prints concrete drone laboratory on-site in Dubai - 3D Printing Industry. (n.d.). Retrieved June 24, 2023, from https://3dprintingindustry.com/news/cybe-construction-3d-prints-concrete-drone-laboratory-site-dubai-114869/

CyBe Mortar — CyBe Construction. (n.d.). Retrieved June 24, 2023, from https://cybe.eu/3d-concrete-printing/mortar/

CyBe RC (Robot Crawler) — CyBe Construction. (n.d.). Retrieved February 4, 2023, from https://cybe.eu/3d-concrete-printing/printers/cybe-robot-crawler/

Dielemans, G., Lachmayer, L., Recker, T., Atanasova, L., Hechtl, C. M., Matthäus, C., Raatz, A., & Dörfler, K. (2022). Mobile Additive Manufacturing: A Case Study of Clay Formwork for Bespoke in Situ Concrete Construction. *RILEM Bookseries*, *37*, 15–21. https://doi.org/10.1007/978-3-031-06116-5_3/COVER

Dörfler, K., Dielemans, G., Lachmayer, L., Recker, T., Raatz, A., Lowke, D., & Gerke, M. (2022). Additive Manufacturing using mobile robots: Opportunities and challenges for building construction. *Cement and Concrete Research*, *158*, 106772. https://doi.org/10.1016/j.cemconres.2022.106772

Dörfler, K., Hack, N., Sandy, T., Giftthaler, M., Lussi, M., Walzer, A. N., Buchli, J., Gramazio, F., & Kohler, M. (2019). Mobile robotic fabrication beyond factory conditions: case study Mesh Mould wall of the DFAB HOUSE. *Construction Robotics*, *3*(1–4), 53–67. https://doi.org/10.1007/s41693-019-00020-w

Dörrie, R., Laghi, V., Arrè, L., Kienbaum, G., Babovic, N., Hack, N., & Kloft, H. (2022). Combined Additive Manufacturing Techniques for Adaptive Coastline Protection Structures. *Buildings*, *12*(11), 1806. https://doi.org/10.3390/buildings12111806

Facade - Additive Tectonics. (n.d.). Retrieved June 23, 2023, from https://www.additive-tectonics.com/facade-regensburg/

Freund, N., & Lowke, D. (2022). Interlayer Reinforcement in Shotcrete-3D-Printing : The Effect of Accelerator Dosage on the Resulting Bond Behavior of Integrated Reinforcement Bars. *Open Conference Proceedings, 1*, 83–95. https://doi.org/10.52825/OCP.V1I.72

Gebhard, L., Mata-Falcón, J., Anton, A., Dillenburger, B., & Kaufmann, W. (2021). Structural behaviour of 3D printed concrete beams with various reinforcement strategies. *Engineering Structures, 240*. https://doi.org/10.1016/J.ENGSTRUCT.2021.112380

Gebhard, L., Mata-Falcón, J., Iqbal, A., & Kaufmann, W. (2023). Structural behaviour of post-installed reinforcement for 3D concrete printed shells – A case study on water tanks. *Construction and Building Materials, 366*, 130163. https://doi.org/10.1016/j.conbuildmat.2022.130163

Grasshopper - algorithmic modeling for Rhino. (n.d.). Retrieved June 21, 2023, from https://www.grasshopper3d.com/

Hack, N., Dressler, I., Brohmann, L., Gantner, S., Lowke, D., & Kloft, H. (2020). Injection 3D Concrete Printing (I3DCP): Basic Principles and Case Studies. *Materials 2020, Vol. 13, Page 1093*, *13*(5), 1093. https://doi.org/10.3390/MA13051093

Hack, N., & Kloft, H. (2020). Shotcrete 3D Printing Technology for the Fabrication of Slender Fully Reinforced Freeform Concrete Elements with High Surface Quality: A Real-Scale Demonstrator. In *RILEM Bookseries* (Vol. 28, pp. 1128–1137). Springer. https://doi.org/10.1007/978-3-030-49916-7_107

Hack, N., & Lauer, W. V. (2014). Mesh-Mould: Robotically Fabricated Spatial Meshes as Reinforced Concrete Formwork. *Architectural Design*, *84*(3), 44–53. https://doi.org/10.1002/ad.1753

Harris, C. W., & Dines, N. T. (1998). *texts Time Saver Standards For Landscape Architecture* .

Huang, S., Xu, W., & Li, Y. (2022). The impacts of fabrication systems on 3D concrete printing building forms. *Frontiers of Architectural Research*, *11*(4), 653–669. https://doi.org/10.1016/j.foar.2022.03.004

Jagoda, J., Diggs-McGee, B., Kreiger, M., & Schuldt, S. (2020). The Viability and Simplicity of 3D-Printed Construction: A Military Case Study. *Infrastructures 2020, Vol. 5, Page 35*, *5*(4), 35. https://doi.org/10.3390/INFRASTRUCTURES5040035

Jud, D., Hurkxkens, I., Girot, C., & Hutter, M. (2021). Robotic embankment. *Construction Robotics 2021 5:2*, *5*(2), 101–113. https://doi.org/10.1007/S41693-021-00061-0

Kloft, H., Empelmann, M., Hack, N., Herrmann, E., & Lowke, D. (2020). Reinforcement strategies for 3D-concrete-printing. *Civil Engineering Design*, *2*(4), 131–139. https://doi.org/10.1002/CEND.202000022

Kloft, H., Gehlen, C., Dörfler, K., Hack, N., Henke, K., Lowke, D., Mainka, J., & Raatz, A. (2021a). TRR 277: Additive manufacturing in construction. *Civil Engineering Design*, *3*, 113–122.

Kloft, H., Gehlen, C., Dörfler, K., Hack, N., Henke, K., Lowke, D., Mainka, J., & Raatz, A. (2021b). TRR 277: Additive manufacturing in construction. *Civil Engineering Design*, *3*(4), 113–122. https://doi.org/10.1002/CEND.202100026

Kloft, H., & Hack, N. (n.d.). *Gradual Transition Shotcrete 3D Printing*. https://doi.org/10.1016/j.matdes.2016.03.097

Kloft, H., Krauss, H.-W., Hack, N., Herrmann, E., Neudecker, S., Varady, P. A., & Lowke, D. (2020). Influence of process parameters on the interlayer bond strength of concrete elements additive manufactured by Shotcrete 3D Printing (SC3DP). *Cement and Concrete Research*, *134*, 106078. https://doi.org/10.1016/j.cemconres.2020.106078

KnitCandela - A flexibly formed thin concrete shell at MUAC, Mexico City, 2018. (n.d.). Retrieved June 20, 2023, from https://block.arch.ethz.ch/brg/project/knit-candela-muac-mexico-city

Lachmayer, L., Dörrie, R., Kloft, H., & Raatz, A. (2021). *Automated shotcrete 3D printing-Printing interruption for extended component complexity*.

Lloret-Fritschi, E., Wangler, T., Gebhard, L., Mata-Falcón, J., Mantellato, S., Scotto, F., Burger, J., Szabo, A., Ruffray, N., Reiter, L., Boscaro, F., Kaufmann, W., Kohler, M., Gramazio, F., & Flatt, R. (2020). From Smart Dynamic Casting to a growing family of Digital Casting Systems. *Cement and Concrete Research*, *134*, 106071. https://doi.org/10.1016/J.CEMCONRES.2020.106071

Lowke, D., Dini, E., Perrot, A., Weger, D., Gehlen, C., & Dillenburger, B. (2018). Particle-bed 3D printing in concrete construction – Possibilities and challenges. *Cement and Concrete Research*, *112*, 50–65. https://doi.org/10.1016/J.CEMCONRES.2018.05.018

Lowke, D., Talke, D., Dressler, I., Weger, D., Gehlen, C., Ostertag, C., & Rael, R. (2020). Particle bed 3D printing by selective cement activation – Applications, material and process technology. *Cement and Concrete Research*, *134*, 106077. https://doi.org/10.1016/J.CEMCONRES.2020.106077

Lowke, D., Vandenberg, A., Pierre, A., Thomas, A., Kloft, H., & Hack, N. (2021). Injection 3D concrete printing in a carrier liquid - Underlying physics and applications to lightweight space frame structures. *Cement and Concrete Composites*, *124*, 104169. https://doi.org/10.1016/j.cemconcomp.2021.104169

Ma, G., Buswell, R., Leal da Silva, W. R., Wang, L., Xu, J., & Jones, S. Z. (2022). Technology readiness: A global snapshot of 3D concrete printing and the frontiers for development. *Cement and Concrete Research*, *156*, 106774. https://doi.org/10.1016/j.cemconres.2022.106774

Mai, I., Brohmann, L., Freund, N., Gantner, S., Kloft, H., Lowke, D., & Hack, N. (2021). Large Particle 3D Concrete Printing—A Green and Viable Solution. *Materials 2021, Vol. 14, Page 6125*, *14*(20), 6125. https://doi.org/10.3390/MA14206125

Mechtcherine, V., Buswell, R., Kloft, H., Bos, F. P., Hack, N., Wolfs, R., Sanjayan, J., Nematollahi, B., Ivaniuk, E., & Neef, T. (2021). Integrating reinforcement in digital fabrication with concrete: A review and classification framework. *Cement and Concrete Composites*, *119*. https://doi.org/10.1016/j.cemconcomp.2021.103964

Meibodi, M. A., Bernhard, M., Jipa, A., & Dillenburger, B. (2019). The Smart Takes From the Strong: *Fabricate 2017*, 210–217. https://doi.org/10.2307/J.CTT1N7QKG7.33

Minibuilders - Institute for Advanced Architecture of Cataloni. (n.d.). Retrieved February 7, 2023, from https://iaac.net/project/minibuilders/#

Moelich, G. M., Janse van Rensburg, J. J., Kruger, J., & Combrinck, R. (2022). The Environment's Effect on the Interlayer Bond Strength of 3D Printed Concrete. *RILEM Bookseries*, *37*, 222–227. https://doi.org/10.1007/978-3-031-06116-5_33/COVER

Pegna, J. (1997). Exploratory investigation of solid freeform construction. *Automation in Construction*, *5*(5), 427–437. https://doi.org/10.1016/S0926-5805(96)00166-5

Popescu, M., Rippmann, M., Liew, A., Reiter, L., Flatt, R. J., Van Mele, T., & Block, P. (2021). Structural design, digital fabrication and construction of the cable-net and knitted formwork of the KnitCandela concrete shell. *Structures*, *31*, 1287–1299. https://doi.org/10.1016/j.istruc.2020.02.013

Popescu, M., Rippmann, M., Van Mele, T., & Block, P. (2018). Automated Generation of Knit Patterns for Non-developable Surfaces. *Humanizing Digital Reality*, 271–284. https://doi.org/10.1007/978-981-10-6611-5_24

Project A 01 - Additive Manufacturing in Construction TRR277. (n.d.). Retrieved June 20, 2023, from https://amc-trr277.de/projects/project-area-a/focus-area-project-a01/

Project A 02 - Additive Manufacturing in Construction TRR277. (n.d.). Retrieved June 20, 2023, from https://amc-trr277.de/projects/project-area-a/focus-area-project-a02/

Project A 03 - Additive Manufacturing in Construction TRR277. (n.d.). Retrieved December 5, 2022, from https://amc-trr277.de/projects/project-area-a/focus-area-project-a03/

R&Drone Laboratory — CyBe Construction. (n.d.). Retrieved June 24, 2023, from https://cybe.eu/cases/rdrone-lab/

Reiter, L., Wangler, T., Anton, A., & Flatt, R. J. (2020). Setting on demand for digital concrete – Principles, measurements, chemistry, validation. *Cement and Concrete Research*, *132*. https://doi.org/10.1016/J.CEMCONRES.2020.106047

Riceour, P. (1961). Universal Civilization and National Cultures. In *History and Truth*.

Rippmann, M., Van Mele, T., Block, P., & Popescu, M. (2016). Complex concrete casting: Knitting stay-in-place fabric formwork. *Spatial Structures in the 21st Century*.

Roussel, N. (2018). Rheological requirements for printable concretes. *Cement and Concrete Research*, *112*, 76–85. https://doi.org/10.1016/j.cemconres.2018.04.005

Schipper, H. R., & Grünewald, S. (2014). Efficient material use through smart flexible formwork method. *ECO-Crete: International Symposium on Environmentally Friendly Concrete, Reykjavik, Iceland, 13-15 August 2014*. https://repository.tudelft.nl/islandora/object/uuid%3A5f767d7f-6ad1-4e37-9efc-1817e9561274

Serra, R., & Foster, H. (2018). *Conversations about Sculpture*.

Striatus 3D concrete printed masonry bridge. (n.d.). Retrieved June 20, 2023, from https://www.striatusbridge.com/

Strohle, M., Sadique, M., Dulaimi, A., & Kadhim, M. A. (2023). Prospect and barrier of 3D concrete: a systematic review. *Innovative Infrastructure Solutions*, *8*(1), 1–19. https://doi.org/10.1007/S41062-022-00975-W/FIGURES/12

Szabo, A. ;, Reiter, L. ;, Lloret-Fritschi, E. ;, Wangler, T. ;, Gramazio, F. ;, Kohler, M. ;, & Flatt, R. J. (2020). *ACDC: The Admixture Controlled Digital Casting and its Application to Thin Folded Concrete Structures Working Paper*. https://doi.org/10.3929/ethz-b-000406770

Taha, N., Walzer, A. N., Ruangjun, J., Bürgin, T., Dörfler, K., Lloret-Fritschi, E., Gramazio, F., & Kohler, M. (2019). Robotic AeroCrete – A novel robotic spraying and surface treatment technology for the production of slender reinforced concrete elements. *Architecture in the Age of the 4th Industrial Revolution – Proceedings of the 37th ECAADe and 23rd SIGraDi Conference*, *3*, 245–254. https://doi.org/10.3929/ETHZ-B-000387276

Talke, D., Henke, K., & Weger, D. (2019). *Selective Cement Activation (SCA)-new possibilities for additive manufacturing in construction*.

Tay, Y. W. D., Ting, G. H. A., Qian, Y., Panda, B., He, L., & Tan, M. J. (2018). Time gap effect on bond strength of 3D-printed concrete. *Https://Doi.Org/10.1080/17452759.2018.1500420*, *14*(1), 104–113. https://doi.org/10.1080/17452759.2018.1500420

The Alexander Plaza | Mikyoung Kim Design. (n.d.). Retrieved June 20, 2023, from https://myk-d.com/projects/the-alexander-art-plaza/

The First Park to be Built Using 3D Printing is in China - 3Dnatives. (n.d.). Retrieved June 20, 2023, from https://www.3dnatives.com/en/first-park-3d-printing-china-151120214/

The LivingRoom: A Freeware Learning Garden Focused on Health, Food, and Nutrition Education | ASLA 2020 Student Awards. (n.d.). Retrieved June 23, 2023, from https://www.asla.org/2020studentawards/1315.html

Walker, I. D., Krovi, V. N., Peerzada, A. B., Raman, A., Rangaraju, P., Schmid, M. J., & Srivastava, M. (2023). 3D Concrete Printing with Macro-micro Robots. *Lecture Notes in Networks and Systems*, *561 LNNS*, 493–498. https://doi.org/10.1007/978-3-031-18344-7_34/COVER

Weger, D., Baier, D., Straßer, A., Prottung, S., Kränkel, T., Bachmann, A., Gehlen, C., & Zäh, M. (2020). Reinforced Particle-Bed Printing by Combination of the Selective Paste Intrusion Method with Wire and Arc Additive Manufacturing – A First Feasibility Study. *RILEM Bookseries*, *28*, 978–987. https://doi.org/10.1007/978-3-030-49916-7_95/COVER

Weger, D., & Gehlen, C. (2021). Particle-Bed Binding by Selective Paste Intrusion—Strength and Durability of Printed Fine-Grain Concrete Members. *Materials 2021, Vol. 14, Page 586*, *14*(3), 586. https://doi.org/10.3390/MA14030586

Williams, A. (2021, November 9). *Robots 3D print park benches, flower beds and sculptures in world first*. New Atlas. https://newatlas.com/3d-printing/world-first-3d-printed-park-shenzhen/

Wolfs, R. J. M., Bos, F. P., Van Strien, E. C. F., & Salet, T. A. M. (2018). A real-time height measurement and feedback system for 3d concrete printing. *Fib Symposium*, 2474–2483. https://doi.org/10.1007/978-3-319-59471-2_282/COVER

Xu, W., Gao, Y., Sun, C., & Wang, Z. (2020). Fabrication and Application of 3D-Printed Concrete Structural Components in the Baoshan Pedestrian Bridge Project. *Fabricate 2020*, 140–147. https://doi.org/10.2307/J.CTV13XPSVW.22

Xu, W., Huang, S., Han, D., Zhang, Z., Gao, Y., Feng, P., & Zhang, D. (2022). Toward automated construction: The design-to-printing workflow for a robotic in-situ 3D printed house. *Case Studies in Construction Materials*, *17*, e01442. https://doi.org/10.1016/j.cscm.2022.e01442